Title
Characterizing nuclear remodeling during budding yeast meiosis

Author
King, Grant Austin

Publication Date
2022

Peer reviewed|Thesis/dissertation

Characterizing nuclear remodeling during budding yeast meiosis

by

Grant Austin King

A dissertation submitted in partial satisfaction of the

requirements for the degree of

Doctor of Philosophy

in

Molecular and Cell Biology

in the

Graduate Division

of the

University of California, Berkeley

Committee in charge:

Professor Elçin Ünal, Chair
Professor Jasper Rine
Professor Rebecca Heald
Professor James Olzmann

Summer 2022

Abstract

Characterizing nuclear remodeling during budding yeast meiosis

by

Grant King

Doctor of Philosophy in Molecular and Cell Biology

University of California, Berkeley

Professor Elçin Ünal, Chair

The nucleus, the defining organelle of the eukaryotic cell, must be remodeled during every cell division in order to accommodate the division of genetic material. While this remodeling has been extensively studied during mitosis, it remains poorly understood how the nucleus is remodeled during meiosis. In this study, we provide a comprehensive analysis of nuclear behavior during meiosis in the model organism budding yeast. First, we find that the nuclear envelope undergoes a five-way division, forming a nuclear-envelope bound compartment that is excluded from gametes. This compartment, termed the Gametogenesis Uninherited Nuclear Compartment or GUNC, contains nuclear pore complexes (NPCs) in all cells and age-induced damage in old cells. The material sequestered to the GUNC is subsequently eliminated by release of vacuolar proteases, establishing this remodeling event as a novel nuclear quality control mechanism that contributes to meiotic cellular rejuvenation. Second, we find that the NPC undergoes two mechanistically-distinct meiotic remodeling events: partial nuclear basket detachment during meiosis I and full nuclear basket detachment during meiosis II. Meiosis I detachment, which involves Nup60 and its binding partner Nup2, is driven by Polo kinase-dependent phosphorylation of Nup60 at its binding interface with the NPC core. Notably, this remodeling event also occurs in the distantly related *Schizosaccharomyces pombe*, suggesting basket detachment involves conserved nuclear basket organizational principles and fulfills an important function. Finally, we find that the nuclear permeability barrier is transiently disrupted during meiosis II, driving intermixing of the cytoplasm and nucleoplasm. Since the nuclear envelope stays intact throughout meiosis, regulation of nuclear transport machinery is likely involved in this event. Several meiotic regulators disrupt barrier loss or return, although their precise mechanistic contributions remain unclear. In all, this work establishes the nuclear periphery as a highly dynamic and regulated entity during budding yeast meiosis. Studying the budding yeast meiotic nucleus will continue to improve our understanding of nuclear organization and its contributions to cellular health for years to come.

for my parents

Table of Contents

Acknowledgements

Graduate school can be incredibly difficult and isolating, at times. In my case, it involved struggling with scientific failure and personal challenges, including learning how to cope with my obsessive-compulsive disorder and surviving a pandemic. As such, I have only been able to complete this dissertation with the support of my colleagues, friends, and family. You have allowed this seven-year experience to be full of grace, growth, and discovery – thank you all.

To the Br-Ün lab, I have learned from each and every one of you. Christiane Brune, lab manager-extraordinaire – thank you for keeping the lab running and for your ongoing technical support. Eric Sawyer, my original mentor in the lab – thank you for patiently teaching me how to yeast and, even more importantly, how to be a fantastic mentor and scientist. Jay Goodman, my dear collaborator – thank you for helping me through the process of publishing our first paper. Tina Sing and Vicki Jorgensen (the Fab 3 a.k.a. granT <3), my wonderful friends and trivia partners – thank you for seeing me through many highs and many lows, for making me laugh with so many Da Bomb taste tests and what-are-the-odds. Cyrus Ruediger, my de facto little brother and the ultimate buddy – thank you for always talking science, offering emotional support, tolerating my antics, and eating meals at whatever random time I deemed appropriate. Keerthana Chetlapalli, Matty Walsh, and Ben Styler, my trainees – thank you for helping me learn how to be a mentor. Keerthana – thank you for taking out every single strain in the strain collection from the freezer and for being the best undergraduate I could've asked for. Matty and Ben, my Team Nucleus – thank you for continuing my work, I'm so excited to see what amazing findings you make over the coming years. But, most of all, I will forever be indebted to my PI, Elçin Ünal. Elçin – thank you for being the perfect graduate school mentor for me. You are a role model for the type of person and scientist I hope to be. Your empathy made it feel like I had family in lab and your scientific intuition pushed to grow as a scientist. You, more than anyone else, are the reason that I am finishing this dissertation.

To the Berkeley science community and my collaborators, I am a better scientist and person for having worked with you. Although not technically part of the lab, Zarah Arce, Alex, and the late Bertha Germany provided the daily support that made this work possible. Jasper Rine, James Olzmann, and Rebecca Heald – thank you for being a wonderful thesis committee and supporting me all the way through getting a postdoctoral position! Jeremy Thorner – thank you for your investment in Berkeley's scientific community, including attending our lab meetings. Joao Matos and Rahel Wettstein – thank you for being kind, generous, and sharp collaborators that made for great synergistic science. Sue Jaspersen and Joseph Varberg – thank you for welcoming me to your lab and for the scientific support you've continued to give me.

To my friends and loved ones, I am only sane at the end of this process because of your companionship. Erik Van Dis and Daniel Saxton, my Fat Apples Crew – thank you for so many deranged morning conversations and evening board game nights. Ashley Albright, Jenna Haines, and Helen Vander Wende, the Cute Mommy Butts Club – thank you for all the wonderful times, ranging from watching fantastic films like *Sex and the City 2* to eating delicious bar-b-que. Jennifer Mahan and Amanda Perry – thank you for being the best friends and travel buddies I could ever ask for, even if one of us (me) has to cry every trip. Summer Si – thank you for sticking by side since the 11th grade and accompanying me through this chapter of my life. Carlos de Sousa – thank you for your emotional support, kindness, and company during the final push of my PhD. Katie Haller, Joon Kim, Kelsey Roberts Kingman, Elora López-Nandam, Wenyi Zhou, Rebecca Sylvers, Alex Co, Maddie Elia – thank you for your continued love and friendship.

To my family, I made it to grad school and finished grad school because of you. My extended family, especially Rihab Habibi, Norma Freiha, and Abeer Yazbek – thank you for making me feel loved, I hope to see you even more over the coming years. My grandparents – the late Richard King, the late Josephine Khuri, and Margaret King – thank you for your unconditional love, I am grateful to have known you. Pita, Turtlese and most especially Rocky – thank you for being such amazing and cute pets. Brad, my little brother – thank you for being there for me, especially since you've moved to the Bay Area. As much as I tease you, I'm proud of you for the amazing doctor and person you are. Hala King and Richard King, my parents – thank you for being a source of laughter and dog pictures, for being my shoulder to cry on and a constant I could always rely on. You have no idea how much that meant to me.

And, last but not least, hyraxes – thank you for always putting on a smile on my face, even during my hardest days. Of course, I had to include a couple of pictures.

Chapter 1

Introduction

The following chapter contains material derived from a publication on which I am first author (King and Ünal, 2020).

1.1 A defining feature of eukaryotes: the nuclear periphery

The nucleus, a membrane-bound organelle encompassing the cell's genetic material, is the defining feature of the eukaryotic cell. This compartmentalization allows for separation of transcription, which occurs within the nucleus, and translation, which occurs within the cytoplasm. The nuclear periphery is the barrier responsible for establishing a distinct nuclear and cytoplasmic identity (reviewed in Hetzer, 2010). In all eukaryotes, this barrier consists of the nuclear envelope, a double lipid bilayer that is a subregion of the endoplasmic reticulum, and nuclear pore complexes (NPCs), large macromolecular structures that mediate selective transport (Figure 1.1). It has become increasingly appreciated that the nuclear periphery is a key location for both natural and pathological aging. As such, improved understanding of the organizational principles of the nuclear periphery is an important area of current cell biology research. In this section, I provide a brief overview of the key features of the nuclear envelope and how they become disrupted in aging cells.

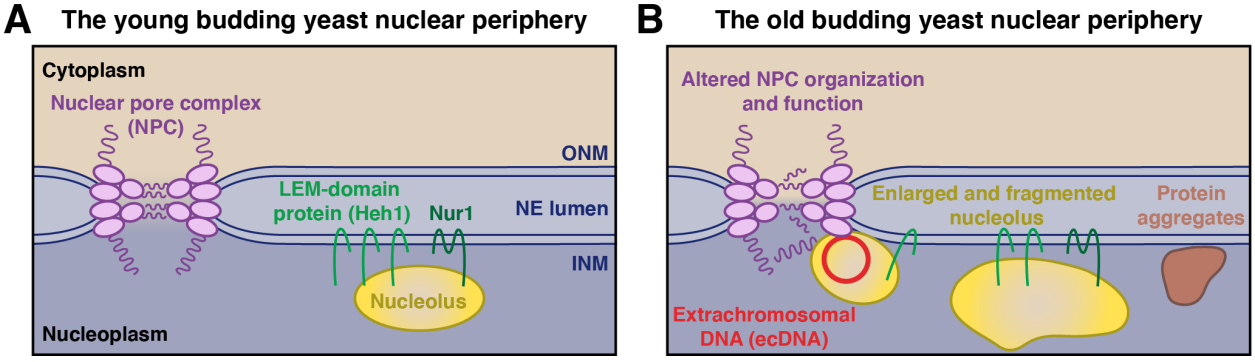

Figure 1.1. Schematic depicting the nuclear periphery in young and old budding yeast cells. A. The nuclear periphery in a young yeast cell. The nuclear envelope (NE) is a double lipid bilayer, consisting of the outer nuclear membrane (ONM), inner nuclear membrane (INM), and the space in between (NE lumen). Nuclear pore complexes (NPCs), embedded in the NE, mediate transport between the cytoplasm and the nucleoplasm. The INM has a distinct proteome and lipidome, including the nucleolar tethers Heh1/Src1 and Nur1 (chromosome linkage INM proteins, or the CLIP complex). **B.** The nuclear periphery in an old yeast cell. Various changes occur to the

nuclear periphery during replicative aging. NPCs become misorganized and exhibit altered transport properties. The nucleolus expands and exhibits fragmentation. Extrachromosomal DNA (ecDNA) forms by recombination within the repetitive rDNA array and accumulates in mother cells. Chaperone-bound protein aggregates form and localize to the INM.

1.1.1 The nuclear envelope

The nuclear envelope is the subregion of the endoplasmic reticulum that surrounds the cell's genetic material (Figure 1.1). The double membrane bilayer consists of the outer nuclear membrane (ONM), the inner nuclear membrane (INM), and a lumen in between the membranes. The composition of the ONM is largely similar to that of the endoplasmic reticulum, with few proteins known to localize specifically to this bilayer. The INM, however, has recently been revealed to have a distinct proteome and lipidome from the rest of the endoplasmic reticulum (Romanauska and Köhler, 2018; Smoyer et al., 2016).

The INM proteome consists of transmembrane proteins that are targeted by multiple mechanisms, including active transport through the NPC and binding to chromatin upon diffusion from the ONM (reviewed in Katta et al., 2014). Some of these proteins, including LEM-domain proteins, are conserved from yeast to humans and generally contribute to nuclear organization (reviewed in Mekhail and Moazed, 2010). Other proteins, such as the cytoskeletal lamins, are present in metazoans but not yeast and likely indicate distinct evolutionary constraints on nuclear structure (reviewed in Gruenbaum and Foisner, 2015). INM proteins can also influence the ONM proteome, via interactions within the nuclear envelope lumen (e.g., SUN-KASH domain proteins; reviewed in Starr and Fridolfsson, 2010). Importantly, distinct quality control pathways exist to monitor the INM proteome, including nucleophagy and nuclear-specific ubiquitin ligase adaptors involved in INM associated-degradation (Foresti et al., 2014; Mochida et al., 2015). The specific INM protein composition is required for proper chromatin organization and function. For example, the transmembrane proteins Heh1/Src1 and Nur1 (chromosome linkage INM proteins, or the CLIP complex) tether the nucleolus to the nuclear periphery in budding yeast, contributing to genome stability (Mekhail et al., 2008).

The INM has recently come to be appreciated as metabolically active, with a lipidome distinct from that of the cortical endoplasmic reticulum or ONM (Romanauska and Köhler, 2021, 2018). Lipid synthesis enzymes localize to the nuclear envelope, resulting in the enrichment of certain lipid species at the INM. Notably, lipid droplets can form at the INM, by a process similar to that observed at other endoplasmic reticulum domains. Due to the recency of these findings, the importance of a distinct INM lipid composition remains largely unknown. However, the dynamic regulation

further establishes the nuclear envelope as a unique membrane domain within the cell, with many mysteries yet to be revealed.

1.1.2 The nuclear pore complex

The nuclear pore complex (NPC) is a well-conserved, supramolecular structure that acts as a gate between the nucleus and cytoplasm (reviewed in Lin and Hoelz, 2019). It is comprised of over 30 distinct subunits organized into six subcomplexes, which in turn organize into eight spokes and a single radially-symmetrical channel (Kim et al., 2018). The core of the NPC interacts with the nuclear envelope and scaffolds intrinsically disordered channel nucleoporins. These channel nucleoporins form a phase-separated hydrogel that acts as the permeability barrier between the nucleus and cytoplasm (Frey and Görlich, 2007). Nuclear transport receptors, including importins and exportins, facilitate transport by locally melting interactions within the channel. Asymmetrically localized nucleoporins, including the nuclear basket and cytoplasmic filaments, facilitate directional export of RNA from the nucleus (reviewed in Strambio-De-Castillia et al., 2010; Wente and Rout, 2010). Additionally, the nuclear basket interacts with chromatin, affecting nuclear processes ranging from gene expression to DNA repair.

Many processes regulate the life cycle of these complex transport machines (reviewed in Dultz et al., 2022). NPC assembly occurs through two distinct mechanisms: insertion into pre-existing nuclear envelope, which occurs throughout the cell cycle in metazoans and budding yeast, and stabilization of a pre-existing membrane hole, which occurs specifically upon nuclear envelope reassembly in metazoans (Otsuka et al., 2018, 2016). Both assembly mechanisms involve stepwise recruitment of nucleoporins to build a complete NPC (Dultz et al., 2008; Onischenko et al., 2020); how additional assembly factors contribute to the process remains poorly understood. NPC disassembly, on the other hand, only occurs during cell divisions in metazoans, via coordinated phosphorylation by multiple cell cycle kinases (Laurell et al., 2011; Linder et al., 2017). In budding yeast and post-mitotic metazoan cells, many NPC subunits are incredibly long-lived and exhibit only limited turnover (D'Angelo et al., 2009; Rempel et al., 2019; Toyama et al., 2013). Receptor-mediated autophagy targets some NPCs for destruction, but whether other mechanisms of NPC turnover exist remains unknown (Allegretti et al., 2020; Lee et al., 2020).

Despite their stability and complexity, NPCs exhibit surprising flexibility in structure and composition. Different NPCs have distinct subsets of nucleoporins: in budding yeast, NPCs can differ in their stoichiometry of certain subcomplexes and a subpopulation of NPCs near the nucleolus lacks members of the nuclear basket (Akey et al., 2022; Galy et al., 2004). Additionally, the NPC can undergo large-scale architectural changes in response to different cellular stimuli, including constriction and dilation (Zimmerli et al., 2021). Further study of NPC dynamics promises to reveal currently unknown regulation and remodeling of these cellular giants.

1.1.3 The aging nuclear periphery

Changes to the nuclear periphery are frequently associated with pathological aging in metazoans (reviewed in Martins et al., 2020). Decreased function of the nuclear permeability barrier occurs in various progressive neurodegenerative diseases, such as amyotrophic lateral sclerosis and Huntington's disease (Chou et al., 2018; Gasset-Rosa et al., 2017; Grima et al., 2017; Zhang et al., 2015). Further, evidence exists that changes in nuclear organization are causal to aging phenotypes, since mutations in the nuclear gene lamin A result in the premature aging disease Hutchison-Gilford progeria syndrome (Eriksson et al., 2003). As such, improved understanding of nuclear changes during natural aging and rejuvenation is an important area of current research.

In metazoans, several nuclear changes have been reported during the natural aging process (Haithcock et al., 2005; Scaffidi and Misteli, 2006). NPCs accumulate damage and display reduced functionality due to their exceptional stability in post-mitotic cells (D'Angelo et al., 2009; Toyama et al., 2013). The nucleolus exhibits increased activity and enlargement, with small nucleolar size even correlated to increased lifespan in diverse metazoans (Buchwalter and Hetzer, 2017; Tiku et al., 2017). Nuclear processes such as splicing are impacted by decline of cellular proteostasis (Sabath et al., 2020). It remains unclear if these changes contribute to age-associated decline in cellular function and, if so, how they might be reversed.

Notably, many of these changes are conserved in budding yeast, a model organism in which aging has been extensively studied (reviewed in Denoth Lippuner et al., 2014). NPCs exhibit altered stoichiometry and reduced function (Rempel et al., 2019), nucleoli exhibit enlargement and increased fragmentation (Paxman et al., 2021; Sinclair et al., 1997), and protein aggregates stably form inside the nucleus (Saarikangas et al., 2017). Additionally, extrachromosomal DNA (ecDNA) accumulates at the nuclear periphery, where it has been hypothesized to contribute to age-induced dysfunction (Neurohr et al., 2018; Sinclair and Guarente, 1997). Further study of these conserved nuclear aging biomarkers in budding yeast promises to improve understanding of their impact and reversibility across organisms.

1.2 Extreme cellular remodeling: the nuclear periphery during cell divisions

Spindle assembly and chromosome division during eukaryotic cell divisions necessitates remodeling of the nuclear periphery (reviewed in Güttinger et al., 2009; Smoyer and Jaspersen, 2014). In different organisms, diverse nuclear morphologies accommodate the division of the nuclear compartment (Figure 1.2): the nuclear periphery can be entirely disassembled ("open" cell divisions), as seen in metazoans, or remain largely intact ("closed" cell divisions), as seen in budding yeast. Despite the utility of this binary, many cellular divisions exhibit a more intermediate nuclear

behavior, with specific parts of the nuclear periphery remaining intact or being disassembled. In this section, I provide a brief overview of nuclear remodeling during mitosis in diverse organisms.

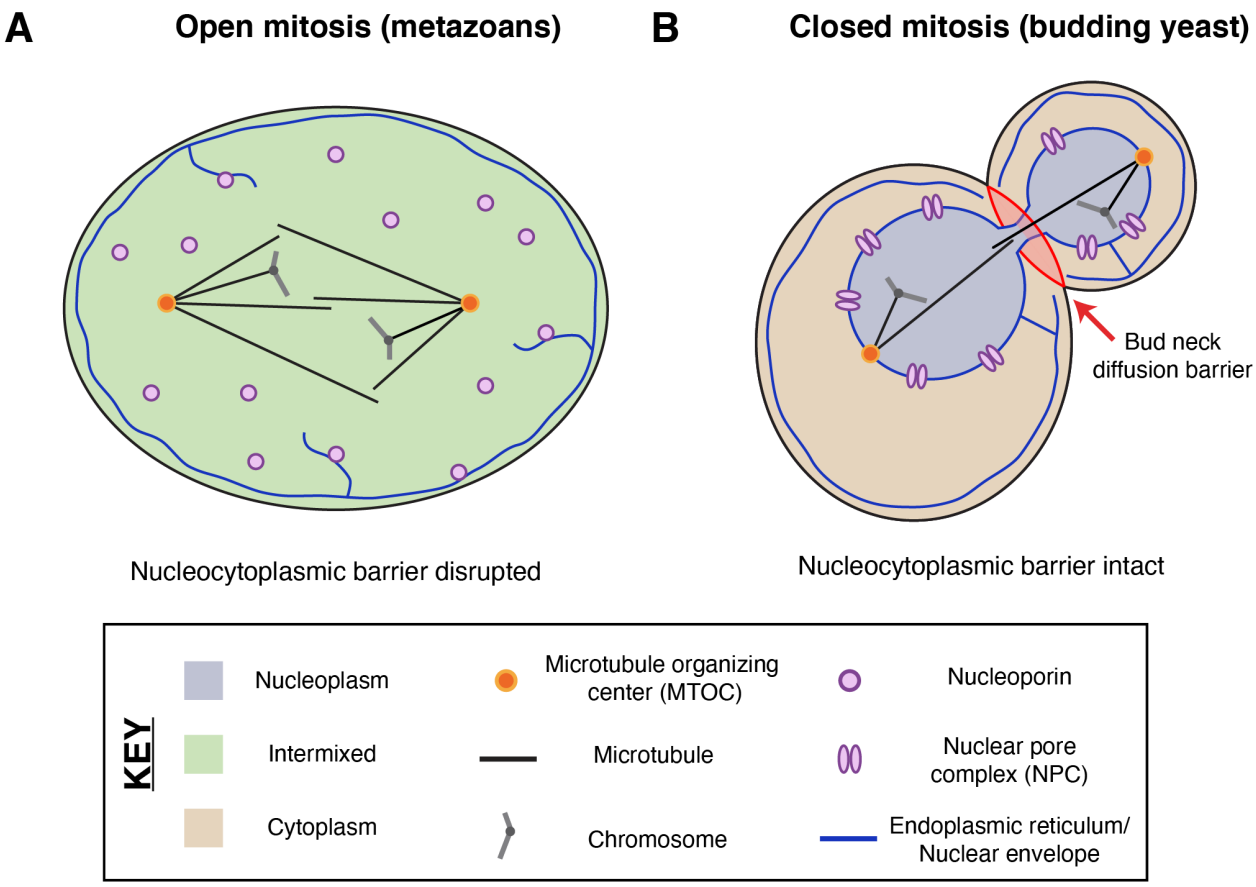

Figure 1.2. Schematic depicting the nuclear periphery during open and closed mitosis. A. A cell undergoing open mitosis, as observed in metazoans. The nuclear envelope is disassembled, retreating into the endoplasmic reticulum network. Nuclear pore complexes (NPCs) undergo cell-cycle dependent phosphorylation, driving their disassembly. As a consequence, the nucleoplasm and cytoplasm intermix, allowing for spindle machinery to access the chromosomes. **B.** A cell undergoing closed mitosis, as observed in budding yeast. The microtubule organizing centers, spindle pole bodies, are embedded in the nuclear envelope, allowing access to chromatin without nuclear envelope disassembly. NPCs also remain intact, resulting in the maintenance of a distinct cytoplasm and nucleoplasm. Different nuclear compartments in mother and daughter cells are established via a lateral diffusion barrier formed at the bud neck.

1.2.1 Open cell divisions

During open mitosis, the nuclear periphery – including both the nuclear envelope and nuclear pore complexes – is largely disassembled and reassembled (Figure 1.2; reviewed in Güttinger et al., 2009). This form of cell division predominates in metazoans, including humans. At the onset of metazoan mitosis, cell-cycle coupled phosphorylation triggers disassembly both of NPCs, initiating loss of nuclear compartmentalization, and lamins, altering the structural integrity of the nucleus (Gerace and Blobel, 1980; Heald and McKeon, 1990; Laurell et al., 2011; Linder et al., 2017). The nuclear envelope is torn by cytoskeletal forces and ultimately retreats into the surrounding endoplasmic reticulum (Beaudouin et al., 2002; Ellenberg et al., 1997; Yang et al., 1997). Mixing of the cytoplasm and nucleoplasm allows microtubule organizing centers to access chromosomes and facilitate spindle assembly. Upon exit from mitosis, chromosomes recruit new nuclear envelope to their surface (Anderson and Hetzer, 2007). NPCs reform on the surface of the chromosomes, maintaining holes in the reforming nuclear envelope (Franz et al., 2007; Walther et al., 2003a, 2003b); the compartment is ultimately sealed by ESCRT-III-dependent membrane remodeling (Olmos et al., 2015).

Altogether, the disruption of the nuclear barrier during open cell divisions provides the machinery involved in spindle assembly easy access to chromosomes. However, exposure of the dividing chromosomes to the cytoplasm involves significant risks. The mis-segregation of a chromosome can result in ectopic formation of the nuclear envelope around it, driving the formation of a faulty micronucleus (Hatch et al., 2013; Liu et al., 2018). Defects in this micronucleus result in massive DNA damage events, such as chromothripsis, that can drive the formation of cancer. Additional defects during open mitosis, such as exit of a chromosome from the organelle-free "exclusion" zone around the spindle, can similarly result in micronucleus formation (Ferrandiz et al., 2022). Open mitosis therefore poses threats to the integrity of the genome, even as it facilitates its division.

1.2.2 Closed cell divisions

During closed mitosis, the nuclear periphery remains largely intact throughout the cell division program (Figure 1.2; reviewed in Boettcher and Barral, 2013). This form of cell division predominates in the model organism, budding yeast, and other unicellular fungi. In the context of budding yeast mitosis, microtubule organizing centers (spindle pole bodies) are embedded within the nuclear envelope, giving them access to chromosomes (Byers and Goetsch, 1975). Spindle assembly and elongation can therefore take place even as the nuclear envelope remains intact. Instead of experiencing disassembly, the nuclear envelope undergoes membrane expansion to facilitate chromosome division, which is regulated by cell-cycle coupled inhibition of lipin (Pah1 in budding yeast; O'Hara et al., 2006). NPCs are similarly present throughout mitosis, experiencing regulated inheritance into daughter cells (Colombi et al., 2013; Khmelinskii et al., 2010; Makio et al., 2013; Winey et al., 1997). As a

consequence, the nucleus and cytoplasm retain their distinct identity during closed divisions. Of note, it still remains poorly understood how karyokinesis, or the separation of the two nuclear compartments, takes place, although evidence exists that this process is linked to cytokinesis (Melloy and Rose, 2017).

Altogether, the nuclear periphery undergoes expansion during closed cell divisions to accommodate spindle formation and chromosome segregation. However, the maintenance of an intact nuclear envelope results in limited opportunity for turnover of deleterious nuclear material, including nuclear age-induced damage. To allow for rejuvenation during mitosis, distinct nuclear envelope composition within mother and daughter cells is established via the formation of a lateral diffusion barrier (Clay et al., 2014; Denoth-Lippuner et al., 2014). The bud neck organizes a sphingolipid-based barrier in the outer nuclear membrane, driving the asymmetric inheritance of age-induced damage by mother cells. Closed mitosis therefore drives accumulation of nuclear age-associated damage, which may contribute to replicative aging.

1.2.3 Beyond the binary

Many cell divisions feature nuclear dynamics that cannot be neatly characterized as either open or closed (reviewed in Dey and Baum, 2021). In metazoans, certain cell types maintain parts of the nuclear periphery around the dividing spindle. For example, in *Drosophila melanogaster* neural stem cells, the nuclear envelope and lamina persist during mitosis, which may contribute to the establishment of distinct cell identities (Roubinet et al., 2021). Similarly, parts of the nuclear envelope persist during syncytial nuclear divisions in early *D. melanogaster* development and during much of the cell cycle in *C. elegans* (Lee et al., 2000; Stafstrom and Staehelin, 1984). In fungi, certain species exhibit partial disruption of the nuclear periphery, resulting in nucleocytoplasmic barrier disruption. In *Aspergillus nidulans,* the NPC undergoes a phosphorylation-driven partial disassembly event, driving compartment intermixing (De Souza et al., 2004). In *Schizosaccharomyces japonicus*, the nuclear envelope is torn due to limited nuclear envelope availability, driven by lipin activity during mitosis (Makarova et al., 2016; Yam et al., 2011). This dramatic evolutionary plasticity suggests nuclear morphology during cell divisions is both subject to changing pressures and surprisingly adaptable.

Of note, nuclear behavior remains poorly characterized in many cell division contexts, including budding yeast meiosis. Electron microscopy indicates that the nuclear envelope remains intact during both divisions, but further characterization remains limited (Moens, 1971; Moens and Rapport, 1971). Excitingly, the distantly related fission yeast *Schizosaccharomyces pombe* exhibits a transient disruption of nuclear permeability during meiosis II, termed virtual nuclear envelope breakdown or vNEBD (Arai et al., 2010; Asakawa et al., 2010). The mechanisms underlying this event remain poorly understood; however, as in budding yeast, the nuclear envelope remains intact throughout the meiotic divisions. Nuclear transport may be subject to

novel pressures and, consequently, modulation during meiosis. Further characterization of different cell division programs promises to provide insight into the how and why diverse nuclear dynamics arise.

1.3 Securing the future: the meiotic developmental program

In sexually reproducing organisms, meiosis is the cell division program by which a diploid progenitor forms haploid gametes. The chromosome dynamics during this process have been extensively studied and are well-conserved from yeast to humans. However, many other cellular changes take place in order to accommodate the formation of healthy gametes, involving nearly every organelle. Importantly, meiosis can reset various forms of age-induced damage, ensuring the next generation is born young (Figure 1.3). Here, I provide an overview of meiotic cellular differentiation, with a particular emphasis on budding yeast.

1.3.1 Overview of meiosis

Meiosis involves two consecutive chromosomal divisions to form haploid gametes (reviewed in Marston and Amon, 2004). During meiotic S-phase, chromosomes undergo a single DNA replication event. During meiotic prophase I, programmed double-strand DNA breaks occur on chromosomes and facilitate homologous recombination, ensuring accurate chromosome segregation and generating novel allelic combinations. The two consecutive meiotic divisions drive the formation of haploid gametes: meiosis I involves the separation of homologous chromosomes and meiosis II involves the separation of sister chromatids. The machinery involved in coordinating these divisions is largely conserved from yeast to humans.

In budding yeast, entry into the meiotic developmental program is triggered by nutrient deprivation and requires respiration-competency (reviewed in Neiman, 2011). Two master transcription factors regulate progression through the meiotic divisions: Ime1, which induces meiotic entry, and Ndt80, which induces the meiotic divisions. Additional transcription factors are likely to be involved in gamete development, although these have yet to be identified. During the course of meiosis, almost every gene undergoes coordinated changes in protein abundance, suggesting that gametogenesis represents a large-scale cellular remodeling program (Brar et al., 2012; Cheng et al., 2018). Excitingly, the regulatory logic and functional relevance of most of these changes have yet to be identified.

1.3.2 Cellular remodeling during meiosis

During meiosis, gametes must inherit the full complement of organelles in addition to the necessary genetic material. In budding yeast, new gamete plasma membranes (known as prospore membranes) nucleate from cytoplasmic face of the spindle pole bodies, packaging one nucleus and the appropriate organellar complement per

gamete (Neiman, 1998). Almost every organelle undergoes dramatic changes to facilitate their inheritance or disinheritance. Mitochondria collapse from the cell periphery onto dividing nuclei, allowing partial entry into nascent gametes (Sawyer et al., 2019; Suda et al., 2007). The cortical endoplasmic reticulum similarly collapses during meiosis and is only partially inherited (Otto et al., 2021; Suda et al., 2007). In contrast, vacuoles, organelles equivalent to metazoan lysosomes, are generated *de novo* within nascent gametes (Roeder and Shaw, 1996). The mother cell vacuole remains outside of the developing gametes, until its coordinated lysis results in the elimination of all material that is not packaged into gametes (Eastwood et al., 2012; Eastwood and Meneghini, 2015).

The behavior of the nuclear periphery, however, remains less well understood during budding yeast meiosis. The nuclear envelope appears to remain continuous during both meiotic divisions, which would seem to suggest that it is largely inherited along with the genetic material (Moens, 1971; Moens and Rapport, 1971). However, limited evidence exists that part of the nucleus – including nucleolar material, nucleoporins, and nuclear envelope – may be excluded outside of gametes (Brewer et al., 1980; Fuchs and Loidl, 2004). A more thorough characterization of the dynamics of different nuclear components is necessary to understand its inheritance and disinheritance.

In metazoans, organelle segregation is also regulated during gametogenesis (reviewed in Goodman et al., 2020). During spermatogenesis, a residual body containing various organellar material is formed and eliminated (Breucker et al., 1985; Huang et al., 2012). During oogenesis, oocytes inherit a subset of organelles from neighboring cells in the form of the Balbiani body (Boke et al., 2016). Further, only one haploid meiotic product is packaged as an egg, with the remaining products discarded as polar bodies (reviewed in Maro and Verlhac, 2002). Notably, multiple forms of organellar quality control have been shown to act during metazoan gametogenesis and fertilization. In *D. melanogaster* oogenesis, mitochondria undergo programmed fragmentation, allowing for autophagy of poorly functioning mtDNA (Lieber et al., 2019). In *C. elegans*, lysosomal acidification triggers clearance of age-induced protein aggregates (Bohnert and Kenyon, 2017). Whether similar organelle quality control processes take place during budding yeast meiosis remains unknown.

1.3.3 A natural rejuvenation pathway

Excitingly, sexual reproduction represents an endogenous context during which age-induced damage is reversed, enabling the rejuvenation of the next generation. In budding yeast, meiosis resets replicative aging (Figure 1.3), such that all four gametes born from an aged mother cell have the same replicative potential as gametes born from a young mother cell (Unal et al., 2011). During this process, various senescence factors – including extrachromosomal DNA (ecDNA), protein aggregates, and excess nucleolar material – are eliminated. The mechanism by which cellular rejuvenation occurs during meiosis remains unknown. Ectopic expression of

the master transcription factor Ndt80 is able to extend lifespan in mitotic cells, indicating that some rejuvenation is driven by transcriptional changes that can be recapitulated outside of a meiotic context. However, Ndt80 is unable to eliminate age-induced damage, including protein aggregates and ecDNA, suggesting that additional meiosis-specific rejuvenation pathways have yet to be uncovered.

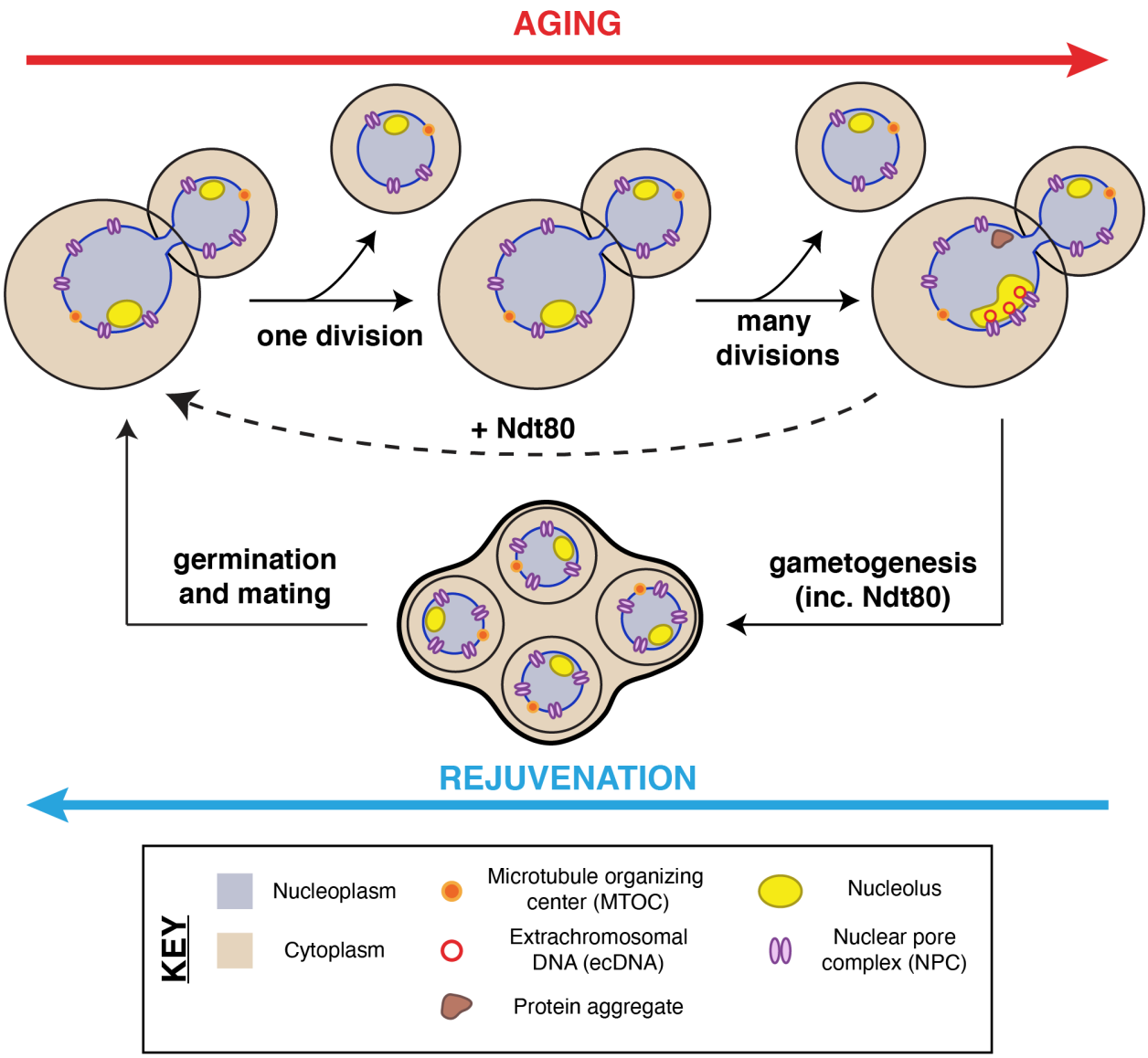

Figure 1.3. Replicative aging and rejuvenation during the budding yeast life cycle. Schematic adapted from Sing et al., 2022. During replicative aging, a mother cell accumulates various forms of age-induced damage, including extrachromosomal DNA (ecDNA), excess nucleolar material, and protein aggregates. Gametogenesis eliminates this damage and resets replicative lifespan in all four gametes, by mechanisms that remain unclear. Ectopic over-expression of the meiotic transcription

factor Ndt80 extends lifespan in mitotically-dividing cells but does not eliminate age-induced damage such as protein aggregates and ecDNA.

The rejuvenation mechanisms that occur during metazoan meiosis and sexual reproduction are also poorly understood. Organellar quality control during gametogenesis and fertilization likely contributes to the youth of nascent zygotes (Bohnert and Kenyon, 2017; Lieber et al., 2019). Of note, expression of embryonic master transcription factors results in epigenetic changes that can rejuvenate somatic cells, similarly to Ndt80 (Ocampo et al., 2016; Sarkar et al., 2020). Further elucidation of endogenous rejuvenation pathways during sexual reproduction therefore promises to shed light on the mechanisms of aging and, eventually, on how aging can be reversed.

Chapter 2

Meiotic Cellular Rejuvenation is Coupled to Nuclear Remodeling in Budding Yeast

The following chapter contains material derived from a publication on which I am co-first author (King et al., 2019).

2.1 Introduction

Aging occurs as an organism loses its ability to maintain homeostasis over time. The cellular changes that accompany aging have been most extensively characterized in the budding yeast, *Saccharomyces cerevisiae* (Figure 2.1A; Denoth Lippuner et al., 2014; Kaeberlein, 2010; Longo et al., 2012). Disrupted protein homeostasis results in the accumulation of protein aggregates that contain oxidatively damaged proteins (Aguilaniu et al., 2003; Erjavec et al., 2007). Many organelles exhibit signs of dysfunction: mitochondria fragment and aggregate, mitochondrial membrane potential decreases, and the vacuole becomes less acidic (Henderson et al., 2014; Hughes and Gottschling, 2012; Veatch et al., 2009). Notably, the nucleus also undergoes a number of changes including enlargement of the nucleolus (Lewinska et al., 2014; Morlot et al., 2019; Sinclair et al., 1997), misorganization of nuclear pore complexes (Lord et al., 2015), and accumulation of extrachromosomal ribosomal DNA (rDNA) circles (Denoth-Lippuner et al., 2014; Sinclair and Guarente, 1997). Many of the cellular changes that accrue with age are conserved across eukaryotes (Colacurcio and Nixon, 2016; David et al., 2010; Sun et al., 2016; Tiku et al., 2017).

In budding yeast mitosis, age-induced damage is asymmetrically retained by the mother cell resulting in the formation of an aged mother cell and a young daughter cell (Mortimer and Johnston, 1959). In contrast, meiotic cells reset aging symmetrically such that all of the meiotic products are born young, independent of their progenitor's age (Unal et al., 2011). Importantly, senescence factors originally present in the aged precursor cells, including protein aggregates, nucleolar damage, and rDNA circles, are no longer present in the newly formed gametes (Unal et al., 2011; Ünal and Amon, 2011). How gametes avoid inheriting age-associated damage and how this event is coupled to the meiotic differentiation program remains unknown.

Meiotic differentiation, also known as gametogenesis, is a tightly regulated developmental program whereby a progenitor cell undergoes two consecutive nuclear divisions, meiosis I and meiosis II, to form haploid gametes. Meiotic differentiation requires extensive cellular remodeling to ensure that gametes inherit the necessary nuclear and cytoplasmic contents. In yeast gametogenesis, the nucleus undergoes a

closed division, with the nuclear envelope remaining continuous until karyokinesis forms four new nuclei (Unal et al., 2011). Mitochondria and cortical endoplasmic reticulum also undergo regulated morphological changes, separating from the cellular cortex and localizing near the nuclear envelope at the transition between meiosis I and II (Gorsich and Shaw, 2004; Miyakawa et al., 1984; Otto et al., 2021; Sawyer et al., 2019; Stevens, B., 1981; Suda et al., 2007). Around the same time, new plasma membranes, also known as prospore membranes, grow from the centrosome-like spindle pole bodies embedded in the nuclear envelope. This directed growth of plasma membrane ensures that nascent nuclei and a fraction of the cytoplasmic contents are encapsulated to form gametes (Brewer et al., 1980; Byers, 1981; Knop and Strasser, 2000; Moens, 1971; Neiman, 1998). Subsequently, the uninherited cellular contents are destroyed by proteases released upon permeabilization of the progenitor cell's vacuole, the yeast equivalent of the mammalian lysosome (Eastwood et al., 2012; Eastwood and Meneghini, 2015). Whether these cellular remodeling events are integral to the removal of age-induced damage has not been characterized.

In this study, we aimed to determine the mechanism by which nuclear senescence factors are eliminated during budding yeast meiosis. Using time-lapse fluorescence microscopy, we found that protein aggregates, rDNA circles, and a subset of nucleolar proteins are sequestered away from chromosomes during meiosis II. Importantly, we show that the core subunits of the nuclear pore complex (NPC) also undergo a similar sequestration process in both young and aged cells. The damaged material localizes to a nuclear envelope-bound compartment containing the excluded NPCs that is eliminated upon vacuolar lysis. Finally, we found that the proper development of plasma membranes is required for the sequestration of core NPCs and senescence factors away from the newly forming gametes. Our study defines a key nuclear remodeling event and demonstrates its involvement in the elimination of age-induced cellular damage during meiotic differentiation.

2.2 Results

2.2.1 Senescence factors are sequestered away from chromosomes in meiosis II and subsequently eliminated

To gain a deeper understanding of gametogenesis-induced rejuvenation, we first sought to characterize the meiotic dynamics of age-induced protein aggregates, rDNA circles, and nucleolar damage using time-lapse fluorescence microscopy. To isolate aged cells, we employed a previously established protocol that uses pulse-labeling of cells with biotin followed by harvesting with anti-biotin magnetic beads (Boselli et al., 2009; Smeal et al., 1996). All three types of damage have been reported to localize to the nuclear periphery in aged mitotic cells (Cabrera et al., 2017; Denoth-Lippuner et al., 2014; Saarikangas et al., 2017; Sinclair and Guarente, 1997). Therefore, we monitored their meiotic localization relative to chromosomes, marked with a

fluorescently tagged chromatin protein: either histone H2A (Hta1) or histone H2B (Htb1).

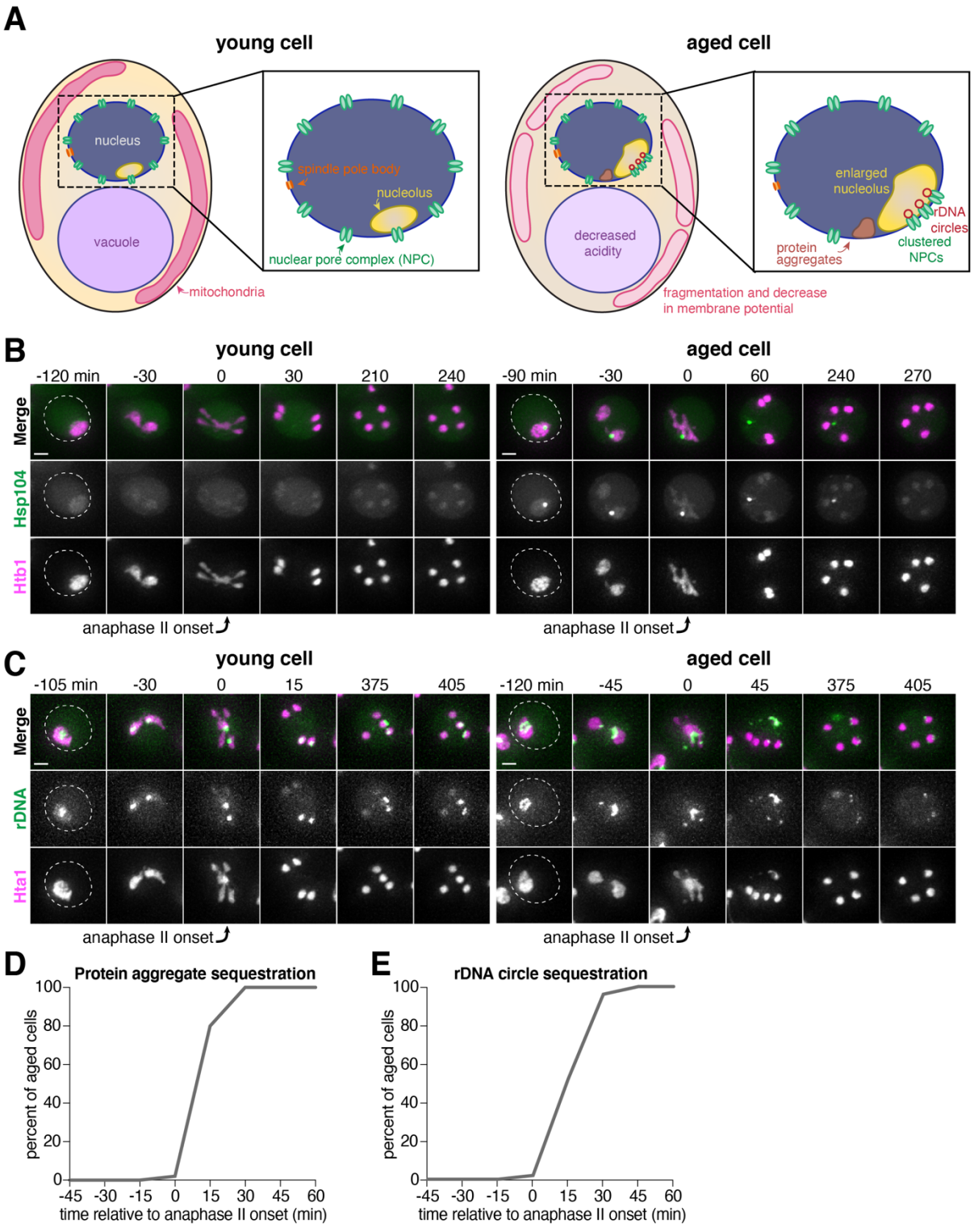

Figure 2.1. Senescence factors are sequestered away from chromosomes in meiosis II and are subsequently eliminated. A. Schematic depiction of a young and aged budding yeast cell. **B.** (left panel) Montage of a young cell (1 generation old) with diffuse Hsp104-eGFP progressing through meiosis (UB9724). (right panel) Montage of an aged cell (7 generations old) containing protein aggregates labeled with Hsp104-eGFP progressing through meiosis (UB9724). Chromosomes were visualized with histone marker Htb1-mCherry. **C.** (left panel) Montage of a young cell (0 generations old) with rDNA repeats, visualized with TetR-GFP binding to tetO arrays in the rDNA repeats, progressing through meiosis (UB17338). (right panel) Montage of an aged cell (9 generations old) containing rDNA circles, visualized with TetR-GFP binding to tetO arrays in the rDNA repeats, progressing through meiosis. (UB17338). Chromosomes were visualized with histone marker Hta1-mApple. For B-C, the time point depicting anaphase II onset was defined as 0 minutes as indicated by the arrows. **D.** Quantification depicting the timing of protein aggregate sequestration relative to the timing of anaphase II onset (median replicative age = 7, mean replicative age = 6.3 ± 1.5, n = 50 cells). **E.** Quantification depicting the timing of rDNA circle sequestration relative to the timing of anaphase II onset (median replicative age = 8, mean replicative age = 8.2 ± 2.4, n = 50 cells). Scale bars, 2 μm.

Similar to mitosis, we observed that protein aggregates, visualized by the fluorescently tagged chaperone Hsp104-eGFP (Glover and Lindquist, 1998; Saarikangas et al., 2017), localized to a perinuclear region inside the nucleus prior to the meiotic divisions and in meiosis I (Figure 2.1B, right panel; Figure 2.2A-B). In contrast, during meiosis II, the protein aggregates localized away from chromosomes, a phenomenon we termed sequestration (Figure 2.1B, D). The sequestration was highly penetrant (>99%) and occurred with consistent timing shortly after the onset of anaphase II (Figure 2.1D). Subsequently, the aggregates disappeared late in gametogenesis (Figure 2.1B). By comparison, young cells did not contain any Hsp104-associated aggregates but instead displayed diffuse Hsp104 signal throughout meiosis (Figure 2.1B, left panel). We conclude that age-associated protein aggregates undergo stereotypical sequestration and elimination during meiotic differentiation, suggesting developmentally controlled induction of these events.

We next tested whether the extrachromosomal rDNA circles that accumulate in aged cells displayed a similar behavior. To visualize ribosomal DNA in single cells, we used a strain carrying five tandem copies of the tetracycline operator sequence integrated within each rDNA repeat in one of the two chromosome XII homologs (tetO-rDNA). The strain additionally contained a tetracycline repressor protein fused to GFP (TetR-GFP) under the control of a meiotic promoter (Li et al., 2011). These two modifications, namely the meiosis-restricted expression of TetR-GFP and the heterozygosity of the tetO-rDNA array, did not affect growth rate in vegetative cells. Using this method, we observed that, in aged cells, a substantial fraction of the tetO-rDNA/TetR-GFP signal and a small fraction of the Hta1-mApple signal were

sequestered away from the dividing chromosomes after the onset of anaphase II and disappeared during late stages of gamete maturation (Figure 2.1C, right panel; Figure 2.1E). By comparison, in young cells, the gamete nuclei retained the entire tetO-rDNA array and histone-bound chromatin after completion of anaphase II (Figure 2.1C, left panel), consistent with previous work (Fuchs and Loidl, 2004; Li et al., 2011). In aged cells carrying TetR-GFP without the tetO-rDNA array, the GFP signal remained diffuse throughout meiosis (Figure 2.2C), confirming that the extrachromosomal GFP puncta were due to sequestered rDNA circles as opposed to TetR-GFP aggregation. These findings demonstrate that, similar to age-associated protein aggregates, extrachromosomal rDNA circles also undergo programmed sequestration and destruction during meiotic differentiation.

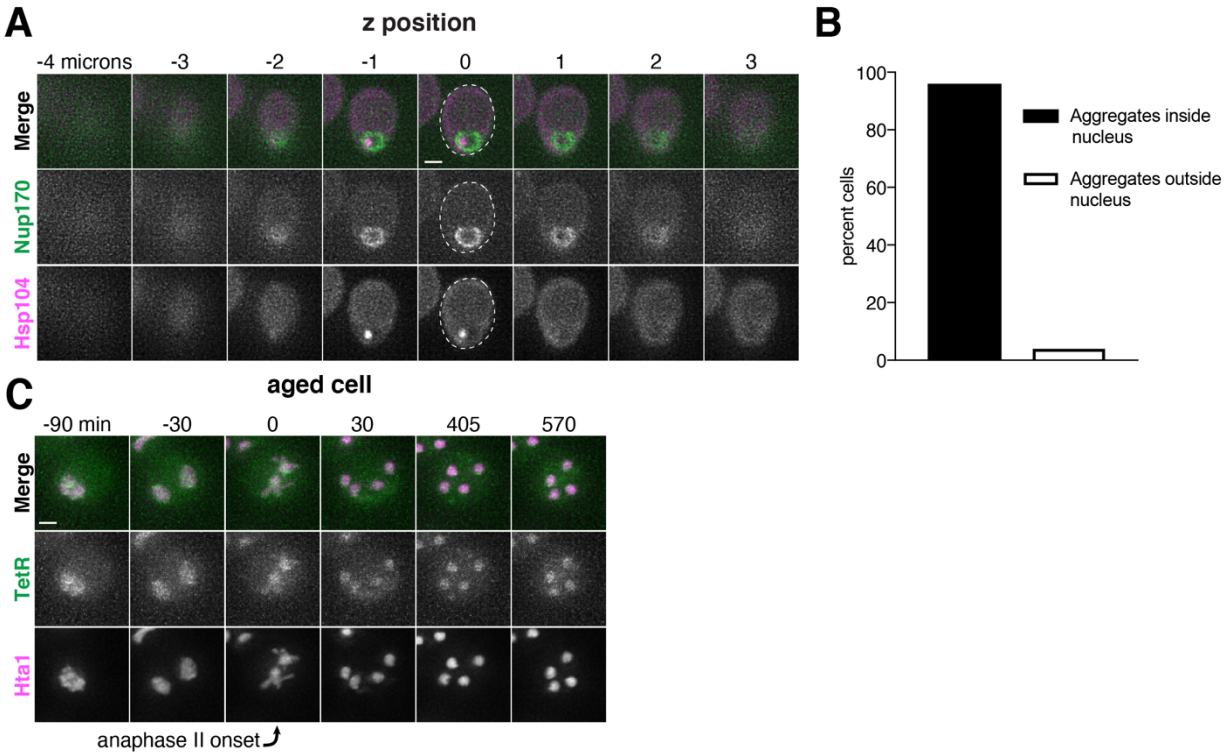

Figure 2.2. Controls for Figure 2.1. A. Z-slices of an aged prophase I cell (7 generations old) depicting localization of NPCs, marked by Nup170-GFP, and protein aggregates, marked by Hsp104-mCherry (UB12975). **B.** Quantification depicting frequency of pre-meiotic cells with protein aggregates inside the nucleus (median replicative age = 6, mean replicative age = 6.2 ± 2.1, n =100 cells). **C.** Montage of an aged cell (9 generations old) containing TetR-GFP but lacking the tetO array (UB17509). Chromosomes were visualized with histone marker Hta1-mApple, and the time point depicting anaphase II onset was defined as 0 minutes as indicated by the arrow. Scale bars, 2 µm.

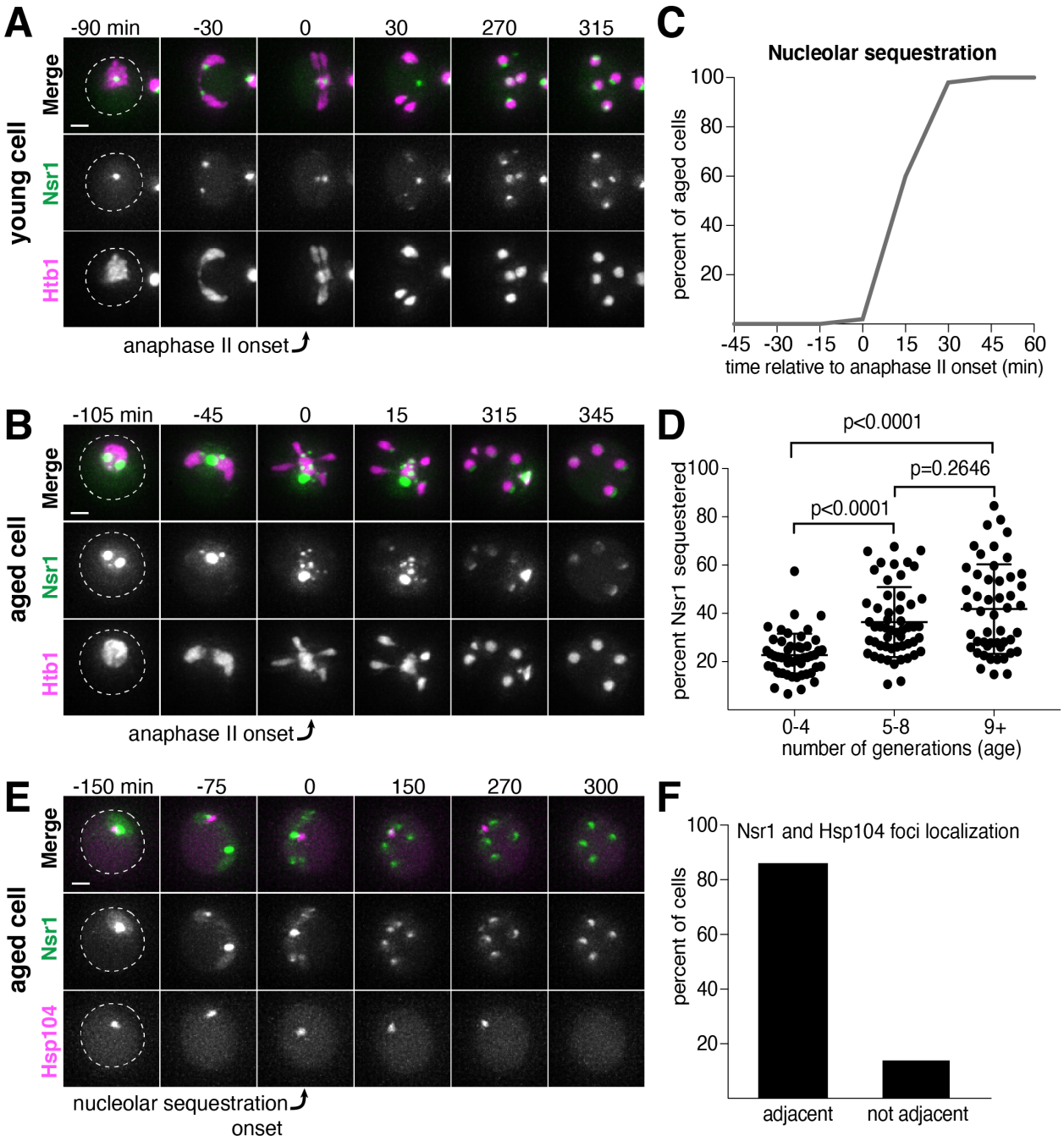

Figure 2.3. Nucleolar material is sequestered away from chromosomes during meiosis II in young and aged cells. A. Montage of a young cell (1 generation old) with the nucleolar tag Nsr1-GFP progressing through meiosis (UB16712). **B.** Montage of an aged cell (9 generations old) containing abnormal nucleolar material, labeled with Nsr1-GFP, progressing through meiosis (UB16712). For A-B, chromosomes were visualized with the histone marker Htb1-mCherry and the time point depicting anaphase II onset was defined as 0 minutes as indicated by the arrows. **C.**

Quantification depicting timing of Nsr1 sequestration relative to timing of anaphase II onset (median replicative age = 8, mean replicative age = 7.2 ± 2.4, n = 50 cells). **D.** Quantification depicting the degree of Nsr1 sequestration in cells of different ages (n = 50 for cells with 0-4 doublings, n = 53 for cells with 5-8 doublings, and n = 49 for cells with 9 or more doublings). The Mann-Whitney nonparametric test was used to test statistical significance, and data were generated from two biological replicates. **E.** Montage of an aged cell (9 generations old) with the nucleolus marked by Nsr1-GFP and protein aggregates marked by Hsp104-mCherry progressing through meiosis (UB13299). For E, the time point depicting Nsr1-GFP sequestration was defined as 0 minutes as indicated by the arrow. **F.** Quantification depicting the frequency of sequestered Hsp104-mCherry aggregates localizing adjacent to sequestered Nsr1-GFP (UB13299) immediately after nucleolar segregation (median replicative age = 7, mean replicative age = 6.7 ± 1.5, n = 100 cells). Adjacency was defined as sequestered Nsr1-GFP signal either neighboring or exhibiting partial overlap with sequestered Hsp104-mCherry signal in individual z-sections. Scale bars, 2 μm.

In addition to rDNA circles, other nucleolar aberrations also accumulate during cellular aging. As a mother cell continues to divide mitotically, factors involved in ribosomal biogenesis are upregulated, leading to the formation of enlarged and fragmented nucleoli (Janssens et al., 2015; Morlot et al., 2019; Sinclair et al., 1997). To visualize nucleoli in more detail, we fluorescently tagged the rRNA processing factor Nsr1 at its endogenous locus (Lee et al., 1992). A previous study found that two other rRNA processing factors, the fibrillarin homolog Nop1 and the high mobility group protein Nhp2, are partially sequestered away from chromosomes during gametogenesis (Fuchs and Loidl, 2004). Nsr1 similarly demonstrated partial sequestration after the onset of anaphase II in young cells (Figure 2.3A). In aged cells, Nsr1 foci appeared enlarged and fragmented prior to the meiotic divisions, consistent with previously reported changes in nucleolar morphology (Figure 2.3B; Janssens et al., 2015; Morlot et al., 2019; Sinclair et al., 1997). As in young cells, Nsr1 was sequestered away from chromosomes following the onset of anaphase II and subsequently eliminated (Figure 2.3B-C). Interestingly, a significantly higher fraction of the total Nsr1 was sequestered in older cells (mean = 23% for 0-3 generation-old cells, 36% for 5-8 generation-old cells and 42% for 9 or more generation-old cells; Figure 2.3D). A portion of the histone H2B (Htb1-mCherry) was also sequestered away from the gamete nuclei, reminiscent of the behavior of histone H2A in the GFP-marked rDNA strain. This chromatin demarcation occurred only in aged cells and always co-localized with the sequestered nucleoli. Since the extrachromosomal histone mass is present in aged cells independent of the GFP-marked rDNA array, the discarded rDNA circles are likely assembled into chromatin, and the extrachromosomal histone signal can be used as a proxy for rDNA circles.

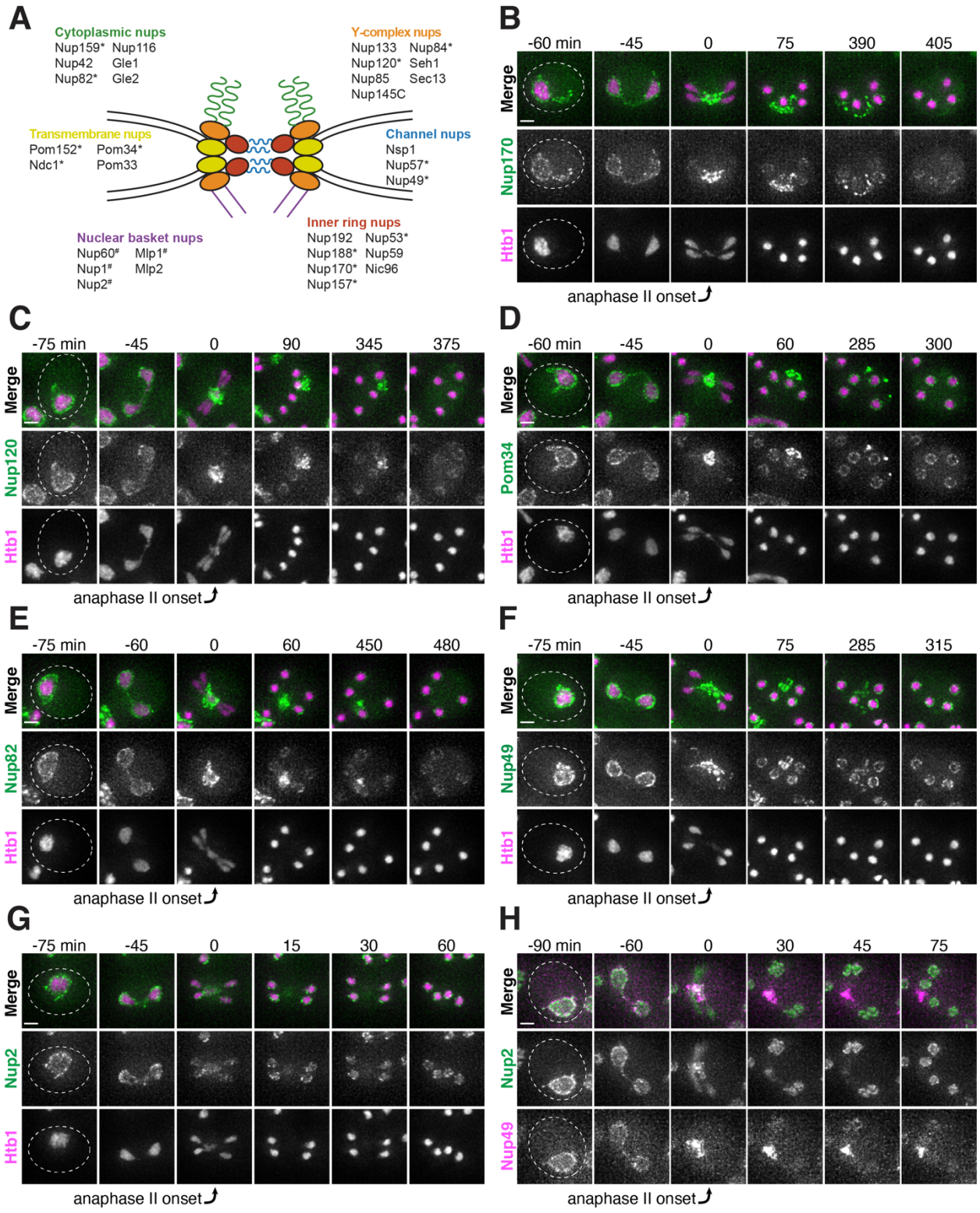
A
Cytoplasmic nups
Nup159* Nup116
Nup42 Gle1
Nup82* Gle2
Y-complex nups
Nup133 Nup84*
Nup120* Seh1
Nup85 Sec13
Nup145C
Transmembrane nups
Pom152* Pom34*
Ndc1* Pom33
Channel nups
Nsp1
Nup57*
Nup49*
Nuclear basket nups
Nup60# Mlp1#
Nup1# Mlp2
Nup2#
Inner ring nups
Nup192 Nup53*
Nup188* Nup59
Nup170* Nic96
Nup157*
B
-60 min -45 0 75 390 405
Merge
Nup170
Htb1
anaphase II onset
C
-75 min -45 0 90 345 375
Merge
Nup120
Htb1
anaphase II onset
D
-60 min -45 0 60 285 300
Merge
Pom34
Htb1
anaphase II onset
E
-75 min -60 0 60 450 480
Merge
Nup82
Htb1
anaphase II onset
F
-75 min -45 0 75 285 315
Merge
Nup49
Htb1
anaphase II onset
G
-75 min -45 0 15 30 60
Merge
Nup2
Htb1
anaphase II onset
H
-90 min -60 0 30 45 75
Merge
Nup2
Nup49
anaphase II onset

Figure 2.4. Nucleoporins from the core of the nuclear pore complex, but not the nuclear basket, are sequestered away from chromosomes during meiosis II and subsequently eliminated in young cells. **A.** A schematic depicting the different nucleoporins and subcomplexes that comprise the nuclear pore complex (NPC). Nup100 and Nup145N are not included in the schematic, since they represent linkers between different subcomplexes. Nomenclature and organization are from Beck and Hurt, 2017; the schematic itself is adapted from Rajoo et al., 2018. Nucleoporins marked with an asterisk are sequestered away from chromosomes; nucleoporins marked with a pound sign return to dividing nuclei. For each nucleoporin, the observed phenotype was observed in all tetrads examined ($n \geq 25$ tetrads). **B-G.** Montages of cells with tagged nucleoporins from each subcomplex progressing through meiosis. Chromosomes were visualized with the histone marker Htb1-mCherry, and the first time point depicting anaphase II was defined as 0 minutes as indicated by the arrows. **B.** Nup170-GFP, an inner ring complex nucleoporin (UB11513) **C.** Nup120-GFP, a Y-complex nucleoporin (UB13499) **D.** Pom34-GFP, a transmembrane nucleoporin (UB13503) **E.** Nup82-GFP, a cytoplasmic nucleoporin (UB14652) **F.** Nup49-GFP, a channel nucleoporin (UB13509) **G.** Nup2-GFP, a nuclear basket nucleoporin (UB15305) **H.** Montage depicting localization of Nup2-GFP, a nuclear basket nucleoporin, and Nup49-mCherry, a channel nucleoporin (UB15672). Scale bars, 2 µm.

Finally, we analyzed the behavior of protein aggregates with respect to nucleoli and found that both the timing and location of the sequestration event were coincident (Figure 2.3E-F). Taken together, these data reveal that distinct types of age-induced damage all undergo a spatiotemporally linked sequestration and elimination process, suggesting a common mode of meiotic regulation

2.2.2 Core nucleoporins exhibit a meiotic behavior similar to senescence factors in young cells

Since nucleolar constituents localize away from dividing chromosomes even in young cells, we reasoned that the sequestration of age-induced nuclear damage might involve a nuclear remodeling event that takes place generally as part of meiotic differentiation. As a means of assessing nuclear behavior, we sought to characterize the dynamics of nuclear pore complexes (NPCs) during meiosis in young cells.

Nuclear pore complexes are large protein structures that span the nuclear envelope and primarily function in selective nucleocytoplasmic transport. NPCs contain multiple copies of at least 30 distinct types of proteins termed nucleoporins. Nucleoporins are organized into different subcomplexes with distinct structural roles (Beck and Hurt, 2017; Kim et al., 2018). Intriguingly, one nucleoporin, Nsp1, has been previously shown to localize away from chromosomes in meiosis II (Fuchs and Loidl, 2004). Using time-lapse microscopy, we surveyed the meiotic dynamics and

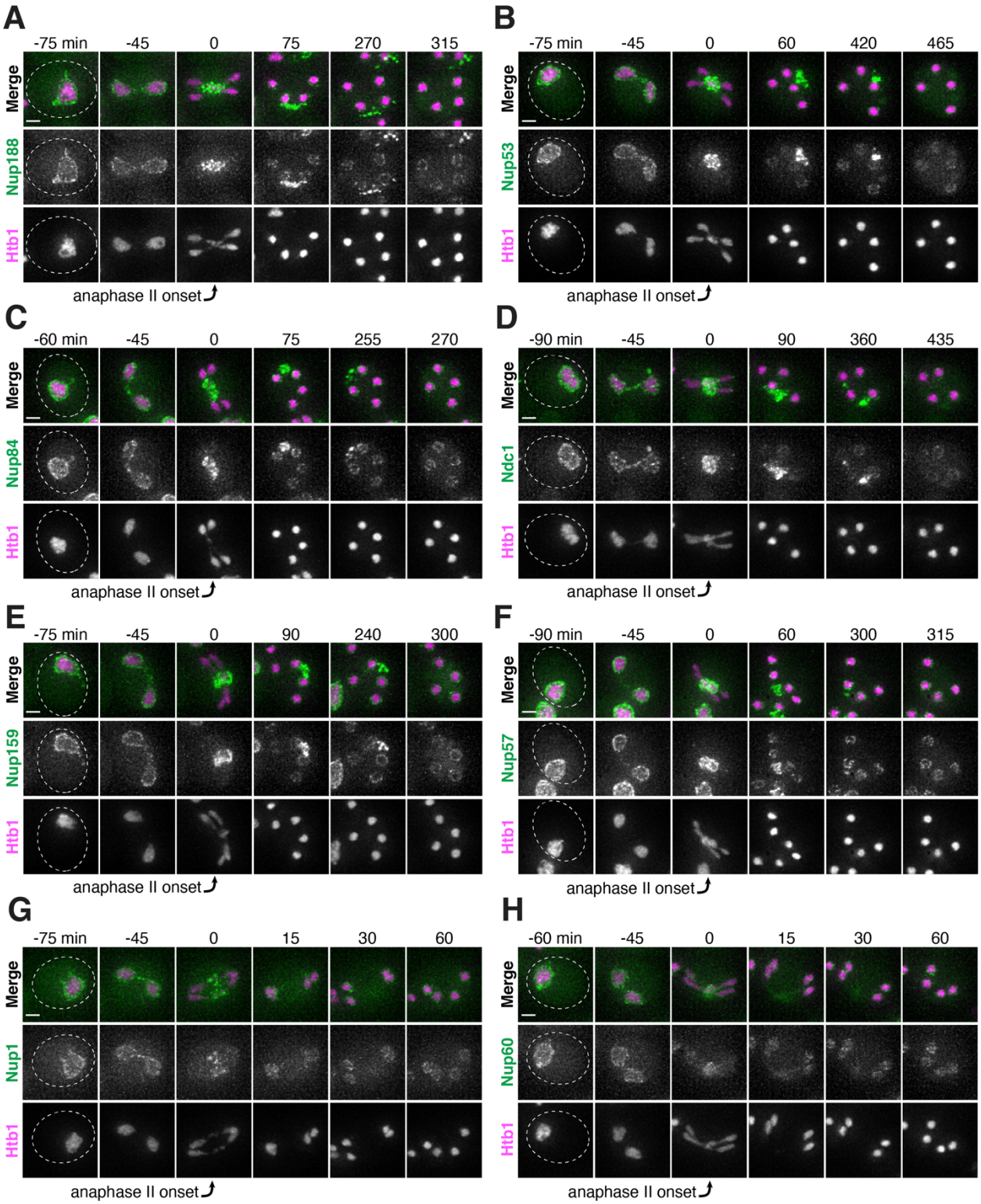
A
-75 min
-45
0
75
270
315
Merge
Nup188
Htb1
anaphase II onset
B
-75 min
-45
0
60
420
465
Merge
Nup53
Htb1
anaphase II onset
C
-60 min
-45
0
75
255
270
Merge
Nup84
Htb1
anaphase II onset
D
-90 min
-45
0
90
360
435
Merge
Ndc1
Htb1
anaphase II onset
E
-75 min
-45
0
90
240
300
Merge
Nup159
Htb1
anaphase II onset
F
-90 min
-45
0
60
300
315
Merge
Nup57
Htb1
anaphase II onset
G
-75 min
-45
0
15
30
60
Merge
Nup1
Htb1
anaphase II onset
H
-60 min
-45
0
15
30
60
Merge
Nup60
Htb1
anaphase II onset

Figure 2.5. Additional nucleoporins exhibit meiotic dynamics consistent with their respective subcomplexes. A-H. Montages of cells with additional tagged nucleoporins from each subcomplex progressing through meiosis. Chromosomes were visualized with the histone marker Htb1-mCherry, and the first time point depicting anaphase II was defined as 0 minutes as indicated by the arrows. **A.** Nup188-GFP, an inner ring complex nucleoporin (UB13505) **B.** Nup53-eGFP, an inner ring complex nucleoporin (UB3810) **C.** Nup84-GFP, a Y-complex nucleoporin (UB13497) **D.** Ndc1-GFP, a transmembrane nucleoporin (UB15301) **E.** Nup159-GFP, a cytoplasmic nucleoporin (UB14650) **F.** Nup57-GFP, a channel nucleoporin (UB14654) **G.** Nup1-GFP, a nuclear basket nucleoporin (UB15303). **H.** Nup60-GFP, a nuclear basket nucleoporin (UB14646). Scale bars, 2 µm.

---

localization of 17 different endogenously GFP-tagged nucleoporins representing different subcomplexes (Figure 2.4A). We found that nucleoporins from five of the six tested subcomplexes, including those most integral to the NPC structure, exhibited sequestration and elimination similar to age-induced damage. The nucleoporins localized to the nuclear periphery before the meiotic divisions and during meiosis I, but largely localized away from chromosomes after the onset of anaphase II (Figure 2.4B-F; Figure 2.5A-F). Although a large fraction of the nucleoporins persisted away from the chromosomes, some nucleoporins re-appeared around the gamete nuclei, either by de novo synthesis or return of the pre-existing pool. Several hours after the meiotic divisions, any remaining nucleoporin signal outside of the gamete nuclei abruptly disappeared (Figure 2.4B-F; Figure2.5A-F)

Interestingly, the nucleoporins from one subcomplex, the nuclear basket, exhibited a markedly different behavior: after briefly localizing outside of the developing nuclei during anaphase II along with the nucleoporins from other subcomplexes, they returned to the nascent nuclei within 30 minutes (Figure 2.4G-H; Figure 2.5G-H). Consistent with the nuclear basket exhibiting different dynamics than the NPC core, the protein abundance patterns of several nuclear basket nucleoporins during meiosis were markedly different than those observed for nucleoporins from core subcomplexes (Cheng et al., 2018, Figure 2.6A-B). Although a few other nucleoporins also had differential protein abundance levels during the meiotic divisions, they were sequestered away from gamete nuclei, similarly to their respective subcomplexes (Figure 2.6C-E). The simplest interpretation of these findings was that the nuclear basket detached from the rest of the NPC during meiosis II. Given that all other NPC subcomplexes tested persist outside of developing nuclei, we propose that intact NPCs without nuclear baskets are left outside of gamete nuclei.

Since senescence factors and NPCs were sequestered with similar timing, we next asked whether they were sequestered to a similar location. We monitored the localization of protein aggregates, rDNA circles, and sequestered nucleolar material relative to NPCs and found that they co-localize with the sequestered NPCs after the

onset of anaphase II (Figure 2.7A-C; Figure 2.8A-B). These results suggest that a common nuclear remodeling event is responsible for the spatial separation of various nuclear components from the dividing chromosomes.

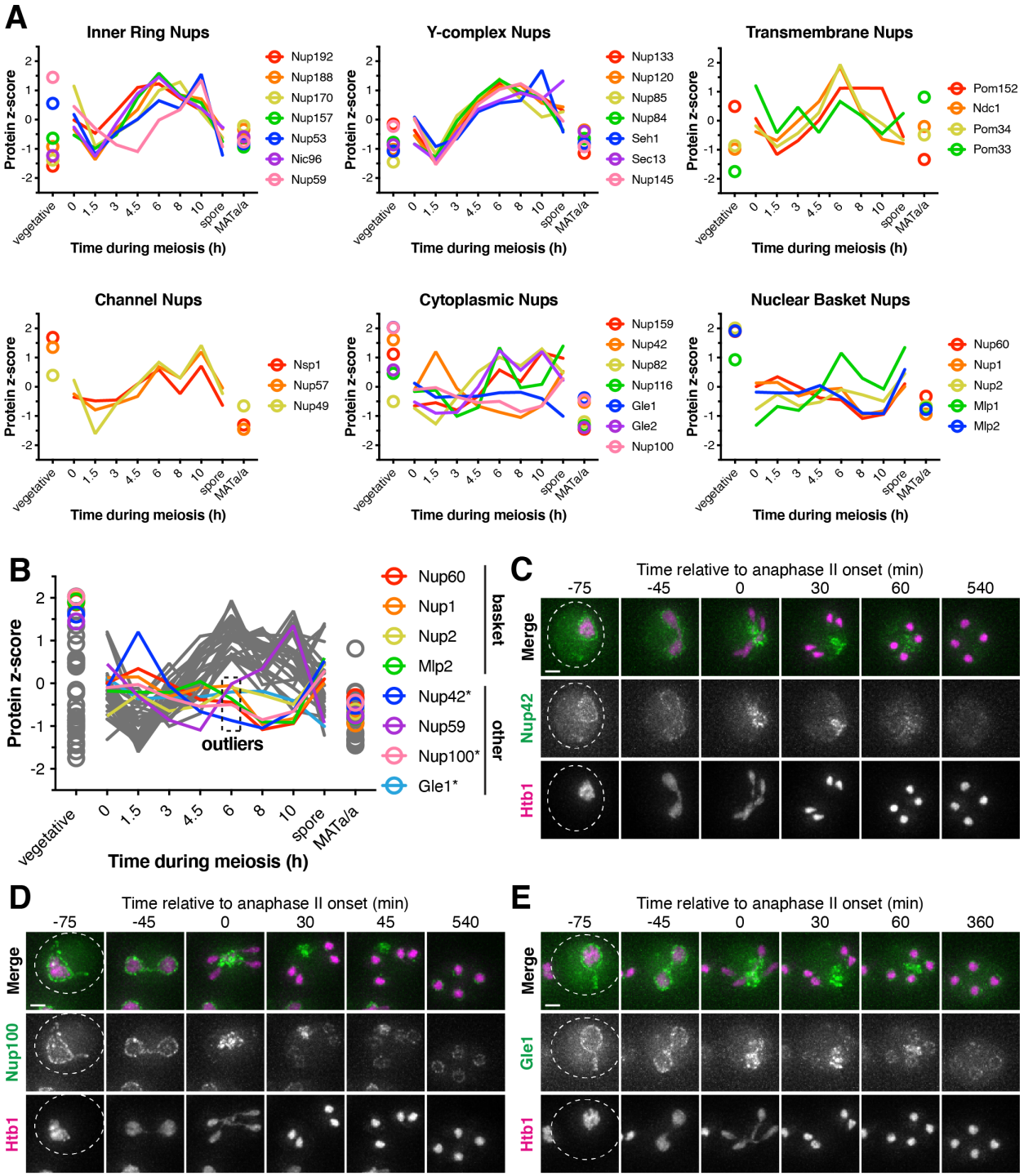

Figure 2.6. Nuclear basket nucleoporins exhibit protein abundance dynamics distinct from those of core nucleoporins during meiosis. A. Protein abundance patterns for nucleoporins during meiosis plotted by subcomplex. Protein z-score data is from Cheng et al., 2018. **B.** Protein abundance patterns of all nucleoporins during budding yeast meiosis plotted together, with outliers during the meiotic divisions (6 h) highlighted in different colors. The outliers include four nuclear basket nucleoporins and four nucleoporins that belong to sequestered subcomplexes. **C-E.** Montages of cells with fluorescently tagged outlier nucleoporins progressing through meiosis. Chromosomes were visualized with the histone marker Htb1-mCherry, and the time point depicting anaphase II onset was defined as 0 minutes. **C.** ye-GFP-Nup42, a cytoplasmic nucleoporin (UB24011) **D.** Nup100-GFP, a linker nucleoporin (UB21660) **E.** Gle1-GFP, a cytoplasmic nucleoporin (UB22741). Scale bars, 2 µm.

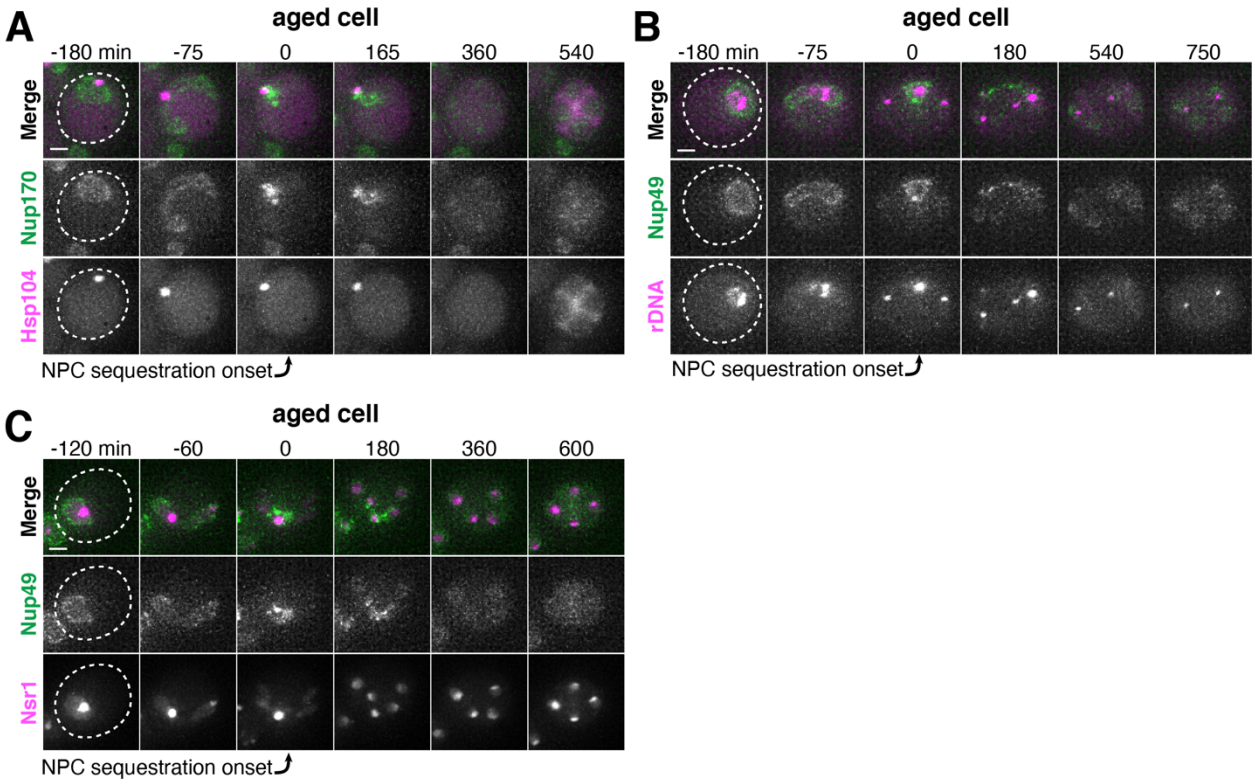

Figure 2.7. Age-dependent nuclear damage is sequestered with disposed NPCs during anaphase II. A. Montage of an aged cell (7 generations old) with protein aggregates, labeled with Hsp104-mCherry, and NPCs, labeled Nup170-GFP, progressing through meiosis (UB12975). **B.** Montage of an aged cell (9 generations old) with rDNA circles, marked by TetR-GFP binding to tetO arrays in the rDNA repeats, and NPCs, labeled with Nup49-mCherry, progressing through meiosis (UB17532). **C.** Montage of an aged cell (7 generations old) with abnormal nucleolar material, marked by Nsr1-GFP, and NPCs, marked by Nup49-mCherry, progressing through meiosis (UB16708). The

first time point depicting NPC sequestration was defined as 0 minutes as indicated by the arrows. Scale bar, 2 µm.

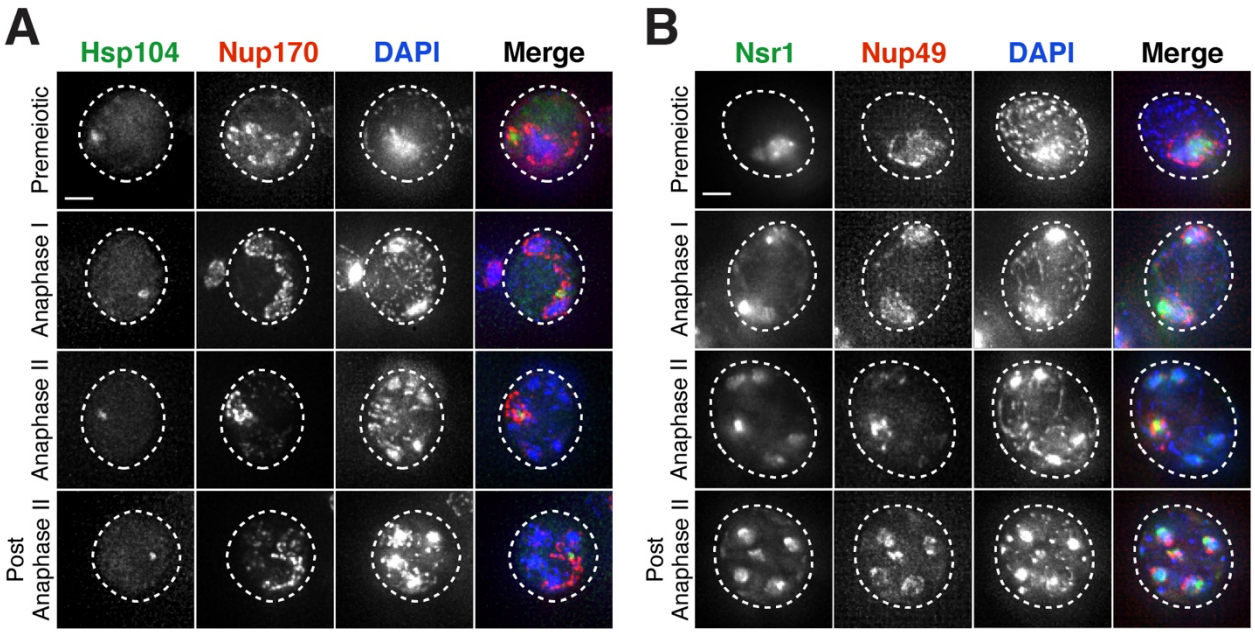

Figure 2.8. Protein aggregates and nucleolar material are sequestered with disposed NPCs during meiosis II. A-B. Maximum intensity projections of fixed premeiotic and meiotic cells depicting localization of NPCs, marked by Nup170-GFP, and either **A.** protein aggregates, marked by Hsp104-mCherry (UB12975), or **B.** nucleolar material, marked by Nsr1-GFP (UB16708). Scale bar, 2 µm.

2.2.3 Sequestered nuclear material localizes to a nuclear envelope-bound compartment

The nuclear envelope remains continuous during budding yeast meiosis, dynamically changing shape to accommodate the chromosomal divisions (Moens, 1971; Moens and Rapport, 1971). After the second meiotic division, karyokinesis occurs to form the nascent nuclei of the four gametes. Given the abrupt change in NPC distribution during anaphase II, we sought to determine how other nuclear membrane proteins behave during this time. We found that the integral LEM-domain protein Heh1 (Gene ID: 854974) and a generic inner nuclear membrane marker, eGFP-h2NLS-L-TM, localized to both nascent gamete nuclei and the sequestered NPCs during anaphase II (Figure 2.9A-B; Figure 2.10A-B; King et al., 2006; Meinema et al., 2011), suggesting the existence of a separate membranous compartment.

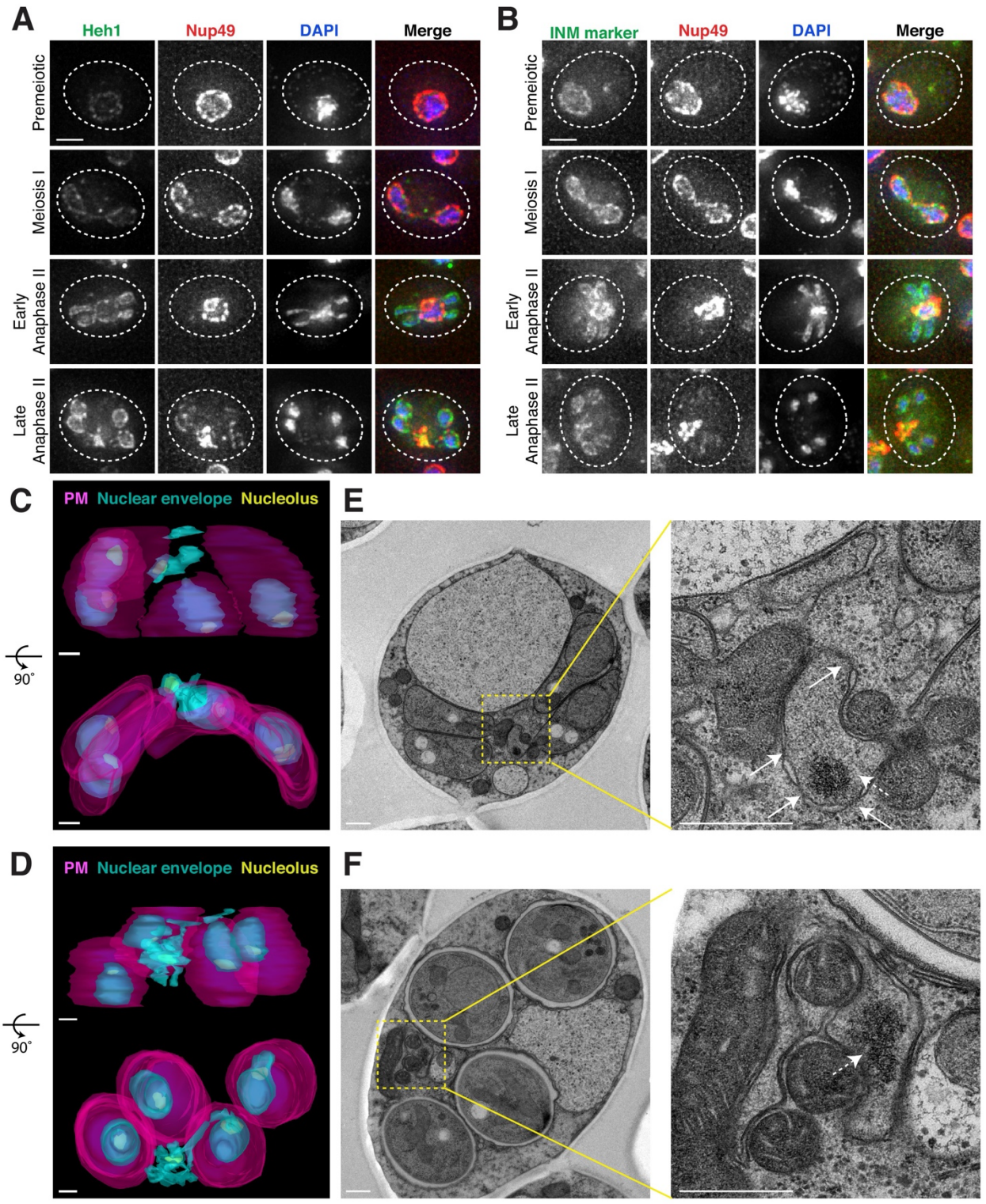

Figure 2.9. Nucleoporins are sequestered to a nuclear envelope-bound compartment during meiosis II. A-B. Maximum intensity projections of fixed young cells depicting

the localization of inner nuclear membrane proteins – **A.** Heh1-3xeGFP (UB14391) and **B.** the synthetic construct eGFP-h2NLS-L-TM from (Meinema et al., 2011; UB12932) – relative to the nucleoporin Nup49-mCherry and DAPI. Scale bars, 2 µm. **C-D.** Reconstructions of **C.** a young late anaphase II cell and **D.** a young post-meiosis II cell from 70 nm serial TEM micrographs (UB11513). Gamete plasma membranes are depicted in magenta, the nuclear envelope is depicted in cyan, and nucleoli are depicted in yellow. **E-F.** Electron micrographs of **E.** a young late anaphase II cell and **F.** a young post-meiosis II cell with insets depicting the nuclear envelope-bound region outside the gamete plasma membranes (UB11513). Solid arrows indicate NPCs; dashed arrows indicate nucleolar mass. Note that the electron micrographs in panel F come from the cell reconstructed in panel D. Scale bars, 0.5 µm.

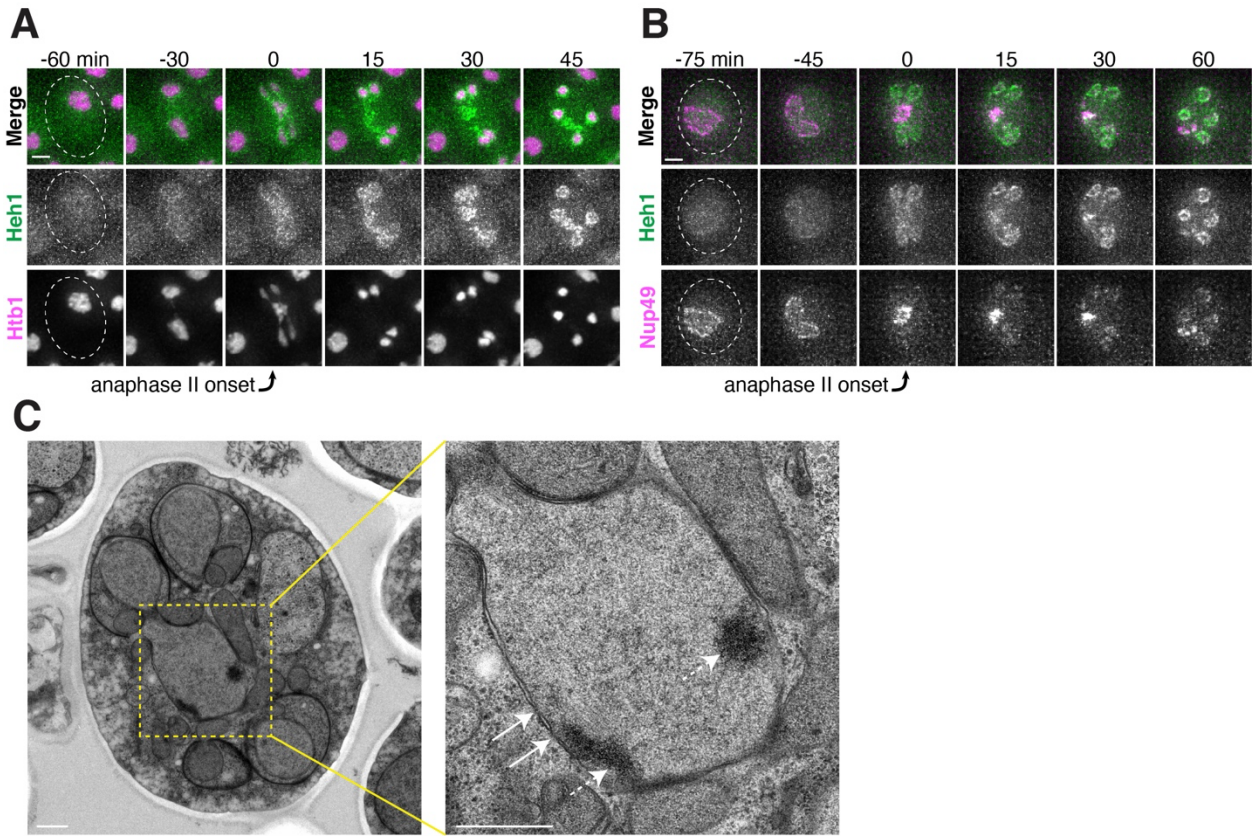

Figure 2.10. Additional evidence for a nuclear envelope bound compartment remaining outside of developing gametes during meiosis II. A-B. Montages of young cells with a fluorescently tagged inner nuclear membrane protein Heh1-3xeGFP and either **A.** Htb1-mCherry, a histone marker (UB14393), or **B.** Nup49-mCherry, a nucleoporin (UB14391). The time point depicting anaphase II onset was defined as 0 minutes as indicated by the arrows. Scale bars, 2 µm. **C.** Electron micrographs of a young early anaphase II cell and an inset of the nuclear envelope-bound region outside the gamete plasma membranes (UB11513). Solid arrows indicate NPCs; dashed arrows indicate nucleolar mass. Scale bars, 0.5 µm.

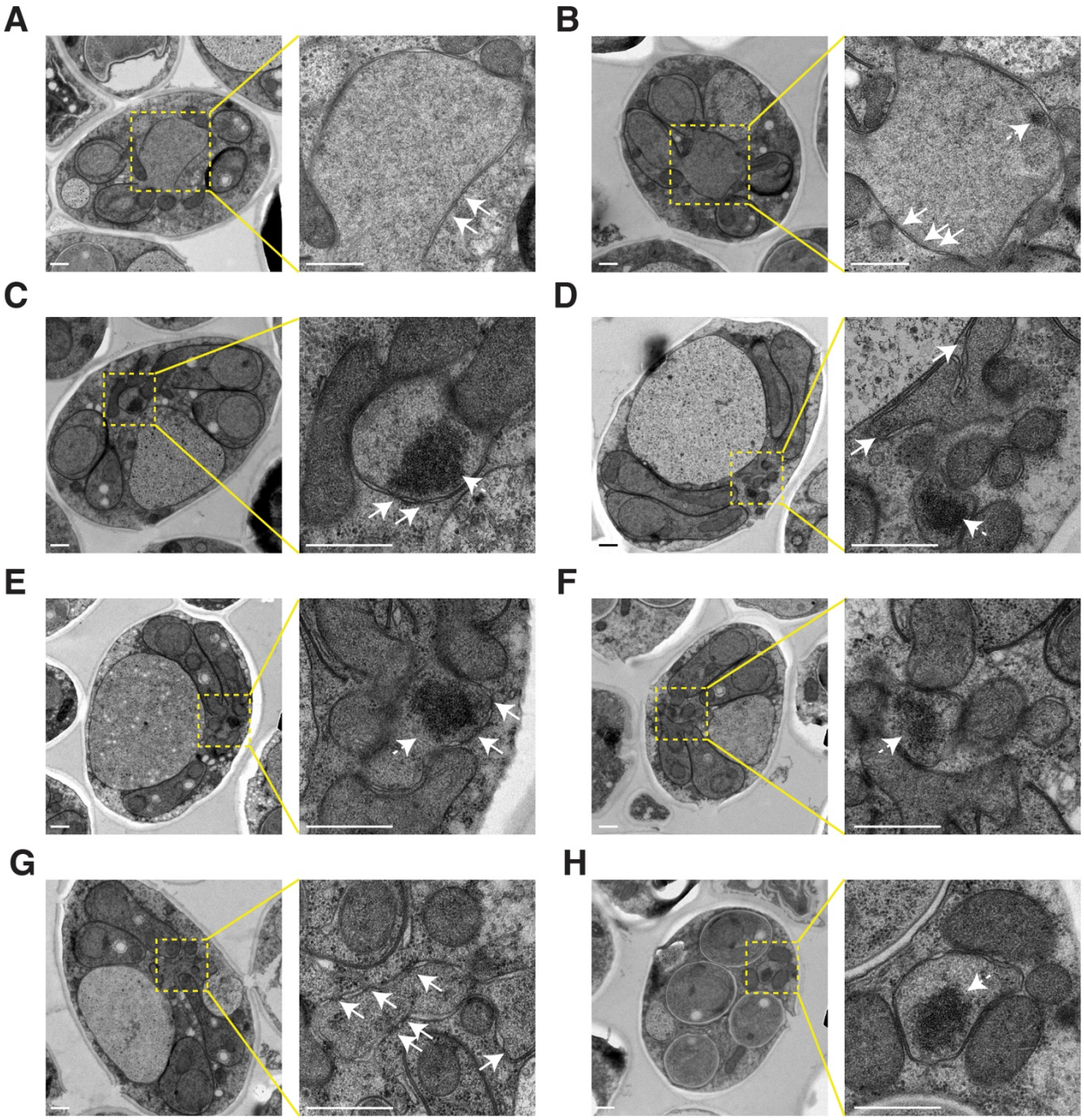

Figure 2.11. Additional electron micrographs demonstrating formation of a nuclear envelope-bound compartment outside of gametes during meiosis II. A-H. Electron micrographs of cells with insets of the nuclear envelope-bound region outside the gamete plasma membranes (UB11513). Solid arrows indicate NPCs; dashed arrows indicate the nucleolar mass. **A-B**. Early anaphase II cells. **C-G.** Late anaphase II cells. **H.** Post-meiotic cell. Scale bars, 0.5 µm.

We next performed serial section transmission electron microscopy (TEM) to observe this compartment directly. Reconstructions of individual cells, either during anaphase II or during gamete development, confirmed the existence of nuclear envelope-bound space outside of the four nuclei (Figure 2.9C-D). The compartment seemed deformed in comparison to the nascent gamete nuclei in that the nuclear envelope membrane structure appeared abnormal and the compartment was often fragmented into multiple nuclear envelope-bound regions (Figure 2.9C-F). These regions were located outside of the gamete plasma membranes, also known as prospore membranes (Figure 2.9C-D). Importantly, individual sections showed that the compartment contained nucleolar material and NPCs (Figure 2.9E and 2.9F; Figure 2.10C; Figure 2.11). We conclude that, during meiosis II, the nuclear envelope undergoes a five-way division to form the four nuclei and a separate compartment containing discarded nuclear proteins.

2.2.4 Core nucleoporins and senescence factors are excluded from developing gametes during meiosis II

The TEM analyses showed that the nuclear envelope-bound compartment localized outside of the developing gamete plasma membranes (Figure 2.9C-D). It remained unclear, however, how the material was sequestered into this compartment. At least two models could explain how the material was left outside of the nascent gametes: (1) the material was being "extruded," removed from the gamete after initial entry, or (2) "excluded," never entering the nascent gametes. To differentiate between these models, we analyzed the localization of a gamete-specific plasma membrane (PM) marker, yeGFP-Spo20$^{51-91}$ (Nakanishi et al., 2004), relative to NPCs and chromosomes. We found that, throughout anaphase II, a sequestered mass of nucleoporins was constrained to a region immediately outside of the nascent plasma membranes and never appeared inside (Figure 2.12A). The rim of the developing plasma membranes marked by Don1-GFP neatly delineated the boundary of the NPC mass (Figure 2.12B, Figure 2.13). Live-cell microscopy confirmed that the NPCs remained outside of nascent plasma membranes throughout their development, supporting "exclusion" as the means by which nuclear material remained outside of the developing gametes (Figure 2.14).

To determine if senescence factors were similarly excluded, we monitored the localization of protein aggregates and nucleolar material relative to the gamete plasma membranes. This analysis revealed that age-induced damage almost never entered into newly forming gametes (Figure 2.12C; Figure 2.15). Only one out of several hundred gametes inherited the Hsp104-associated protein aggregates (Figure 2.12D); strikingly, this Hsp104 punctum persisted after gamete maturation, suggesting that the elimination of age-associated damage is dependent on its prior exclusion. These results highlight the existence of an active mechanism in meiotic cells that precludes the inheritance of NPCs and senescence factors by the nascent gametes.

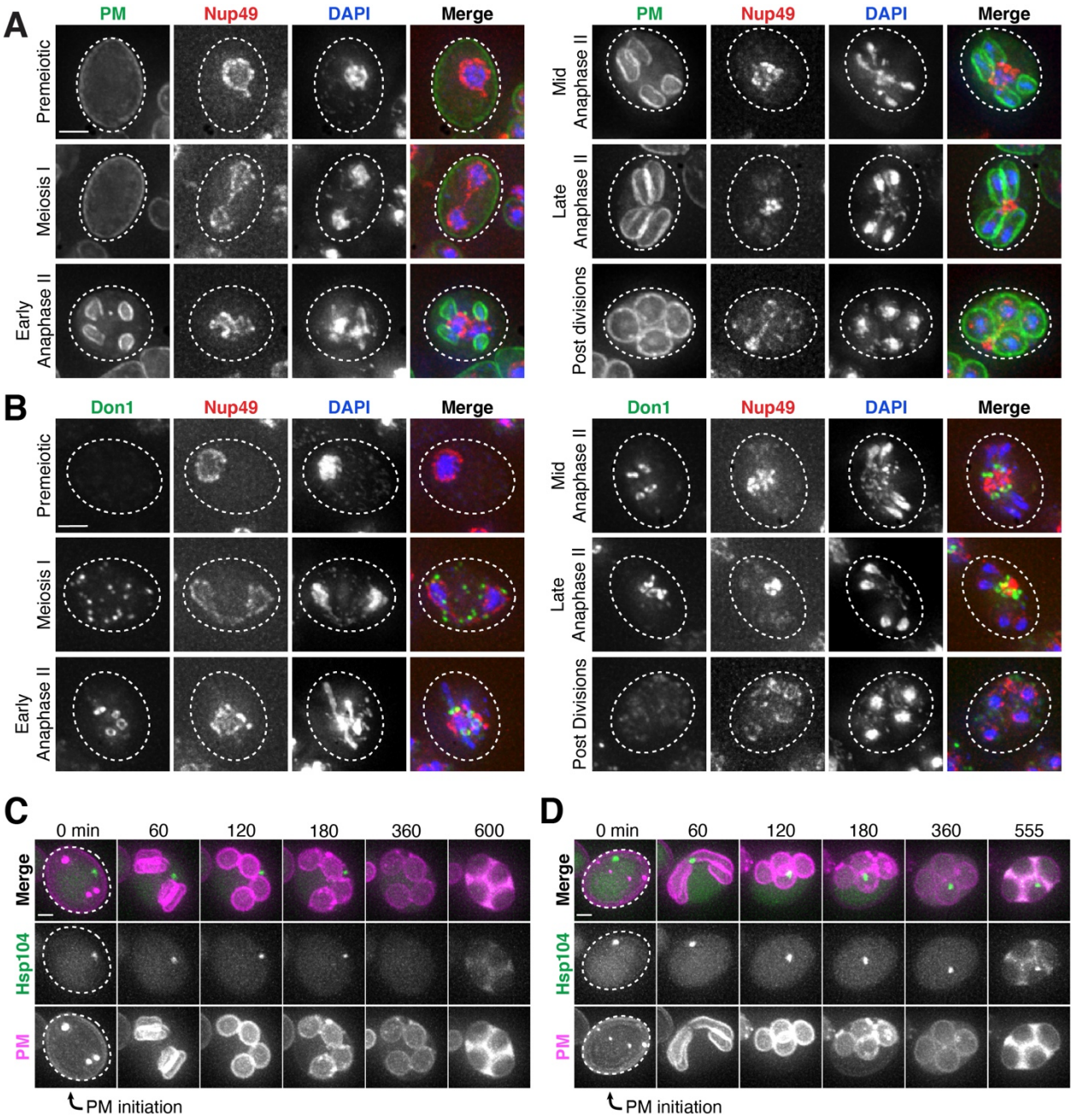

Figure 2.12. Core nucleoporins and age-dependent damage are excluded from developing gametes during meiosis II. A. Maximum intensity projections over 6 µm of fixed young cells depicting localization of the gamete plasma membrane marker yeGFP-Spo20$^{51-91}$ relative to the nucleoporin Nup49-mCherry and DAPI (UB12342). **B.** Maximum intensity projections over 8 µm of fixed young cells depicting localization of the leading edge complex tag Don1-GFP relative to the nucleoporin Nup49-mCherry and DAPI (UB12436). **C-D.** Montages of cells with a protein aggregate tag,

Hsp104-mCherry, and a marker of the gamete plasma membrane, yeGFP-Spo20$^{51-91}$ (UB11821). **C.** An aged cell (6 generations old) that excluded its protein aggregate from developing gametes. **D.** An aged cell (6 generations old) that failed to exclude its protein aggregate from developing gametes. For C-D, the first time point depicting gamete plasma membrane nucleation was defined as 0 minutes as indicated by the arrows. Scale bars, 2 µm.

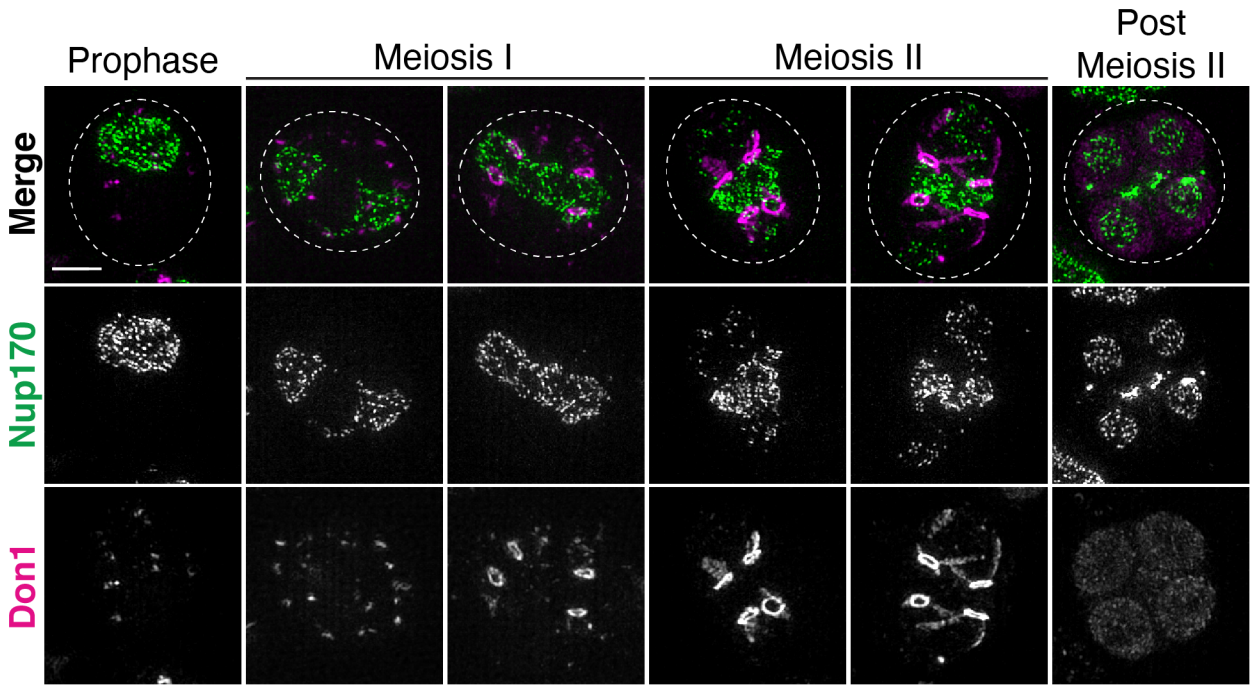

Figure 2.13. Super-resolution imaging demonstrating that core nucleoporins are excluded from developing gametes during meiosis II. Structured illumination microscopy (SIM) images of fixed cells with Nup170-GFP, a core nucleoporin, and Don1-mCherry, a leading edge complex subunit (UB20613). Scale bars, 2 µm.

2.2.5 Elimination of excluded nuclear material coincides with vacuolar lysis

Following gamete formation, permeabilization of the precursor cell's vacuolar membrane causes the release of proteases, which degrade the cellular contents left in the precursor cell cytosol in a process termed mega-autophagy (Eastwood et al., 2012; Eastwood and Meneghini, 2015). To determine whether mega-autophagy was responsible for the degradation of the excluded nuclear material, we monitored the disappearance of NPCs and age-associated protein aggregates relative to the lysis of the vacuolar membrane as monitored by either Vph1-eGFP or Vph1-mCherry. We found that both events coincided with the onset of vacuolar lysis (Figure 2.16A-D). To further assess nucleoporin degradation, we measured the protein levels of GFP-

tagged Nup84 and Nup170 by immunoblotting (Figure 2.16E-F). Since GFP is relatively resistant to vacuolar proteases, degradation of tagged proteins leads to the accumulation of free GFP (Kanki and Klionsky, 2008). We found that free GFP accumulated in wild-type cells 12 hours after meiosis induction, consistent with vacuolar proteases driving the elimination of Nup84 and Nup170 (Figure 2.16E-F). Importantly, we confirmed that the degradation of both nucleoporins depends on the meiotic transcription factor Ndt80. Ndt80 is a master transcription factor necessary for the meiotic divisions and gamete maturation (Xu et al., 1995). In the absence of *NDT80*, cells exhibit a prolonged arrest during prophase I and fail to undergo vacuolar lysis (Eastwood et al., 2012). Altogether, these analyses highlight mega-autophagy as the probable degradation mechanism for NPCs and nuclear senescence factors.

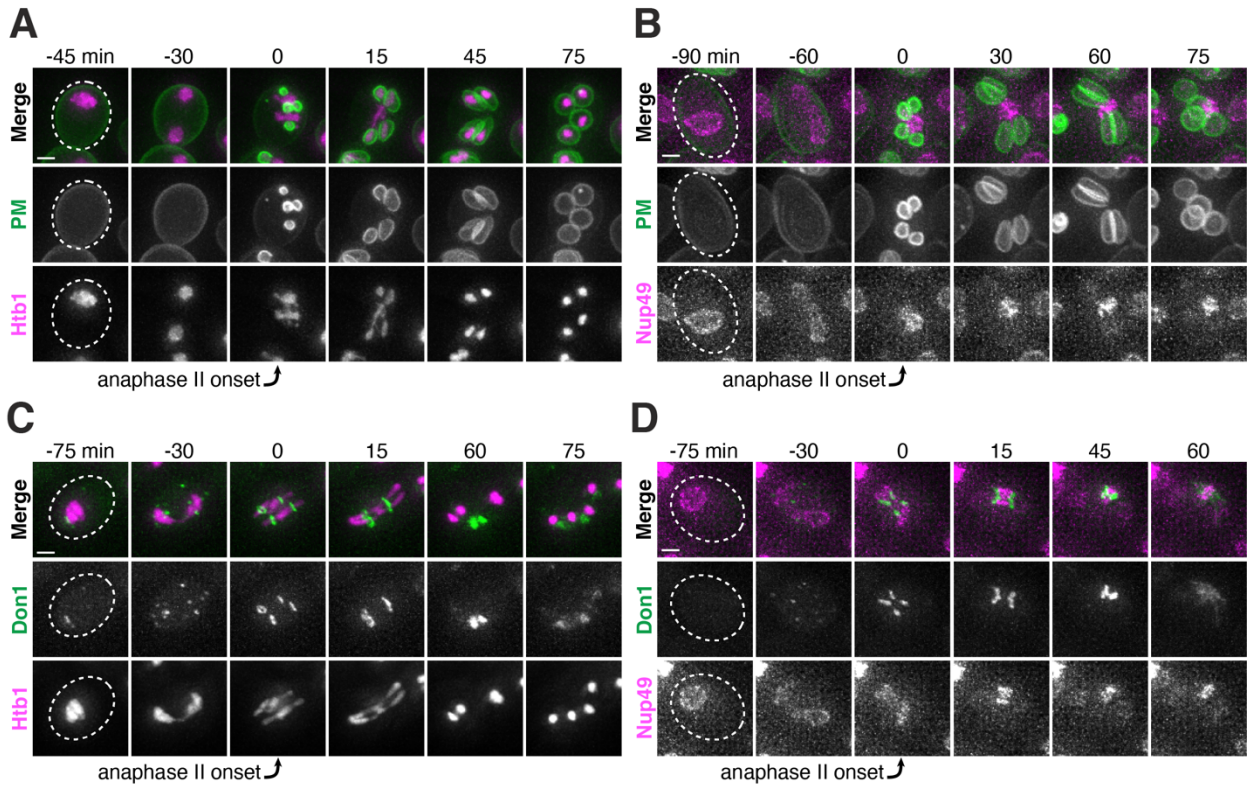

Figure 2.14. Dynamic localization of sequestered nucleoporins relative to gamete plasma membranes. A-B. Montages of young cells progressing through the meiotic divisions with a gamete plasma membrane marker yeGFP-Spo20$^{51-91}$ and either **A.** a histone marker Htb1-mCherry (UB12434), or **B.** a nucleoporin marker Nup49-mCherry (UB12342). **C-D.** Montages of young cells progressing through the meiotic divisions with the leading edge complex subunit Don1-GFP and either **C.** a histone marker Htb1-mCherry (UB12438), or **D.** a nucleoporin marker Nup49-mCherry (UB12436). The time point depicting anaphase II onset was defined as 0 minutes as indicated by the arrows. Scale bars, 2 µm.

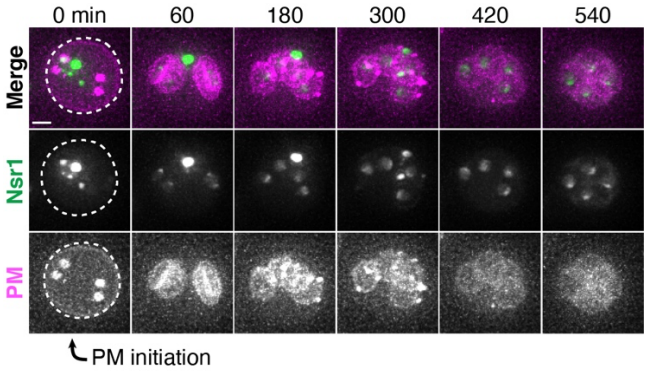

Figure 2.15 Nucleolar material in aged cells is excluded from the developing gametes. Montage of an aged cell (7 generations old) excluding nucleolar material marked by Nsr1-GFP during meiosis II (UB16710). Gamete plasma membranes were marked by mKate-Spo20$^{51-91}$. The time point depicting anaphase II onset was defined as 0 minutes as indicated by the arrow. Scale bar, 2 µm.

2.2.6 Sequestration of nuclear pore complexes requires gamete plasma membrane development

What drives the nuclear remodeling event in meiotic cells? Given that the boundaries of the excluded NPC mass co-localize with the rims of developing gamete plasma membranes (Figure 2.12B, Figure 2.13), we posited that plasma membrane development itself was required for NPC sequestration. To test this hypothesis, we monitored NPC localization in mutants with disrupted plasma membrane formation. Plasma membrane development is initiated from the cytoplasmic face of the spindle pole body, which is converted from a microtubule-nucleation center to a membrane-nucleation center during meiosis II (Knop and Strasser, 2000). *SPO21* (also known as *MPC70*) is required for this conversion event, and its deletion completely inhibits *de novo* plasma membrane formation (Knop and Strasser, 2000). We found that, in *spo21Δ* cells, nucleoporins remained around chromosomes during anaphase II instead of being sequestered away (Figure 2.17A-B).

As an independent test of the role of plasma membrane development in NPC remodeling, we perturbed plasma membrane development by an orthogonal method. The formation of fewer than four plasma membranes can be induced by low carbon conditions, since carbon concentration affects the conversion of the spindle pole body into a membrane nucleator (Davidow et al., 1980; Okamoto and Iino, 1981; Taxis et al., 2005). Under such conditions, we found that the gamete nuclei displayed reciprocal localization of plasma membranes and NPCs: only the nuclei that were devoid of plasma membranes were enriched for NPCs (Figure 2.17C-E). This was consistent with the observation that, even in high carbon conditions, cells fated to

form three or two mature gametes would often have one or two nuclei enriched for NPCs, respectively (Figure 2.17B).

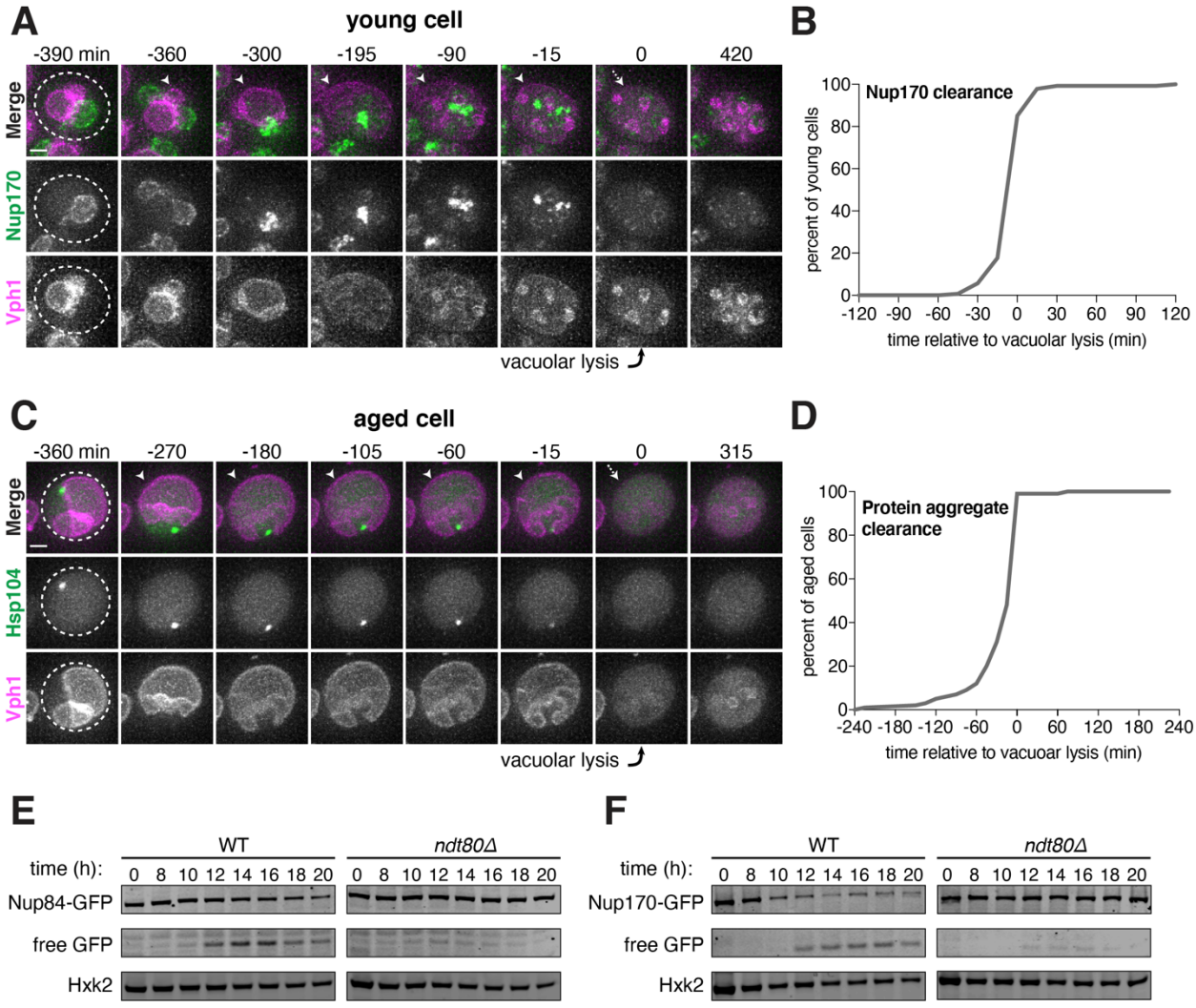

Figure 2.16. Core nucleoporins and protein aggregates are turned over coincident with vacuolar lysis. A. Montage of a young cell with an inner ring complex nucleoporin tag, Nup170-GFP, and a marker for the vacuole, Vph1-mCherry (UB15890). Images are maximum intensity projections over 6 µm; the first time point depicting vacuolar lysis was defined as 0 minutes as indicated by the arrow. **B.** Quantification of the experiment in panel A. Timing of the excluded Nup170-GFP clearance relative to vacuolar lysis (n = 141 cells). **C.** Montage of an aged cell (8 generations old) with a protein aggregate tag, Hsp104-mCherry, and a marker for the vacuolar membrane, Vph1-eGFP (UB12163). Images are maximum intensity projections over 8µm; the first time point depicting vacuolar lysis was defined as 0 minutes as indicated by the arrow. **D.** Quantification of the experiment in panel C. Timing of excluded Hsp104-

mCherry clearance relative to vacuolar lysis (median replicative age = 6, mean replicative age = 5.9 ± 1.5, n = 100 cells). For panels A and C, solid arrows indicate the intact vacuolar membrane of mother cell and dashed arrows indicate vacuolar permeabilization. For panels B and D, vacuolar lysis was scored as the time of vacuolar membrane disappearance. Scale bars, 2 µm. Immunoblot assay measuring degradation of **E.** Nup84-GFP in wild type (UB13497) and *ndt80Δ* cells (UB19929) **F.** Nup170-GFP in wild type (UB11513) and *ndt80Δ* cells (UB19927). Hxk2 levels were measured as a loading control.

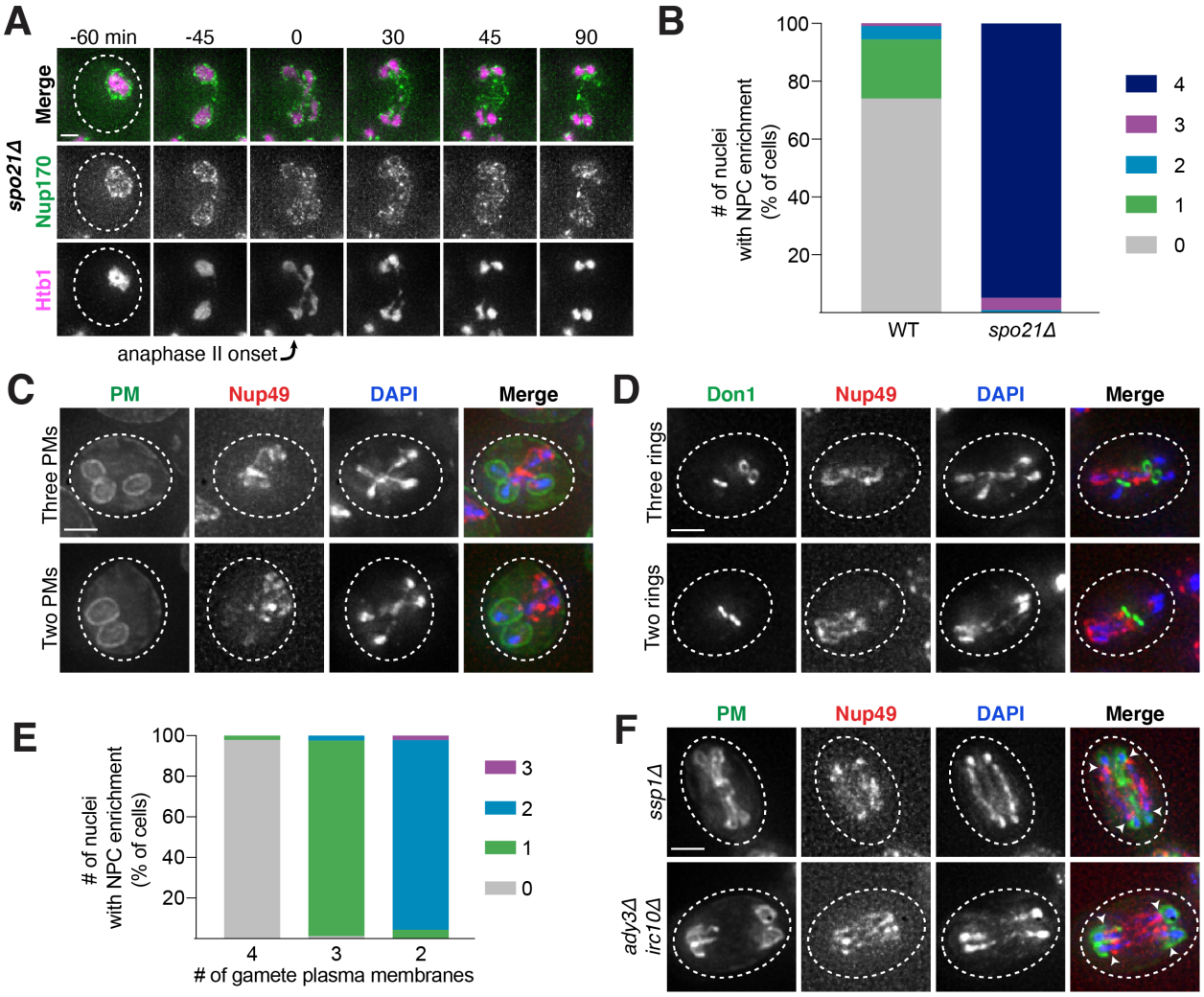

Figure 2.17. Gamete plasma membrane development is necessary for nucleoporin sequestration. A. Montage of inner ring complex nucleoporin Nup170-GFP localization relative to Htb1-mCherry in a young *spo21Δ* cell (UB13377). The first time point depicting anaphase II was defined as 0 minutes as indicated by the arrow. **B.** Quantification of the experiment in panel A for *spo21Δ* and Figure 2.4B for wild type (WT). Number of nuclei enriched for nucleoporins following anaphase II in WT

or *spo21Δ* cells (n = 108 cells for WT, n = 118 cells *spo21Δ*). **C-D.** Maximum intensity projections of fixed young cells depicting **C.** gamete plasma membrane yeGFP-Spo20$^{51-91}$ (UB12342) or **D.** leading edge Don1-GFP (UB12436) localization relative to nucleoporin Nup49-mCherry localization in low-carbon conditions that promoted the formation of fewer than four gamete plasma membranes. **E.** Quantification of the experiment in panel C. Number of nuclei enriched for nucleoporins following anaphase II in cells with variable numbers of gamete plasma membranes (4 PSMs: n = 48; 3 PSMs: n = 80; 2 PSMs: n = 46). **F.** Maximum intensity projections of fixed young cells showing gamete plasma membrane (yeGFP-Spo20$^{51-91}$) and nucleoporin (Nup49-mCherry) localization in mutants defective in leading edge complex formation, *ssp1Δ* (UB13473) or *ady3Δ irc10Δ* (UB13583). Arrowheads on merged images denote location of DAPI constrictions. Scale bars, 2 µm.

Finally, we examined how defects in leading edge complex formation, the structure that forms at the rim of the developing plasma membranes, affect NPC sequestration. Specifically, the absence of the organizing member Ssp1 or simultaneous deletion of the Ady3 and Irc10 subunits, results in the formation of misshapen plasma membranes with narrow rims (Lam et al., 2014; Moreno-Borchart et al., 2001). We found that both *ssp1Δ* and *ady3Δ irc10Δ* cells had defective NPC sequestration, with NPCs often remaining partially around anaphase II nuclei (Figure 2.17F; Figure 2.18). The boundary of NPC removal from the nuclei was marked by constrictions in the DAPI or histone signal and corresponded to the extent of plasma membrane formation (Figure 2.17F; Figure 2.18). In contrast, dramatically widening the rim of the plasma membrane by deleting the membrane shaping protein Sma2 resulted in gamete nuclei inheriting more NPCs, suggesting that the physical proximity of the plasma membrane and nuclear envelope may be important for sequestration (Maier et al., 2008; Figure 2.19). The varying NPC inheritance observed in *sma2Δ* cells (compare 2.19A to 2.19B) may therefore stem from variation in plasma membrane lip diameter. Taken together, these data support the conclusion that NPC sequestration and exclusion are driven by the development of plasma membranes around nascent gamete nuclei.

We also tested a number of additional proteins for a role in nuclear pore complex sequestration (Figure 2.20, Table 2.1, Table 2.2). Contrary to a recent report, we found that deleting the nuclear adaptors of the ESCRT-III complex Heh1, Heh2, and Chm7 did not grossly disrupt NPC sequestration, although more subtle effects on inheritance remain possible (Koch et al., 2020; Figure 2.20A-E). The discrepancy between our work and the recently published study is partially attributable to the failure of Koch et al. to differentiate between packaged (NPC sequestering) and unpackaged (NPC inheriting) gamete nuclei, since cells without the ESCRT-III adaptors exhibit reduced sporulation efficiency (Figure 2.20F). Genes involved in other candidate nuclear and meiotic processes were also largely dispensable for NPC sequestration (Table 2.1 and Table 2.2). The specific molecular players involved in

NPC sequestration therefore remain elusive; a genetic screen may reveal the involvement of unanticipated or currently unknown pathways (Appendix A).

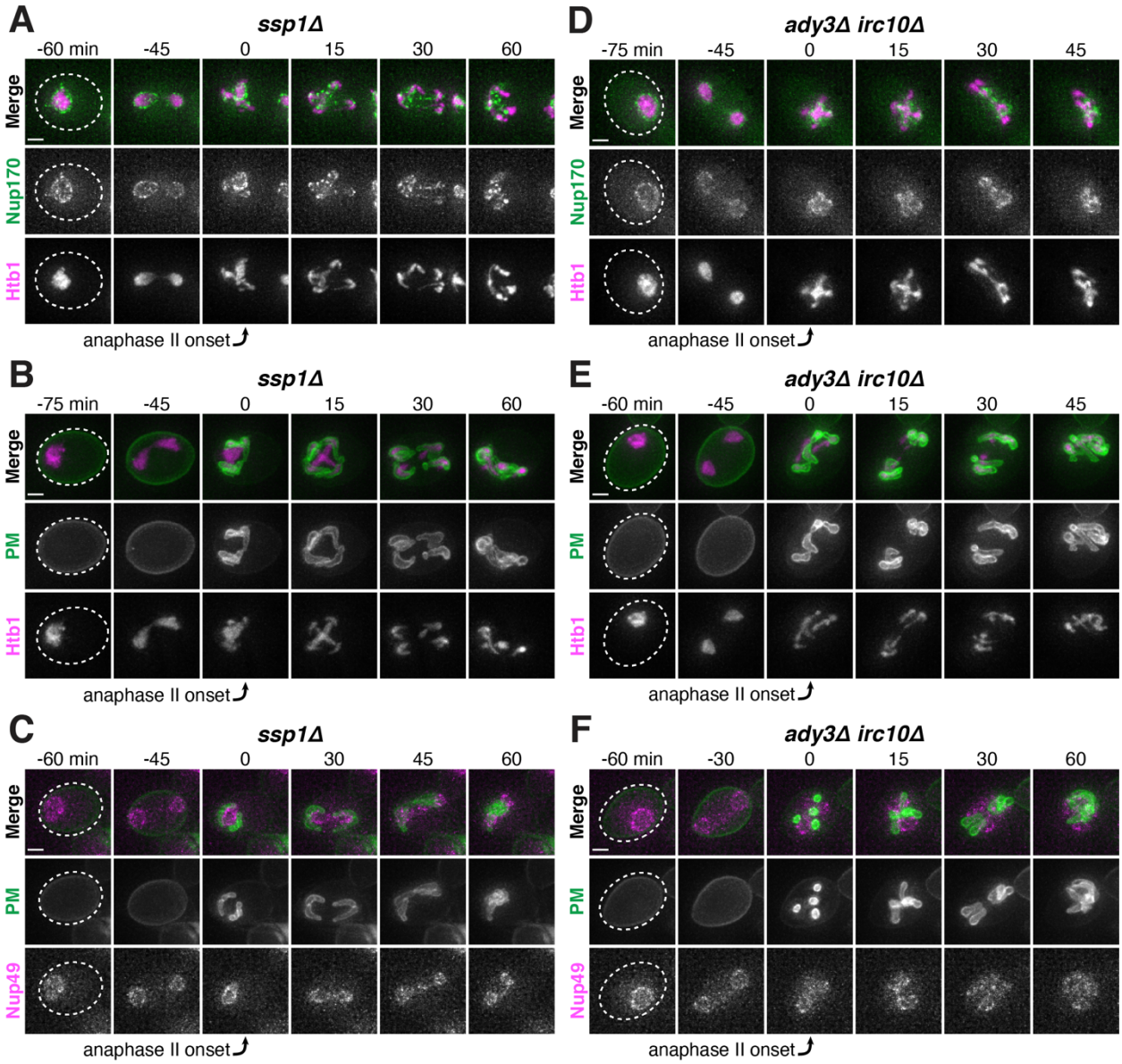

Figure 2.18. Leading edge complex members are required for proper gamete plasma membrane formation and nucleoporin sequestration. A-C. Montages of young *ssp1Δ* cells progressing through the meiotic divisions with the following tags: **A.** nucleoporin Nup170-GFP and histone Htb1-mCherry (UB13373); **B.** gamete plasma membrane yeGFP-Spo20$^{51-91}$ and histone Htb1-mCherry (UB13475); **C.** and gamete plasma membrane yeGFP-Spo20$^{51-91}$ and nucleoporin Nup49-mCherry (UB13473). **D-F.** Montages of young *ady3Δ irc10Δ* cells progressing through the meiotic divisions with the following tags: **D.** nucleoporin Nup170-GFP and histone Htb1-mCherry

(UB12465); **E.** gamete plasma membrane yeGFP-Spo20$^{51-91}$ and histone Htb1-mCherry (UB13585); **F.** and gamete plasma membrane yeGFP-Spo20$^{51-91}$ and nucleoporin Nup49-mCherry (UB13583). The time point depicting anaphase II onset was defined as 0 minutes as indicated by the arrows. Scale bars, 2 µm.

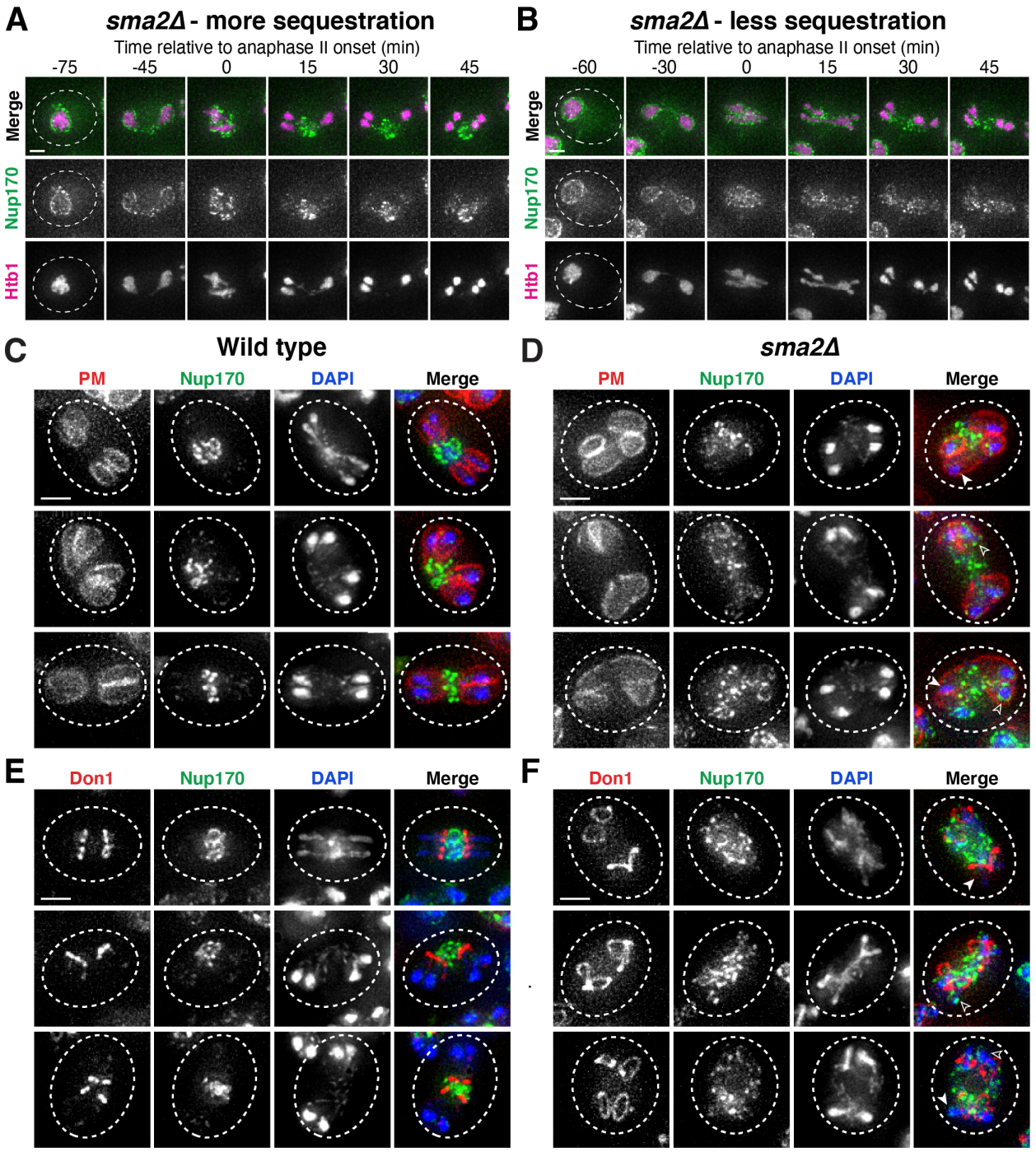

Figure 2.19. Wider plasma membranes result in NPC sequestration defects. A-B. Montages of young *sma2Δ* cells progressing through the meiotic divisions with the nucleoporin Nup170-GFP and histone Htb1-mCherry (UB20074). Cells can exhibit diverse sequestration phenotypes, ranging from **A.** sequestration more like wild type to **B.** sequestration more like *spo21Δ* cells. **C-D.** Maximum intensity projections over 10 µm of fixed **C.** wild type (UB20615) or **D.** *sma2Δ* (UB20767) young cells, visualizing the plasma membrane (PM) marker Spo20-mKate, the nucleoporin Nup170-GFP, and DAPI-stained chromatin. **E-F.** Maximum intensity projections over 10 µm of fixed **E.** wild type (UB20613) or **F.** *sma2Δ* young cells (UB20765), visualizing the leading edge complex member Don1-mCherry, the nucleoporin Nup170-GFP, and DAPI-stained chromatin. Filled arrowheads indicate nuclei exhibiting NPC sequestration; hollow arrowheads indicate nuclei exhibiting NPC inheritance. Note that for C-F, the microscope software was set to 60x despite the images being acquired with a 100x objective, resulting in sub-optimal deconvolution. Intensity values are not scaled identically for all images in C-F. Scale bars, 2 µm.

2.2.7 Sequestration of senescence factors requires gamete plasma membrane development

Since the sequestration of NPCs and nuclear senescence factors were spatially and temporally coupled, we reasoned that a common mechanism could mediate both events. We therefore monitored the sequestration of protein aggregates in *spo21Δ* cells, which are defective in NPC sequestration. In comparison to wild-type cells, we found that *spo21Δ* mutants exhibited a dramatic increase in the association of protein aggregates with chromosomes during anaphase II (48% vs. 0%; Figure 2.21A-B). Regardless of whether or not the protein aggregate was sequestered away from chromosomes in *spo21Δ* cells, the protein aggregates always co-localized with the nuclear envelope, as marked by NPCs (Figure 2.22A-B). Thus, without the nascent plasma membranes, protein aggregates appeared randomly distributed along the nuclear periphery.

We next assessed how nucleolar sequestration is affected in *spo21Δ* cells by monitoring the formation of the sequestered Nsr1 focus in young cells. We found that in 39% of the *spo21Δ* cells, the nucleoli failed to be sequestered in meiosis II and instead co-segregated with chromosomes (Figure 2.21C-D). In contrast, none of the wild-type cells displayed this behavior. Furthermore, Nsr1 remained co-localized to the nuclear envelope in *spo21Δ* cells in a similar manner to protein aggregates (Figure 2.22C-D). Altogether, these findings support the notion that meiotic exclusion of age-induced protein aggregates and nucleolar material is coupled to a nuclear remodeling event that is driven by gamete plasma membrane formation.

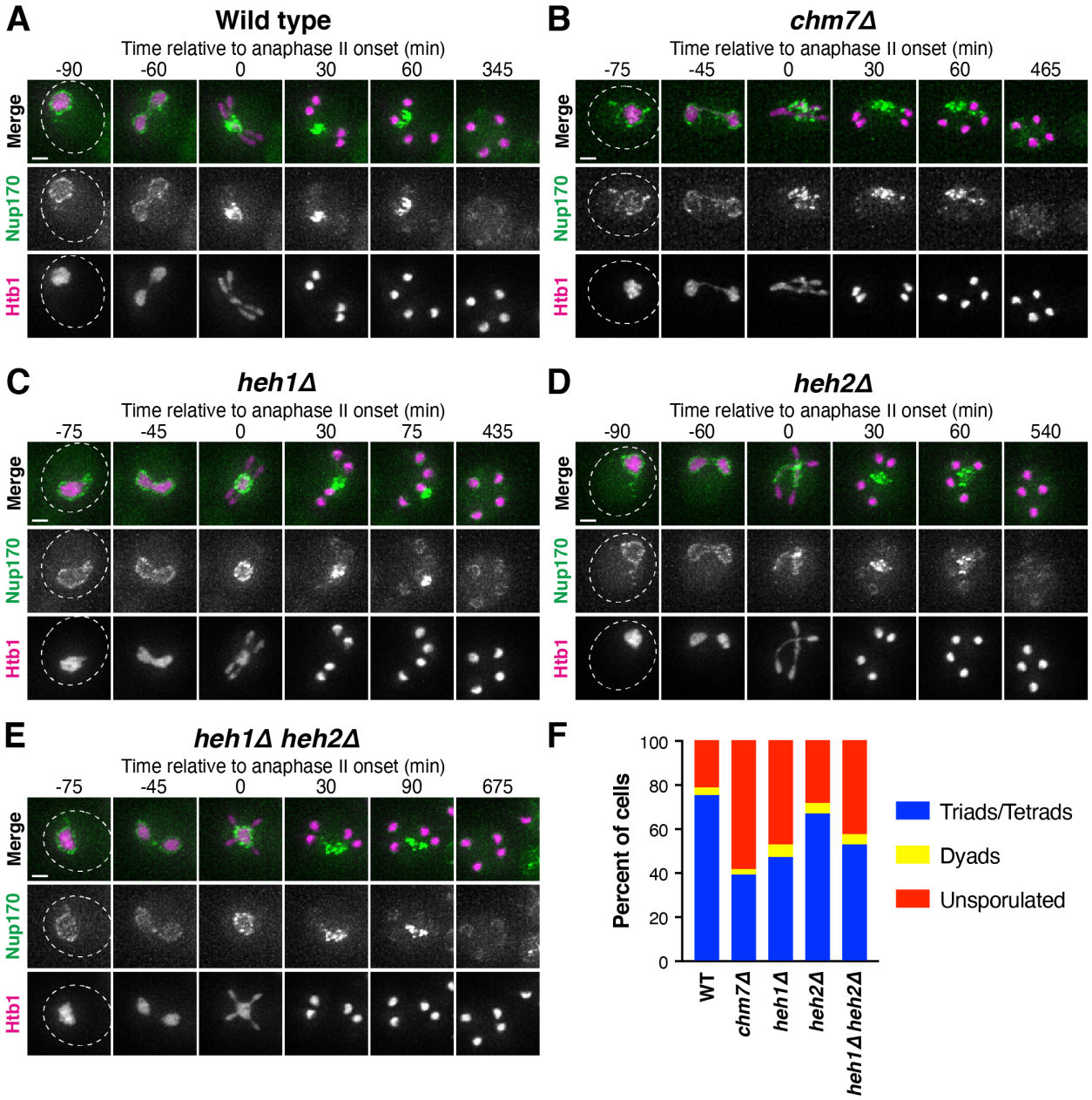

Figure 2.20. Nuclear ESCRT-III adaptors are largely dispensable for NPC sequestration. A-E. Montages of cells with a fluorescently tagged core nucleoporin Nup170-GFP and histone Htb1-mCherry progressing through meiosis. Representative cells of different ESCRT-III nuclear adaptor mutants are shown: **A.** wild type (UB11513), **B.** *chm7Δ* (UB14376), **C.** *heh1Δ* (UB14378), **D.** *heh2Δ* (UB14380), and **E.** *heh1Δ heh2Δ* (UB14382). Note that for B, the microscope software was set to 100x despite the images being acquired with a 60x objective, resulting in sub-optimal deconvolution. The first time point depicting anaphase II was defined as 0 minutes as indicated by the arrows. Scale bars, 2 µm. **F.** The sporulation efficiency

for the different genotypes displayed in A-E. At least 200 cells were counted for each strain.

Table 2.1. Meiotic septin and leading edge complex genes are not required for nuclear pore complex or protein aggregate sequestration. Movies of strains with the indicated deletion, and either (1) a fluorescently tagged inner ring complex nucleoporin (Nup170-GFP) and a meiotic staging marker (Htb1-mCherry) or (2) a fluorescently tagged chaperone that marks age-induced protein aggregates (Hsp104-mCherry) and a gamete plasma membrane marker (yeGFP-Spo20$^{51-91}$) were generated. For mutants with successful gamete packaging, at least 25 tetrads were observed. For mutants with poor or unsuccessful gamete packaging, at least 50 cells that proceeded through MII were observed and compared to wild type (UB11513 for Nup170-GFP; UB11821 for Hsp104-mCherry).

Function	Gene	NPC Strain (Nup170-GFP)	Protein Aggregate strain (Hsp104-mCherry)
Leading edge	*ady3Δ*	UB12414	UB19758
	don1Δ	UB12461	UB19756
	irc10Δ	UB12463	UB19762
Meiotic septins	*spr3Δ*	UB15307	UB19752
	spr28Δ	UB15426	UB19754
	spr3Δspr28Δ	UB15428	UB19760

Table 2.2. Additional candidate genes are not required for nuclear pore complex sequestration. Movies of strains with the indicated allele, a fluorescently tagged inner ring complex nucleoporin (Nup170-GFP), and a meiotic staging marker (Htb1-mCherry) were generated. For mutants with successful gamete packaging, at least 25 tetrads were observed. For mutants with poor or unsuccessful gamete packaging, at least 50 cells that proceeded through MII were observed and compared to wild type (UB11513 for Nup170-GFP). For *cdc15-as1*, the inhibitor 1-NA-PP1 was added to a final concentration of 10 μM after 4.25 hours in Spo.

Function	Allele and strain number
Meiotic kinase	*sps1Δ* (UB13379), *smk1Δ* (UB13381), *cdc15-as1* (UB13513)
Meiotic regulators	*gip1Δ* (UB13375), *ama1Δ* (UB13383),
Autophagy	*atg39Δ* (UB14372), *atg40Δ* (UB14374), *nvj1Δ* (UB14386)
Other	*nsg1Δ* (UB12752), *spo19Δ* (UB20076), *msc1Δ* (UB20218), *hos3Δ* (UB25672), *nur1Δ* (UB25676)

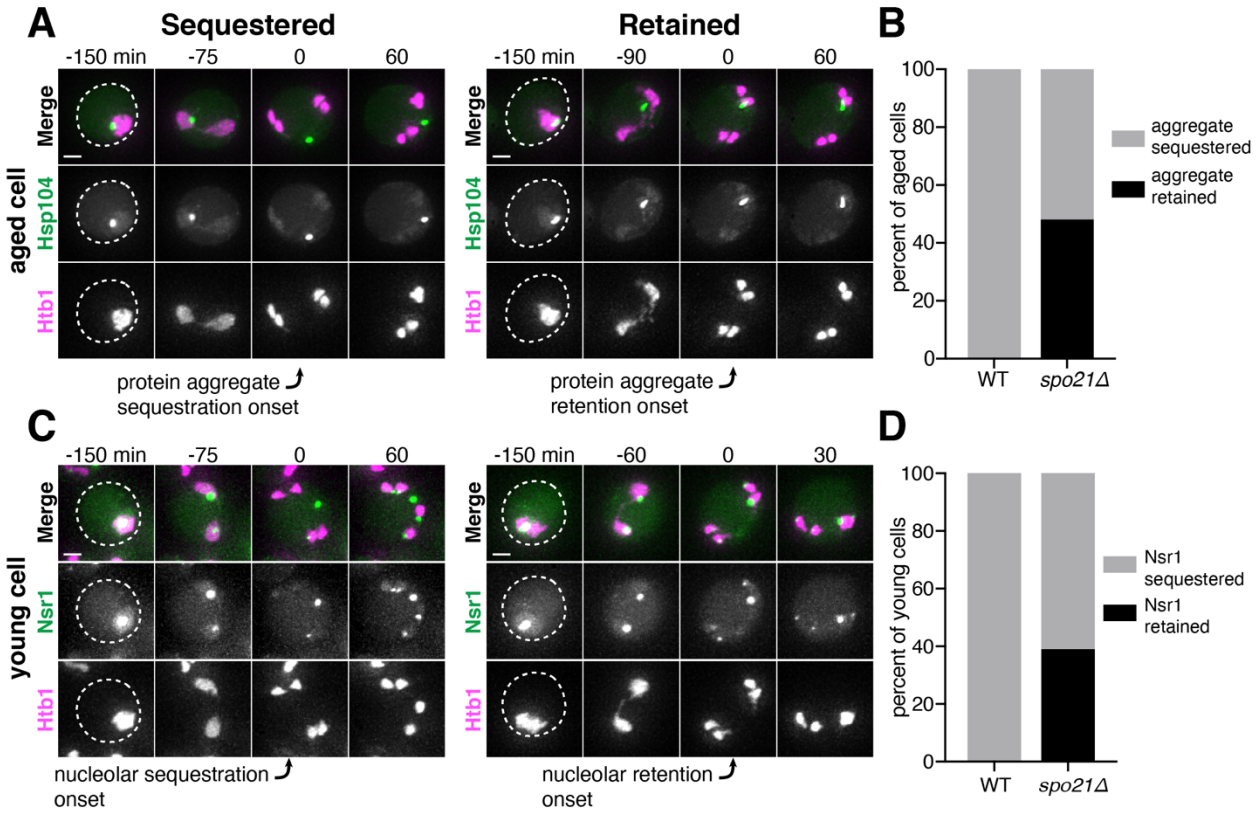

Figure 2.21. Protein aggregate and nucleolar sequestration is coupled to NPC sequestration via gamete plasma membrane development. **A**. Montages of aged *spo21Δ* cells in which protein aggregates marked by Hsp104-eGFP were either (left panel) sequestered away from (5 generations old) or (right panel) retained by (6 generations old) chromosomes during anaphase II (UB14418). **B.** Quantification of protein aggregate retention in aged in wild type (WT, UB9724) and *spo21Δ* cells (UB14418). Median replicative age = 7, mean replicative age = 6.5 ± 1.5, n = 100 for WT cells; median replicative age = 6, mean replicative age = 6.2 ± 1.2, n = 100 for *spo21Δ* cells. **C.** Montages of young *spo21Δ* cells in which nucleolar material was either (left panel) sequestered away from or (right panel) retained by chromosomes during anaphase II (UB14419). **D.** Quantification of Nsr1 retention in young WT (UB15118) and *spo21Δ* cells (UB14419). n = 100 for WT cells, n = 100 for *spo21Δ* cells. For A and C, chromosomes were visualized with the histone marker Htb1-mCherry. For A, the first time point depicting protein aggregate sequestration or retention was defined as 0 minutes as indicated by the arrows. For C, the first time point depicting nucleolar sequestration or retention was defined as 0 minutes as indicated by the arrows. Scale bars, 2 µm.

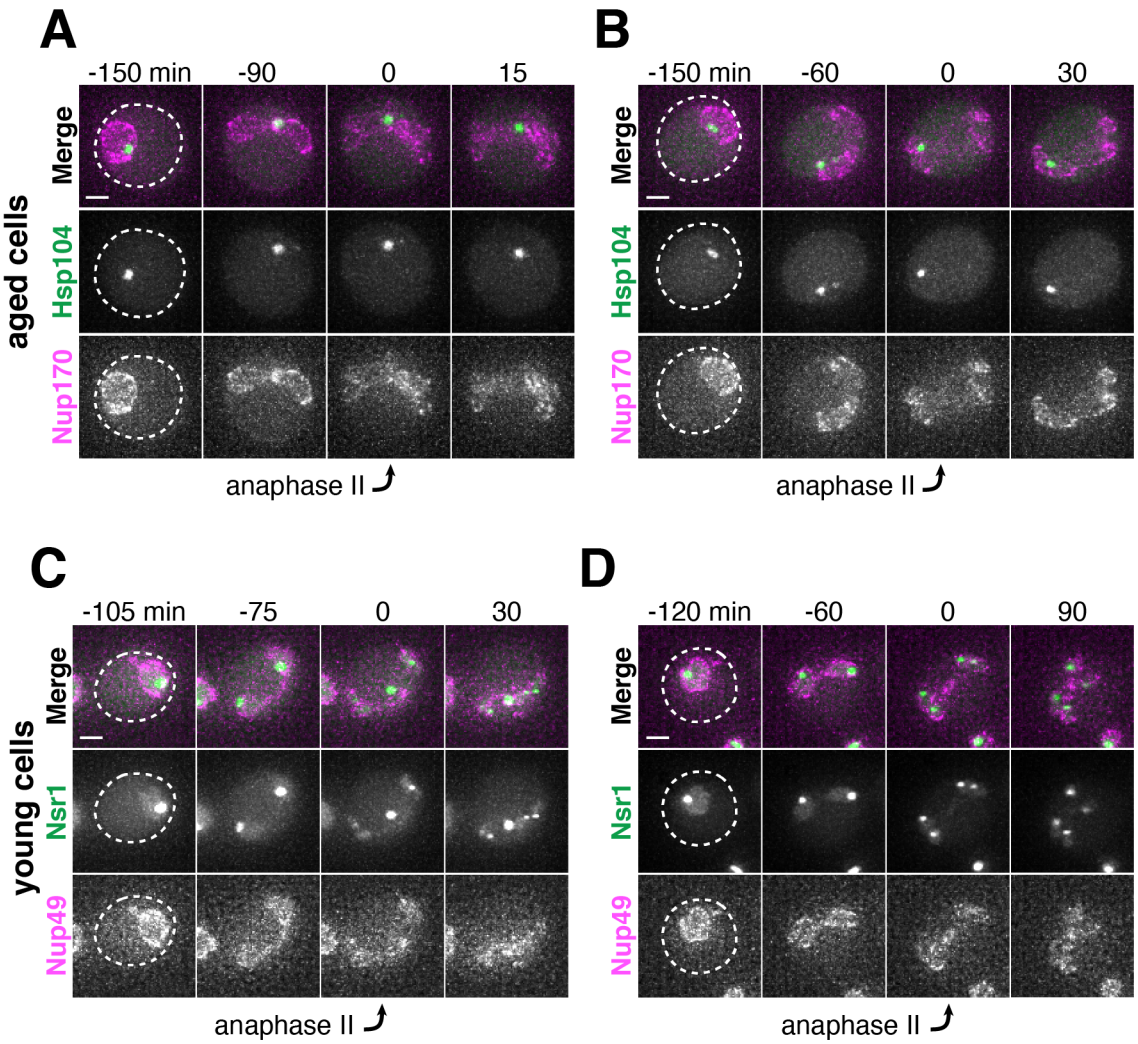

Figure 2.22. Protein aggregates and nucleolar material co-localize with NPCs during anaphase II in *spo21Δ* cells. A-B. Montages of aged *spo21Δ* cells with protein aggregates labeled with Hsp104-mCherry and NPCs labeled with Nup170-GFP (UB13568). **A.** Montage of a cell that sequesters protein aggregates during meiosis II (7 generations old). **B.** Montage of a cell that retains protein aggregates during meiosis II (6 generations old). **C-D.** Montages of young *spo21Δ* cells with nucleolar material labeled with Nsr1-GFP and NPCs labeled with Nup49-mCherry (UB14425). **C.** Montage of a cell that sequesters an Nsr1-GFP punctum during meiosis II. **D.** Montage of a cell that retains all Nsr1-GFP during meiosis II. The time point depicting anaphase II was defined as 0 minutes as indicated by the arrows. Scale bars, 2 µm.

2.3 Discussion

This study defines a meiotic quality control mechanism that eliminates nuclear senescence factors in budding yeast. In an aged precursor cell, many of its nuclear contents, including nuclear pore complexes, rDNA circles, nucleolar proteins and protein aggregates, are sequestered in a membranous compartment away from the chromosomes that are destined for future gametes (Figure 2.23). We term this compartment the Gametogenesis Uninherited Nuclear Compartment, or GUNC. The GUNC and its contents are eliminated upon programmed lysis of the vacuole, an organelle functionally equivalent to the lysosome. We further show that *de novo* plasma membrane growth is required for the sequestration of nuclear material (Figure 2.23). Together, our findings define a meiosis-specific nuclear remodeling event that physically separates age-induced cellular damage away from gametes and highlights its role in cellular rejuvenation.

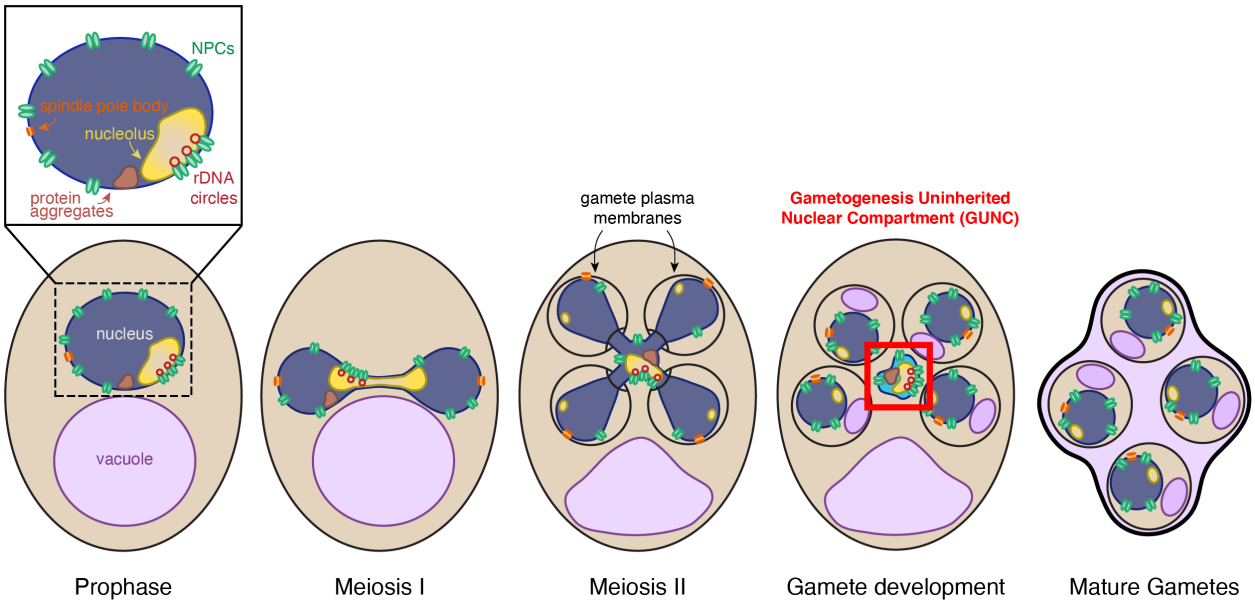

Figure 2.23. Nuclear rejuvenation during meiosis. Aged yeast cells accumulate nuclear damage including extrachromosomal rDNA circles (red), nuclear-associated protein aggregates (brown), abnormal and enlarged nucleoli (yellow), and damaged long-lived proteins including nucleoporins (green). During meiosis II, a nuclear envelope-bound compartment, termed the GUNC (for Gametogenesis Uninherited Nuclear Compartment), containing much of this age-associated damage is formed and remains outside of the developing gametes. The material in the GUNC is turned over coincident with vacuolar lysis, completing rejuvenation of the gamete nuclei. Sequestration of the age-dependent damage away from gamete nuclei requires proper gamete plasma membrane development during anaphase II.

2.3.1 Selective inheritance of nuclear contents during meiotic differentiation

We found that a subset of nuclear components is sequestered away from chromosomes during anaphase II: core nucleoporins, nucleolar proteins involved in rRNA transcription and processing, extrachromosomal rDNA circles, and protein aggregates. However, other nuclear proteins – including histones, the rDNA-associated protein Cfi1, and the Ran exchange factor Prp20 – are largely retained with dividing nuclei during anaphase II (unpublished data). A more thorough cataloging of nuclear components is needed to identify parameters that differentiate excluded nuclear material from retained nuclear material. Strong association with chromatin, as in the case for histones, Cfi1 and Prp20, may be one way to mediate the selective inheritance of nuclear proteins into gametes (Aebi et al., 1990; Dilworth et al., 2005; Li et al., 2003; Straight et al., 1999). On the other hand, strong association with NPCs may facilitate sequestration – for example, extrachromosomal rDNA circles have been shown to interact with NPCs in mitotic cells (Denoth-Lippuner et al., 2014).

It is currently unclear whether a mechanism exists to enrich for damaged proteins in the sequestered pool, such that any proteins remaining with the gamete nuclei are preferentially undamaged. Since some nucleoporins and nucleolar proteins are sequestered and eliminated in young cells, it is likely that undamaged proteins are destroyed during meiosis for reasons that are yet to be determined. However, the observation that the fraction of discarded nucleolar proteins is higher in aged cells than young cells is consistent with the possibility that damaged nucleolar proteins are selectively enriched in the sequestered material. Since both nucleolar proteins and NPCs have been shown to accumulate age-related damage (Denoth-Lippuner et al., 2014; Lord et al., 2015; Rempel et al., 2019; Sinclair et al., 1997), selective elimination and subsequent de novo synthesis could be vital to ensuring gamete rejuvenation.

Unexpectedly, we found that nuclear basket nucleoporins dissociate from the rest of the nuclear pore complex and remain with nascent nuclei during meiosis II. Consistent with this finding, nuclear basket nucleoporins have been shown to be more dynamic than core nucleoporins (Denning et al., 2001; Dilworth et al., 2001; Niepel et al., 2013) and sub-populations of NPCs without certain nuclear basket nucleoporins are present near the nucleolus (Galy et al., 2004). We propose that the nuclear basket segregates with gamete nuclei through re-association with chromatin, which in turn facilitates the formation of new NPCs. In both vertebrates and in the fungus *Aspergillus nidulans*, the nuclear basket nucleoporin Nup2 and its metazoan ortholog Nup50 associate with dividing chromatin during mitosis and contribute to the segregation of NPCs into daughter nuclei (Dultz et al., 2008; Markossian et al., 2015; Suresh et al., 2017). The nuclear basket nucleoporins Nup1 and Nup60 have innate membrane binding and shaping capabilities, making them attractive

candidates to initiate insertion of new NPCs (Mészáros et al., 2015). Indeed, deletion of non-essential nuclear basket nucleoporins results in reduced sporulation efficiency and impaired gamete viability, supporting an important functional role during the meiotic program (Chu et al., 2017).

2.3.2 Formation of gamete plasma membranes is required for the sequestration of nuclear material

We found that gamete plasma membrane formation is required for the selective sequestration of nuclear contents. When plasma membrane development is prevented, NPCs are retained and age-induced damage becomes randomly distributed along the nuclear periphery. The mechanism by which the newly forming plasma membrane creates distinct nuclear envelope domains inside and outside of developing gametes remains unclear. A direct physical blockade, while possible, seems unlikely given that large organelles such as mitochondria enter through the rims of developing plasma membranes (Byers, 1981; Suda et al., 2007). On the other hand, the sequestration boundary at the leading edge is reminiscent of the outer nuclear envelope lateral diffusion barrier that forms at the bud neck during budding yeast mitosis (Caudron and Barral, 2009; Clay et al., 2014). In this context, septins localize to the bud neck and organize a signaling cascade, generating a sphingolipid region in the nuclear envelope that constrains the movement of nuclear envelope proteins (Clay et al., 2014). In meiosis, deletion of meiosis-specific septins (*spr3Δ* and *spr28Δ*; De Virgilio et al., 1996; Fares et al., 1996; Ozsarac et al., 1995) and leading edge complex components (*ady3Δ*, *irc10Δ*, and *don1Δ*; Knop and Strasser, 2000; Lam et al., 2014; Moreno-Borchart et al., 2001) does not grossly alter NPC or protein aggregate sequestration, beyond impacting plasma membrane morphology (Figure 2.17F, Table 2.1). However, an unidentified scaffold might exist to organize a nuclear envelope diffusion barrier. Determining the mechanism by which gamete plasma membranes sequester nuclear material will reveal important principles of nuclear organization and compartmentalization.

After the sequestration event, core nucleoporins begin to re-appear around nascent gamete nuclei, either by *de novo* synthesis or return from the sequestered mass. This raises the intriguing possibility that some core nucleoporins may be able to overcome the physical or diffusion barrier imposed by the plasma membrane. In mitosis, an active transmission mechanism involving the nucleoporin Nsp1 is required for NPCs to pass the bud neck diffusion barrier and enter into daughter cells (Colombi et al., 2013; Makio et al., 2013). Whether any factors facilitate selective NPC inheritance into gametes during meiosis II is an important direction for future studies. Further, daughter-inherited NPCs are modified by the deacetylase Hos3 as they pass through the bud neck, resulting in the formation of a daughter nucleus with distinct cell-cycle behaviors from the mother nucleus (Kumar et al., 2018). Transmission through the leading edge of the gamete plasma membrane might similarly provide an opportunity for any inherited NPCs to acquire gamete-specific modifications and functions.

Further characterizing the reintegration of core nucleoporins at the gamete nuclear periphery will improve our understanding of how NPC remodeling contributes to gamete fitness.

2.3.3 A five-way nuclear division facilitates the subsequent elimination of discarded nuclear material by vacuolar lysis

The sequestration of nuclear damage into a membranous compartment outside of gametes makes it accessible to the degradation machinery active in the progenitor cell cytoplasm during gamete maturation. Due to the strong correlation between the timing of vacuolar lysis and the disappearance of sequestered material as well as the meiosis-specific appearance of NPC degradation intermediates, we propose that mega-autophagy is responsible for the elimination of nuclear senescence factors (Eastwood et al., 2012; Eastwood and Meneghini, 2015). The release of proteases from the vacuole could eliminate protein aggregates and other sequestered nuclear proteins, as has already been observed for unsuccessfully packaged nuclei (Eastwood et al., 2012). Another mechanism, however, is necessary for the elimination of rDNA circles. The endonuclease G homolog, Nuc1, is released from mitochondria during mega-autophagy and therefore could be responsible for the elimination of rDNA circles (Eastwood et al., 2012).

2.3.4 Nuclear remodeling as a driver of gamete health and rejuvenation

Our study highlights a mechanism that facilitates the elimination of age-induced damage during meiosis. Given that extensive nuclear remodeling occurs even in young cells, the reorganization of the nuclear periphery appears to be integral to gamete fitness. Importantly, the sequestration of NPCs in budding yeast meiosis is similar to a NPC reorganization event observed in the spermatogenesis of metazoans, including humans (Fawcett and Chemes, 1979; Ho, 2010; Troyer and Schwager, 1982). In this context, acrosome formation, potentially akin to gamete plasma membrane formation, corresponds to the redistribution of nuclear pores to the caudal end of the nucleus, coincident with chromatin condensation and elimination of un-inherited nuclear material. Whether removal of age-induced damage is also coupled to nuclear remodeling during metazoan spermatogenesis remains to be determined.

Elimination of age-induced damage during gamete maturation may be integral to gamete rejuvenation. In *C. elegans* gametogenesis, oocyte maturation involves the elimination of age-induced protein aggregates by lysosomal activation (Bohnert and Kenyon, 2017; Goudeau and Aguilaniu, 2010). Further determining the mechanism of age-induced damage sequestration and elimination could aid in the development of strategies to counteract cellular aging in somatic cells. The selective inheritance of distinct types of age-induced damage could provide a means of determining whether a given senescence factor is a cause or consequence of aging. In this manner, meiotic differentiation offers a unique and natural context to uncover quality control mechanisms that eliminate the determinants of cellular aging.

Chapter 3

Meiotic Nuclear Pore Complex Remodeling Provides Key Insights into Nuclear Basket Organization

The following chapter contains material derived from a publication on which I am co-first author (King et al., 2022).

3.1 Introduction

The nuclear pore complex (NPC) is a conserved supramolecular structure embedded in the nuclear envelope that acts as the gatekeeper between the nucleus and cytoplasm (reviewed by Hampoelz et al., 2019; Lin and Hoelz, 2019). NPCs are composed of multiple copies of approximately 30 proteins called nucleoporins organized into six modular subcomplexes, which in turn form eight symmetric spokes. Despite its size and complexity, the makeup and structure of the NPC is surprisingly plastic. Individual NPCs within the same cell can differ in composition (Akey et al., 2022b; Galy et al., 2004) and exhibit conformational changes in response to the cellular environment (Schuller et al., 2021; Zimmerli et al., 2021). NPCs also undergo extensive organizational changes during fungal and metazoan mitosis, including partial or full disassembly, that often result in alteration of nucleocytoplasmic transport (De Souza et al., 2004; Dey et al., 2020; Expósito-Serrano et al., 2020; Laurell et al., 2011; Linder et al., 2017; reviewed in Kutay et al., 2021). The extent of NPC plasticity in many other cellular contexts, however, remains largely uncharacterized.

In the budding yeast *Saccharomyces cerevisiae*, the nuclear envelope and its constituent NPCs remain largely intact during both mitosis and meiosis (King et al., 2019; Moens, 1971; Winey et al., 1997). During mitosis, a cytoplasmic pool of the channel nucleoporin Nsp1 mediates NPC inheritance to daughter cells (Colombi et al., 2013; Makio et al., 2013). During meiosis, a large-scale NPC turnover event occurs (King et al., 2019). Core NPC subcomplexes (Figure 3.1A-B) are sequestered to a nuclear envelope-bound compartment, the GUNC (for Gametogenesis Uninherited Nuclear Compartment), that remains outside of gametes and is ultimately degraded during gamete maturation (King et al., 2019; King and Ünal, 2020). In contrast, the entire nuclear basket is inherited: it detaches from the NPC core and returns to nascent gamete nuclei (King et al., 2019). The precise molecular events that control meiotic NPC remodeling are unknown.

The nuclear basket serves as the connection between the nuclear periphery and chromatin, playing roles in diverse nuclear processes including mRNA export and the

DNA-damage response (reviewed in Buchwalter et al., 2019; Strambio-De-Castillia et al., 2010). Organizational understanding of the nuclear basket, however, remains limited due to the highly disordered nature of many basket nucleoporins (Cibulka et al., 2022). Five nucleoporins comprise the budding yeast nuclear basket: Nup1, Nup2, Nup60, Mlp1, and Mlp2. Nup1 and Nup60 contain lipid-binding amphipathic-helices that bind the nuclear envelope and helical regions that bind the NPC core (Mészáros et al., 2015). Nup60 recruits Mlp1 and Nup2 to the NPC via short linear sequence motifs, and Mlp1 is in turn required for Mlp2 localization to the NPC (Cibulka et al., 2022; Dilworth et al., 2001; Feuerbach et al., 2002; Palancade et al., 2005). It is unclear if these features are regulated to achieve nuclear basket detachment during meiosis and whether other currently unknown organizational principles are involved.

In this study, we undertook a mechanistic investigation of nuclear basket remodeling during budding yeast meiosis. Using high time-resolution live-cell fluorescence microscopy, we elucidated two NPC remodeling events in meiosis: partial nuclear basket detachment during meiosis I, involving Nup60 and Nup2, and full nuclear basket detachment during meiosis II. Focusing on the meiosis I remodeling event, we found that partial nuclear basket detachment is coupled to meiotic progression by the Polo kinase Cdc5. We used an unbiased proteomics approach to identify Nup60 as a target of Cdc5-dependent phosphorylation and demonstrated that this phosphorylation drives Nup60 detachment by disrupting its interaction with the NPC core. Nup60 reattachment to the NPC requires its lipid-binding amphipathic helix; this reattachment is necessary for the timely association and organization of the entire nuclear basket in gametes. Differences in dynamics between basket nucleoporins during meiosis I resulted in the discovery of new organizational principles for the nuclear basket, including that Mlp1 can remain associated with the NPC independently of its recruiter Nup60. Notably, meiosis I nuclear basket remodeling is conserved in *Schizosaccharomyces pombe*, a distantly-related yeast without NPC sequestration to the GUNC, suggesting that GUNC formation and basket modularity are functionally separable features of NPC remodeling during meiosis. Our study uncovers a new mode of NPC plasticity in a developmental context and provides mechanistic insights into nuclear basket organization.

3.2 Results

3.2.1 A subset of nuclear basket nucleoporins transiently detaches from the nuclear periphery during meiosis I

We previously demonstrated that nuclear basket nucleoporins Nup60, Nup2, and Nup1 behave distinctly from the NPC core, returning to gamete nuclei during meiosis II instead of remaining sequestered to the GUNC (Figure 3.1B; King et al., 2019). To gain a deeper understanding of the nuclear basket behavior, we first performed denser time-resolution, live-cell imaging of various GFP-tagged nucleoporins in meiotic cells along with a fluorescently tagged histone (Htb1-mCherry) to track

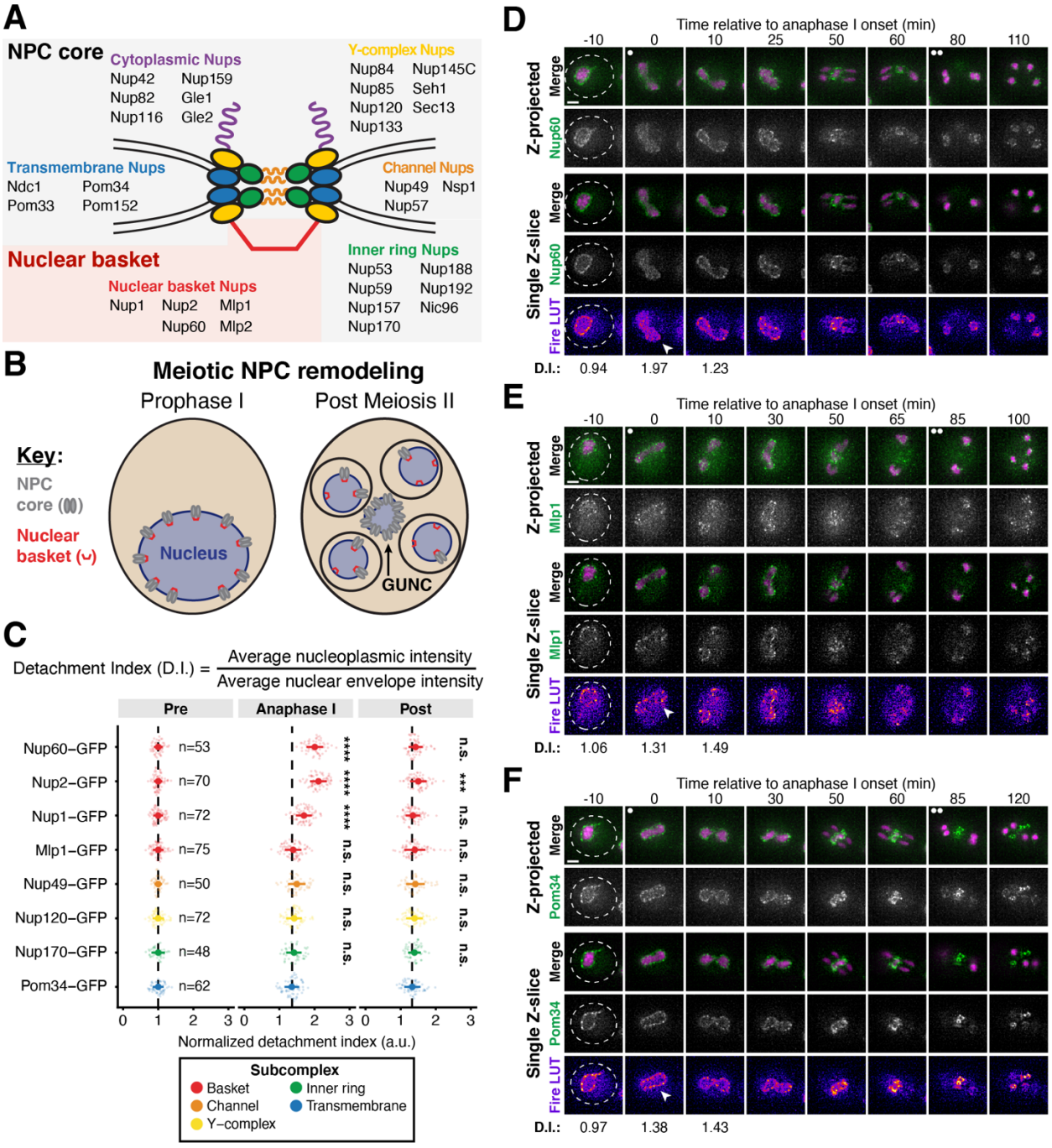

Figure 3.1. A subset of basket nucleoporins relocalize from the nuclear periphery to the nucleoplasm during anaphase I. A. Schematic of the nuclear pore complex (NPC), adapted from King et al., 2019. Nup100 and Nup145N are linkers between subcomplexes and not depicted in the schematic. The gray background denotes the subcomplexes that comprise the NPC core; the red background denotes the nuclear basket. **B.** A schematic depicting NPC remodeling during meiosis as described in King

et al., 2019. Core nucleoporins are sequestered to the Gametogenesis Uninherited Nuclear Compartment (or GUNC) during meiosis II, while basket nucleoporins return to nascent gamete nuclei. **C.** Quantification of nucleoporin detachment before (-10 min, "Pre"), coincident with (0 min, "Anaphase I"), and after (10 min, "Post") the onset of anaphase I. The detachment index (DI) for individual cells was calculated from single z-slices by dividing the average nucleoplasmic signal intensity by the average nuclear envelope signal intensity. For each nucleoporin (color coded by subcomplex), individual DI values were normalized to the average DI at the "Pre" time point. Asterisks indicate statistical significance calculated using Dunn's test for multiple comparisons when each nucleoporin was compared to Pom34-GFP, a transmembrane nucleoporin, for a given time point (see Materials and Methods for an explanation as to why mean DI values for Pom34-GFP change at different meiotic stages). The dashed lines indicate the average DI for Pom34-GFP for each time point. Sample sizes (n) are the number of cells quantified for each nucleoporin; for Nup120-GFP and Nup49-GFP, cells from two independent replicates were pooled. For all figures in this paper, mean and standard deviation are displayed as a dot and whiskers and significance values are denoted with asterisks: *, $p<0.05$; **, $p<0.01$; ***, $p<0.001$; and ****, $p<0.0001$. **D.** Montage of a cell with Nup60-GFP, a nuclear basket nucleoporin, and Htb1-mCherry, a histone, progressing through meiosis (UB14646). **E.** Montage of a cell with Mlp1-GFP, a nuclear basket nucleoporin, and Htb1-mCherry, a histone, progressing through meiosis (UB14648). **F.** Montage of a cell with Pom34-GFP, a transmembrane nucleoporin, and Htb1-mCherry, a histone, progressing through meiosis (UB13503). For all panels, the onset of anaphase I was defined as the Htb1-mCherry chromatin mass exhibiting distortion from a spherical shape consistent with chromosome segregation. For each montage, normalized DI values are indicated when calculated. The white arrowheads in the "Fire LUT" images denote nuclei at the onset of anaphase I, the stage when Nup60-Nup2 detachment is observed. For all figures in this paper, the "Merge" rows display both the GFP and RFP signals together, and the "Fire LUT" (Lookup Table) row displays the GFP signal pseudocolored using the Fire LUT in FIJI (Schindelin et al., 2012). A single white dot (see merged z-projection panels) denotes the time of the meiosis I remodeling event (defined as Nup60-Nup2 relocalization to the nucleoplasm) and two white dots denote the time of the meiosis II remodeling event (defined as near complete nuclear basket return to gamete nuclei). Scale bars, 2 µm.

---

chromatin. Surprisingly, in addition to the previously characterized meiosis II event, the nuclear basket exhibited dynamic behavior during meiosis I (Figure 3.1). Nup60-GFP and its binding partner Nup2-GFP became transiently nucleoplasmic during anaphase I (Figures 3.1C-D, 3.2A-B), undergoing detachment from and subsequent reattachment to the nuclear periphery. Both changes in localization took place within a narrow timeframe (Figure 3.2A), with detachment coinciding with the onset of anaphase I chromosome segregation (within <5 minutes for all cells observed) and lasting for approximately 10 minutes (mean ± standard deviation: replicate 1 = 10.3

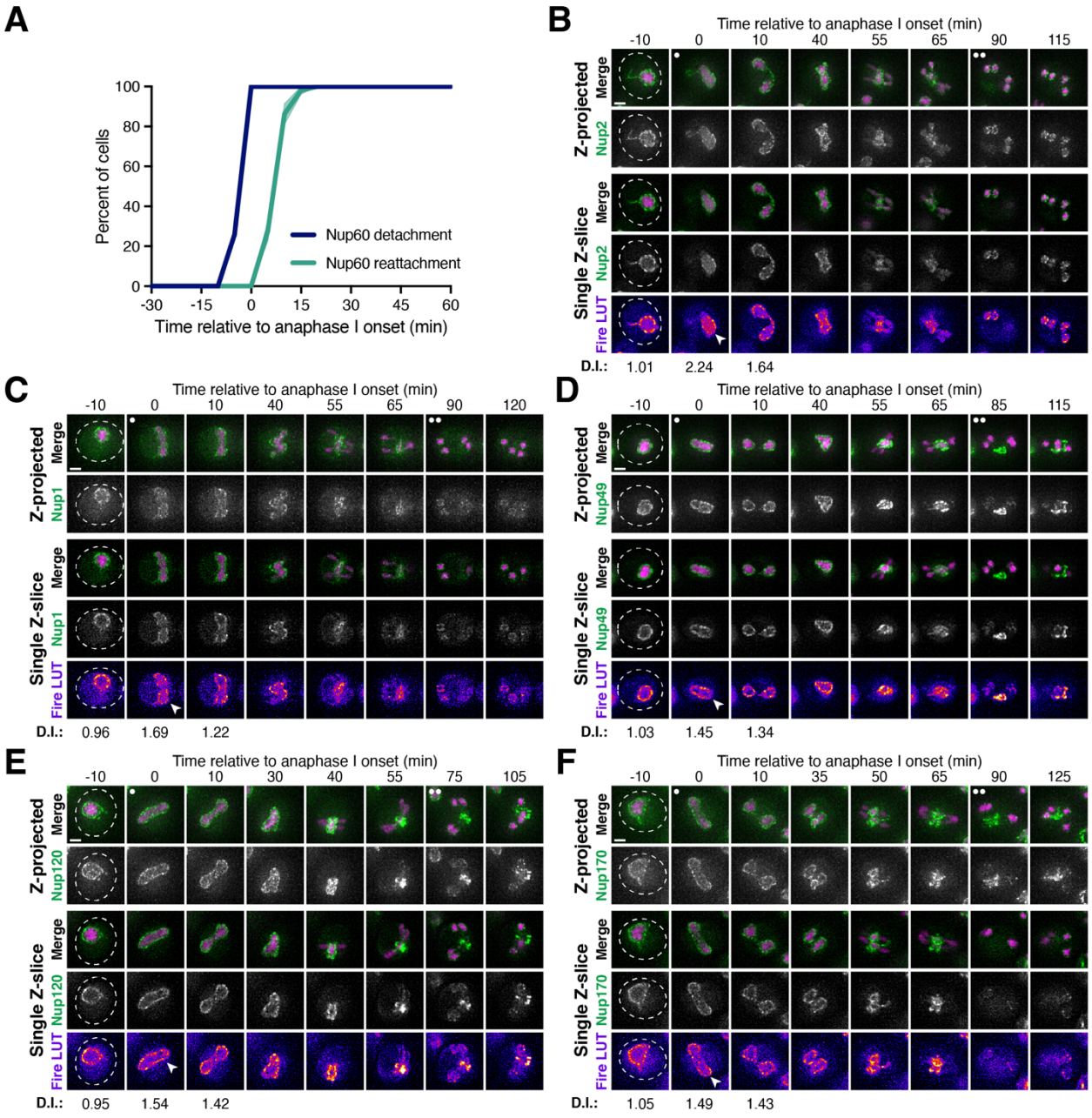

Figure 3.2. Supporting data pertaining to the meiotic behavior of nucleoporins from various NPC subcomplexes. A. Quantification of Nup60-GFP detachment and reattachment timing relative to anaphase I onset, corresponding to B. The mean ± range (shaded range) of two independent biological replicates is displayed (n = 58 cells for replicate 1, 53 cells for replicate 2). **B-F.** Montages of cells with different fluorescently tagged nucleoporins and Htb1-mCherry, a histone, progressing through meiosis: **B.** Nup2-GFP, a nuclear basket nucleoporin (UB15305); **C.** Nup1-GFP, a nuclear basket nucleoporin (UB15303); **D.** Nup49-GFP, a channel nucleoporin

(UB13509); **E.** Nup120-GFP, a Y-complex nucleoporin (UB13499); and **F.** Nup170-GFP, an inner ring complex nucleoporin (UB11513). For each montage, normalized DI values (relative to the average value at the pre-anaphase I time point for each nucleoporin) are indicated when calculated. The onset of anaphase I was defined as the Htb1-mCherry chromatin mass exhibiting distortion from a spherical shape consistent with chromosome segregation. The white arrowheads in the "Fire LUT" images denote nuclei at the onset of anaphase I, the stage when Nup60-Nup2 detachment is observed. Scale bars, 2 µm.

± 2.9 minutes, replicate 2: 11.1 ± 3.3 minutes). Nup1-GFP exhibited a moderate detachment phenotype, with prominent peripheral localization throughout meiosis I (Figures 3.1C, 3.2C), while Mlp1-GFP remained peripheral throughout meiosis I (Figure 3.1C, 3.1E). Mlp2-GFP could not be monitored during the meiotic divisions due to its weak signal, likely as a result of lower expression relative to other nuclear basket members (Cheng et al., 2018). Importantly, all members of the NPC core that were tested, including the transmembrane nucleoporin Pom34-GFP and members of three other subcomplexes, remained peripheral throughout meiosis I (Figures 3.1C, 3.1F, 3.2D-F). Taken altogether, these data reveal that the nuclear basket is partially disassembled during meiosis I, with Nup60 and Nup2 robustly and transiently detaching from the nuclear periphery in a previously overlooked NPC remodeling event.

3.2.2 The nuclear pore complex undergoes two distinct remodeling events during budding yeast meiosis

Our microscopy data established that members of the nuclear basket dissociate from the nuclear periphery during both meiotic divisions (Figure 3.1); however, the relationship between these two dissociation events remained unclear. Since different subsets of basket nucleoporins underwent detachment during meiosis I and meiosis II, we hypothesized that the nuclear basket undergoes two distinct remodeling events. Accordingly, we predicted that: (1) the basket members that detach during both meiosis I and II (Nup60 and Nup2) should be reincorporated into NPCs between the two meiotic divisions; and (2) basket nucleoporins exhibiting different dynamics should be able to detach from the NPC independently of one another.

To assess whether the nuclear basket was reassembled after meiosis I, we performed structured illumination microscopy (SIM) of fixed yeast cells containing Nup2-GFP, a basket nucleoporin that detaches during both meiosis I and II, and Pom34-mCherry, a transmembrane nucleoporin marking the NPC core. Nup2 localization is also a proxy for Nup60 localization, since Nup60 is necessary for Nup2 recruitment to the NPC (Dilworth et al., 2001). We found that Nup2-GFP co-localized with Pom34-mCherry both before and after meiosis I (Figure 3.3A), indicating that Nup2 and Nup60 were indeed reassociating with individual NPCs between meiosis I and II.

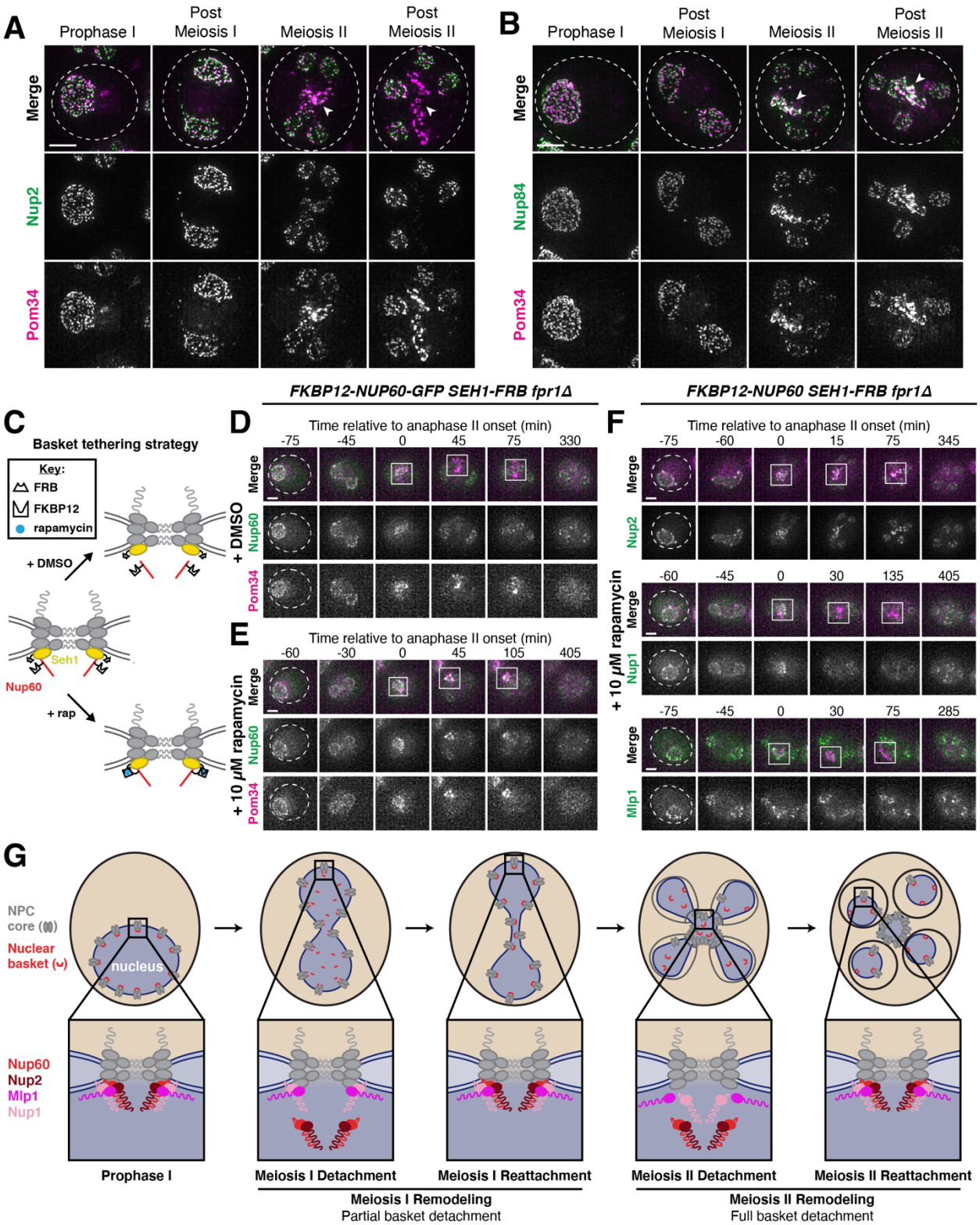
A
Prophase I
Post Meiosis I
Meiosis II
Post Meiosis II
Merge
Nup2
Pom34
B
Prophase I
Post Meiosis I
Meiosis II
Post Meiosis II
Merge
Nup84
Pom34
C
Basket tethering strategy
Key:
FRB
FKBP12
rapamycin
+ DMSO
Seh1
Nup60
+ rap
FKBP12-NUP60-GFP SEH1-FRB fpr1Δ
D
Time relative to anaphase II onset (min)
-75 -45 0 45 75 330
Merge
+ DMSO
Nup60
Pom34
E
Time relative to anaphase II onset (min)
-60 -30 0 45 105 405
+ 10 μM rapamycin
Merge
Nup60
Pom34
FKBP12-NUP60 SEH1-FRB fpr1Δ
F
Time relative to anaphase II onset (min)
-75 -60 0 15 75 345
Merge
Nup2
-60 -45 0 30 135 405
+ 10 μM rapamycin
Merge
Nup1
-75 -45 0 30 75 285
Merge
Mlp1
G
NPC core
Nuclear basket
nucleus
Nup60
Nup2
Mlp1
Nup1
Prophase I
Meiosis I Detachment
Meiosis I Reattachment
Meiosis I Remodeling
Partial basket detachment
Meiosis II Detachment
Meiosis II Reattachment
Meiosis II Remodeling
Full basket detachment

Figure 3.3. Two distinct nuclear pore complex remodeling events occur during budding yeast meiosis. A. Structured illumination microscopy (SIM) images of fixed cells with Nup2-GFP, a nuclear basket nucleoporin, and Pom34-mCherry, a transmembrane nucleoporin (UB20080). **B.** SIM of fixed cells with Nup84-GFP, a Y-complex nucleoporin, and Pom34-mCherry, a transmembrane nucleoporin (UB21079). For A-B, the white arrowheads in the "Merge" images denote the Gametogenesis Uninherited Nuclear Compartment (GUNC). **C.** Schematic of the FKBP12-FRB inducible dimerization approach used to tether Nup60, a nuclear basket nucleoporin, to Seh1, a Y-complex nucleoporin. **D-E.** Montages of cells containing FKBP12-Nup60-GFP and Seh1-FRB, treated with either **D.** DMSO or **E.** 10 µM rapamycin after 4 h in SPM (UB27298). **F.** Montages of cells with different fluorescently tagged basket nucleoporins – Nup2-GFP (UB25843), Nup1-GFP (UB27143), and Mlp1-GFP (UB27725) – and the inducible Nup60 tether (FKBP12-Nup60 and Seh1-FRB) treated with 10 µM rapamycin after 4 h in SPM. For D-F, the transmembrane nucleoporin Pom34-mCherry was used to monitor the NPC core, with the GUNC indicated by a white box. The onset of anaphase II was defined as the first time point with GUNC formation. All cells were *fpr1Δ* to facilitate rapamycin access to the tether. **G.** Model depicting the two distinct NPC remodeling events that occur during budding yeast meiosis: (1) partial basket detachment (Nup60 and Nup2) during meiosis I and (2) full basket detachment (Nup60, Nup2, Nup1, and Mlp1) during meiosis II. Note that, although Nup1 is depicted as remaining associated with the NPC core during meiosis I, it exhibits moderate detachment. Mlp2 is not shown as we were unable to monitor its localization during meiosis. Scale bars, 2 µm.

Moreover, we confirmed at high-resolution that the NPC core and basket behave differently during meiosis II: Nup2-GFP largely returned to gamete nuclei during meiosis II, while Pom34-mCherry was largely sequestered to the GUNC (Figure 3.3A). In contrast, two core nucleoporins – the Y-complex member Nup84-GFP and the transmembrane Pom34-mCherry – colocalized throughout both meiotic divisions, including upon GUNC formation during meiosis II (Figure 3.3B). The reassociation of Nup60 and Nup2 with NPCs after meiosis I indicates that they indeed detach from the NPC in two distinct events.

To determine if basket nucleoporins exhibiting different meiotic behaviors dissociate from the NPC independently, we tethered individual basket members to the NPC core using the FKBP12-FRB inducible dimerization system and then monitored whether other basket nucleoporins still exhibited detachment during meiosis II (Haruki et al. 2008). Based on the interaction between the nuclear basket and the Y-complex in the cryo-EM structure of the NPC, we tagged the N-terminus of Nup60 or Mlp1 in conjunction with the C-terminus of Seh1 to minimally disrupt native NPC organization (Kim et al., 2018). Tethering of Nup60 (FKBP12-Nup60) to the NPC core (Seh1-FRB) resulted in its sequestration to the GUNC during meiosis II, indicating that active detachment from the sequestered NPC core enables nuclear basket return

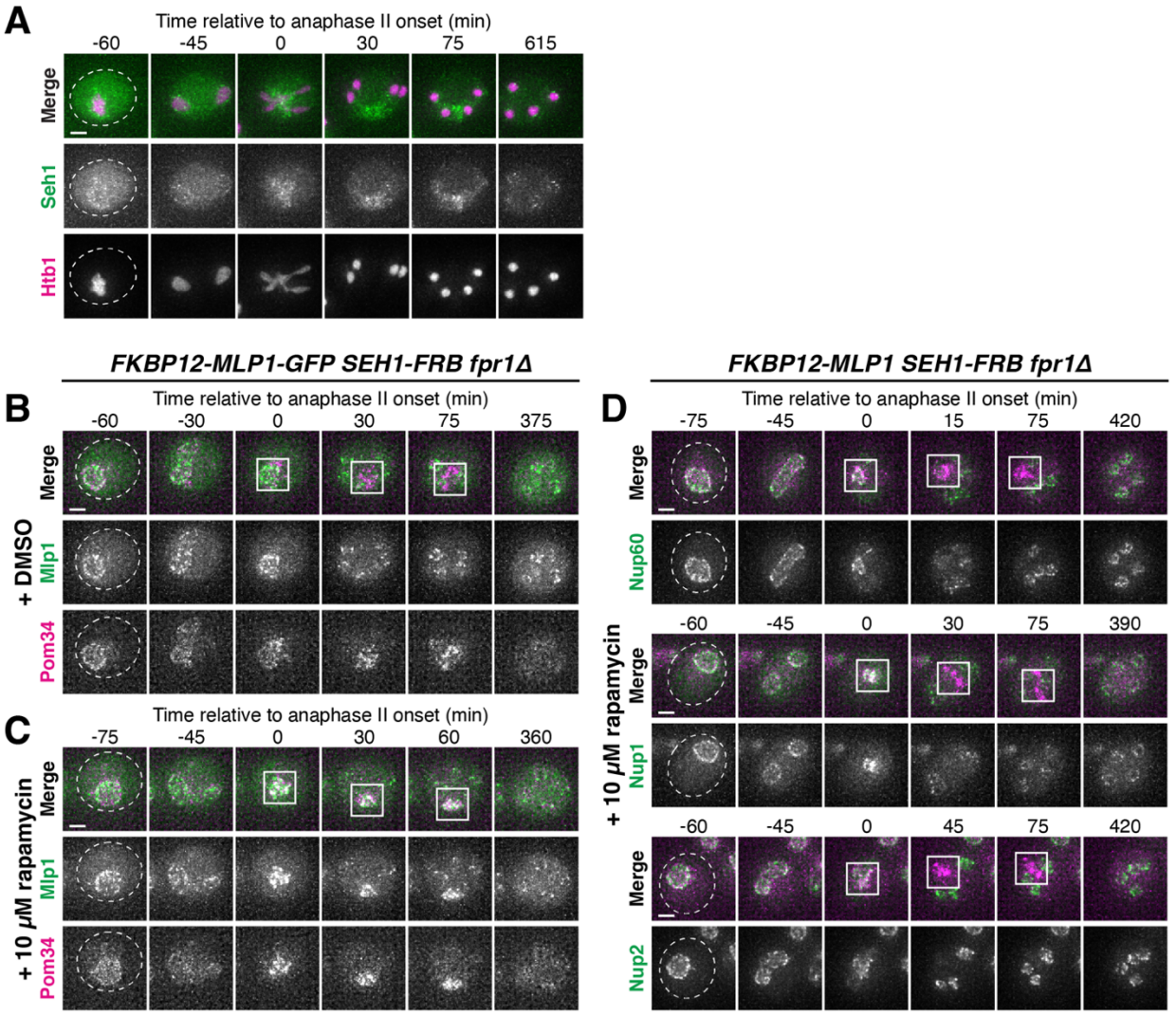

Figure 3.4. Supporting data pertaining to the ability of nuclear basket members to behave independently during meiosis. A. Montage of a cell with Seh1-GFP, a Y-complex nucleoporin, and Htb1-mCherry, a histone, progressing through meiosis (UB24613). The onset of anaphase II was defined by the presence of four Htb1-mCherry lobes. **B-C.** Montages of cells containing FKBP12-Mlp1-GFP and Seh1-FRB, treated with either **B.** DMSO or **C.** 10 µM rapamycin after 4 h in SPM (UB29337). **D.** Montages of cells with different fluorescently tagged basket nucleoporins – Nup60-GFP (UB30174), Nup2-GFP (UB30168), and Nup1-GFP (UB30166) – and the inducible Mlp1 tether (FKBP12-Mlp1 and Seh1-FRB) treated with 10 µM rapamycin after 4 h in SPM. For B-D, the transmembrane nucleoporin Pom34-mCherry was used to monitor the core of the NPC, with the Gametogenesis Uninherited Nuclear Compartment (GUNC) indicated by a white box. The onset of anaphase II was defined as the first time point with GUNC formation. All cells were *fpr1Δ* to facilitate rapamycin access to the tether. Scale bars, 2 µm.

to gamete nuclei (Figures 3.3C-E, 3.4A). Among the basket nucleoporins tested, only Nup2 followed tethered Nup60 to the GUNC; both Mlp1 and Nup1 were still able to detach from the NPC core and return to gamete nuclei (Figure 3.3F). Nup60 and Nup2 therefore remain physically coupled during meiosis, suggesting that they form a distinct submodule that detaches from the NPC together. Tethering Mlp1 (FKBP12-Mlp1) to the NPC core resulted in only its sequestration to the GUNC: Nup2, Nup1, and Nup60 were all able to return to gamete nuclei (Figure 3.4B-D). These results confirm that the nuclear basket does not behave as a uniform entity during meiosis, explaining how nuclear basket nucleoporins are able to exhibit differential meiotic localization patterns.

We therefore propose that two distinct remodeling events occur during budding yeast meiosis, whereby NPCs adopt different forms with varying nucleoporin constituents. During meiosis I, partial nuclear basket disassembly takes place, with Nup60 and Nup2 transiently and robustly detaching from the NPC (Figure 3.3G, "Meiosis I Remodeling"). During meiosis II, full nuclear basket disassembly takes place, with all tested basket nucleoporins (Nup1, Nup2, Mlp1, Nup60) detaching from the NPC and returning to the gamete nuclear periphery (Figure 3.3G, "Meiosis II Remodeling"). Consequently, the nuclear basket is inherited, while the NPC core remains in the GUNC. This nuclear basket remodeling is a new form of NPC structural plasticity that appears to be under strict temporal regulation in meiosis, offering a unique opportunity to deeply interrogate the principles of NPC organization in a developmental context.

3.2.3 The Polo kinase Cdc5 is necessary for partial nuclear basket detachment during meiosis I

We next sought to gain mechanistic insight into how nuclear basket detachment is regulated by focusing on the remodeling event that occurs during meiosis I. To more precisely stage when the Nup60-Nup2 detachment took place, we monitored Nup60-GFP in a strain with a fluorescently tagged spindle pole body (SPB) marker, Spc42-mCherry (Figure 3.5A). Nup60 detachment was stereotyped with respect to SPB behavior (Figure 3.5B), taking place ~25 minutes after metaphase I SPB separation (mean ± standard deviation: replicate 1 = 24.2 ± 5.4 minutes, replicate 2 = 24.5 ± 7.2 minutes). The rapid and precisely-timed detachment of Nup60-Nup2 led us to reason that it may be regulated by a cell cycle-dependent kinase. The Polo kinase Cdc5 was an attractive candidate, as it is induced shortly before the meiotic divisions and is necessary for proper meiosis I chromosome segregation (Clyne et al., 2003; Lee and Amon, 2003). Moreover, Polo kinases have been shown to phosphorylate nucleoporins and regulate NPC disassembly during mitosis in human and worm cells (Linder et al., 2017; Martino et al., 2017).

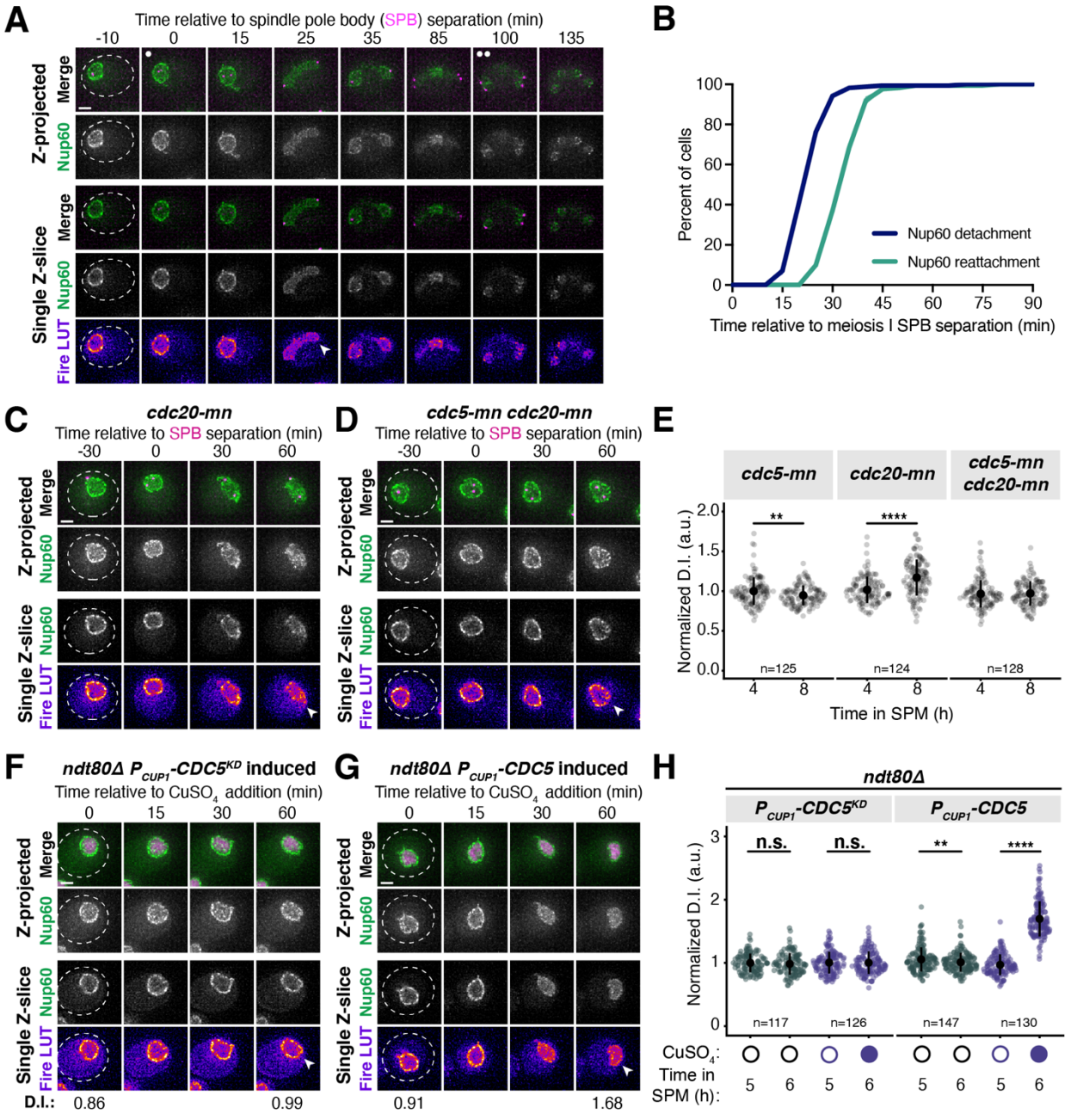

Figure 3.5. *CDC5* is necessary and sufficient for partial nuclear basket disassembly. **A.** Montage of a cell with Nup60-GFP, a nuclear basket nucleoporin, and Spc42-mCherry, a spindle pole body (SPB) component, progressing through meiosis (UB28201). **B.** Quantification of Nup60-GFP detachment and reattachment timing relative to meiosis I SPB separation, corresponding to A. The mean ± range (shaded range) of two independent biological replicates is displayed (n = 91 cells for replicate 1, 81 cells for replicate 2). **C-D.** Montages of cells with Nup60-GFP, a nuclear basket

nucleoporin, and Spc42-mCherry, a spindle pole body component, entering metaphase I arrest in the following strains: **C.** *cdc20-mn* (UB29253) or **D.** *cdc5-mn cdc20-mn* (UB29249). Note that *cdc20-mn* nuclei become highly deformed during extended metaphase I arrest. **E.** Quantification of Nup60-GFP detachment before (4 h in SPM) or during (8 h in SPM) metaphase I arrest in *cdc5-mn* (UB28492), *cdc20-mn* (UB28211) and *cdc5-mn cdc20-mn* (UB28614) cells. Htb1-mCherry, a histone, was used to define the nucleoplasm; due to slightly altered meiotic progression with Htb1-mCherry, a wild type strain (UB14646) was used to assess sporulation progression and determine comparable timing to Spc42-mCherry containing strains. Individual DI values were normalized to the average DI for *cdc5-mn* cells (UB28492) at the pre-meiosis I time point (4 h in SPM, Figure 3.7A). Asterisks indicate statistical significance calculated using a Wilcoxon signed-rank test when metaphase I arrest (8 h in SPM) values were compared to pre-meiotic entry (4 h in SPM) values for each genetic background. Sample sizes (n) are the number of cells quantified for each genetic background. For panels A-D, SPB separation was defined as the first time point that two distinct Spc42-mCherry puncta were visible. **F-G.** Montages of cells with Nup60-GFP, a nuclear basket nucleoporin, and Htb1-mCherry, a histone, in prophase I arrest (*ndt80Δ*) with **F.** P_{CUP1}-*CDC5*^{KD}-*3xFLAG-10xHis* induced (UB29069) or **G.** P_{CUP1}-*CDC5-3xFLAG-10xHis* induced (UB29129). *CDC5* expression was induced at 5 h in SPM with 50 µM $CuSO_4$. **H.** Quantification of Nup60 detachment for the experiment depicted in F-G and S3B. Individual DI values were normalized to the average DI for uninduced P_{CUP1}-*CDC5*^{KD}-*3xFLAG-10xHis* cells at the pre-induction time point (5 h in SPM). Asterisks indicate statistical significance calculated using a Wilcoxon signed-rank test when post-induction (6 h in SPM) values were compared to pre-induction (5 h in SPM) values for each treatment regimen. Sample sizes (n) are the number of cells quantified for each treatment regimen. For F-G, normalized DI values are indicated when calculated. For all montages, the white arrowheads in the "Fire LUT" images denote nuclei exhibiting Nup60-GFP detachment or nuclei from a relevant control at an equivalent time point. Scale bars, 2 µm.

To determine whether the Polo kinase Cdc5 was necessary for nuclear basket remodeling in meiosis I, we utilized a meiotic null allele of *CDC5* where the endogenous promoter is replaced by that of *CLB2*, a B-type cyclin that is transcriptionally repressed during meiosis (*cdc5-mn*; Lee and Amon, 2003). We ensured stage-matched comparison between *CDC5* and *cdc5-mn* cells by performing these experiments in cells depleted for the anaphase-promoting complex/cyclosome (APC/C) activator Cdc20 (*cdc20-mn*) and therefore arrested in metaphase I (Lee and Amon, 2003). We found that Nup60-GFP detached from the nuclear periphery in *cdc20-mn* cells carrying the wild type *CDC5* allele following SPB separation (Figure 3.5C, 3.5E), albeit to a lesser extent than observed in a wild type meiosis (Figure 3.1C). In contrast, Nup60-GFP remained associated with the nuclear periphery in *cdc5-mn cdc20-mn* cells (Figure 3.5D-E). Similar results were obtained using the

cdc5-mn allele alone (Figure 3.7A). We therefore conclude that the Polo kinase Cdc5 couples partial nuclear basket disassembly to meiotic cell cycle progression.

We tested several additional meiotic kinases and regulators for a role in meiosis I or meiosis II nuclear basket detachment by monitoring Nup2-GFP localization. All candidates were dispensable for both remodeling events (Table 3.1), although it remains possible that they could regulate the meiotic dynamics of other basket nucleoporins. Interestingly, in diverse genotypes, Nup2-GFP often became constitutively nucleoplasmic in unpackaged nuclei after meiosis II (data not shown). The relocalization took place after the meiotic divisions, suggesting that this event is distinct from meiotic NPC remodeling. Testing additional candidate genes for a role in the dynamics of different basket nucleoporins will be important to identify other molecular players involved in meiotic NPC remodeling.

Table 3.1. Additional candidate genes do not have a gross effect on nuclear basket detachment during meiosis I or meiosis II. Movies of strains with the indicated allele, a fluorescently tagged nuclear basket nucleoporin (Nup2-GFP), and a fluorescently tagged core nucleoporin (Pom34-mCherry) were generated. Note that subtle differences in meiosis I detachment may have been missed since movies were acquired every 15 minutes instead of every 5 minutes. For many genotypes, Nup2 relocalizes to the nucleoplasm after meiosis II in unpackaged nuclei. For *ime2-as1*, 1-NA-PP1 was added to a final concentration of 20 μM after 5 hours in Spo. For *cdc15-as1*, 1-NA-PP1 was added to a final concentration of 10 μM after 4 hours in Spo.

Function	Allele and strain number
Meiotic kinase	*sps1Δ* (UB24018), *smk1Δ* (UB24020), *ime2-as1* (UB24022), *cdc15-as1* (UB24130)
Meiotic regulator	*spo21Δ* (UB23087), *gip1Δ* (UB25445)

3.2.4 Ectopic Polo kinase activity is sufficient for partial detachment of the nuclear basket

The lack of Nup60-Nup2 detachment in *cdc5-mn* mutants could indicate a direct role for the Polo kinase in mediating nuclear basket detachment or an indirect role via facilitation of proper meiotic progression. To distinguish between these two possibilities, we sought to determine whether ectopic Cdc5 activity was sufficient to drive partial detachment of the nuclear basket outside of the meiotic divisions. *CDC5* is a direct target of the meiotic transcription factor Ndt80 (Clyne et al., 2003). In the absence of *NDT80* function *(ndt80Δ)*, cells successfully enter meiosis but arrest in prophase I, since many of the genes critical for meiotic progression including *CDC5* are not expressed (Chu and Herskowitz, 1998; Xu et al., 1995). As expected, Nup60-

GFP remained at the nuclear periphery during *ndt80Δ* prophase I arrest (0 min, Figures 3.5F-H, 3.7B). We then specifically reintroduced Cdc5 activity in *ndt80Δ* cells by inducing either a wild type *(CDC5)* or kinase-dead *CDC5* transgene (*CDC5*^{KD}, carrying the K110M mutation; Charles et al., 1998) from a copper-inducible promoter (*P*$_{CUP1}$). Strikingly, upon induction of *CDC5*, we observed a significant increase in nucleoplasmic localization of Nup60-GFP (Figure 3.5G-H). Induction of *CDC5*^{KD}, however, had no observable effect on Nup60 localization (Figure 3.5F, 3.5H). Thus, ectopic Polo kinase activity is sufficient to induce Nup60 detachment from the NPC.

3.2.5 SWATH-MS proteomics identifies a Cdc5-dependent Nup60 phosphorylation site and additional novel Polo kinase targets

Our data so far indicate that the Polo kinase Cdc5 regulates nuclear basket remodeling in meiosis I; however, the downstream targets that are critical for this regulation remained unknown. It is possible that Cdc5 phosphorylates one or more nucleoporins, or another factor, to exert its effect. The nuclear basket is anchored to the NPC core via interactions with the Y-complex (Kim et al., 2018; Mészáros et al., 2015). Therefore, nucleoporins belonging to either of these two subcomplexes are potential candidates for Cdc5-dependent phosphorylation. To identify downstream Cdc5 targets, we employed an unbiased approach using Sequential Window Acquisition of All Theoretical Fragment Ion Mass Spectra (SWATH-MS; Gillet et al., 2012; Ludwig et al., 2018; Schubert et al., 2015) that allowed mapping of Cdc5-dependent phosphorylation sites across the proteome (Figure 3.6A). We induced either *CDC5* or *CDC5*^{KD} expression in *ndt80Δ* prophase I-arrested cells and collected samples over several time points after *CDC5* induction (Figure 3.6A). Approximately 7,500 phosphopeptides were identified in each of the samples analyzed, with the vast majority being detected in all samples (Figure 3.7C-D).

To determine which phosphopeptides accumulated in response to Polo kinase activity, we compared the peptide identifications made in either *CDC5* or *CDC5*^{KD} expressing cells and calculated the fold change in abundance (Cdc5/Cdc5^{KD}). We focused specifically on samples collected at 2-5 hours following induction, which showed robust Cdc5 protein expression levels (Figure 3.7E). This analysis recapitulated the identification of several known targets of the Polo kinase Cdc5, including Slk19, Spo13, Net1 and Sgs1 (Grigaitis et al., 2020; Matos et al., 2008; Park et al., 2008; Shou et al., 2002; Figure 3.6B, dark blue dots) , validating our approach. Notably, it also led to the identification of various putative novel targets of Cdc5 (Figure 3.6B, dark gray dots).

The proteome-wide dataset identified 88 phosphorylation sites among 16 nucleoporins from various NPC subcomplexes (Figure 3.6C). All the basket nucleoporins displayed prominent phosphorylation. However, only one of the sites, Nup60 S89, had increased phosphorylation in response to *CDC5* induction with high statistical confidence ($p<0.01$; Figure 3.6C-D). Consistent with Nup60 being a target of Polo kinase, we observed higher mobility species of Nup60 during a wild type

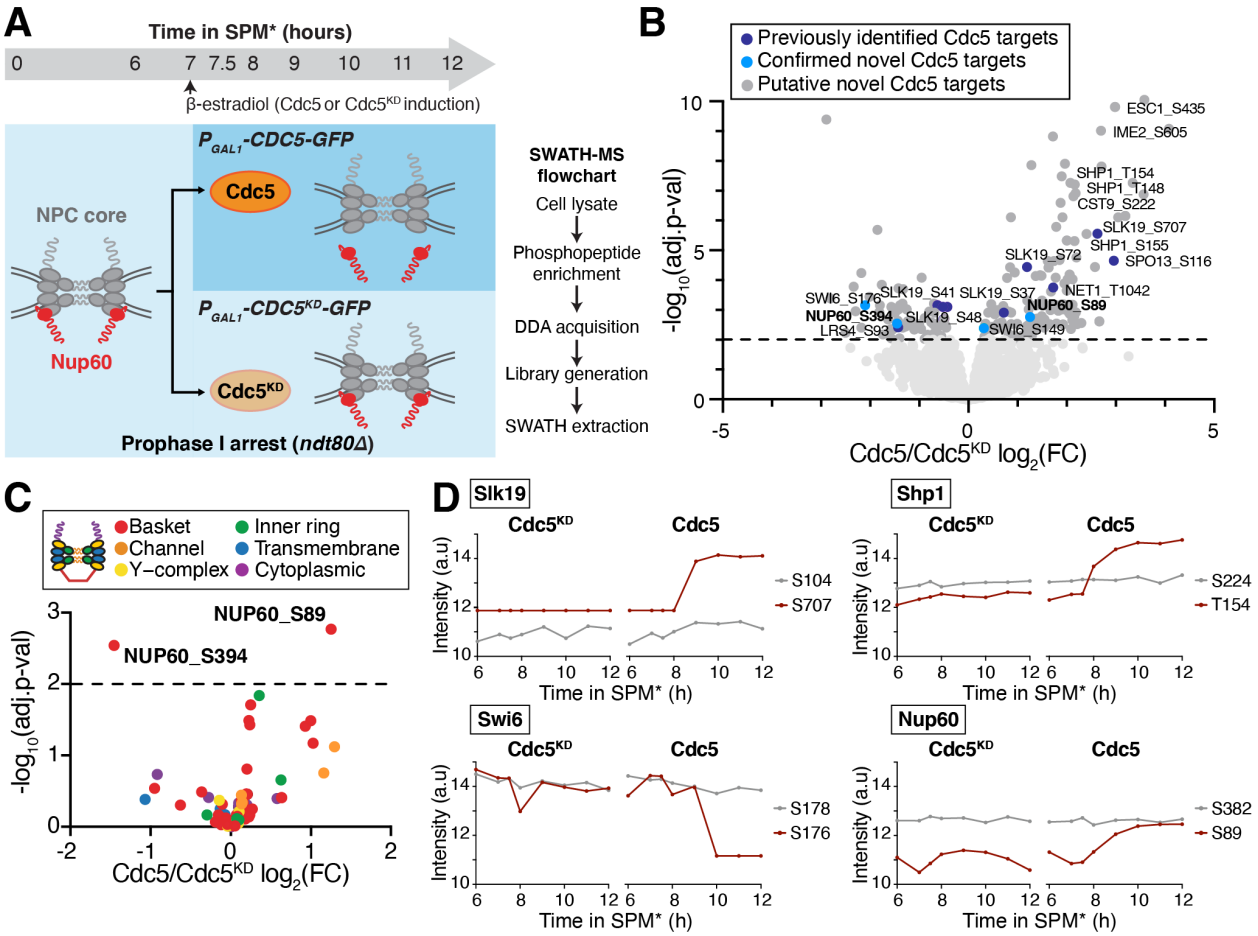
A
Time in SPM* (hours)
0 6 7 7.5 8 9 10 11 12
β-estradiol (Cdc5 or Cdc5KD induction)
PGAL1-CDC5-GFP
Cdc5
NPC core
Nup60
PGAL1-CDC5KD-GFP
Cdc5KD
Prophase I arrest (ndt80Δ)
SWATH-MS flowchart
Cell lysate
Phosphopeptide enrichment
DDA acquisition
Library generation
SWATH extraction
B
Previously identified Cdc5 targets
Confirmed novel Cdc5 targets
Putative novel Cdc5 targets
-log10(adj.p-val)
Cdc5/Cdc5KD log2(FC)
ESC1_S435
IME2_S605
SHP1_T154
SHP1_T148
CST9_S222
SLK19_S707
SHP1_S155
SLK19_S72
SPO13_S116
NET1_T1042
NUP60_S89
SWI6_S176
SLK19_S41
SLK19_S37
NUP60_S394
SLK19_S48
LRS4_S93
SWI6_S149
C
Basket
Inner ring
Channel
Transmembrane
Y–complex
Cytoplasmic
NUP60_S89
NUP60_S394
-log10(adj.p-val)
Cdc5/Cdc5KD log2(FC)
D
Slk19
Shp1
Swi6
Nup60
Cdc5KD
Cdc5
Intensity (a.u)
Time in SPM* (h)
S104
S707
S224
T154
S178
S176
S382
S89
E
NUP60-9myc
Time in SPM* (h): 0 2 4 6 8 10 12
Nup60
Cdc5
Crm1
F
NUP60-9myc cdc20-mn
CDC5
cdc5-mn
Time in SPM* (h): 0 2 4 6 8 10 12
Nup60
Cdc5
Crm1
G
NUP60-9myc ndt80Δ PCUP1-CDC5
Time in SPM* (h): 0 2 4 6 8 8
CuSO4
Nup60
Cdc5
Crm1
H
NUP60-9myc cdc20-mn
NUP60
NUP60-S89A
Time in SPM* (h): 0 2 4 6 8 10 12
Nup60
Cdc5
Crm1

Figure 3.6. SWATH-MS proteomics identifies Nup60 as a target of Cdc5-dependent phosphorylation. A. Schematic illustration of the experimental setup and flowthrough used for the proteomics screen. *ndt80Δ* strains carrying either P_{GAL1}-*CDC5-GFP* (YML3993) or P_{GAL1}-*CDC5*^{KD}-*GFP* (YML3994) were induced to enter meiosis by transfer to SPM* and, after 7h in SPM*, treated with 2 μM ß-estradiol to initiate Cdc5 or Cdc5^{KD} expression, respectively. Samples for protein analyzes, western blot or SWATH-MS proteomics, were collected at the indicated time points after transfer to SPM*. The experiment was performed in biological triplicates. **B.** Volcano plot depicting the differential phosphorylation of peptides in cells ectopically expressing Cdc5 or Cdc5^{KD}, as described in (A). For peptides of interest, the protein name and the phosphorylation site are indicated. The $\log_2$ fold change ($\log_2$(FC)) is plotted on the x-axis and the p-value corrected by false discovery rate (-$\log_{10}$(adj. p-value)) is plotted on the y-axis. Phosphopeptides with adjusted p-values > 0.01 are represented by light gray dots below the dashed line. Phosphopeptides with adjusted p-values ≤ 0.01 are represented by dark gray dots and are putative Cdc5 targets. Within this category, phosphopeptides marked in dark blue belong to previously reported Cdc5 targets and phosphopeptides marked in light blue belong to novel Cdc5 targets further validated in this study. **C.** Volcano plot depicting the differential phosphorylation of nucleoporin peptides in cells ectopically expressing Cdc5 or Cdc5^{KD}. The data was plotted as in (B), but with phosphopeptides colored according to the subcomplex that the nucleoporin belongs to. **D.** Examples of phosphopeptides in Slk19, Shp1, Swi6, and Nup60 that either do not change (gray lines) or change (red lines) in abundance upon Cdc5 expression. Phosphopeptide abundance (the average of the measurements from three biological replicates) is plotted upon either *CDC*^{KD} induction (left plot) or *CDC5* induction (right plot). In samples where a peptide could not be detected, data was imputed for that time point and used for plotting and statistical analysis (e.g., see the Slk19 S707 plot upon *CDC*^{KD} induction). Note: In the case of Swi6, the peptide containing phosphorylated S176 is downregulated upon Cdc5 expression. Such downregulation may be a consequence of concurrent phosphorylation of a second/multiple residue(s) in the same peptide, not detected in this study. Therefore, the Cdc5 target site(s) would not be S176, but the additional site(s) in the same peptide. The same effect may be relevant for other disenriched peptides in (B) and (C). **E.** Immunoblots of Nup60-9myc and Cdc5 protein in a meiotic time course (YML6662). Samples were collected in two-hour intervals and cover the full meiotic cell division program. **F.** Immunoblots for Nup60-9myc and Cdc5 protein from either *cdc20-mn* (YML6665) or *cdc20-mn cdc5-mn* (YML6664) cells during metaphase I arrest. **G.** Immunoblots for Nup60-9myc and Cdc5 protein (YML12234) before (0 h – 6 h in SPM) or after (8 h in SPM) treatment (either addition of copper or not) during prophase I arrest (*ndt80Δ*). Cdc5 was under control of the *CUP1* promoter (P_{CUP1}-*CDC5*). **H.** Immunoblots for Nup60-9myc (YML6665) or Nup60^{S89A}-9myc (YML7956) in *cdc20-mn* strains induced to enter meiosis and arrest in metaphase I. For E-H, Crm1 was used as a loading control and the brackets to the right of the blots denote apparent phosphoshifts.

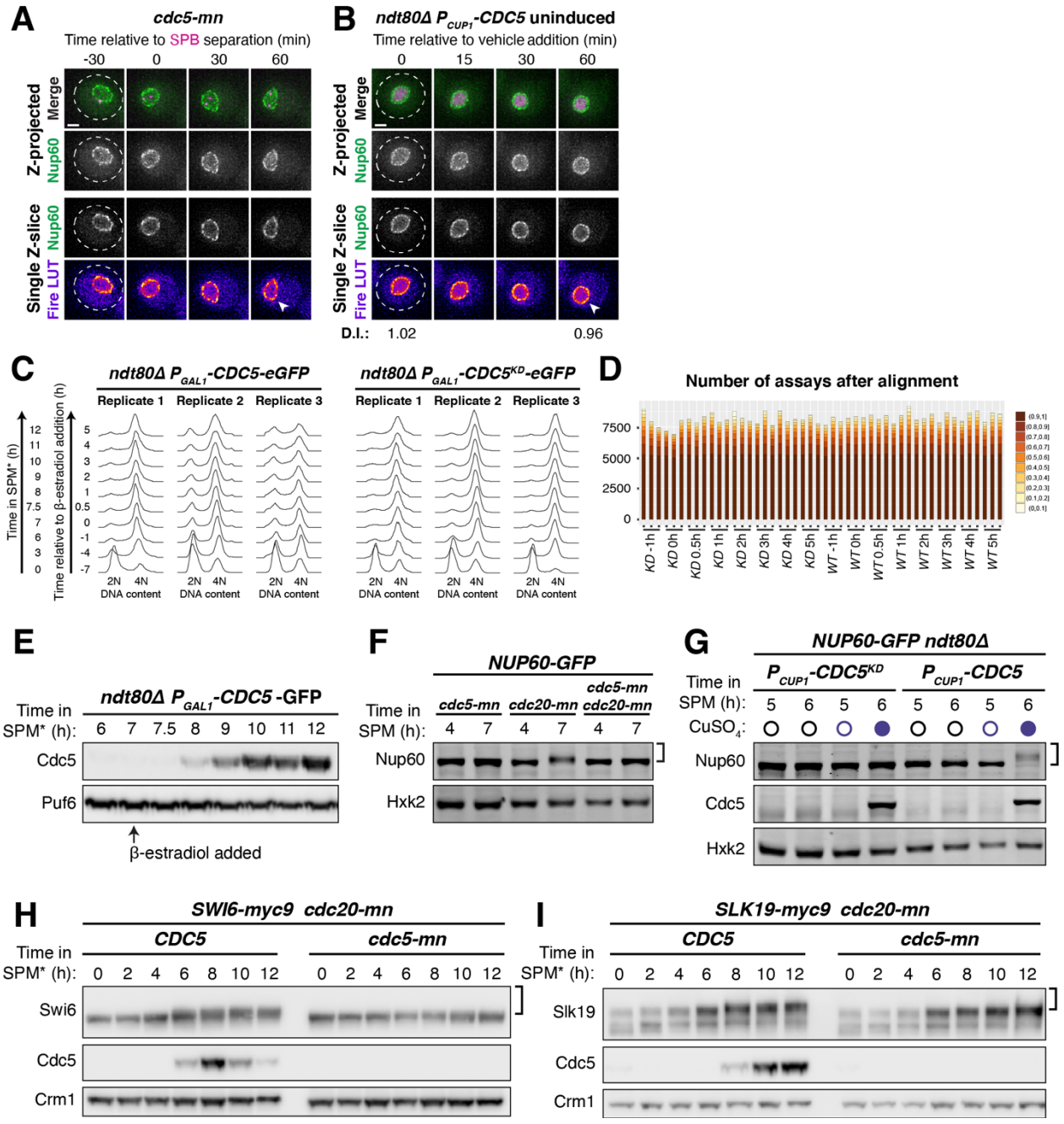

Figure 3.7. Supporting data pertaining to Cdc5-dependent phosphorylation of Nup60 and other novel meiotic targets. A. Montage of a cell with Nup60-GFP, a nuclear basket nucleoporin, and Spc42-mCherry, a spindle pole body component, entering metaphase I arrest caused by *cdc5-mn* (UB29251). **B.** Montage of a cells with Nup60-GFP, a nuclear basket nucleoporin, and Htb1-mCherry, a histone, in prophase I arrest (*ndt80Δ*) with *P*$_{CUP1}$*-CDC5-3xFLAG-10xHis* uninduced (UB29129). Normalized DI values are indicated when calculated (see Figure 3.5H legend for

description of normalization). For A-B, the white arrowheads in the "Fire LUT" images denote nuclei exhibiting Nup60-GFP detachment or nuclei from a relevant control at an equivalent time point. Scale bars, 2 µm. **C.** FACS profiles of DNA content of meiotic time courses used for SWATH MS proteomics in Figure 3.6A-D (Cdc5: YML3993, $Cdc5^{KD}$: YML3994). Three independent replicates are shown for reach strain. **D.** Number of phosphopeptide precursors identified in each sample. The color scale represents the consistency of identification as a fraction over all runs. **E.** Representative immunoblot of Cdc5 expression in cells treated as described in Figure 3.6A. Cells with *P_{GAL1}-CDC5-eGFP* (YML3993) were induced to enter meiosis by transfer to SPM and, after 7h in SPM, treated with 2 µM ß-estradiol to initiate Cdc5 expression. Puf6 was used as a loading control. **F.** Immunoblot for Nup60-GFP before (4 h in SPM) or during (7 h in SPM) metaphase I arrest for the strains imaged in panels 3C-D and S3A (*cdc5-mn*: UB29251*, cdc20-mn*: UB29253, and *cdc5-mn cdc20-mn*: UB29249). Hxk2 was used as a loading control. **G.** Immunoblots for Nup60-GFP and $Cdc5^{KD}$-3xFLAG-10xHis (UB29069) or Cdc5-3xFLAG-10xHis (UB29129) before (5 h in SPM) or after (6 h in SPM) treatment (either addition of copper or not) during prophase I arrest (*ndt80Δ*). The protein samples were collected from the strains imaged in 3F-G and S3B. Hxk2 was used as a loading control. **H.** Immunoblots of Swi6-9myc and Cdc5 in *cdc20-mn* (YML8836) or *cdc20-mn cdc5-mn* (YML8837) strains induced to enter meiosis and arrest in metaphase I. Crm1 was used as loading control. **I.** Immunoblots for Slk19-9myc and Cdc5 in *cdc20-mn* (YML7800) or *cdc20-mn cdc5-mn* (YML7801) cells induced to enter meiosis and arrest in metaphase I. Crm1 was used as loading control. For F-I, the brackets to the right of the blots denote apparent phosphoshifts.

---

meiosis at time points when the Cdc5 protein was expressed (Figure 3.6E). Importantly, Polo kinase activity was both necessary and sufficient for Nup60 phosphorylation (Figures 3.6F-G, 3.7F-G) with Cdc5-dependent phosphorylation coinciding precisely with Nup60-Nup2 detachment from NPCs (compare Figure 3.7F-G with Figure 3.5C-H). As described in detail below, these findings provided an important clue to further investigate how the Polo kinase regulates nuclear basket remodeling in meiosis I.

We note that the SWATH-MS dataset offers a valuable tool to identify previously uncharacterized Polo kinase targets in meiosis (see additional notes regarding data interpretation in Appendix C). As a proof of concept, we confirmed that putative targets Swi6 and Slk19 were modified in a Cdc5-dependent manner during meiosis (Figures 3.6D and 3.7H-I). We predict that the SWATH-MS dataset described here will serve as a broad resource for the study of various other processes regulated by the Polo kinase during meiosis.

3.2.6 Identification of additional phosphorylation sites required for Cdc5-mediated Nup60 detachment

To determine the extent to which the Cdc5-dependent phosphosite Serine 89 contributes meiotic Nup60 phosphorylation, we generated strains expressing a phosphorylation-resistant mutant, *NUP60-S89A-9myc*, at the endogenous locus. The Nup60^{S89A} mutant protein displayed a reduced yet detectable mobility shift (Figure 3.6H), indicating that S89 is phosphorylated but that additional residues may be concurrently modified during meiosis. To identify these additional sites, we took advantage of a second SWATH-MS dataset that characterizes the phosphoproteome during the entire budding yeast meiotic program (Wettstein et al., *in preparation*). This new dataset has comprehensive coverage of the NPC, with a total of 155 phosphopeptides and 106 individual phosphosites for nucleoporins including 20 phosphosites in Nup60.

In the new dataset, S89 phosphorylation peaked during the meiotic divisions (Figure 3.8A, red line), consistent with Cdc5 mediating its modification during a wild type meiosis. Given the well-defined pattern of S89 phosphorylation, we reasoned that Cdc5-responsive phosphorylation sites would likely have a similar temporal profile to S89. This led to the identification of eight additional Nup60 phosphorylation sites exhibiting similar upregulation during meiosis (Figure 3.8A). These sites were located in an N-terminal cluster (T112, S118, S171, S162) and a C-terminal cluster (S371, S374, S394, S395). Many of the phosphosites (T112, S118, S171, S371, S374) exhibited additional signatures of Cdc5-dependence, with low phosphorylation during prophase I arrest (*ndt80Δ*) and high phosphorylation during metaphase I arrest (*cdc20-mn*). Excitingly, the N-terminal phosphosite cluster overlapped with Nup60's helical region (HR), which mediates interaction with the NPC core (Figure 3.8B; Mészáros et al., 2015, Niño et al., 2016). Mapping of the phosphosites on the cryo-EM structure of the budding yeast NPC highlighted that both N- and C-terminal phosphosite clusters were well-positioned to regulate Nup60 binding to the Y-complex (Figure 3.8C; Kim et al., 2018).

To determine whether the identified phosphosites in Nup60 play a role in regulating its detachment from the NPCs, we constructed a series of *NUP60* phosphorylation-resistant mutants tagged with GFP (Figure 3.8B): *NUP60-S89A*, *NUP60-Nterm3A* and *NUP60-Nterm5A*, in which the N-terminal phosphosites were mutated to alanine; *NUP60-Cterm4A*, in which the C-terminal phosphosites were mutated to alanine; and *NUP60-9A* in which both the N- and C-terminal phosphosites were mutated to alanine. Using these alleles, we monitored Nup60 localization and phosphorylation upon ectopic *CDC5* induction during prophase I arrest (*ndt80Δ* background, Figure 3.8D-F). Consistent with our previous data, mutation of the S89 phosphosite alone (Nup60^{S89A}) slightly reduced Nup60 mobility; however, this mutation did not abrogate *CDC5*-dependent Nup60 detachment (Figure 3.8D-F).

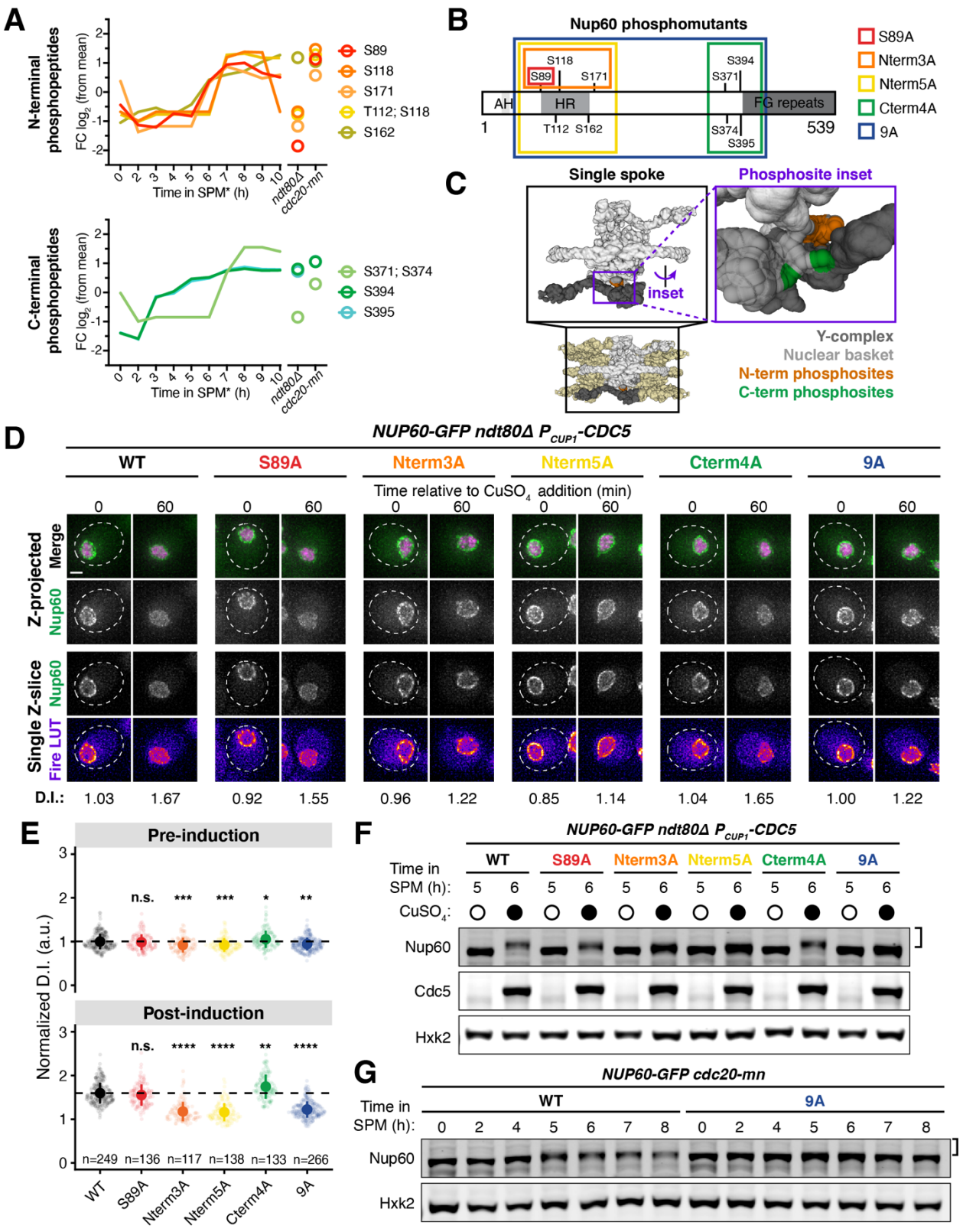
A
N-terminal phosphopeptides
FC log2 (from mean)
Time in SPM* (h)
ndt80Δ cdc20-mn
S89
S118
S171
T112; S118
S162
C-terminal phosphopeptides
S371; S374
S394
S395
B
Nup60 phosphomutants
S89A
Nterm3A
Nterm5A
Cterm4A
9A
AH
HR
FG repeats
1
539
C
Single spoke
Phosphosite inset
inset
Y-complex
Nuclear basket
N-term phosphosites
C-term phosphosites
D
NUP60-GFP ndt80Δ P CUP1 -CDC5
WT
S89A
Nterm3A
Nterm5A
Cterm4A
9A
Time relative to CuSO4 addition (min)
Z-projected Merge
Nup60
Single Z-slice Nup60
Fire LUT
D.I.:
1.03 1.67 0.92 1.55 0.96 1.22 0.85 1.14 1.04 1.65 1.00 1.22
E
Pre-induction
Post-induction
Normalized D.I. (a.u.)
n.s. *** *** * **
n.s. **** **** ** ****
n=249 n=136 n=117 n=138 n=133 n=266
F
NUP60-GFP ndt80Δ P CUP1 -CDC5
Time in SPM (h):
CuSO4:
Nup60
Cdc5
Hxk2
G
NUP60-GFP cdc20-mn
Time in SPM (h):
Nup60
Hxk2

Figure 3.8. Identification of Nup60 phosphosites at the interface with the NPC core that mediate Cdc5-dependent detachment. A. N-terminal and C-terminal Nup60 phosphopeptides that exhibit meiotic upregulation (data from Wettstein et al., *in preparation*). Each line represents an individual phosphopeptide originating from Nup60 protein, measured in 1-hour intervals across the entire meiotic cell division program, as well as in prophase I arrested cells (*ndt80Δ*, 8 h in SPM*) and metaphase I arrested cells (*cdc20-mn*, 10 h in SPM*). $\log_2$ fold change ($\log_2$(FC)) relative to mean expression over all samples of each phosphopeptide is plotted on the y-axis. Average measurement of triplicates is plotted. **B.** Schematic of Nup60 depicting the position of phosphosites relative to known structural features. The phosphomutants generated are indicated by colored boxes. **C.** Visualization of the N-terminal (orange) and C-terminal phosphosites (green) of Nup60 on a cryo-EM structure of the NPC (Kim et al., 2018) visualized using Mol* (Sehnal et al., 2021). **D.** Montages of cells containing different *NUP60-GFP* alleles and *HTB1-mCherry* in a prophase I arrest (*ndt80Δ*) before (5 h in SPM) and after (6 h in SPM) induction of P_{CUP1}*-CDC5-3xFLAG-10xHis*. The following alleles were tested: *NUP60-GFP* (UB29129), *NUP60-S89A-GFP* (UB29560), *NUP60-Nterm3A-GFP* (UB29636), *NUP60-Nterm5A-GFP* (UB29638), *NUP60-Cterm4A-GFP* (UB29562), and *NUP60-9A-GFP* (UB29564). Induction was performed at 5 h in SPM medium with 50 µM $CuSO_4$. **E.** Quantification of Nup60 detachment for the experiment depicted in D. Individual DI values were normalized to the average DI for Nup60-GFP cells at the pre-induction time point (5 h in SPM). Asterisks indicate statistical significance calculated using Dunn's test for multiple comparisons when each allele was compared to wild type for a given time point. Sample sizes (n) are the number of cells quantified for each strain; for Nup60-GFP and Nup60^{9A}-GFP, cells from two independent replicates were pooled. **F.** Immunoblot for different Nup60-GFP alleles and Cdc5-3xFLAG-10xHis before (5 h in SPM) or after (6 h in SPM) copper induction during prophase I arrest (*ndt80Δ*), corresponding to the images in D. Hxk2 was used as a loading control. **G.** Immunoblot for Nup60-GFP (UB29253) or Nup60^{9A}-GFP (UB30438) in *cdc20-mn* background. Hxk2 was used as a loading control. For F-G the brackets to the right of the blots denote apparent phosphoshifts. For each montage, normalized DI values are indicated when calculated. Scale bars, 2 µm.

Strikingly, mutating the additional N-terminal phosphosites (Nup60^{Nterm3A} and Nup60^{Nterm5A}) strongly reduced both Nup60 phosphorylation and detachment (Figure 3.8D-F). In contrast, mutating the C-terminal phosphosites alone did not impair Nup60 phosphorylation or detachment (Nup60^{Cterm4A}). Likewise, we did not observe any additional defects when the N- and C-terminal phospho-mutations were combined (Nup60^{9A}; Figure 3.8D-F). Notably, all phosphorylation-resistant mutants besides *NUP60-Cterm4A* exhibited reduced phosphorylation in a *cdc20-mn* background, suggesting that the same sites are responsible for regulating Nup60 detachment from NPCs during meiosis I (Figures 3.8G, S3.10A, S3.10C, S3.10E, S3.10G). Overall, these data demonstrate that the Polo kinase Cdc5 regulates the

phosphorylation of Nup60's helical region (HR), resulting in Nup60 detachment from NPCs.

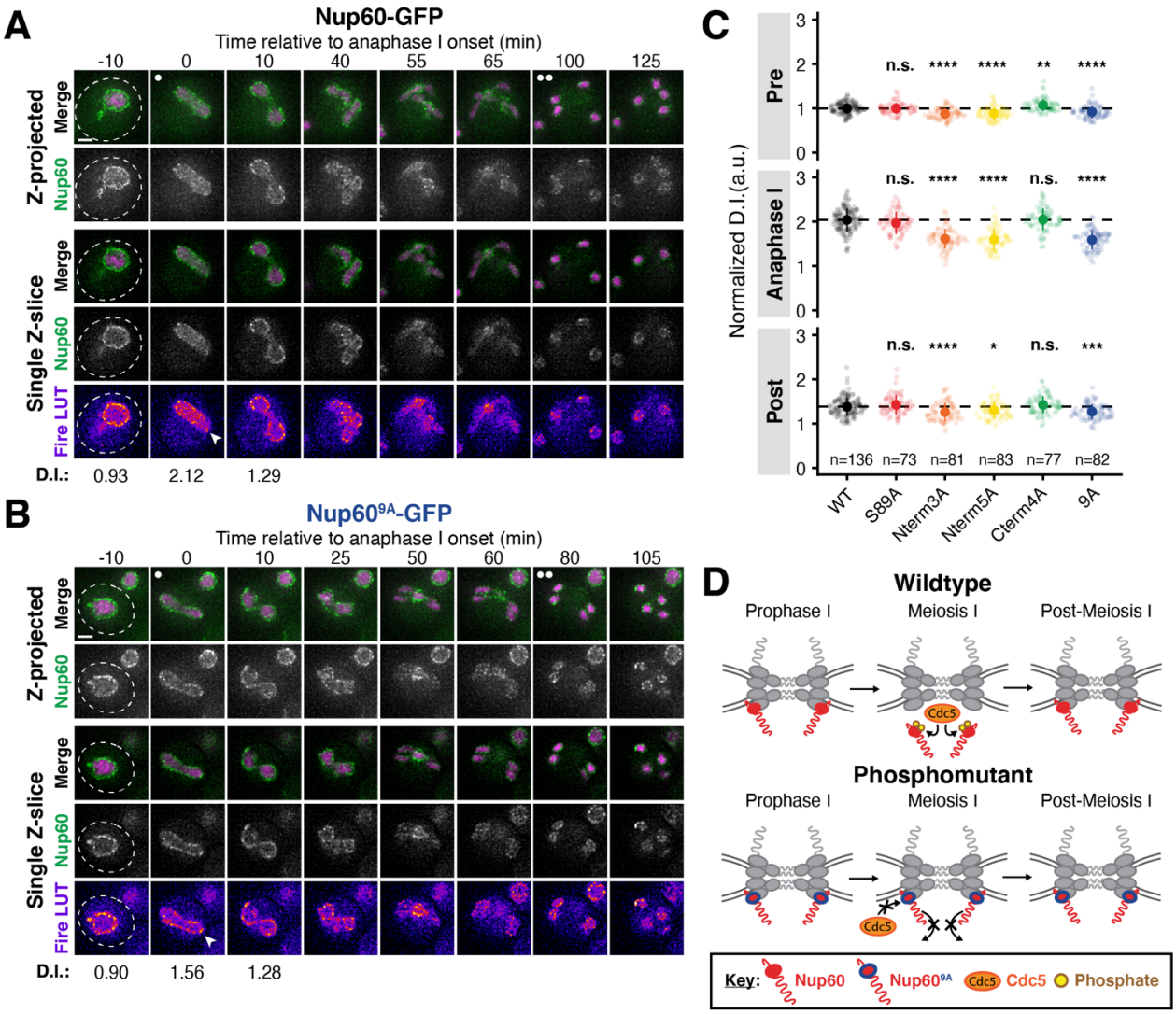

Figure 3.9. Cdc5-dependent Nup60 phosphorylation mediates meiosis I, but not meiosis II, nuclear pore complex remodeling. A-B. Montages of cells with **A.** Nup60-GFP (UB14646) or **B.** Nup60^{9A}-GFP (UB29358) and Htb1-mCherry progressing through meiosis. **C.** Quantification of Nup60 detachment before (-10 min, "Pre"), coincident with (0 min, "Anaphase I"), and after (10 min, "Post") the onset of anaphase I. Individual DI values were normalized to the average DI of Nup60-GFP at the "Pre" time point. Asterisks indicate statistical significance calculated using Dunn's test for multiple comparisons when each allele was compared to Nup60-GFP for a given time point. The dashed lines indicate the average DI for Nup60-GFP for each time point. Sample sizes (n) are the number of cells quantified for each allele; for Nup60-GFP, cells from two independent replicates were pooled. **D.** A schematic that depicts Cdc5-

dependent phosphorylation of Nup60 driving detachment from the NPC during meiosis I in wild type, but not phosphomutant, cells. For all panels, the onset of anaphase I was defined as the Htb1-mCherry chromatin mass exhibiting distortion from a spherical shape consistent with chromosome segregation. For each montage, normalized DI values are indicated when calculated. Scale bars, 2 µm.

3.2.7 Cdc5-dependent Nup60 phosphorylation mediates meiosis I NPC remodeling

Since Nup60 and Nup2 detach during both meiosis I and meiosis II, it was unclear whether similar mechanisms underly both NPC remodeling events. Cdc5 is present during both meiotic divisions, but individual Cdc5 substrates can be targets of phosphorylation exclusively during meiosis I (Attner et al., 2013). To elucidate the role of Cdc5-driven Nup60 phosphorylation in NPC plasticity, we assessed localization of the Nup60-GFP phosphorylation-resistant mutants by live-cell imaging throughout meiosis (Figure 3.9). During meiosis I, we observed significantly reduced detachment for the same phosphomutants that exhibited reduced phosphorylation and detachment upon ectopic *CDC5* expression (Figures 3.8, 3.9A-C, 3.10B, 3.10D, 3.10F, 3.10H). This confirms that Cdc5-dependent phosphorylation drives the meiosis I NPC remodeling event by disrupting Nup60 interaction with the NPC core (Figure 3.9D). During meiosis II, however, we found that Nup60 detachment and return to gamete nuclei occurred normally for all phosphorylation-resistant mutants tested (Figures 3.9A-C, 3.10B, 3.10D, 3.10F, 3.10H). Nup60 detachment is therefore regulated by different means during meiosis I and II. These data indicate that the two meiotic NPC remodeling events are mechanistically separable, further establishing them as distinct cellular phenomena.

3.2.8 The lipid-binding N-terminus of Nup60 is required for NPC reassociation

Nup60 detachment during meiosis I is rapidly followed by its reassociation with the NPC (Figure 3.1C-D). While we had gained mechanistic insight into how Nup60's interaction with the NPC is disrupted by Cdc5-dependent phosphorylation, it remained unclear what structural features facilitate its reattachment to the NPC. Two N-terminal regions of Nup60 mediate its recruitment to the nuclear periphery: an amphipathic-helix (AH), which binds directly to the inner nuclear membrane, and a helical region (HR), which interacts with the NPC core itself (Mészáros et al., 2015). Since Cdc5-dependent phosphorylation likely disrupts binding of the helical region to the Y-complex, we hypothesized that the amphipathic helix may become crucial in mediating NPC reassembly after meiosis I. To test this hypothesis, we generated a mutant in which the N-terminal region of Nup60 spanning its amphipathic helix was deleted (*nup60-ΔAH [nup60-Δ2-47]*, Figure 3.11A; Mészáros et al., 2015). Prior to the

meiotic divisions, Nup60$^{\Delta AH}$-GFP largely localized to the nuclear periphery, exhibiting only minor nucleoplasmic mislocalization (~45 min, Figure 3.11B-C).

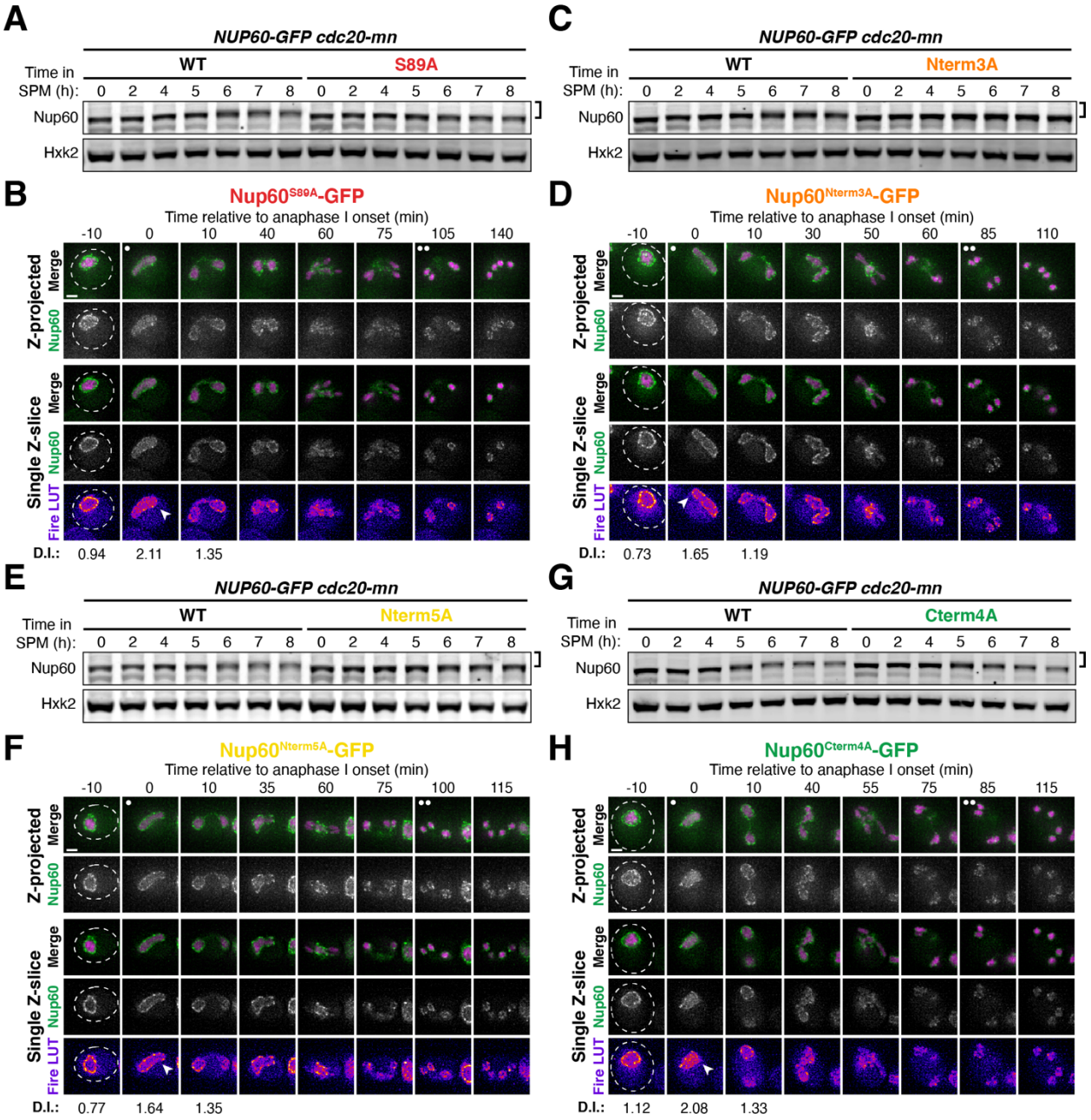

Figure 3.10. Supporting data pertaining to Nup60 phosphomutant localization and phosphorylation. A, C, E, G. Immunoblots of different Nup60 phosphomutants compared to Nup60-GFP (UB29253) in *cdc20-mn* background. Hxk2 was used as a loading control. The phosphomutants tested are: **A.** Nup60^{S89A}-GFP (UB30327); **C.** Nup60^{Nterm3A}-GFP (UB30329); **E.** Nup60^{Nterm5A}-GFP (UB30331); and **G.** Nuup60^{Cterm4A}-GFP (UB30333). The Nup60-GFP control for A, C, and E are all re-

runs of the same replicate; the Nup60-GFP control for G is a re-run of the replicate from Figure 5G. The brackets to the right of the blots denote apparent phosphoshifts. **B, D, F, H.** Montages of cells with different fluorescently tagged Nup60 phosphomutants and Htb1-mCherry progressing through meiosis. The alleles visualized are: **B.** Nup60^{S89A}-GFP (UB29265); **D.** Nup60^{Nterm3A}-GFP (UB29441); **F.** Nup60^{Nterm5A}-GFP (UB29443); and **H.** Nup60^{Cterm4A}-GFP (UB29267). For panels B, D, F, and H, the white arrowheads in the "Fire LUT" images denote nuclei at the onset of anaphase I, the stage when Nup60-Nup2 detachment is observed. Scale bars, 2 µm

---

During meiosis I, Nup60$^{\Delta AH}$-GFP detached from the NPC core similarly to Nup60-GFP (-10 min and 0 min, Figure 3.11B-C). However, instead of subsequently reattaching to NPCs, Nup60$^{\Delta AH}$-GFP remained largely nucleoplasmic, with only a small fraction returning to the nuclear periphery (+10 min, Figure 3.11B-C). Strikingly, the nucleoplasmic localization of Nup60$^{\Delta AH}$-GFP persisted during both meiotic divisions and during subsequent gamete formation (Figure 3.11C). A point mutation in the amphipathic helix that renders it unable to bind the nuclear envelope (*nup60-I36R*; Mészáros et al., 2015) also exhibited impaired NPC reassociation (Figure 3.11D), confirming that the observed defect was due to disruption of lipid-binding. Nup60 protein levels were reduced in both nup*60-ΔAH and nup60-I36R* mutants during the meiotic divisions, suggesting that binding to the nuclear envelope or NPCs is important for Nup60 stability (Figure 3.12A-C). The meiotic program is therefore a cellular context in which lipid-binding by a nuclear basket nucleoporin is essential for proper NPC organization.

The meiotic role of Nup60's amphipathic helix was specific, since removing a similar amphipathic helix in Nup1 (*nup1-ΔAH*) had no effect on meiotic localization (Figure 3.12D-E). We hypothesized that the observed specificity stemmed from the amphipathic helix of Nup60 becoming essential for its interaction with NPCs downstream of Cdc5-dependent detachment. To directly assess this prediction, we monitored Nup60$^{\Delta AH}$-GFP dynamics during metaphase I arrest with or without Cdc5 activity (Figure 3.11E). Nup60$^{\Delta AH}$-GFP exhibited significant detachment from the nuclear periphery and increased phosphorylation in *cdc20-mn* cells, but not in *cdc5-mn cdc20-mn* cells (Figure 3.11E-G). *cdc5-mn* single mutants were indistinguishable from *cdc5-mn cdc20-mn* double mutants (Figure 3.11E-G). Ectopic *CDC5* expression was also sufficient to trigger complete detachment of Nup60$^{\Delta AH}$-GFP from the nuclear periphery during prophase I (Figure 3.12F-H). Cdc5-mediated disruption of the interaction between the helical region and the NPC core therefore results in the amphipathic helix becoming the primary means of Nup60 association with the NPC. Consistent with the amphipathic helix and helical region acting in parallel to coordinate proper Nup60 localization, the extent of detachment in *nup60-ΔAH cdc20-mn* cells was more profound than what we observed for *NUP60 cdc20-mn* cells (compare Figure 3.11E-G with Figure 3.5C-E). Our data reveal that the N-terminus of Nup60 facilitates both detachment and reattachment with the NPC core during

meiosis I: Polo kinase-dependent phosphorylation of the helical region results in Nup60 detachment and redocking by the amphipathic helix results in Nup60 reattachment (Figure 3.11H).

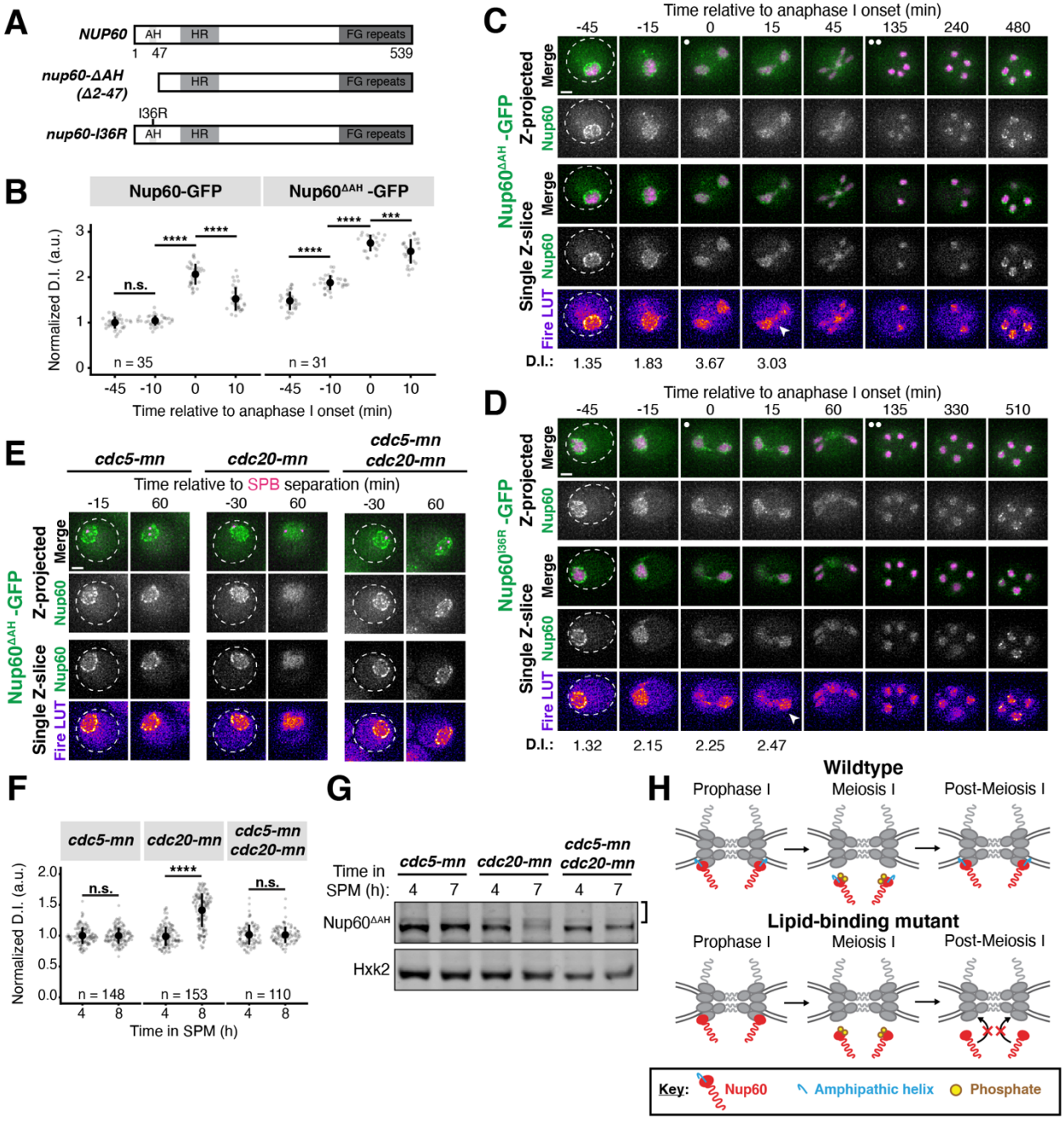

Figure 3.11. The lipid-binding N-terminus of Nup60 mediates return to the nuclear periphery after meiotic detachment. A. Schematic of different *NUP60* lipid-binding mutants generated: *nup60-ΔAH*, which lacks its N-terminal amphipathic helix, and *nup60-I36R*, containing a point mutation in its N-terminal amphipathic helix. **B.**

Quantification of Nup60 detachment for Nup60-GFP (UB14646) and Nup60$^{\Delta AH}$-GFP (UB25731) at -45 min, -10 min, 0 min, and +10 min relative the onset of anaphase I. Individual DI values were normalized to the average DI of Nup60-GFP at the -45 min time point. Asterisks indicate statistical significance calculated using Wilcoxon signed-rank tests when each time point was compared to the previous time point for a given allele. Sample sizes (n) are the number of cells quantified for each allele. **C-D.** Montages of cells with **C.** Nup60$^{\Delta AH}$-GFP (UB25731) or **D.** Nup60^{I36R}-GFP (UB27189) and Htb1-mCherry progressing through meiosis. For C-D, the white arrowheads in the "Fire LUT" images denote nuclei after anaphase I that continue to exhibit Nup60 detachment. **E.** Montages of cells with Nup60$^{\Delta AH}$-GFP and Spc42-mCherry entering metaphase I arrest in the following strains: *cdc5-mn* (UB29257), *cdc20-mn* (UB29259), or *cdc5-mn cdc20-mn* (UB29255). **F.** Immunoblot for Nup60$^{\Delta AH}$-GFP before (4 h in SPM) or during (7 h in SPM) metaphase I arrest for the strains in panels E. Hxk2 was used as a loading control. The bracket to the right of the blot denotes the apparent phosphoshift. **G.** Quantification of Nup60$^{\Delta AH}$-GFP detachment before (4 h in SPM) or during (8 h in SPM) metaphase I arrest in *cdc5-mn* (UB28494), *cdc20-mn* (UB28213), and *cdc5-mn cdc20-mn* (UB28616) cells. Htb1-mCherry, a histone, was used to define the nucleoplasm; due to slightly altered meiotic progression with Htb1-mCherry, a wild type strain (UB25731) was used to assess sporulation progression and determine comparable timing to Spc42-mCherry containing strains. Asterisks indicate significance determined using Wilcoxon signed-rank tests when metaphase I arrest (8 h in SPM) values were compared to pre-meiotic entry (4 h in SPM) values for each genetic background. **H.** A schematic that depicts the role of Nup60's amphipathic helix in mediating return to the NPC after meiosis I detachment. For all panels, the onset of anaphase I was defined as the Htb1-mCherry chromatin mass exhibiting distortion from a spherical shape consistent with chromosome segregation. For each montage, normalized DI values are indicated when calculated. Scale bars, 2 µm.

3.2.9 Nup60 reattachment is required for proper gamete nuclear basket organization

Nup60 is a key subunit of the nuclear basket, responsible for recruiting both Nup2 and Mlp1 to NPCs (Dilworth et al., 2001; Feuerbach et al., 2002). We therefore hypothesized that reassociation of Nup60 with the NPCs might be necessary for proper nuclear basket organization in gamete nuclei. Accordingly, all the nuclear basket subunits that we tested were mislocalized in *nup60-ΔAH* gametes (Figures 3.13 and 3.14). Nup2-GFP phenocopied Nup60$^{\Delta AH}$-GFP, remaining nucleoplasmic instead of returning to the gamete nuclear periphery (Figure 3.14A-B). Nup1-GFP was barely detectable at the gamete nuclear periphery after meiosis II (Figure 3.13A-B). Mlp1-GFP exhibited nucleoplasmic mislocalization and often formed puncta akin to those observed in *nup60Δ* cells, structural abnormalities that persisted for hours after the meiotic divisions (Feuerbach et al., 2002; Figure 3.13D-F). Mlp1

misorganization was similar in *nup60-I36R* gametes (Figure 3.14C-E), confirming that the basket defects observed were due to defective Nup60 reassociation with the nuclear periphery. Proper execution of meiotic NPC remodeling is therefore required for nuclear basket organization in gametes.

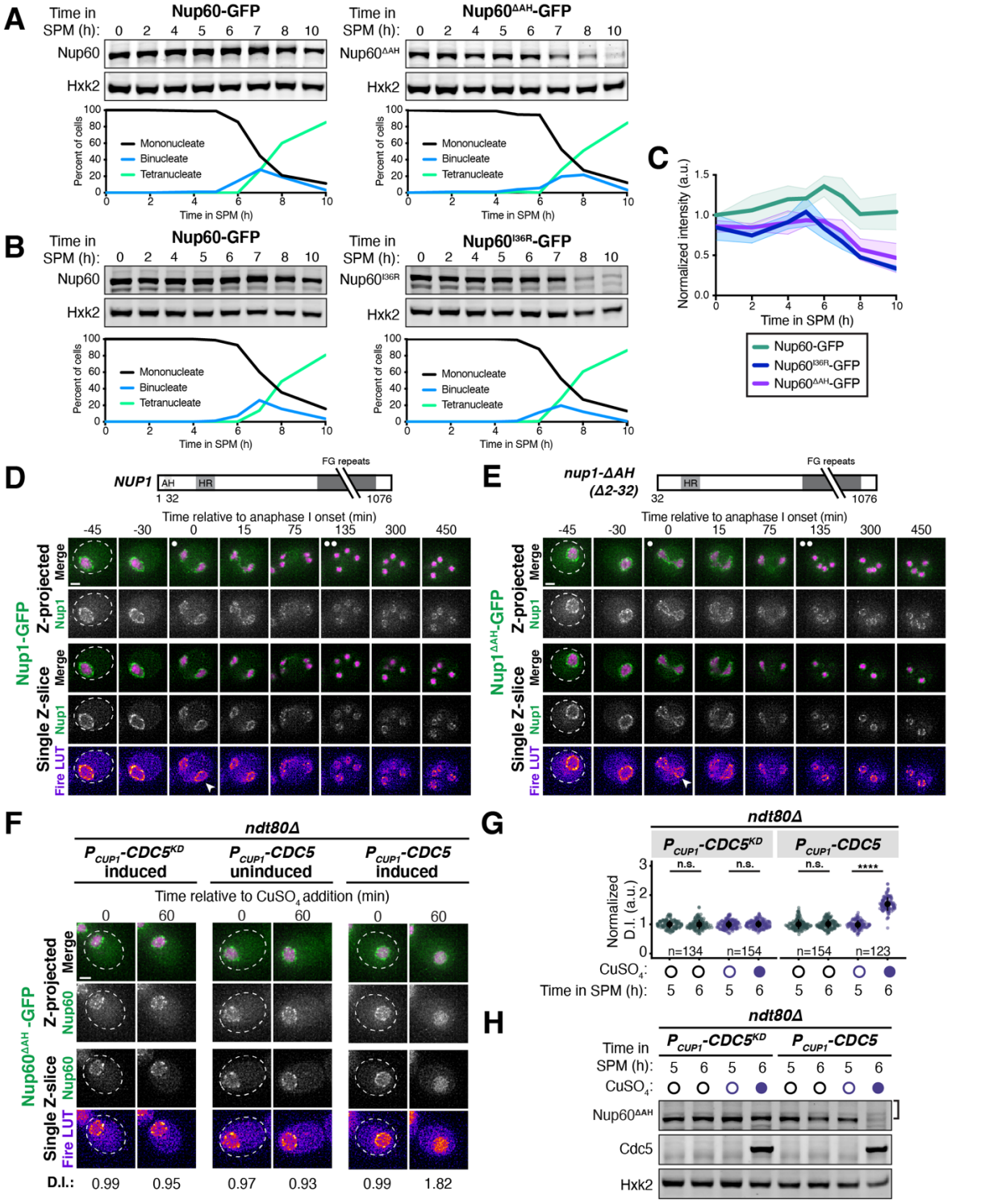

Figure 3.12. Supporting data pertaining to a meiotic role for the Nup60 amphipathic helix. A. Immunoblots of Nup60-GFP (UB14646) and Nup60$^{\Delta AH}$-GFP (UB25731) in cells progressing through meiosis. **B.** Immunoblots of Nup60-GFP (UB14646) and Nup60^{I36R}-GFP (UB27189) in cells progressing through meiosis. For A-B, Hxk2 was used as a loading control and meiotic staging corresponding to the displayed blots was assessed using Htb1-mCherry. **C.** Quantification of different Nup60 mutant protein levels during meiosis, corresponding to A-B. Background subtracted Nup60 intensity was divided by Hxk2 intensity to control for loading and then normalized to Nup60-GFP levels at 0 h in SPM (using the control run on the same blot). For Nup60-GFP, the mean ± standard deviation (shaded range) of four independent biological replicates is displayed. For Nup60$^{\Delta AH}$-GFP and Nup60^{I36R}-GFP, the mean ± range (shaded area) of two independent biological replicates is displayed. **D-E.** Montages of cells with either **D.** Nup1-GFP (UB15303) or **E.** Nup1$^{\Delta AH}$-GFP (UB25727) and Htb1-mCherry going through meiosis. Schematics of *NUP1* and *nup1-ΔAH*, which lacks its N-terminal amphipathic helix, are displayed above their respective montages. For panels D-E, the white arrowheads in the "Fire LUT" images denote nuclei during meiosis I, a time point when Nup60$^{\Delta AH}$ detachment is apparent. **F.** Montages of cells with Nup60$^{\Delta AH}$-GFP and Htb1-mCherry exposed to different Cdc5 treatments in prophase I arrest (*ndt80Δ*): *P$_{CUP1}$-CDC5^{KD}-3xFLAG-10xHis* induced (UB29073), *P$_{CUP1}$-CDC5-3xFLAG-10xHis* uninduced (UB29071), and *P$_{CUP1}$-CDC5-3xFLAG-10xHis* induced (UB29071). Induction of Cdc5 protein was performed at 5 h in SPM with 50 µM $CuSO_4$. **G.** Quantification of Nup60$^{\Delta AH}$ detachment for the experiment depicted in F. Individual DI values were normalized to the average DI for uninduced *P$_{CUP1}$-CDC5^{KD}-3xFLAG-10xHis* cells at the pre-induction time point (5 h). Asterisks indicate statistical significance calculated using a Wilcoxon signed-rank test when post-induction (6 h in SPM) values were compared to pre-induction (5 h in SPM) values for each treatment regimen. Sample sizes (n) are the number of cells quantified for each treatment regimen. **H.** Immunoblots for Nup60$^{\Delta AH}$-GFP and Cdc5^{KD}-3xFLAG-10xHis (UB29073) or Cdc5-3xFLAG-10xHis (UB29071) before (5 h in SPM) or after (6 h in SPM) treatment (either addition of copper or not) during prophase I arrest (*ndt80Δ*), corresponding to the images in F. Hxk2 was used as a loading control. The bracket to the right of the blot denotes the apparent phosphoshift. For each montage, normalized DI values are indicated when calculated. Scale bars, 2 µm.

3.2.10 Meiotic dynamics reveal underlying principles of nuclear basket organization

Intriguingly, the meiotic phenotypes displayed by basket nucleoporins in *nup60-ΔAH* cells were suggestive of previously unknown organizational principles for the nuclear basket. Nup1, for example, appears to partially rely on Nup60 for its localization. Even before the meiotic divisions, Nup1 localization to the nuclear periphery was reduced in *nup60-ΔAH* mutants (Figure 3.13C). This dependence on Nup60 might

also explain the partial detachment of Nup1 from the nuclear periphery during meiosis I (Figure 3.1C). Most strikingly, Mlp1 remained peripheral during meiosis I after Nup60$^{\Delta AH}$ became entirely nucleoplasmic, despite Nup60 being required for Mlp1 recruitment to the NPC (Figure 3.13E-F). Mlp1 only began to exhibit mislocalization after it detached from the NPC core during meiosis II (Figure 3.13E-F). This led us to hypothesize that Nup60 has two separate roles in organizing nuclear basket nucleoporins: (1) recruitment of basket nucleoporins to the NPCs, as seen for both Nup2 and Mlp1, and (2) retention of basket nucleoporins at the NPCs, as seen for Nup2 but not Mlp1 (Figure 3.15A). This model could also explain how Mlp1, but not Nup2, remains associated with NPCs when Nup60 detaches during meiosis I (Figure 3.3G).

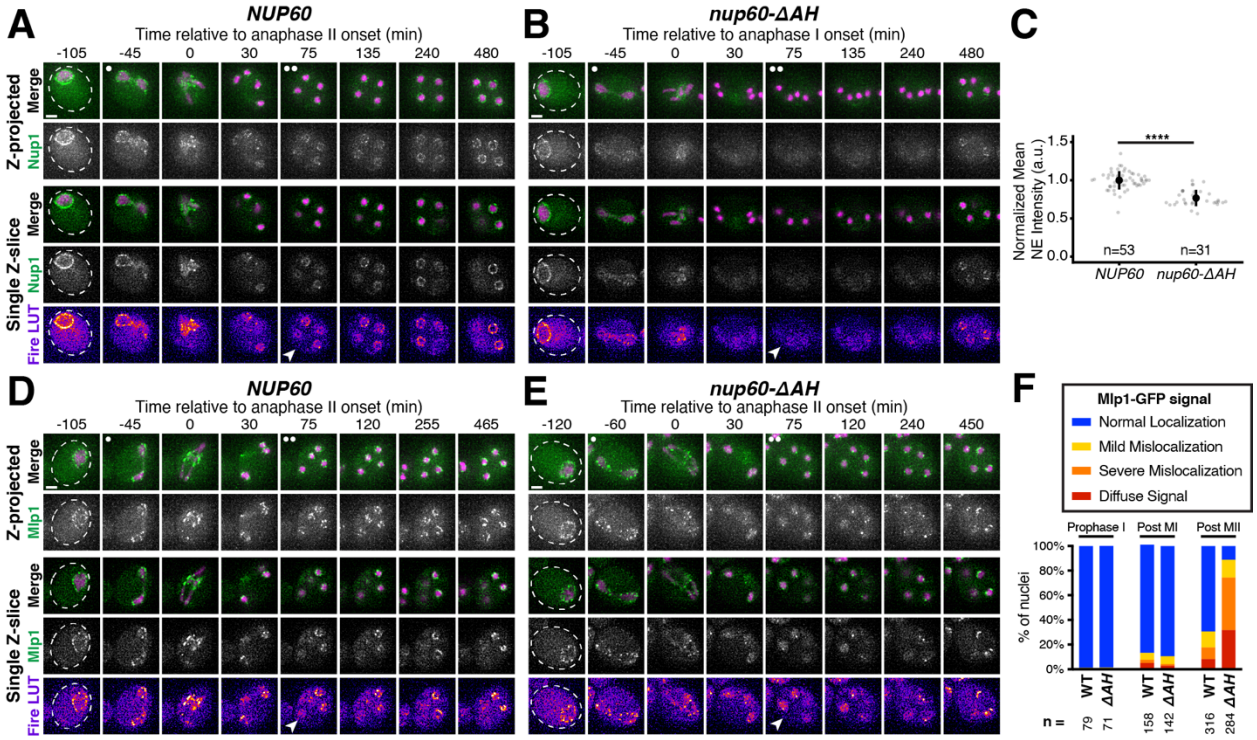

Figure 3.13. Peripheral Nup60 is required for proper gamete nuclear basket organization. A-B. Montages of cells with Nup1-GFP, a nuclear basket nucleoporin, and Htb1-mCherry, a histone, progressing through meiosis in either **A.** a *NUP60* (UB15303) or **B.** a *nup60-ΔAH* (UB30628) genetic background. **C.** Quantification of average nuclear envelope intensity of Nup1-GFP during prophase I (defined as one hour prior to the anaphase I, the presence of two clear Htb1-mCherry lobes) in *NUP60* and *nup60-ΔAH* cells, as shown in A-B. Individual intensity values were normalized to the average nuclear envelope intensity in *NUP60* cells. Asterisks indicate significance determined using a Wilcoxon rank sum test. Sample sizes (n) are the number of cells quantified in each background. **D-E.** Montages of cells with Mlp1-GFP, a nuclear basket nucleoporin, and Htb1-mCherry, a histone, progressing

through meiosis in either **D.** a *NUP60 (*UB14648) or **E.** a *nup60-ΔAH* (UB30632) genetic background. **F.** Quantification of Mlp1-GFP organization for the strains in D-E during prophase I (defined as an hour before the post-MI time point), post-MI (defined as the presence of two clear Htb1-mCherry lobes), and post-MII (defined as 2 h after the presence of four clear Htb1-mCherry lobes). Sample sizes (n) indicate the number of nuclei scored for Mlp1 organization. For panels A-B and D-E, the white arrowheads in the "Fire LUT" images denote cells after anaphase II when gamete nuclear basket organization or misorganization is apparent. Scale bars, 2 µm.

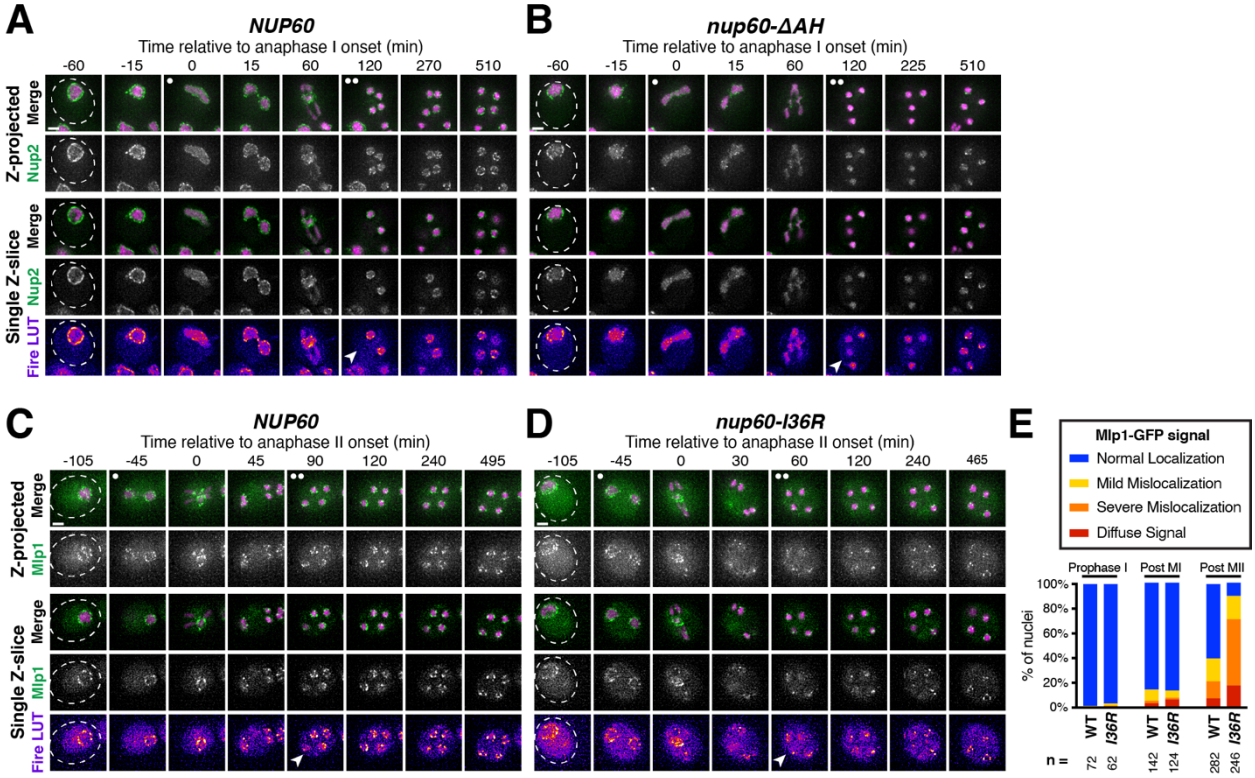

Figure 3.14. Supporting data pertaining to the role of Nup60 in gamete nuclear basket organization. A-B. Montages of cells with Nup2-GFP, a nuclear basket nucleoporin, and Htb1-mCherry, a histone, progressing through meiosis in either **A.** a *NUP60* (UB15305) or **B.** a *nup60-ΔAH* (UB30630) genetic background. **C-D.** Montages of cells with Mlp1-GFP, a nuclear basket nucleoporin, and Htb1-mCherry, a histone, progressing through meiosis in either **C.** a *NUP60* (UB14648) or **D.** a *nup60-I36R* (UB30640) genetic background. **E.** Quantification of Mlp1-GFP organization for the strains in C-D during prophase I (defined as an hour before the post-MI time point), post-MI (defined as the presence of two clear Htb1-mCherry lobes), and post-MII (defined as 2 h after the presence of four clear Htb1-mCherry lobes). Sample sizes (n) indicate the number of nuclei scored for Mlp1 organization. For panels A-D, the white arrowheads in the "Fire LUT" images denote cells after

anaphase II when gamete nuclear basket organization or misorganization is apparent. Scale bars, 2 μm.

To directly test this model, we monitored Mlp1-GFP and Nup2-GFP localization upon different Nup60 conditional depletion regimens. We generated strains with an auxin-inducible degron fused to Nup60 (Nup60-3V5-IAA17) as well as a copper-inducible F-box receptor (P_{CUP1}-*osTIR1*^{F74G}), allowing us to achieve rapid depletion of Nup60 in both mitotic and meiotic cells (Figure 3.15B; Yesbolatova et al., 2020). If Nup60 is required for nuclear basket recruitment to the NPCs, then constitutive depletion in mitotic cells should result in mislocalization of newly synthesized Mlp1 and Nup2 (Figure 3.15A). Indeed, both Mlp1 and Nup2 exhibited mislocalization upon constitutive mitotic depletion, similar to that observed in *nup60Δ* cells (Figure 3.15C-D, 3.15F-G). If Nup60 is required for retention of basket nucleoporins, then transient depletion should also result in rapid mislocalization, since Mlp1 and Nup2 would no longer be anchored to the NPCs. To ensure that the cells were matched for meiotic stage, we induced transient depletion during prophase I arrest (*ndt80Δ* background). We found that, while Nup2 rapidly became nucleoplasmic upon Nup60 depletion, Mlp1 was retained at the nuclear periphery for hours (Figure 3.15E, 3.15H). Mlp1 can therefore remain associated with the NPC core independently of Nup60 after its initial recruitment. Moreover, retention of Mlp1 upon Nup60 depletion suggests that association of Mlp1 with the NPC core is very stable, as it remained perinuclear for hours without any Nup60-mediated recruitment (Figure 3.15H). The distinct organization of Mlp1 within the nuclear basket explains how the two modes of NPC remodeling observed during budding yeast meiosis are possible.

3.2.11 Meiotic nuclear pore complex remodeling is conserved in *S. pombe*

Our work established that the nuclear basket displays extensive remodeling during budding yeast meiosis; the extent to which basket remodeling is conserved remained unknown (Figure 3.3G). To address this question, we monitored nuclear basket dynamics in the fission yeast *Schizosaccharomyces pombe* (Sp), which is highly diverged from the budding yeast *Saccharomyces cerevisiae* (Sc; Sipiczki, 2000). *S. pombe* cells do not form a nuclear envelope compartment akin to the GUNC and their gametes inherit the NPC core during meiosis (Asakawa et al., 2010). Excitingly, SpNup60 (the ortholog of ScNup60) and SpNup61 (the ortholog of ScNup2) both detached from the nuclear periphery during meiosis I with similar timing to that observed in *S. cerevisiae* (Figure 3.16A-C). On the other hand, SpNup124 (the ortholog of ScNup1), SpNup211 (the ortholog of ScMlp1 and ScMlp2), and SpAlm1 (a putative Tpr-like nucleoporin without an *S. cerevisiae* ortholog) all remained associated with the NPC throughout meiosis I (Figures 3.16D-E, 3.17A). The transmembrane nucleoporin SpPom34 (the ortholog of ScPom34) also remained peripheral, consistent with the core remaining intact during partial basket detachment (Figure 3.16F). Together, these data suggest that the meiosis I NPC

remodeling event is conserved and occurs independent of NPC sequestration to the GUNC.

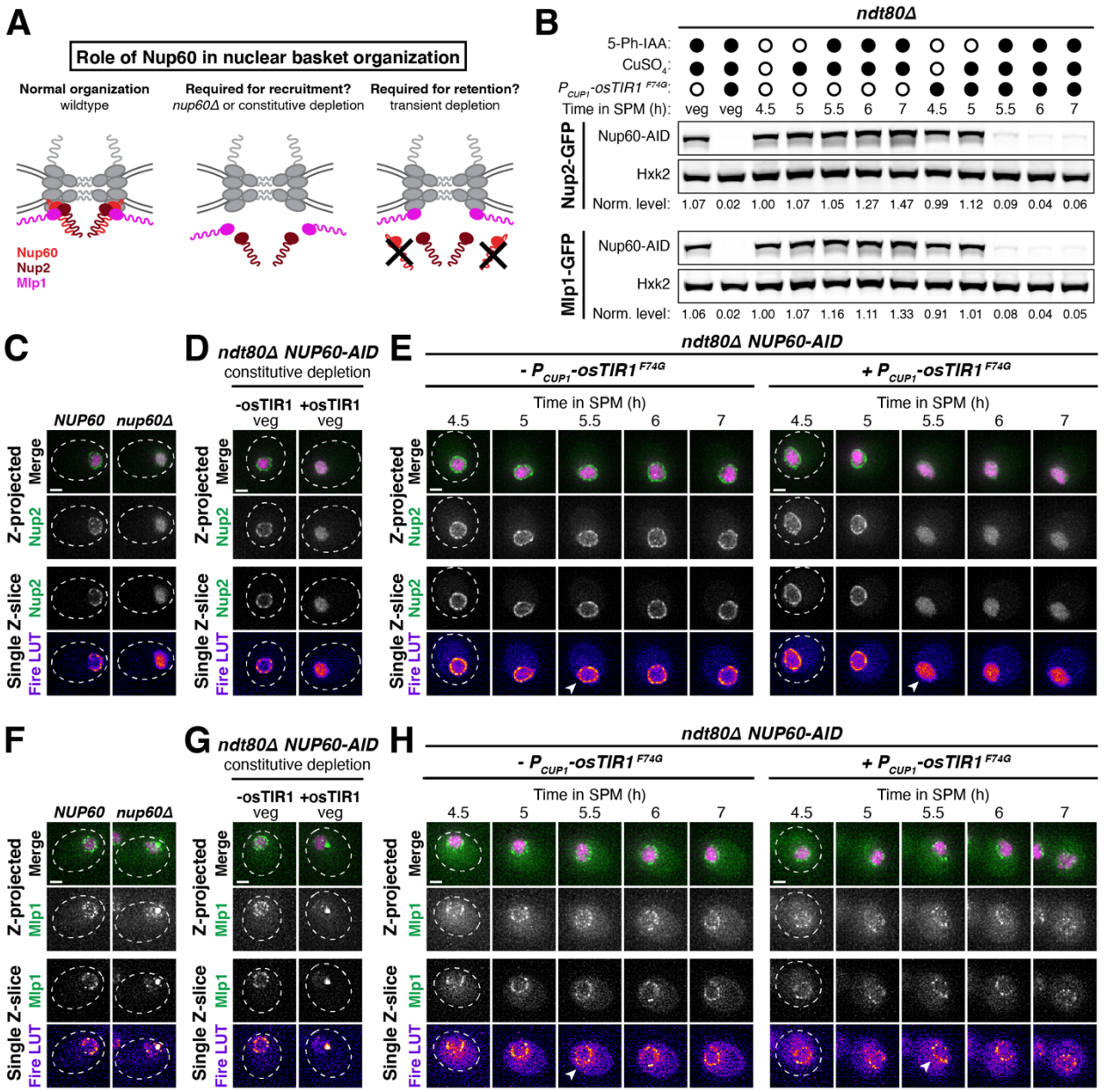

Figure 3.15. Nup60 is not required for the retention of Mlp1 at the nuclear periphery, explaining differences in the meiotic dynamics of basket nucleoporins. A. Schematic depicting a hypothesis for two distinct roles of Nup60 in nuclear basket organization: (1) a role in recruitment (for both Mlp1 and Nup2), tested by monitoring nucleoporin localization in a *nup60Δ* background or upon constitutive Nup60 depletion using the *NUP60-AID* allele, and (2) a role in retention (for Nup2, but not Mlp1), tested by monitoring nucleoporin localization upon transient Nup60 depletion using the

NUP60-AID allele. **B.** Immunoblot of Nup60-3V5-IAA17 (Nup60-AID) levels in strains with Nup2-GFP or Mlp1-GFP, in the absence or presence of P_{CUP1}-*osTIR1-F74G*. (Nup2-GFP: -osTIR1 = UB32240 and +osTIR1 = UB32238; Mlp1-GFP: -osTIR1 = UB32248 and +osTIR1 = UB32246). Hxk2 was used as a loading control. Vegetative depletion was induced with 50 µM $CuSO_4$ and 100 µM 5-Ph-IAA immediately upon inoculation of a logarithmic YPD culture at 0.25 OD/mL and continued for 10 h. For meiotic depletion, cells were maintained in prophase I arrest (*ndt80Δ*), and depletion was induced by adding 50 µM $CuSO_4$ at 4.5 h in SPM and 100 µM 5-Ph-IAA at 5 h in SPM. Background subtracted Nup60 protein levels were divided by Hxk2 levels to control for loading and then normalized to the -osTIR1 strain at 4.5 h in SPM. **C.** Nup2-GFP localization in *NUP60* (UB15305) and *nup60Δ* (UB31600) cells from a saturated YPD culture. **D.** Nup2-GFP localization in -osTIR1 (UB32240) or +osTIR1 (UB32238) cells from a saturated YPD culture after constitutive Nup60 depletion. **E.** Nup2-GFP localization in -osTIR1 (UB32240) or +osTIR1 (UB32238) cells before and after Nup60 depletion during prophase I arrest. **F.** Mlp1-GFP localization in *NUP60* (UB14648) and *nup60Δ* (UB31262) cells from a saturated YPD culture. **G.** Mlp1-GFP localization in -osTIR1 (UB32248) or +osTIR1 (UB32246) cells from a saturated YPD culture after constitutive Nup60 depletion. **H.** Mlp1-GFP localization in -osTIR1 (UB32248) or +osTIR1 (UB32246) cells before and after Nup60 depletion during prophase I arrest. For panels E and H, the white arrowheads in the "Fire LUT" images denote nuclei at the time point when Nup60-AID was largely depleted in +osTIR1 strains. Scale bars, 2 µm.

During meiosis II, SpNup60 and SpNup61 again detached from the nuclear periphery and SpPom34 remained associated with the NPC (Figure 3.17B-C, 3.17G). However, unlike in *S. cerevisiae*, SpNup124, SpAlm1, and SpNup211 did not detach (Figure 3.17D-F). The meiosis II NPC remodeling event is therefore less well conserved and its relationship to GUNC formation remains unclear. Importantly, since the same nuclear basket nucleoporins detach from the NPC with similar timing in both *S. pombe* and *S. cerevisiae*, the organizational principles of the nuclear basket uncovered in this study seem to be conserved across four hundred million years of evolution.

3.3 Discussion

In this study, we provide key mechanistic insights into two distinct NPC remodeling events in budding yeast meiosis (Figure 3.3G). During meiosis I, two nuclear basket nucleoporins – Nup60 and Nup2 – transiently dissociate from NPCs. The Polo kinase Cdc5 drives detachment of Nup60 and Nup2 from the NPCs, via developmentally programmed phosphorylation at the interface between Nup60 and the Y-complex. Nup60 and Nup2 subsequently reassociate with NPCs in a manner dependent on the lipid-binding amphipathic helix of Nup60. During meiosis II, the entire nuclear basket detaches from the NPC core and returns to gamete nuclei, avoiding

sequestration to the GUNC. Nuclear basket organization is therefore subject to extensive plasticity during gametogenesis, with potential implications for gamete health.

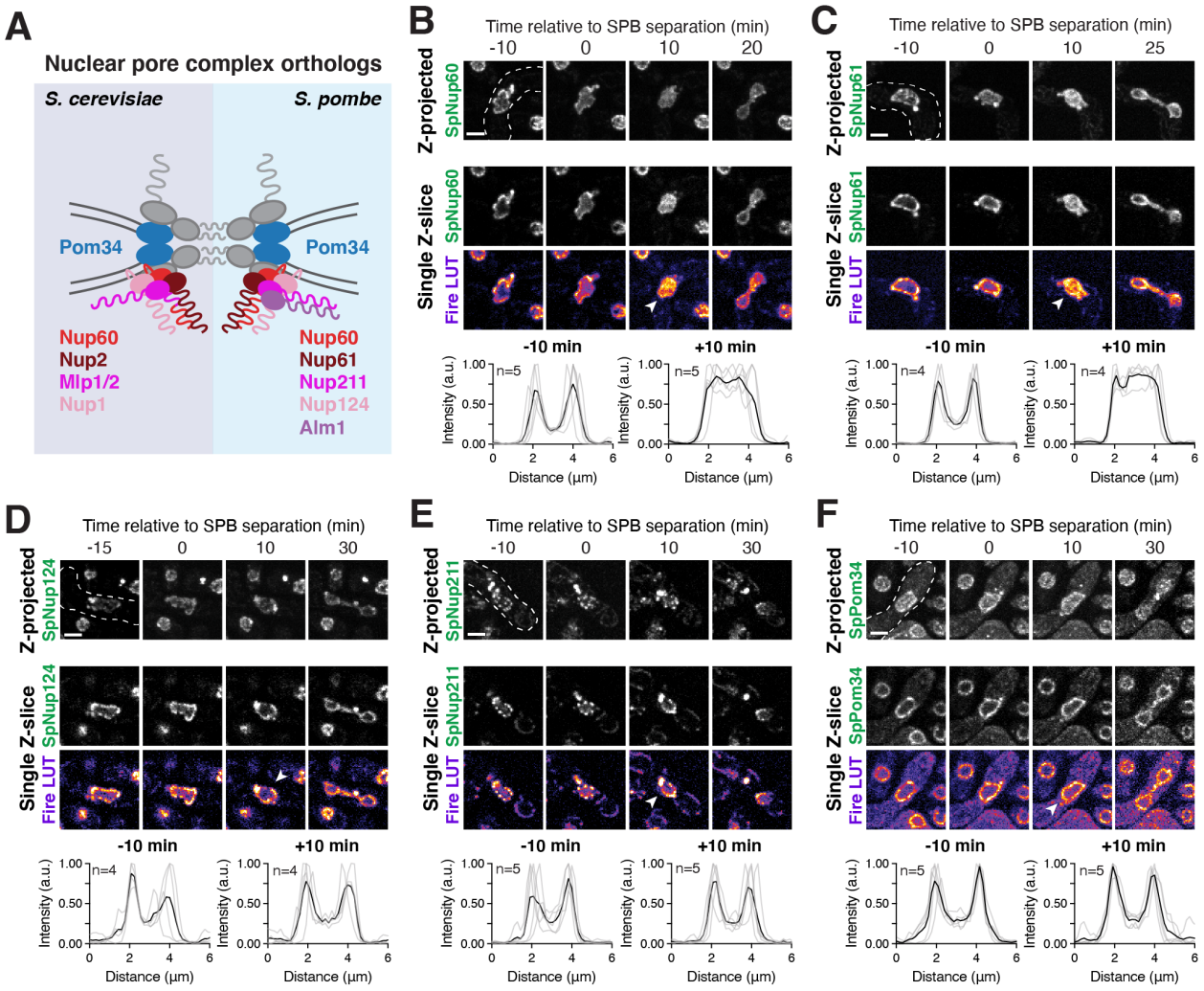

Figure 3.16. Meiosis I nuclear pore complex remodeling is conserved in *Schizosaccharomyces pombe*. A. A schematic depicting nuclear basket nucleoporin orthologs in *S. cerevisiae* and *S. pombe*. **B-F.** Maximum intensity projections (top row) and single z-slice image montages of cells with various GFP-tagged nucleoporins progressing through meiosis I and staged according to the timing of meiosis I SPB separation as visualized using SpPpc89-mCherry (not shown). For each nucleoporin, individual (gray) and mean (black) Nup-GFP intensity profiles measured on single z-slices are shown below for the indicated number of individual nuclei (n), 10 minutes before and after SPB separation. The following nucleoporins were visualized: **B.** SpNup60-GFP, the ortholog of ScNup60 (fySLJ730 x fySLJ479); **C.** SpNup61-GFP, the ortholog of ScNup2 (fySLJ840 x fySLJ479); **D.** SpNup124-GFP, the ortholog of ScNup1 (fySLJ456 x fySLJ989); **E.** SpNup211-GFP, the ortholog of ScMlp1 and

ScMlp2 (fSLJ456 x FySLJ990); and **F.** SpPom34-GFP, the ortholog of ScPom34 (fySLJ1242 x fySLJ1243). For panels B-F, the white arrowheads in the "Fire LUT" images denote nuclei after meiosis I SPB separation, at the stage when SpNup60-SpNup2 detachment is observed. Scale bars, 3 µm.

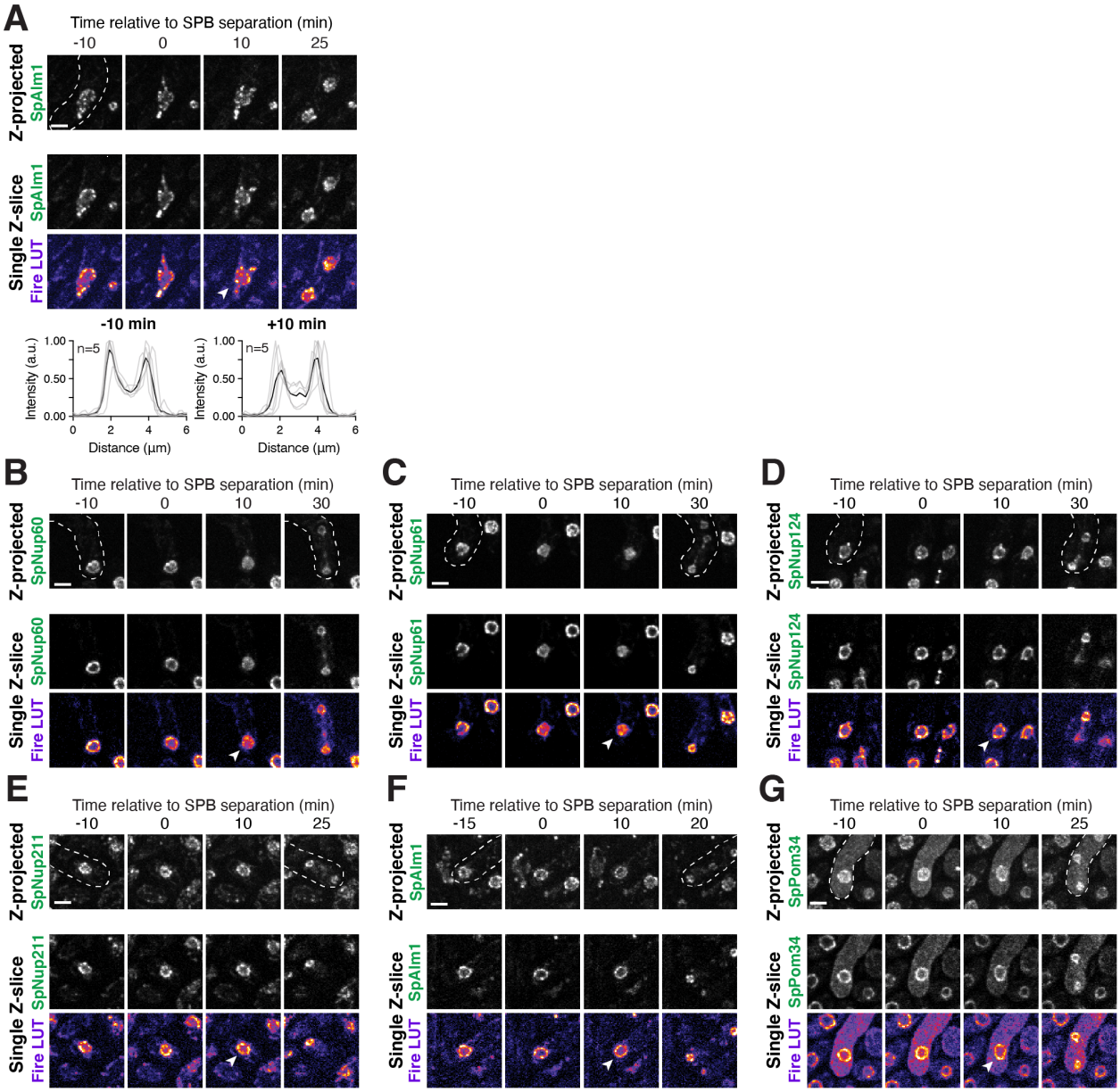

Figure 3.17. Supporting data pertaining to nuclear basket behavior during S. pombe meiosis. A. Maximum intensity projections (top row) and single z-slice image montages of cells with SpAlm1-GFP, a putative Tpr-like nucleoporin with no apparent *S. cerevisiae* ortholog (fySLJ842 x fySLJ479), progressing through meiosis I and staged according to the timing of meiosis I SPB separation as visualized using SpPpc89-mCherry (not shown). The individual (gray) and mean (black) SpAlm1-GFP

intensity profiles measured on single z-slices are shown below for the indicated number of individual nuclei (n), 10 minutes before and after SPB separation. The white arrowhead in the "Fire LUT" images denote a nucleus after meiosis I SPB separation, at the stage when SpNup60-SpNup2 detachment is observed. **B-G.** Montages of strains with the various GFP-tagged nucleoporins during meiosis II: **B.** SpNup60-GFP (fySLJ730 x fySLJ479); **C.** SpNup61-GFP (fySLJ840 x fySLJ479); **D.** SpNup124-GFP (fySLJ456 x fySLJ989); **E.** SpNup211-GFP (fSLJ456 x FySLJ990); **F.** SpAlm1-GFP (fySLJ842 x fySLJ479); and **G.** SpPom34-GFP (fySLJ1242 x fySLJ1243). Cells were staged according to the timing of meiosis II SPB separation as visualized using SpPpc89-mCherry. For panels B-G, the white arrowheads in the "Fire LUT" images denote nuclei after meiosis II SPB separation, at the time point when the second SpNup60-SpNup2 detachment occurs. Scale bars, 3 µm.

3.3.1 A new type of nuclear pore complex remodeling during cell division: nuclear basket detachment

We characterize a new form of NPC remodeling during cell division: specific disassembly and reassembly of part or all of the nuclear basket (Figure 3.1). Disassembly of the nuclear basket during other NPC remodeling events, including during metazoan and fungal mitosis, is coupled to disassembly of channel nucleoporins, driving a loss of nucleocytoplasmic compartmentalization (De Souza et al., 2004; Dey et al., 2020; Dultz et al., 2008; Osmani et al., 2006). In contrast, both core and channel nucleoporins remain peripheral during budding and fission yeast meiosis (Figures 3.1 and 3.16), likely resulting in largely intact NPCs without a subset of or all nuclear basket nucleoporins. Despite their distinct outcomes, meiosis I basket detachment and previously characterized NPC remodeling events share a similar mechanistic underpinning: phosphorylation driven by a cell-cycle kinase disrupts nucleoporin interactions to facilitate disassembly (Figures 3.5, 3.6, 3.8). Moreover, Polo kinases are involved in both fungal and metazoan NPC remodeling – Cdc5 in budding yeast, PLK-1 in worms, and PLK1 in human cells – indicating that the same regulatory machinery can be used to achieve different NPC structural states (Linder et al., 2017; Martino et al., 2017).

The nuclear basket is the most dynamic and heterogenous subcomplex of the NPC, in addition to being the least structurally and functionally understood. Individual basket members disassociate and reassociate with the NPC with rapid kinetics in yeast and metazoan cells (Buchwalter et al., 2014; Hakhverdyan et al., 2021; Rabut et al., 2004). Individual NPCs within the same yeast cell exhibit variable basket composition, with "basketless" NPCs near the nucleolus lacking Mlp1 and Mlp2 (Akey et al., 2022b; Galy et al., 2004; Varberg et al., 2022). Budding yeast meiosis represents a developmental context in which NPCs change their nuclear basket composition *en masse* (Figure 3.1). Moreover, distinct nuclear basket states are achieved during meiosis I and meiosis II due to partial or full basket disassembly (Figure 3.3).

Studying nuclear transport during the meiotic divisions or upon ectopic modification of nuclear basket organization using meiotic mechanisms may help illuminate how nuclear basket plasticity affects NPC function.

3.3.2 Insights into nuclear basket organization from meiotic remodeling

Our study provides key insights into how the structural principles of the nuclear basket can be exploited to achieve disassembly and reassembly (Figures 3.5, 3.6, 3.8, 3.9, 3.11). During meiosis I, we find that the N-terminus of Nup60 facilitates both detachment and reattachment: phosphorylation of its helical region (HR) disrupts interaction with the NPC core and lipid-binding by its amphipathic helix (AH) allows for redocking on the NPCs. These principles may be similarly utilized in other cellular contexts. For example, monoubiquitylation of the helical region of Nup60 has also been implicated in altering its association with the NPC (Niño et al., 2016). Excitingly, meiosis represents a developmental context where the direct membrane-binding function of the nuclear basket becomes essential for proper NPC organization (Figures 3.11, 3.13). In addition to facilitating reassociation of Nup60 and Nup2 with NPCs following meiosis I, the Nup60 amphipathic helix is necessary for the timely recruitment of all nuclear basket nucleoporins to the gamete nuclear periphery after meiosis II (Figure 3.13).

Moreover, the distinct behaviors of basket nucleoporins during partial nuclear basket disassembly drove insights into how Nup60 coordinates nuclear basket organization. Nup60 is involved in the recruitment of Mlp1 and Nup2 to NPCs (Cibulka et al., 2022; Dilworth et al., 2001; Galy et al., 2004); however, Mlp1 remained associated with the nuclear periphery during meiosis I despite Nup60 exhibiting robust detachment (Figure 3.1). By depleting Nup60 either constitutively or acutely using the auxin-AID system (Nishimura et al., 2009; Yesbolatova et al., 2020), we uncovered two distinct roles for Nup60: recruitment and retention. Although Nup60 is required to recruit both Nup2 and Mlp1, Nup60 is not required for the retention of Mlp1 at the nuclear periphery (Figure 3.15). The ability of Mlp1 to remain associated with the NPC in the absence of Nup60 suggests the existence of additional interactions at the nuclear periphery. Consistent with this notion, Mlp1 is the slowest maturing member of the yeast NPC (Onischenko et al., 2020). It has been suggested that Mlp1 and Mlp2 interact to form a network between neighboring NPCs (Niepel et al., 2013), which could explain its persistence at the nuclear periphery in the absence of Nup60. Determining whether Nup60 mediates retention of other proteins that require it for peripheral localization, such as the SUMO protease Ulp1 (Zhao et al., 2004), will provide insight into their meiotic regulation and the organizational hierarchy of the nuclear basket.

How the entire nuclear basket is detached from NPCs following meiosis II remains less well understood. Phosphorylation-resistant Nup60 mutants that fail to detach during meiosis I were still able to detach in meiosis II, indicating that the two nuclear basket detachment events are mechanistically distinct (Figure 3.9). Additionally,

individual nuclear basket nucleoporins detached from NPCs independently during meiosis II, with Mlp1 and Nup1 able to return to gamete nuclei even when the bulk of Nup60 was targeted to the GUNC through artificial tethering to NPC core (Figure 3.3). It is therefore likely that modifications on multiple nucleoporins facilitate their dissociation from the NPC core, perhaps via the coordinated activity of multiple kinases as in metazoan mitosis (Laurell et al., 2011). Further elucidation of NPC remodeling in meiosis II will improve our understanding of how the basket is held together and how it can come apart.

3.3.3 Nuclear pore complex remodeling in gametogenesis

Why NPCs exhibit such extensive modularity during meiosis remains a key area for future investigation. The basket nucleoporins Nup60 and Nup2 are required for proper gametogenesis in budding yeast (Chu et al., 2017; Komachi and Burgess, 2022). It has been hypothesized that their meiotic function involves tethering chromosomes to the nuclear periphery during prophase I, in parallel to the telomere bouquet protein Ndj1 and the linker of the nucleoskeleton and cytoskeleton (LINC) complex. Basket detachment during the meiotic divisions might therefore facilitate the release of chromatin from the nuclear envelope as chromosomes undergo segregation. Moreover, full basket detachment during meiosis II enables inheritance of the nuclear basket but not the NPC core by nascent gametes. The metazoan basket nucleoporin Nup153 (the ortholog of ScNup60 and ScNup1) mediates NPC assembly in interphase cells (Vollmer et al., 2015); it is tempting to speculate that Nup60 and Nup1 could similarly facilitate insertion of newly synthesized NPCs in gametes after large-scale meiotic turnover. Determining whether and how NPC remodeling contributes to gamete health may reveal novel roles for the nuclear basket in nuclear organization.

Strikingly, nuclear basket disassembly during meiosis I is conserved in the distantly related fission yeast *Schizosaccharomyces pombe* (Figure 3.16). This conservation over 400 million years of evolution is consistent with basket detachment serving an important meiotic function (Sipiczki, 2000). It also establishes that nuclear basket detachment is an NPC remodeling event distinct from GUNC formation, since NPC sequestration does not take place in *S. pombe* (Asakawa et al., 2010). In addition to NPCs being partially disassembled, the nuclear permeability barrier is transiently disrupted during meiosis II in *S. pombe* and possibly *S. cerevisiae* (Arai et al., 2010; Asakawa et al., 2010; Shelton et al., 2021), suggesting that several hallmarks of metazoan cell divisions occur within the context of these fungal cell divisions. This work adds to growing evidence that nuclear periphery dynamics during cell divisions exist across an evolutionary spectrum, rather than fitting a binary where the nuclear periphery is either completely intact ("closed" divisions) or completely disrupted ("open" divisions).

Altogether, our study provides insights into a new type of NPC remodeling during cell divisions: nuclear basket disassembly and reassembly. Whether nuclear basket detachment occurs in other contexts, including mammalian meiosis, remains unclear. Notably, the metazoan basket nucleoporin Nup50 (the ortholog of ScNup2) was originally cloned from mice testis due to its high expression levels (Fan et al., 1997; Guan et al., 2000). During spermatogenesis, Nup50 exhibits a familiar localization pattern: it relocalizes from the nuclear periphery in spermatocytes (pre-meiosis II) to the nucleoplasm in spermatids (post-meiosis II), before returning to the nuclear periphery in spermatozoa (mature gametes). Nuclear basket detachment may therefore represent a widespread feature of gametogenesis programs. Future interrogation of how cells achieve complex and dynamic meiotic regulation of the NPC promises to improve our understanding of NPC organization and function.

Chapter 4

Transient disruption of the nuclear permeability barrier during budding yeast meiosis

4.1 Introduction

During cell division, a eukaryotic cell must remodel its nuclear envelope in order to accommodate the division of genetic material. Cells have reached divergent evolutionary solutions for this problem, ranging from "open" to "closed" cell divisions (reviewed in Boettcher and Barral, 2013). In open cell divisions such as those observed in metazoans, the nuclear envelope and its constituent nuclear pore complexes (NPCs) are largely disassembled, resulting in intermixing of the nucleoplasm and cytoplasm. In closed cell divisions such as those observed in budding yeast, the nuclear periphery and the nuclear permeability barrier instead remain largely intact. The evolutionary pressures underpinning these distinct nuclear modalities during cell division are poorly understood.

It has become increasingly appreciated that many forms of cell division do not fit this binary and instead exist between the two extremes (reviewed in Dey and Baum, 2021). In some metazoan cell types, the nuclear periphery remains partially intact throughout the cell cycle (Roubinet et al., 2021). In diverse fungal cell divisions, different disruptions of the nuclear periphery and nuclear transport occur, ranging from partial disassembly of NPCs to tearing of the nuclear envelope (De Souza et al., 2004; Yam et al., 2011). The changes underlying these differences in nuclear behavior can be surprisingly simple, relating to changes in even a single gene (Makarova et al., 2016). This evolutionary plasticity in nuclear division suggests that distinct cellular contexts can impose different demands on nuclear dynamics.

Budding yeast mitosis and meiosis have historically been considered "closed" cell divisions, since electron microscopy indicates that the nuclear envelope remains largely intact (Moens, 1971; Moens and Rapport, 1971). However, our recent work has demonstrated that budding yeast meiosis has properties resembling an "open" cell division. Formation of the Gametogenesis Uninherited Nuclear Compartment (GUNC) facilitates the turnover of nuclear material, in a manner similar to nuclear envelope breakdown (Chapter 2, King et al., 2019). The NPC undergoes phosphorylation-driven partial disassembly, coordinated by a cell cycle kinase also involved in metazoan NPC disassembly (Chapter 3, King et al., 2022). These dramatic differences relative to mitotic nuclear behavior raise the possibility that meiotic nuclear transport might also exhibit more "open" behaviors.

Here, we use live-cell microscopy to demonstrate that the nuclear permeability barrier is transiently disrupted during meiosis II, with multiple nucleoplasmic markers dispersing from and subsequently returning to developing gamete nuclei. This disruption is similar to what has been observed during meiosis in the distantly related fission yeast *Schizosaccharomyces pombe*, an event termed virtual nuclear envelope breakdown or vNEBD (Arai et al., 2010; Asakawa et al., 2010). We begin initial phenotypic and mechanistic characterization of this event in budding yeast, identifying several meiotic genes with effects on either barrier loss or return. Further insight into this permeability disruption promises to improve our understanding of how diverse nuclear remodeling regimes contribute to cellular health.

4.2 Results

4.2.1 The nuclear permeability barrier is transiently disrupted after anaphase II in budding yeast

We first set out to characterize whether any changes to nuclear transport occur during the meiotic divisions in budding yeast. To do this, we monitored a frequently-used marker of the nucleoplasm, GFP-Npl3, relative to the dividing chromatin marked with Htb1-mCherry (Gilbert et al., 2001; Figure 4.1A). Excitingly, we observed that GFP-Npl3 transiently diffused away from the nucleus shortly after meiosis II, coincident with the completion of anaphase II chromosome segregation (Figure 4.1A, 4.1D). The signal remained diffuse for approximately 30 minutes (mean ± standard deviation: 31.1 ± 13.1 minutes; Figure 4.1E), before robustly returning to gamete nuclei. We favor a model by which the GFP-Npl3 is dispersed and reimported into nuclei, instead of one in which it is destroyed and resynthesized, given the rapid kinetics of the event and the diffuse signal visible after anaphase II. We therefore posit that nuclear transport undergoes two dramatic changes during budding yeast meiosis: nuclear permeability barrier loss and return. Notably, this phenotype is strikingly similar to the virtual nuclear envelope breakdown (vNEBD) observed in *S. pombe* meiosis, suggesting that this event has been conserved over 400 million years of evolution (Arai et al., 2010; Asakawa et al., 2010).

We next confirmed that nuclear permeability barrier loss and return was a general event by monitoring the meiotic behavior of two additional nucleoplasmic markers: an entirely synthetic construct, 2xmCherry-SV40NLS, and another yeast protein, Trz1-GFP (Figure 4.1B-C; Kalderon et al., 1984). As with GFP-Npl3, both markers became diffuse at the end of anaphase II before robustly returning to gamete nuclei around 45 minutes later (Figure 4.1B-E; 2xmCherry-SV40NLS - mean ± standard deviation = 46.5 ± 12.0 minutes; Trz1-GFP - mean ± standard deviation = 50.4 ± 13.5 minutes). Importantly, these markers span a range of sizes (GFP-Npl3 = ~72 kDa, 2xmCherry-SV40NLS = ~57 kDa, Trz1-GFP = ~124 kDa) and utilize distinct nuclear import pathways (GFP-Npl3 = Kap111/Mtr10, 2xmCherry-SV40NLS = Srp1/Kap95; Pemberton and Paschal, 2005), supporting the notion that nuclear transport

undergoes a global change after meiosis II. The markers did, however, exhibit subtle differences in dynamics, with barrier loss as assayed by GFP-Npl3 appearing weaker and more transient than barrier loss as assayed by 2xmCherry-SV40NLS (Figure 4.1D-F). Based on the behavior observed for these diverse nucleoplasmic markers, we conclude that nuclear transport is unexpectedly dynamic during budding yeast meiosis.

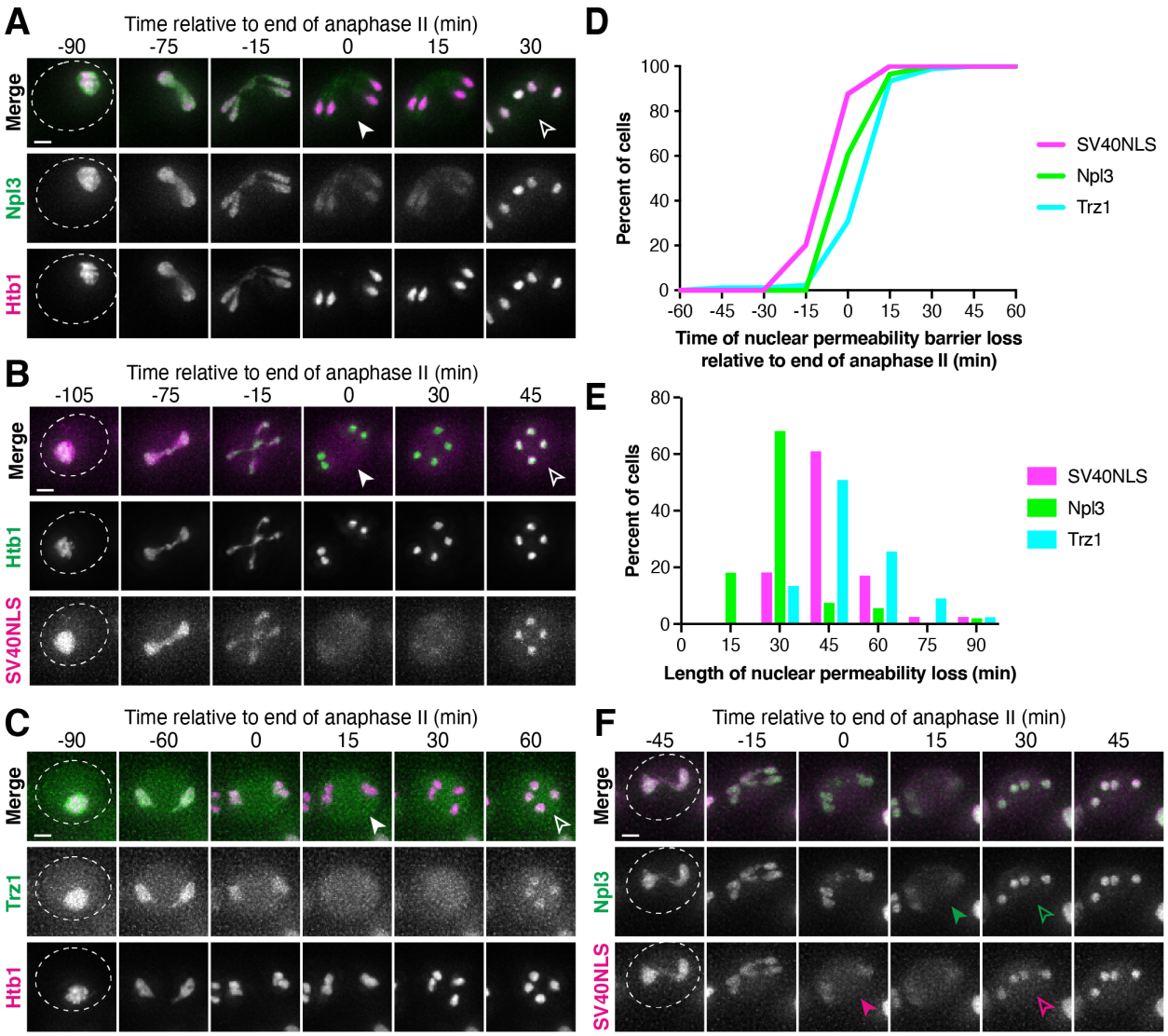

Figure 4.1. The nuclear permeability barrier is transiently disrupted during budding yeast meiosis. A-C. Montages of cells with different nucleoplasmic markers progressing through the meiotic divisions. Chromosomes were visualized with the histone marker Htb1-mCherry or Htb1-eGFP, and the time point of completion of anaphase II chromosome segregation was defined as 0 minutes. **A.** GFP-Npl3 (UB18509). **B** 2xmCherry-SV40NLS (UB21380). **C.** Trz1-GFP (UB20609). **D-E.** Quantification of **D.** time of nuclear permeability barrier loss relative to the end of

anaphase II or **E.** nuclear permeability barrier loss duration, corresponding to the experiments in A-C. Sample sizes were: n = 56 cells for GFP-Npl3, n = 89 cells for 2xmCherry-SV40NLS, n = 91 cells for Trz1-GFP. **F.** Montage of a cell with two different nucleoplasmic markers, GFP-Npl3 and 2xmCherry-SV40NLS, progressing through meiosis (UB20617). In all figures in this chapter, nuclear permeability barrier loss is indicated with a filled-in arrowhead and nuclear permeability barrier return is indicated with a hollow arrowhead. Nuclear permeability barrier loss was defined as the first time point when a significant portion of the nucleoplasmic marker diffused from the nucleoplasm; nuclear permeability barrier return was defined as the first time point when a significant portion of the nucleoplasmic marker returned to the nucleoplasm. Scale bars, 2 µm.

4.2.2 Timing of nuclear permeability disruption relative to key meiotic events

This disruption of the nuclear permeability barrier is similar to the compartment intermixing that occurs during nuclear envelope disassembly in open cell divisions. However, the nuclear envelope remains largely intact throughout budding yeast meiosis, as demonstrated in this work and previously (Figure 2.9-2.11; Moens, 1971; Moens and Rapport, 1971). We were therefore interested in understanding how nuclear permeability barrier disruption relates temporally to other key meiotic nuclear remodeling events. We first assessed the relationship between timing of barrier loss and NPC sequestration to the GUNC, since GUNC formation involves the large-scale turnover of nuclear transport machinery (Chapter 2). We found that the two events were temporally distinct: NPCs were sequestered to the GUNC early during anaphase II, whereas transient loss of the nuclear permeability barrier occurred largely after anaphase II (Figure 4.2A). As such, we reason that NPC sequestration is unlikely to be driving barrier loss or return. We next assessed the timing of barrier disruption relative to plasma membrane closure or cytokinesis, which we used as a proxy for karyokinesis and the establishment of distinct gamete nuclei. Although a link has not yet been established in meiosis, karyokinesis and cytokinesis are closely linked in mitosis (Melloy and Rose, 2017). We found that return of the permeability barrier tightly coincided with plasma membrane closure and, probably, nuclear division (Figure 4.2B-C). Further work is required to determine whether karyokinesis itself or an event coincident with cytokinesis is responsible for this temporal correlation. Of note, barrier return does not occur in unpackaged nuclei, further suggesting that a link exists between cytokinesis and restoration of nuclear transport (Figure 4.2D). Staging barrier loss and return relative to meiotic exit events promises to shed light on the function and mechanism of nuclear transport disruption.

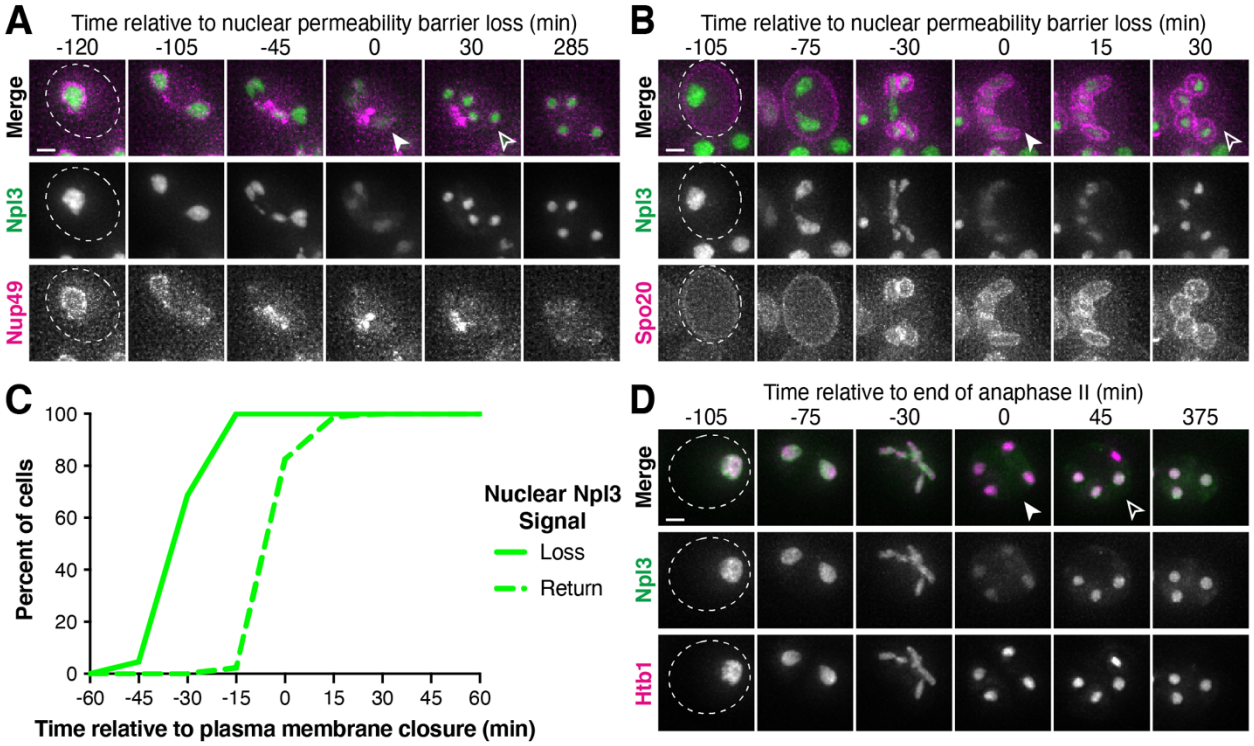

Figure 4.2. Timing of nuclear permeability barrier disruption relative to other meiotic nuclear events. A-B. Montages of cells with a nucleoplasmic marker GFP-Npl3 and either **A.** a fluorescently tagged core nucleoporin Nup49-mCherry (UB8746) or **B.** a gamete plasma membrane marker mKate-Spo20$^{50\text{-}91}$ (UB18511) progressing through the meiotic divisions. The time point of nuclear permeability barrier loss was defined as 0 minutes. For A, meiosis was induced by adding 1 µM ß-estradiol after 5 h in Spo, since UB8746 contained *P_{GAL}-NDT80.* **C.** Quantification of GFP-Npl3 signal loss and return relative to plasma membrane closure, corresponding to B. Plasma membrane closure was defined as the time point at which the gamete plasma membranes went from being elongated to round (Diamond et al., 2009; n = 86 cells). **D.** Montage of a cell that becomes a triad progressing through meiosis, with a nucleoplasmic marker GFP-Npl3 and a fluorescently tagged histone Htb1-mCherry (UB18509). The time point of completion of anaphase II chromosome segregation was defined as 0 minutes. Scale bars, 2 µm.

4.2.3 Mechanism of nuclear permeability loss and return

Since no global disruption of the nuclear envelope occurs, barrier loss and return seem likely to be driven by modulation of nuclear transport machinery. In *S. pombe*, barrier loss has been proposed to be driven by changes in the Ran gradient, the cycle that establishes directionality of nuclear transport (Figure 4.3A; reviewed in Joseph,

2006). Nuclear GTP-bound Ran (Ran-GTP) facilitates transport out of the nucleus, while cytoplasmic GDP-bound Ran (Ran-GDP) facilitates transport into the nucleus.

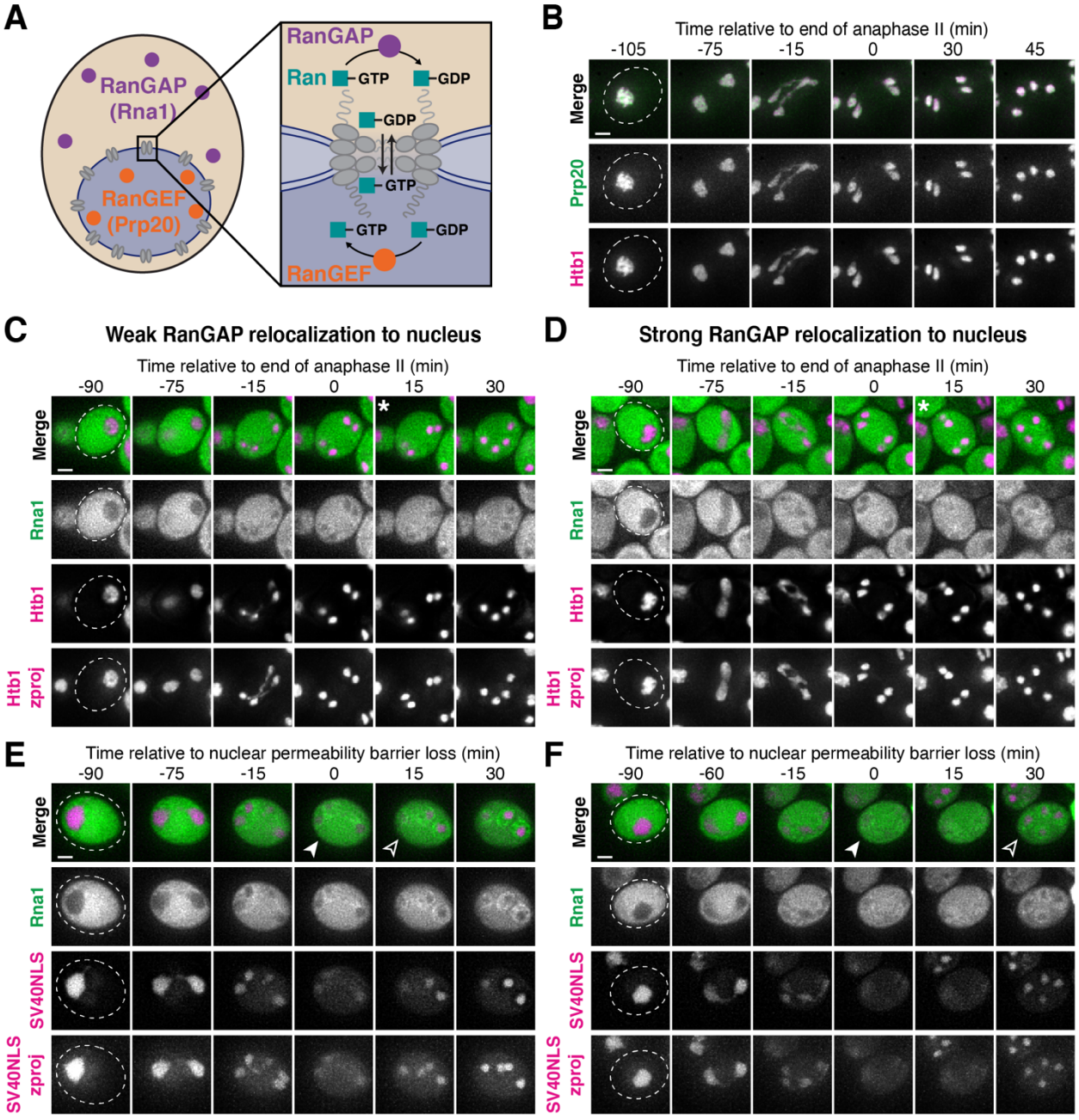

Figure 4.3. Behavior of the Ran gradient during nuclear permeability barrier loss and return. A. Schematic of the Ran gradient, which mediates directional nuclear transport (reviewed in Joseph, 2006). Nuclear Ran-GTP drives nuclear export, while cytoplasmic Ran-GDP drives nuclear import. The Ran guanine nucleotide exchange factor (RanGEF) Prp20 converts Ran-GDP to Ran-GTP in the nucleus; the Ran GTPase activating protein (RanGAP) Rna1 converts Ran-GTP to Ran-GDP in the

cytoplasm. **B.** Montage of a cell with the RanGEF Prp20-GFP and histone Htb1-mCherry progressing through meiosis (UB20161). **C-F.** Montages of cells with the RanGAP Rna1-3xGFP and **C-D.** the histone Htb1-mCherry (UB20153) or **E-F.** the nucleoplasmic marker 2xmCherry-SV40NLS (UB20155) progressing through meiosis. Both cells with (**C, E**) less dramatic and (**D**, **F**) more dramatic RanGAP relocalization into the nucleus are shown. For B-D, the time point of anaphase II chromosome segregation completion was defined as 0 minutes. The asterisks indicate the time point of maximal RanGAP nuclear localization. For E-F, the time point of nuclear permeability barrier loss was defined as 0 minutes. Scale bars, 2 µm.

This gradient is established by the asymmetric localization of Ran guanine nucleotide exchange factor (RanGEF, or Prp20 in budding yeast) to the nucleus and Ran GTPase activating protein (RanGAP, or Rna1 in budding yeast) to the cytoplasm (Becker et al., 1995; Belhumeur et al., 1993). We therefore monitored Prp20 or Rna1 during meiosis to determine whether changes in their localization might drive barrier loss (Figure 4.3B-D). As reported in *S. pombe*, the RanGEF Prp20 remained nuclear throughout both meiotic divisions, likely due to its association with chromatin, making it an unlikely candidate for driving nuclear permeability loss (Figure 4.3B; Arai et al., 2010; Asakawa et al., 2010). In contrast, the RanGAP Rna1 appeared to partially enter into gamete nuclei after anaphase II, albeit to a variable extent in different cells (Figure 4.3C-F). Notably, barrier loss could sometimes be observed without visible nuclear RanGAP entry (Figure 4.3E-F), suggesting either that a small nuclear pool of RanGAP is sufficient to drive barrier loss or that RanGAP nuclear entry is not causative. Further quantitative characterization of RanGAP localization is necessary to determine whether its relocalization is consistent with a role in barrier loss or whether modulation of other transport factors is likely involved.

Due to the tight coupling of barrier loss to key meiotic events (Figure 4.1-4.2), we reasoned that a meiotic regulatory factor is likely upstream of any modulation of nuclear transport. As such, we tested various meiotic genes for a role in either barrier loss or return (Table 4.1, Figure 4.4). Of the genes we tested, only loss of Ime2 function affected barrier loss (Figure 4.4A). However, a constitutively active allele of Ime2 (*IME2st*; Berchowitz et al., 2013) was not sufficient to drive barrier loss, indicating that Ime2 may play a more indirect role in the phenomenon (Figure 4.4B). A number of genes caused disruption in barrier return, likely due at least in part to pleiotropic issues with meiotic progression (Table 4.1). We highlight the two genes with the most dramatic effects – *AMA1*, a meiosis-specific adaptor of the anaphase promoting complex, and *GIP1*, a meiosis-specific regulator of the phosphatase Glc7 – reasoning that these are most likely to be playing a specific role (Cooper et al., 2000; Tachikawa et al., 2001; Figure 4.4C-F). Both *ama1Δ* and *gip1Δ* cells exhibit barrier return less frequently than wild type cells and, when it does occur, with a delay and to fewer nuclei (Figure 4.4D, 4.4F). Interestingly, plasma membrane development was dispensable for nuclear transport modulation, as *spo21Δ* cells exhibited barrier loss

and return with relatively normal kinetics, indicating that NPC sequestration to the GUNC and barrier disruption can be completely decoupled (Figure 4.4G-H). ESCRT-III adaptors (Chm7, Heh1, and Heh2) also only had minor effects on barrier return, if any, suggesting either that they are not required for nuclear membrane remodeling or that additional pathways play an important role (Table 4.1). This initial characterization of candidate genes will hopefully facilitate more detailed mechanistic follow-up in the future.

Table 4.1. Additional genes tested for a role in nuclear permeability barrier loss or return. Movies of strains with the indicated allele, a fluorescent nucleoplasmic marker (GFP-Npl3), and a marker for meiotic progression (Htb1-mCherry) were generated. When phenotypes of interest were observed, movies of strains with the same allele and a second nucleoplasmic marker (2xmCherry-SV40NLS) were generated to assess whether the effect was general. For *ime2-as1*, cells were induced to enter the meiotic divisions after 5 hours in Spo with 1 μM ß-estradiol (since the strains contained P_{GAL}-*NDT80*) and *ime2-as1* was inhibited after 7 hours in Spo with 20 μM 1-NA-PP1. Alleles with results of particular interest are bolded and in red.

Allele	Strain number	Phenotype
heh1Δ	GFP-Npl3: UB20157	GFP-Npl3: In a small subset of nuclei (~5% of MII cells), barrier return is faulty. Nuclei can exhibit long-term loss or multiple transient losses of compartmentalization for hours after meiosis, even if successfully packaged.
heh2Δ	GFP-Npl3: UB20163	GFP-Npl3: Barrier loss and return are relatively normal
heh1Δ heh2Δ	GFP-Npl3: UB20274	GFP-Npl3: Same as *heh1Δ*
chm7Δ	GFP-Npl3: UB20863	GFP-Npl3: Barrier loss and return are relatively normal
chm7Δ heh1Δ	GFP-Npl3: UB20983	GFP-Npl3: Same as *heh1Δ*
spr3Δ	GFP-Npl3: UB22987	GFP-Npl3: Barrier loss and return are relatively normal
spr28Δ	GFP-Npl3: UB23203	GFP-Npl3: Barrier loss and return are relatively normal
spr3Δ spr28Δ	GFP-Npl3: UB23866	GFP-Npl3: Barrier loss and return are relatively normal
ssp1Δ	GFP-Npl3: UB20159 2xmCherry-SV40NLS: UB21817	GFP-Npl3: Delayed barrier loss from the nuclear region surrounded by misformed plasma membranes; heterogenous return afterwards

		2xmCherry-SV40NLS: A delay in barrier loss for specific nuclear regions is not observed, suggesting that the *ssp1Δ* phenotype observed for GFP-Npl3 is not general; defects in barrier return are present
sma2Δ	GFP-Npl3: UB20605	GFP-Npl3: Messy and variable, but barrier loss and return occur to some extent
ssp1Δ sma2Δ	GFP-Npl3: UB20761	GFP-Npl3: Somewhere in between *ssp1Δ* and *sma2Δ* single deletes; barrier loss and return occur to some extent
nup60Δ	GFP-Npl3: UB23658 2xmCherry-SV40NLS: UB25072	GFP-Npl3: Signal remains nuclear throughout meiosis, suggesting no barrier loss 2xmCherry-SV40NLS: Barrier loss and return are mostly normal, suggesting that the *nup60Δ* phenotype observed for GFP-Npl3 is not general
ime2-as1	GFP-Npl3: UB26767 2xmCherry-SV40NLS: UB26769	GFP-Npl3: Barrier loss seems less complete than in wild type 2xmCherry-SV40NLS: Barrier loss seems less complete than in wild type
ama1Δ	GFP-Npl3: 20607 2xmCherry-SV40NLS: 25650	GFP-Npl3: Barrier return is pretty defective – no return in some cells and, when return occurs, often weak and to only a few nuclei. Of all mutants tested, the second strongest defect in barrier return. 2xmCherry-SV40NLS: Barrier return is pretty defective, with a similar phenotype to that observed in GFP-Npl3
gip1Δ	GFP-Npl3: 18824 2xmCherry-SV40NLS: 21614	GFP-Npl3: Barrier return is very defective – no return in many cells and, when return occurs, often weak and to only a few nuclei. Of all mutants tested, the strongest defect in barrier return. 2xmCherry-SV40NLS: Barrier return is very defective, with a similar phenotype to that observed in GFP-Npl3
spo21Δ	GFP-Npl3: 18859 2xmCherry-SV40NLS: 21612 (new Htb1-eGFP), 18822 (old Htb1-GFP)	GFP-Npl3: Barrier loss and return occur with relatively normal kinetics, before a subsequent permanent loss. Of note, return almost always takes place to all four nuclei, instead of a subset (in wild type cells, return occurs to only packaged nuclei)

		2xmCherry-SV40NLS: Barrier loss occurs with normal kinetics. Barrier return is much weaker than in wild type but with normal kinetics for the new Htb1-eGFP. Barrier return occurs more strongly and with normal kinetics for the old Htb1-GFP, for reasons that are unclear.
sps1Δ	GFP-Npl3: UB26148 2xmCherry-SV40NLS: UB26150	GFP-Npl3: Barrier return is defective and heterogenous 2xmCherry-SV40NLS: Barrier return is defective and heterogenous
ama1Δ spo21Δ	GFP-Npl3: UB26152	GFP-Npl3: Barrier loss seems to be somewhat permanent; more like *ama1Δ* than *spo21Δ* 2xmCherry-SV40NLS: Somewhat difficult to interpret, since *spo21Δ* return is far more subtle for this marker; barrier loss seems to be more or less permanent in the double delete
gip1Δ spo21Δ	GFP-Npl3: UB26154 2xmCherry-SV40NLS: UB26156	GFP-Npl3: Barrier loss and return occurs somewhat normally, before a subsequent permanent loss; more like *spo21Δ* than *gip1Δ* 2xmCherry-SV40NLS: Somewhat difficult to interpret, since *spo21Δ* return is far more subtle for this marker; barrier loss seems to be more or less permanent in the double delete
sps1Δ ama1Δ	GFP-Npl3: UB26364 2xmCherry-SV40NLS: UB26283	GFP-Npl3: Barrier return is defective and heterogenous; unclear whether more like *sps1Δ* or *ama1Δ*, but no clear synergistic defect 2xmCherry-SV40NLS: Barrier return is defective, perhaps to a greater extent than *sps1Δ* or *ama1Δ* alone

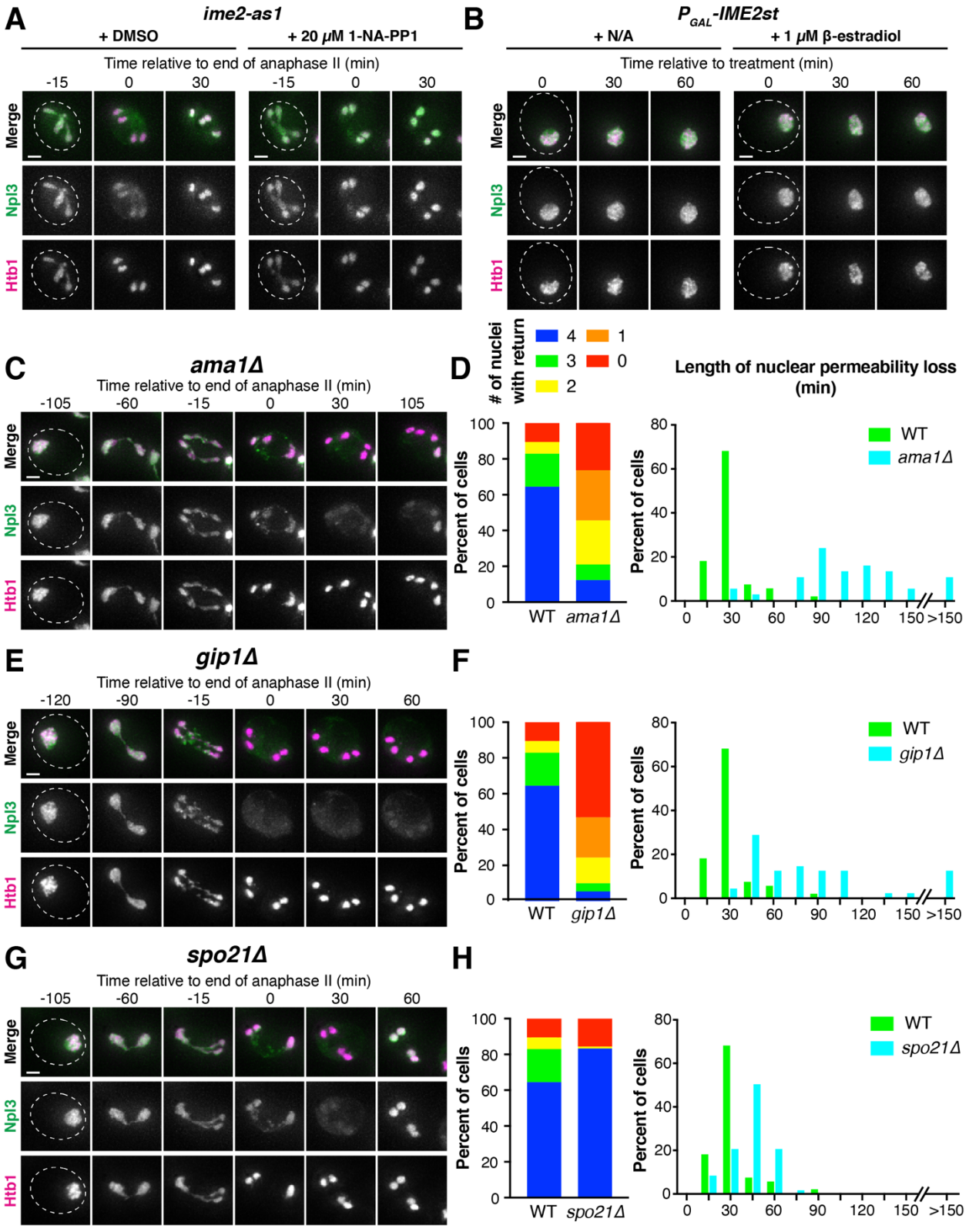
A
ime2-as1
+ DMSO
+ 20 μM 1-NA-PP1
Time relative to end of anaphase II (min)
-15
0
30
Merge
Npl3
Htb1
B
P GAL -IME2st
+ N/A
+ 1 μM β-estradiol
Time relative to treatment (min)
0
30
60
C
ama1Δ
Time relative to end of anaphase II (min)
-105
-60
-15
0
30
105
D
# of nuclei with return
4
3
2
1
0
Length of nuclear permeability loss (min)
Percent of cells
WT
ama1Δ
>150
E
gip1Δ
-120
-90
F
gip1Δ
G
spo21Δ
H
spo21Δ

Figure 4.4. Candidate meiotic regulators of barrier loss and return. A, C, E, G. Montages of mutant cells with a nucleoplasmic marker GFP-Npl3 and fluorescently tagged histone Htb1-mCherry progressing through meiosis. The following mutant genotypes are depicted: **A.** *ime2-as1*, treated with 1 μM ß-estradiol after 5 hours in Spo to induce P_{GAL}-*NDT80* and either (left) DMSO or (right) 20 μM 1-NA-PP1 after 7 hours in Spo to inhibit Ime2 (UB26767). **C.** *ama1Δ* (UB20607). **E.** *gip1Δ* (UB18824). **G.** *spo21Δ* (UB18859). **B.** Montage of a cell arrested in prophase (*ndt80Δ*) with induction of P_{GAL}-*IME2st* by addition of either (left) nothing or (right) 1 μM ß-estradiol after 6 hours in Spo (UB27197). **D, F, H.** Quantification of (left) number of nuclei exhibiting return per cell and (right) for cells exhibiting loss and return, duration of nuclear permeability loss. **D.** *ama1Δ*, corresponding to C (n = 57 cells total, 38 cells exhibiting loss and return). **F.** *gip1Δ*, corresponding to E (n = 111 cells total, 49 cells exhibiting loss and return). **H.** *spo21Δ*, corresponding to F (n = 96 cells total, 74 cells exhibiting loss and return). All wild type values are from the same control (n = 76 cells total, 56 cells exhibiting loss and return; UB18509). Scale bars, 2 μm.

4.3 Discussion

In this chapter, we demonstrate that the nuclear permeability barrier is transiently disrupted during budding yeast meiosis (Figure 4.5), consistent with a recent report (Shelton et al., 2021). Given that the nuclear envelope remains largely intact during meiosis, we propose that modulation of nucleocytoplasmic transport machinery drives this rapidly reversible event. Barrier loss may be driven by relocalization of the RanGAP to the nucleoplasm, as has been suggested in fission yeast (Arai et al., 2010; Asakawa et al., 2010). Barrier return is temporally connected to cytokinesis and likely karyokinesis, although a direct mechanistic link remains to be established. Importantly, we identify multiple meiotic genes with effects on barrier loss and barrier return, providing the groundwork for future mechanistic analysis.

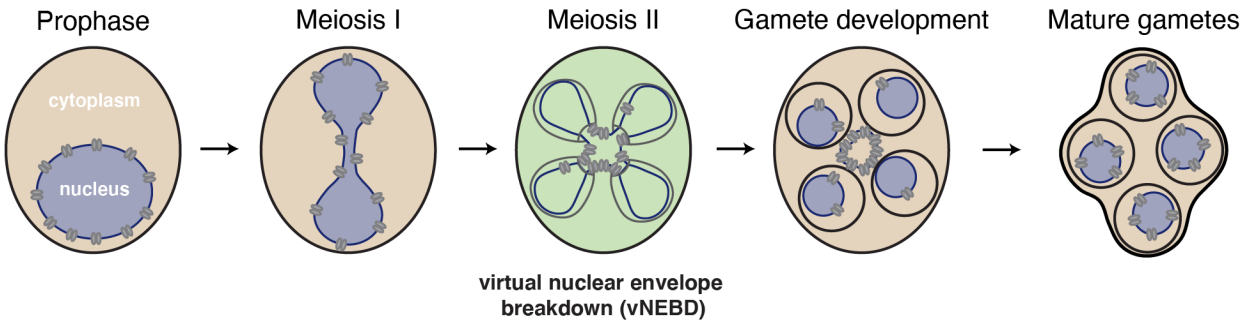

Figure 4.5. Nuclear transport during budding yeast meiosis. Schematic depicting the transient disruption of the nuclear permeability barrier during meiosis II. Barrier loss occurs after nuclear pore sequestration to the GUNC; barrier return occurs coincident with plasma membrane closure. The timing of the event is strikingly

similar to virtual nuclear envelope breakdown (vNEBD) observed during fission yeast meiosis (Arai et al., 2010; Asakawa et al., 2010).

The nature of the nuclear permeability barrier disruption requires additional characterization. Given that the RanGAP becomes partially nucleoplasmic, it seems likely that meiotic transport disruption is bidirectional as in *S. pombe*, with cytoplasmic proteins able to enter the nucleus (Figure 4.3; Arai et al., 2010; Asakawa et al., 2010). However, monitoring a nuclear export signal (NES)-containing cargo is necessary to definitively establish that the cytoplasmic and nucleoplasmic compartments fully intermix. Further, it remains to be determined whether a size limit affects what material transits between the cytoplasm and nucleoplasm. Monitoring the ability of very large particles, such as nucGEMs, to diffuse between the two compartments could provide mechanistic insight into barrier loss, differentiating between modulation of nuclear transport machinery and larger-scale disruption of the nuclear envelope (Shu et al., 2022). Assessing these properties is necessary to fully understand how barrier disruption in budding yeast meiosis relates what is observed in other cell division contexts.

Of note, barrier loss and return are not coupled to GUNC formation, since plasma membrane biogenesis is not required for alteration of nuclear transport (Figure 4.4). The sequestration of NPCs was also temporally distinct from barrier loss, providing further evidence that this turnover event does not drive barrier loss (Figure 4.2). Interestingly, gamete nuclei become transport-competent very shortly after packaging, suggesting that either newly synthesized or inherited NPCs are sufficient to drive robust nuclear transport (Figure 4.2). Given that fission yeast exhibit barrier loss but do not exhibit large-scale NPC remodeling, we favor a model whereby barrier disruption is driven by modulation of other transport machinery, with NPC destruction and resynthesis contributing to gamete health in other ways (Asakawa et al., 2010).

Towards identification of such a mechanism, we identified meiotic regulators of nuclear barrier disruption, including genes that affect both barrier loss and return (Table 4.1, Figure 4.4). Notably, one candidate regulator of loss is a meiotic kinase (Ime2; Benjamin et al., 2003) and one candidate regulator of return is a meiotic phosphatase interactor (Gip1; Tachikawa et al., 2001), suggesting that a cell-cycle coupled phosphorylation event could be modulating nuclear transport. This regulatory logic would be analogous to what is observed in metazoans, where phosphorylation-driven disassembly of NPCs facilitates nuclear envelope breakdown (Laurell et al., 2011; Linder et al., 2017). Identifying the mechanism underpinning nuclear permeability barrier disruption may elucidate novel means by which cells control nuclear transport.

Our work continues to blur the line between open and closed divisions, suggesting that many divisions fall somewhere in between. The functional relevance of these nuclear dynamics remains elusive, although the conservation of this event to fission yeast argues for a fundamental role in gamete health (Arai et al., 2010; Asakawa et al., 2010). Virtual nuclear envelope breakdown has been proposed to facilitate spindle disassembly in fission yeast (Flor-Parra et al., 2018); however, all identified mutants affecting barrier loss also affect sporulation progression, preventing any analysis of how barrier disruption contributes to gamete health. Improved understanding of meiotic nuclear transport promises to shed light on plasticity of nuclear behavior during the cell cycle and its impact on cell health.

Chapter 5

Conclusions

The following chapter contains material derived from a publication on which I am first author (King and Ünal, 2020).

5.1 The dynamic nuclear periphery during budding yeast meiosis

Collectively, our work establishes that almost every aspect of the nuclear periphery undergoes striking remodeling during the meiotic divisions. The nuclear envelope forms a fifth compartment (the Gametogenesis Uninherited Nuclear Compartment, or GUNC) that is excluded from gametes, containing nuclear pore complexes and age-induced damage (Chapter 2). The nuclear pore complex experiences two disassembly events: partial basket detachment during meiosis I and complete basket detachment during meiosis II (Chapter 3). The nuclear permeability barrier itself is transiently disrupted, with the cytoplasm and nucleoplasm intermixing occurring after anaphase II (Chapter 4). This in-depth characterization of nuclear behavior has inspired many new questions about meiotic nuclear dynamics; answering them promises to provide fundamental insight into how the nucleus is organized. Below, I summarize our key findings and outline important areas for future inquiry.

5.1.1 The nucleus undergoes a five-way division

We made the striking finding that the nucleus undergoes a five-way division during budding yeast meiosis, driving the formation of the Gametogenesis Uninherited Nuclear Compartment or GUNC (Figure 5.1A; Chapter 2; King et al., 2019; King and Ünal, 2020). In young cells, nuclear pore complexes (NPCs) are largely sequestered to the compartment; in old cells, various forms of age-induced damage – including extrachromosomal rDNA circles, nucleolar material, and protein aggregates – are also sequestered to the compartment. The GUNC is eliminated during gamete maturation via the programmed release of proteases from the vacuole. Proper sequestration of nuclear components to the GUNC, and therefore their eventual elimination, depends on the formation of *de novo* gamete plasma membranes.

Key questions about the GUNC formation have yet to be answered (Figure 5.1B), including how material is sequestered to the GUNC and whether selectivity mechanisms exist to regulate its composition. The sequestration of material to the GUNC requires gamete plasma membranes, suggesting the existence of a lateral membrane diffusion barrier akin to that observed at the bud neck during mitosis (Clay et al., 2014). Candidate proteins informed by the mitotic mechanism – including

leading edge complex members and meiotic septins – are largely not required for sequestration; as such, we have begun the set-up of a genetic screen to identify relevant factors (Appendix A). Intriguingly, the sequestration mechanism only acts on certain classes of nuclear material (e.g., NPCs are sequestered but nuclear baskets are not). Association with chromatin is one property that might govern inheritance, but a further cataloguing of sequestered components is necessary to understand the rules governing inheritance and disinheritance. Purification of the GUNC in young and old cells, followed by mass spectrometry, could allow for high throughput analysis of its composition. Future work should also address whether a quality control mechanism exists to selectively target damaged nuclear components, such as old NPCs, to the GUNC. Preliminary evidence suggests both new and old NPCs are eliminated (Appendix B.1), but experiments have yet to be performed in old or stressed cells. Understanding GUNC formation and composition will contribute to our general understanding of how organelle sub-compartmentalization is achieved.

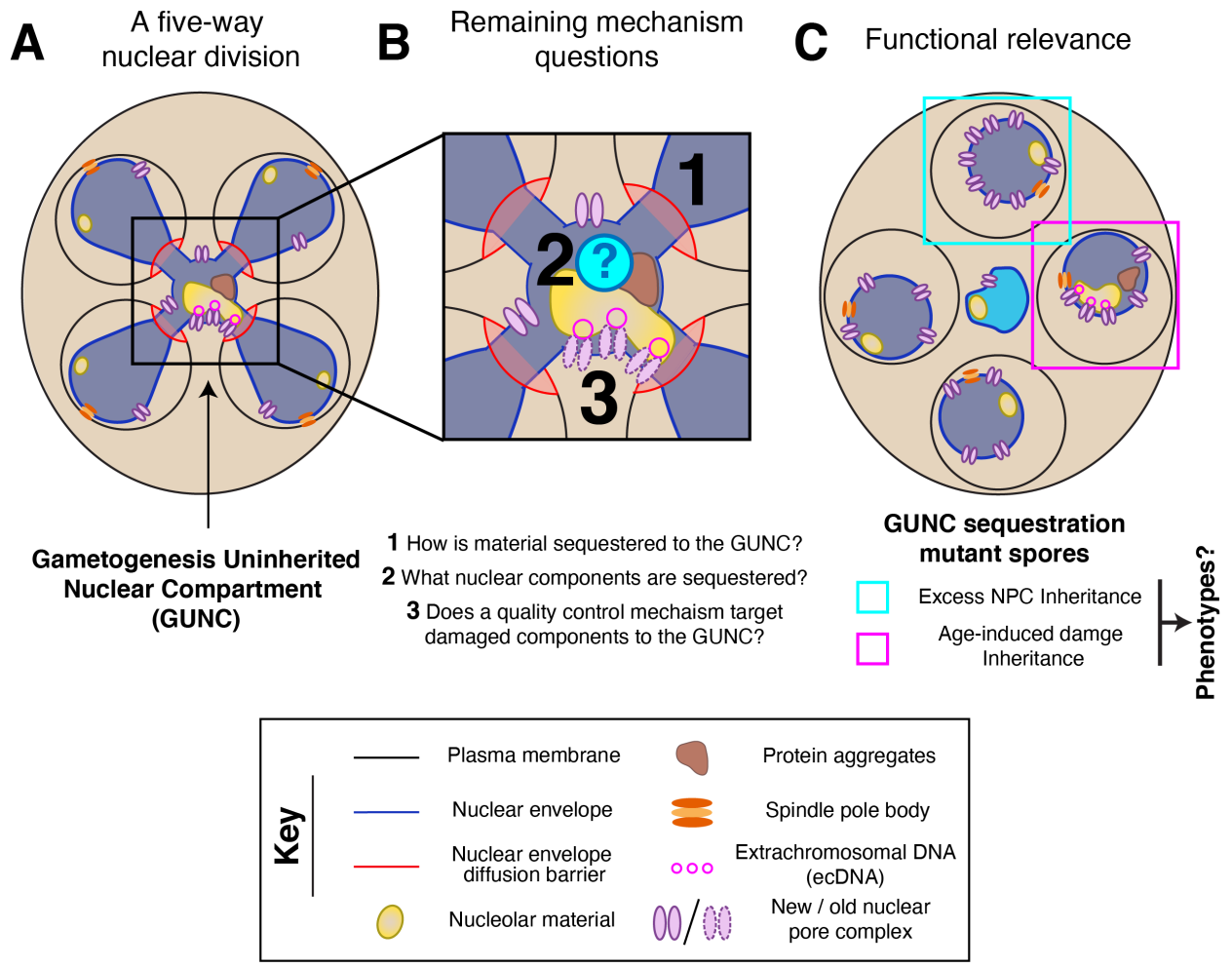

Figure 5.1. Outstanding mechanistic and functional questions relating to GUNC formation. A. Schematic summarizing the formation of the Gametogenesis

Uninherited Nuclear Compartment (GUNC; King et al., 2019). Nuclear pore complexes (NPCs) and age-induced damage are sequestered to a fifth nuclear envelope bound compartment during meiosis II. This requires formation of gamete plasma membranes, which likely create a lateral diffusion barrier in the nuclear envelope. **B.** Schematic depicting outstanding mechanistic questions regarding GUNC formation, outlined below the figure. **C.** Schematic depicting how the functional relevance of GUNC formation might be evaluated with a GUNC sequestration mutant. Gametes with excess NPC inheritance or age-induced damage inheritance could be isolated, and subsequently analyzed for phenotypes related to gamete fitness and lifespan.

The purpose of GUNC formation likewise remains enigmatic (Figure 5.1C). Functional analysis will be facilitated by the identification of mutants that are defective in sequestration of nuclear material to the GUNC (Appendix A). Since the GUNC drives elimination of various forms of age-induced damage in old cells, its formation may contribute to meiotic rejuvenation. Life-span analysis of viable gametes from sequestration-defective mutants will allow for testing of this hypothesis. In parallel, rare gamete nuclei that spontaneously inherit age-induced damage could be analyzed using a fluorescence dissection scope. Notably, the large-scale NPC turnover observed in young cells suggests that GUNC formation has functions beyond rejuvenation, especially since NPC remodeling is observed in diverse gametogenesis programs (Fawcett and Chemes, 1979; Ho, 2010; Troyer and Schwager, 1982). Sporulation efficiency, spore viability, and nuclear transport should therefore also be assessed for gametes of identified sequestration mutants. Additionally, more subtle phenotypes may be revealed by genomic approaches, such as differences in gamete transcription by RNA-seq or in chromatin compaction by Hi-C. This analysis will provide important insight into how nuclear remodeling contributes to gamete health across diverse organisms.

5.1.2 The nuclear pore complex undergoes phosphorylation-driven partial disassembly

We found that, in addition to experiencing bulk turnover, NPCs undergo cell-cycle driven changes in composition (Figure 5.2A; Chapter 3; King et al., 2022, 2019). During meiosis I, partial nuclear basket disassembly takes place, with Nup60 and its binding partner Nup2 detaching from the NPC. The Polo kinase Cdc5 drives this detachment, with Cdc5-dependent Nup60 phosphorylation disrupting its interaction with the Y-complex. Subsequent reattachment requires a lipid-binding amphipathic helix in Nup60 and facilitates proper gamete nuclear basket organization. Importantly, this NPC remodeling event is conserved in the distantly related fission yeast. During meiosis II, complete nuclear basket disassembly takes place, with all members of the nuclear basket returning to gamete nuclei. This results in the inheritance of the nuclear basket, even as the core of the NPC is disinherited.

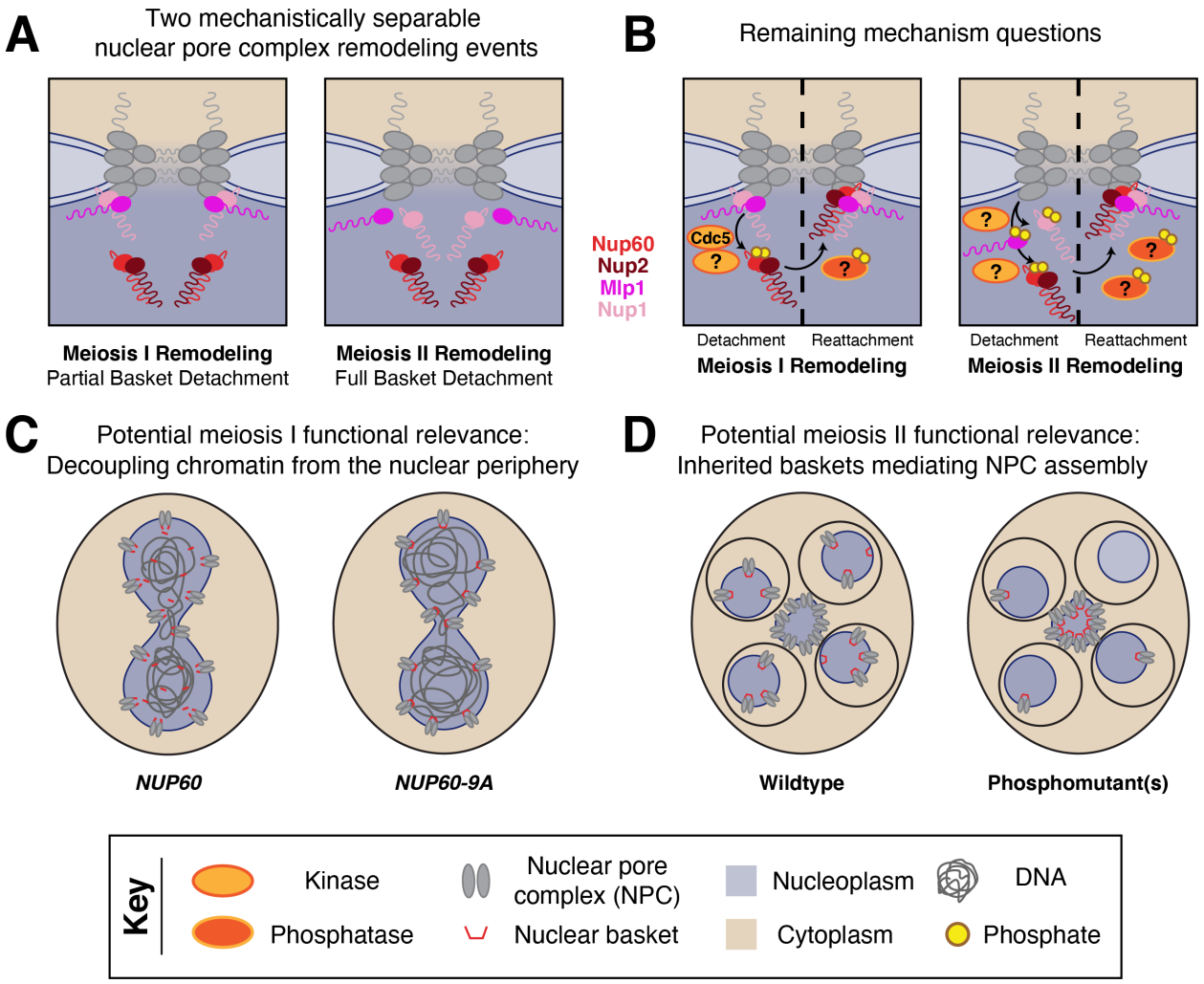

Figure 5.2. Outstanding mechanistic and functional questions relating to meiotic nuclear pore complex remodeling. A. Schematic summarizing the two nuclear pore complex (NPC) remodeling events that occur during budding yeast meiosis (King et al., 2022): partial nuclear basket detachment of Nup60 and Nup2 during meiosis I and full nuclear basket detachment during meiosis II. **B.** Schematic depicting outstanding mechanistic questions related to meiosis I and meiosis II NPC remodeling, including: (1) Is an unknown kinase acting upstream or downstream of Cdc5 to facilitate Nup60 detachment during meiosis I? (2) Does an unknown phosphatase facilitate Nup60 reattachment during meiosis I? (3) Do multiple unknown kinases and phosphatases coordinate detachment and reattachment of different basket nucleoporins during meiosis II? **C.** Schematic depicting a potential function for meiosis I partial nuclear basket detachment. The conserved detachment of Nup60-Nup2 may facilitate decoupling of chromatin from the nuclear periphery, resetting the extensive connections that are made during meiotic prophase. **D.** Schematic depicting a potential function for meiosis II full nuclear basket

detachment. The inheritance of the nuclear basket may facilitate the insertion of new NPCs in gamete nuclei.

The mechanism of meiosis I partial nuclear basket detachment has been well-characterized; in contrast, the mechanisms of meiosis I reattachment and meiosis II remodeling remain unknown (Figure 5.2B). Meiosis I detachment is driven by Cdc5-dependent phosphorylation of Nup60, although it remains unclear whether another kinase cooperates with Cdc5 to drive this phosphorylation event. Meiosis I reattachment likely involves dephosphorylation of Nup60 by an unknown phosphatase, similar to NPC reassembly during mitotic exit in metazoans (Hattersley et al., 2016). Given their precise timing, meiosis II detachment and reattachment also seem likely be driven by cell cycle-coupled phosphorylation and dephosphorylation. Additional candidate meiotic kinases and phosphatase regulators should therefore be tested for a role in dynamics of individual nucleoporins during both meiotic divisions. Multiple kinases may coordinate the detachment of different nucleoporins during meiosis II, as observed during NPC disassembly during mitosis in metazoans (Laurell et al., 2011; Linder et al., 2017). Relevant phosphosites involved in basket detachment might then be identified by looking for residues with differential phosphorylation during the meiotic divisions (using the dataset in Wettstein et al. 2022, in preparation), the approach used to identify Nup60 phosphosites during meiosis I. Improved understanding of how the nuclear basket comes apart and back together during the meiotic divisions will improve our understanding of its organization.

The two nuclear basket detachment events likely serve distinct functions, given their mechanistic separability and distinct evolutionary histories (Figure 5.2C-D). The meiosis I detachment event is conserved in *S. pombe* and therefore likely unrelated to GUNC formation. Its timing at the onset of anaphase I suggests it may decouple chromosomes and the nuclear periphery, resetting the extensive connections formed between them during prophase (Figure 5.2C; Zetka et al., 2020). Further analysis of Nup60 phosphomutants, including assessing whether they affect various metrics of gamete fitness and whether they exhibit genetic interactions, will help determine the function of this detachment event. It may also be necessary to identify additional Cdc5-dependent phosphosites on Nup60 in order to generate a phosphomutant with completely abolished phosphorylation and detachment. The meiosis II detachment event, which is specific to *S. cerevisiae*, drives basket inheritance coincident with GUNC formation. The returning basket nucleoporins may nucleate the formation of new NPCs after GUNC-dependent NPC turnover, since basket-dependent NPC assembly has been observed in metazoans (Figure 5.2D; Martino et al., 2017). Determining the mechanism of meiosis II remodeling, however, is necessary to study its functional relevance. By analyzing NPC remodeling during meiosis, new contributions of the nuclear basket to cellular health are likely to be uncovered.

5.1.3 The nucleocytoplasmic barrier undergoes a transient disruption

We found that, despite the nuclear envelope remaining intact during meiosis, the nucleus and cytoplasm transiently intermix after anaphase II (Figure 5.3A; Chapter 4). A similar alteration of nuclear transport is observed in fission yeast, suggesting that the regulatory architecture and functional relevance of the event may be deeply conserved (Arai et al., 2010; Asakawa et al., 2010). The disruption of the nuclear permeability barrier was independent from NPC sequestration to the GUNC but may be driven by changes in the Ran gradient. We identified meiotic regulators that affect both barrier loss and barrier return, laying the groundwork for more fine-scale mechanistic analysis.

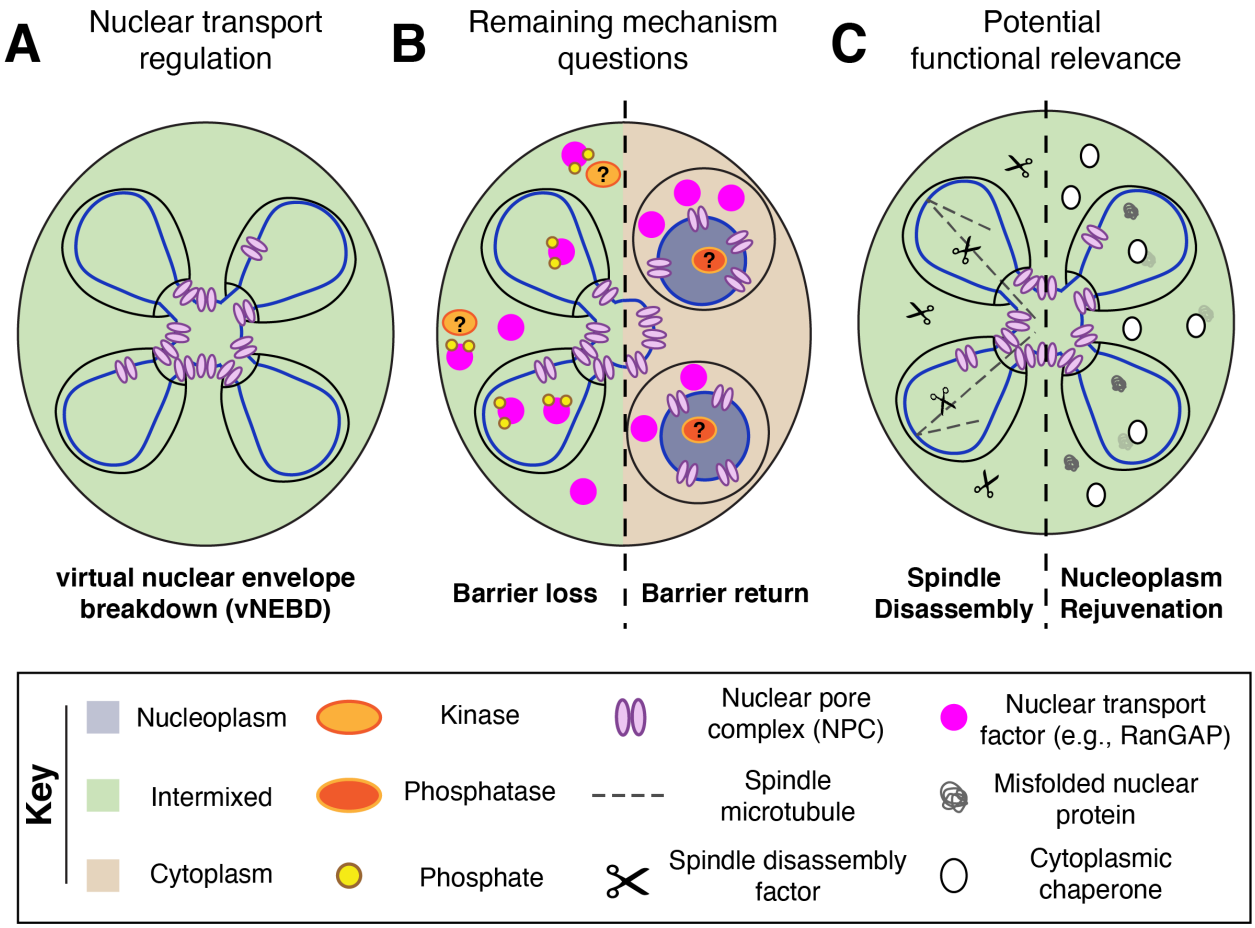

Figure 5.3. Outstanding mechanistic and functional questions relating to the transient nuclear permeability barrier disruption during budding yeast meiosis. A. Schematic depicting transient nuclear permeability barrier disruption after anaphase II, an event termed virtual nuclear envelope breakdown (vNEBD). **B.** Schematic depicting a possible mechanism of vNEBD, involving cell-cycle coupled phosphorylation and dephosphorylation of a nuclear transport factor. Key

mechanistic questions include: (1) Is barrier loss and return driven by regulation of a nuclear transport factor? (2) If so, what molecular players – such as meiotic kinases and phosphatases – are involved in this regulation? C. Schematic depicting potential functions of barrier loss, including spindle disassembly (as suggested in Flor-Parra et al., 2018) via nuclear access of a spindle disassembly factor and rejuvenation of the nucleoplasm via nuclear access of a cytoplasmic chaperone.

The proximate cause of compartment intermixing is enigmatic (Figure 5.3B). Determining the nature of barrier disruption – including whether size limits what is able to diffuse between the nucleoplasm and cytoplasm – will help determine if nuclear envelope perforation or modification of nuclear transport machinery is driving the disruption. We favor a model involving cell cycle-coupled phosphorylation and dephosphorylation of transport machinery, given that the event is well-timed with respect to other meiotic events. Phosphorylation-driven disassembly of NPCs similarly initiates nuclear barrier loss in metazoans (Laurell et al., 2011; Linder et al., 2017). Since all current candidate genes affecting barrier disruption are likely pleiotropic, additional meiotic kinases and phosphatases should be tested for a role in barrier loss and return. If no candidates seem promising after initial validation, the susceptibility of barrier disruption to various types of drug-based inhibition (e.g., nocodazole for microtubules, latrunculin for actin) may provide a mechanistic foothold. A cleverly designed genetic screen would allow for the identification of unanticipated players, but generating a permanent readout for a transient event has proven to be non-trivial. Regardless of whether a novel mechanism or convergent evolution is involved in barrier disruption, this work will provide insight into the regulation of nuclear transport during the cell cycle.

The conservation of virtual nuclear envelope breakdown in fission yeast suggests a deeply rooted function (Figure 5.3C). Initial work has implicated barrier disruption in meiosis II spindle breakdown (Flor-Parra et al., 2018), but it remains unclear why spindle disassembly machinery is unable to be imported into the nucleus as during meiosis I. Alternatively, compartment intermixing could allow access of quality control pathways to different substrates (e.g., cytoplasmic chaperones to nuclear damage), contributing to rejuvenation. The nucleoplasm has limited opportunities for turnover during closed divisions; as such, barrier loss could facilitate rejuvenation of the nucleoplasm, similarly to GUNC formation driving rejuvenation of the nuclear periphery. Identification of mutants that prevent barrier disruption but enable gamete survival will allow for determination of how nuclear transport affects gamete health and lifespan. Importantly, this functional analysis is likely to reveal the different selective pressures acting on the nucleus during asexual (mitotic) and sexual (meiotic) cell divisions.

5.2 The future of the meiotic nucleus

While I'm sad that my time studying the meiotic nucleus is coming to a close, I'm excited that my research has opened the door to many new research directions. The nuclear periphery has historically been viewed as a passive entity that functions only to encase genomic material; my work has added to a growing body of evidence that suggests, instead, it is a highly dynamic and regulated organelle with many remaining secrets. The findings that will come from studying these processes in the coming years promise to have relevance far outside of the humble (but miraculous) budding yeast, ranging from improving our understanding of nuclear aging to revealing novel functions of the nuclear basket. I'm grateful to have had the opportunity to pursue basic, mechanism-driven research during my PhD; I hope this system will provide that opportunity for many others. I am confident that, for as long as it is studied, the budding yeast meiotic nucleus will provide fundamental insights into how the eukaryotic cell works.

References

Aebi, M., Clark, M.W., Vijayraghavan, U., Abelson, J., 1990. A yeast mutant, PRP20, altered in mRNA metabolism and maintenance of the nuclear structure, is defective in a gene homologous to the human gene RCC1 which is involved in the control of chromosome condensation. Mol. Gen. Genet. MGG 224, 72–80. https://doi.org/10.1007/BF00259453

Aguilaniu, H., Gustafsson, L., Rigoulet, M., Nyström, T., 2003. Asymmetric inheritance of oxidatively damaged proteins during cytokinesis. Science 299, 1751–1753. https://doi.org/10.1126/science.1080418

Akey, C.W., Singh, D., Ouch, C., Echeverria, I., Nudelman, I., Varberg, J.M., Yu, Z., Fang, F., Shi, Y., Wang, J., Salzberg, D., Song, K., Xu, C., Gumbart, J.C., Suslov, S., Unruh, J., Jaspersen, S.L., Chait, B.T., Sali, A., Fernandez-Martinez, J., Ludtke, S.J., Villa, E., Rout, M.P., 2022a. Comprehensive structure and functional adaptations of the yeast nuclear pore complex. Cell 185, 361-378.e25. https://doi.org/10.1016/j.cell.2021.12.015

Akey, C.W., Singh, D., Ouch, C., Echeverria, I., Nudelman, I., Varberg, J.M., Yu, Z., Fang, F., Shi, Y., Wang, J., Salzberg, D., Song, K., Xu, C., Gumbart, J.C., Suslov, S., Unruh, J., Jaspersen, S.L., Chait, B.T., Sali, A., Fernandez-Martinez, J., Ludtke, S.J., Villa, E., Rout, M.P., 2022b. Comprehensive structure and functional adaptations of the yeast nuclear pore complex. Cell 185, 361-378.e25. https://doi.org/10.1016/j.cell.2021.12.015

Allegretti, M., Zimmerli, C.E., Rantos, V., Wilfling, F., Ronchi, P., Fung, H.K.H., Lee, C.-W., Hagen, W., Turoňová, B., Karius, K., Börmel, M., Zhang, X., Müller, C.W., Schwab, Y., Mahamid, J., Pfander, B., Kosinski, J., Beck, M., 2020. In-cell architecture of the nuclear pore and snapshots of its turnover. Nature 586, 796–800. https://doi.org/10.1038/s41586-020-2670-5

Anand, R., Memisoglu, G., Haber, J., 2017. Cas9-mediated gene editing in Saccharomyces cerevisiae. Protoc. Exch. https://doi.org/10.1038/protex.2017.021a

Anderson, D.J., Hetzer, M.W., 2007. Nuclear envelope formation by chromatin-mediated reorganization of the endoplasmic reticulum. Nat. Cell Biol. 9, 1160–1166. https://doi.org/10.1038/ncb1636

Arai, K., Sato, M., Tanaka, K., Yamamoto, M., 2010. Nuclear compartmentalization is abolished during fission yeast meiosis. Curr. Biol. CB 20, 1913–1918. https://doi.org/10.1016/j.cub.2010.09.004

Asakawa, H., Kojidani, T., Mori, C., Osakada, H., Sato, M., Ding, D.-Q., Hiraoka, Y., Haraguchi, T., 2010. Virtual breakdown of the nuclear envelope in fission yeast meiosis. Curr. Biol. CB 20, 1919–1925. https://doi.org/10.1016/j.cub.2010.09.070

Attner, M.A., Miller, M.P., Ee, L., Elkin, S.K., Amon, A., 2013. Polo kinase Cdc5 is a central regulator of meiosis I. Proc. Natl. Acad. Sci. U. S. A. 110, 14278–14283. https://doi.org/10.1073/pnas.1311845110

Barrantes, F.J., 2021. Chapter Nine - Fluorescence sensors for imaging membrane lipid domains and cholesterol, in: Model, M.A., Levitan, I. (Eds.), Current Topics in Membranes, New Methods and Sensors for Membrane and Cell Volume Research. Academic Press, pp. 257–314. https://doi.org/10.1016/bs.ctm.2021.09.004

Beaudouin, J., Gerlich, D., Daigle, N., Eils, R., Ellenberg, J., 2002. Nuclear Envelope Breakdown Proceeds by Microtubule-Induced Tearing of the Lamina. Cell 108, 83–96. https://doi.org/10.1016/S0092-8674(01)00627-4

Beck, M., Hurt, E., 2017. The nuclear pore complex: understanding its function through structural insight. Nat. Rev. Mol. Cell Biol. 18, 73–89. https://doi.org/10.1038/nrm.2016.147

Becker, J., Melchior, F., Gerke, V., Bischoff, F.R., Ponstingl, H., Wittinghofer, A., 1995. RNA1 Encodes a GTPase-activating Protein Specific for Gsp1p, the Ran/TC4 Homologue of Saccharomyces cerevisiae*. J. Biol. Chem. 270, 11860–11865. https://doi.org/10.1074/jbc.270.20.11860

Belhumeur, P., Lee, A., Tam, R., DiPaolo, T., Fortin, N., Clark, M.W., 1993. GSP1 and GSP2, genetic suppressors of the prp20-1 mutant in Saccharomyces cerevisiae: GTP-binding proteins involved in the maintenance of nuclear organization. Mol. Cell. Biol. 13, 2152–2161. https://doi.org/10.1128/mcb.13.4.2152-2161.1993

Benjamin, K.R., Zhang, C., Shokat, K.M., Herskowitz, I., 2003. Control of landmark events in meiosis by the CDK Cdc28 and the meiosis-specific kinase Ime2. Genes Dev. 17, 1524–1539. https://doi.org/10.1101/gad.1101503

Berchowitz, L.E., Gajadhar, A.S., van Werven, F.J., De Rosa, A.A., Samoylova, M.L., Brar, G.A., Xu, Y., Xiao, C., Futcher, B., Weissman, J.S., White, F.M., Amon, A., 2013. A developmentally regulated translational control pathway establishes the meiotic chromosome segregation pattern. Genes Dev. 27, 2147–2163. https://doi.org/10.1101/gad.224253.113

Boettcher, B., Barral, Y., 2013. The cell biology of open and closed mitosis. Nucl. Austin Tex 4, 160–165. https://doi.org/10.4161/nucl.24676

Bohnert, K.A., Kenyon, C., 2017. A lysosomal switch triggers proteostasis renewal in the immortal C. elegans germ lineage. Nature 551, 629–633. https://doi.org/10.1038/nature24620

Boke, E., Ruer, M., Wühr, M., Coughlin, M., Lemaitre, R., Gygi, S.P., Alberti, S., Drechsel, D., Hyman, A.A., Mitchison, T.J., 2016. Amyloid-like Self-assembly of a Cellular Compartment. Cell 166, 637–650. https://doi.org/10.1016/j.cell.2016.06.051

Boselli, M., Rock, J., Unal, E., Levine, S.S., Amon, A., 2009. Effects of age on meiosis in budding yeast. Dev. Cell 16, 844–855. https://doi.org/10.1016/j.devcel.2009.05.013

Brar, G.A., Yassour, M., Friedman, N., Regev, A., Ingolia, N.T., Weissman, J.S., 2012. High-resolution view of the yeast meiotic program revealed by ribosome profiling. Science 335, 552–557. https://doi.org/10.1126/science.1215110

Breucker, H., Schäfer, E., Holstein, A.F., 1985. Morphogenesis and fate of the residual body in human spermiogenesis. Cell Tissue Res. 240, 303–309. https://doi.org/10.1007/BF00222339
Brewer, B.J., Zakian, V.A., Fangman, W.L., 1980. Replication and meiotic transmission of yeast ribosomal RNA genes. Proc. Natl. Acad. Sci. U. S. A. 77, 6739–6743. https://doi.org/10.1073/pnas.77.11.6739
Buchwalter, A., Hetzer, M.W., 2017. Nucleolar expansion and elevated protein translation in premature aging. Nat. Commun. 8, 328. https://doi.org/10.1038/s41467-017-00322-z
Buchwalter, A., Kaneshiro, J.M., Hetzer, M.W., 2019. Coaching from the sidelines: the nuclear periphery in genome regulation. Nat. Rev. Genet. 20, 39–50. https://doi.org/10.1038/s41576-018-0063-5
Buchwalter, A.L., Liang, Y., Hetzer, M.W., 2014. Nup50 is required for cell differentiation and exhibits transcription-dependent dynamics. Mol. Biol. Cell 25, 2472–2484. https://doi.org/10.1091/mbc.e14-04-0865
Byers, B., 1981. Cytology of the yeast life cycle., in: The Molecular Biology of the Yeast Saccharomyces: Life Cycle and Inheritance, J.N. Strathern, E.W. Jones, and J.R. Broach, Eds. Cold Spring Harbor Laboratory Press, Cold Spring Harbor, NY, pp. 59–96.
Byers, B., Goetsch, L., 1975. Behavior of spindles and spindle plaques in the cell cycle and conjugation of Saccharomyces cerevisiae. J. Bacteriol. 124, 511–523. https://doi.org/10.1128/jb.124.1.511-523.1975
Cabrera, M., Novarina, D., Rempel, I.L., Veenhoff, L.M., Chang, M., 2017. A simple microfluidic platform to study age-dependent protein abundance and localization changes in Saccharomyces cerevisiae. Microb. Cell Graz Austria 4, 169–174. https://doi.org/10.15698/mic2017.05.573
Carlile, T.M., Amon, A., 2008. Meiosis I is established through division-specific translational control of a cyclin. Cell 133, 280–291. https://doi.org/10.1016/j.cell.2008.02.032
Caudron, F., Barral, Y., 2009. Septins and the lateral compartmentalization of eukaryotic membranes. Dev. Cell 16, 493–506. https://doi.org/10.1016/j.devcel.2009.04.003
Chao, J.T., Wong, A.K.O., Tavassoli, S., Young, B.P., Chruscicki, A., Fang, N.N., Howe, L.J., Mayor, T., Foster, L.J., Loewen, C.J.R., 2014. Polarization of the Endoplasmic Reticulum by ER-Septin Tethering. Cell 158, 620–632. https://doi.org/10.1016/j.cell.2014.06.033
Charles, J.F., Jaspersen, S.L., Tinker-Kulberg, R.L., Hwang, L., Szidon, A., Morgan, D.O., 1998. The Polo-related kinase Cdc5 activates and is destroyed by the mitotic cyclin destruction machinery in S. cerevisiae. Curr. Biol. 8, 497–507. https://doi.org/10.1016/S0960-9822(98)70201-5
Cheng, Z., Otto, G.M., Powers, E.N., Keskin, A., Mertins, P., Carr, S.A., Jovanovic, M., Brar, G.A., 2018. Pervasive, Coordinated Protein-Level Changes Driven by Transcript Isoform Switching during Meiosis. Cell 172, 910-923.e16. https://doi.org/10.1016/j.cell.2018.01.035

Chou, C.-C., Zhang, Y., Umoh, M.E., Vaughan, S.W., Lorenzini, I., Liu, F., Sayegh, M., Donlin-Asp, P.G., Chen, Y.H., Duong, D.M., Seyfried, N.T., Powers, M.A., Kukar, T., Hales, C.M., Gearing, M., Cairns, N.J., Boylan, K.B., Dickson, D.W., Rademakers, R., Zhang, Y.-J., Petrucelli, L., Sattler, R., Zarnescu, D.C., Glass, J.D., Rossoll, W., 2018. TDP-43 pathology disrupts nuclear pore complexes and nucleocytoplasmic transport in ALS/FTD. Nat. Neurosci. 21, 228–239. https://doi.org/10.1038/s41593-017-0047-3

Chu, D.B., Gromova, T., Newman, T.A.C., Burgess, S.M., 2017. The Nucleoporin Nup2 Contains a Meiotic-Autonomous Region that Promotes the Dynamic Chromosome Events of Meiosis. Genetics 206, 1319–1337. https://doi.org/10.1534/genetics.116.194555

Chu, S., Herskowitz, I., 1998. Gametogenesis in Yeast Is Regulated by a Transcriptional Cascade Dependent on Ndt80. Mol. Cell 1, 685–696. https://doi.org/10.1016/S1097-2765(00)80068-4

Chudakov, D.M., Lukyanov, S., Lukyanov, K.A., 2007. Using photoactivatable fluorescent protein Dendra2 to track protein movement. BioTechniques 42, 553–563. https://doi.org/10.2144/000112470

Cibulka, J., Bisaccia, F., Radisavljević, K., Gudino Carrillo, R.M., Köhler, A., 2022. Assembly principle of a membrane-anchored nuclear pore basket scaffold. Sci. Adv. 8, eabl6863. https://doi.org/10.1126/sciadv.abl6863

Clay, L., Caudron, F., Denoth-Lippuner, A., Boettcher, B., Buvelot Frei, S., Snapp, E.L., Barral, Y., 2014. A sphingolipid-dependent diffusion barrier confines ER stress to the yeast mother cell. eLife 3, e01883. https://doi.org/10.7554/eLife.01883

Clyne, R.K., Katis, V.L., Jessop, L., Benjamin, K.R., Herskowitz, I., Lichten, M., Nasmyth, K., 2003. Polo-like kinase Cdc5 promotes chiasmata formation and cosegregation of sister centromeres at meiosis I. Nat. Cell Biol. 5, 480–485. https://doi.org/10.1038/ncb977

Colacurcio, D.J., Nixon, R.A., 2016. Disorders of lysosomal acidification-The emerging role of v-ATPase in aging and neurodegenerative disease. Ageing Res. Rev. 32, 75–88. https://doi.org/10.1016/j.arr.2016.05.004

Colombi, P., Webster, B.M., Fröhlich, F., Lusk, C.P., 2013. The transmission of nuclear pore complexes to daughter cells requires a cytoplasmic pool of Nsp1. J. Cell Biol. 203, 215–232. https://doi.org/10.1083/jcb.201305115

Cooper, K.F., Mallory, M.J., Egeland, D.B., Jarnik, M., Strich, R., 2000. Ama1p is a meiosis-specific regulator of the anaphase promoting complex/cyclosome in yeast. Proc. Natl. Acad. Sci. U. S. A. 97, 14548–14553. https://doi.org/10.1073/pnas.250351297

D'Angelo, M.A., Raices, M., Panowski, S.H., Hetzer, M.W., 2009. Age-dependent deterioration of nuclear pore complexes causes a loss of nuclear integrity in postmitotic cells. Cell 136, 284–295. https://doi.org/10.1016/j.cell.2008.11.037

D'Aquino, K.E., Monje-Casas, F., Paulson, J., Reiser, V., Charles, G.M., Lai, L., Shokat, K.M., Amon, A., 2005. The protein kinase Kin4 inhibits exit from

mitosis in response to spindle position defects. Mol. Cell 19, 223–234. https://doi.org/10.1016/j.molcel.2005.06.005
David, D.C., Ollikainen, N., Trinidad, J.C., Cary, M.P., Burlingame, A.L., Kenyon, C., 2010. Widespread protein aggregation as an inherent part of aging in C. elegans. PLoS Biol. 8, e1000450. https://doi.org/10.1371/journal.pbio.1000450
De Souza, C.P.C., Osmani, A.H., Hashmi, S.B., Osmani, S.A., 2004. Partial Nuclear Pore Complex Disassembly during Closed Mitosis in Aspergillus nidulans. Curr. Biol. 14, 1973–1984. https://doi.org/10.1016/j.cub.2004.10.050
De Virgilio, C., DeMarini, D.J., Pringle, J.R., 1996. SPR28, a sixth member of the septin gene family in Saccharomyces cerevisiae that is expressed specifically in sporulating cells. Microbiol. Read. Engl. 142 (Pt 10), 2897–2905. https://doi.org/10.1099/13500872-142-10-2897
Denning, D., Mykytka, B., Allen, N.P., Huang, L., Al Burlingame, null, Rexach, M., 2001. The nucleoporin Nup60p functions as a Gsp1p-GTP-sensitive tether for Nup2p at the nuclear pore complex. J. Cell Biol. 154, 937–950. https://doi.org/10.1083/jcb.200101007
Denoth Lippuner, A., Julou, T., Barral, Y., 2014. Budding yeast as a model organism to study the effects of age. FEMS Microbiol. Rev. 38, 300–325. https://doi.org/10.1111/1574-6976.12060
Denoth-Lippuner, A., Krzyzanowski, M.K., Stober, C., Barral, Y., 2014. Role of SAGA in the asymmetric segregation of DNA circles during yeast ageing. eLife 3. https://doi.org/10.7554/eLife.03790
Dey, G., Baum, B., 2021. Nuclear envelope remodelling during mitosis. Curr. Opin. Cell Biol., Cell Nucleus 70, 67–74. https://doi.org/10.1016/j.ceb.2020.12.004
Dey, G., Culley, S., Curran, S., Schmidt, U., Henriques, R., Kukulski, W., Baum, B., 2020. Closed mitosis requires local disassembly of the nuclear envelope. Nature 585, 119–123. https://doi.org/10.1038/s41586-020-2648-3
Diamond, A.E., Park, J.-S., Inoue, I., Tachikawa, H., Neiman, A.M., 2009. The Anaphase Promoting Complex Targeting Subunit Ama1 Links Meiotic Exit to Cytokinesis during Sporulation in Saccharomyces cerevisiae. Mol. Biol. Cell 20, 134–145. https://doi.org/10.1091/mbc.E08-06-0615
Dilworth, D.J., Suprapto, A., Padovan, J.C., Chait, B.T., Wozniak, R.W., Rout, M.P., Aitchison, J.D., 2001. Nup2p Dynamically Associates with the Distal Regions of the Yeast Nuclear Pore Complex. J. Cell Biol. 153, 1465–1478.
Dilworth, D.J., Tackett, A.J., Rogers, R.S., Yi, E.C., Christmas, R.H., Smith, J.J., Siegel, A.F., Chait, B.T., Wozniak, R.W., Aitchison, J.D., 2005. The mobile nucleoporin Nup2p and chromatin-bound Prp20p function in endogenous NPC-mediated transcriptional control. J. Cell Biol. 171, 955–965. https://doi.org/10.1083/jcb.200509061
Dultz, E., Wojtynek, M., Medalia, O., Onischenko, E., 2022. The Nuclear Pore Complex: Birth, Life, and Death of a Cellular Behemoth. Cells 11, 1456. https://doi.org/10.3390/cells11091456
Dultz, E., Zanin, E., Wurzenberger, C., Braun, M., Rabut, G., Sironi, L., Ellenberg, J., 2008. Systematic kinetic analysis of mitotic dis- and reassembly of the

nuclear pore in living cells. J. Cell Biol. 180, 857–865. https://doi.org/10.1083/jcb.200707026
Eastwood, M.D., Cheung, S.W.T., Lee, K.Y., Moffat, J., Meneghini, M.D., 2012. Developmentally programmed nuclear destruction during yeast gametogenesis. Dev. Cell 23, 35–44. https://doi.org/10.1016/j.devcel.2012.05.005
Eastwood, M.D., Meneghini, M.D., 2015. Developmental Coordination of Gamete Differentiation with Programmed Cell Death in Sporulating Yeast. Eukaryot. Cell 14, 858–867. https://doi.org/10.1128/EC.00068-15
Eisenberg, A.R., Higdon, A., Keskin, A., Hodapp, S., Jovanovic, M., Brar, G.A., 2018. Precise Post-translational Tuning Occurs for Most Protein Complex Components during Meiosis. Cell Rep. 25, 3603-3617.e2. https://doi.org/10.1016/j.celrep.2018.12.008
Ellenberg, J., Siggia, E.D., Moreira, J.E., Smith, C.L., Presley, J.F., Worman, H.J., Lippincott-Schwartz, J., 1997. Nuclear Membrane Dynamics and Reassembly in Living Cells: Targeting of an Inner Nuclear Membrane Protein in Interphase and Mitosis. J. Cell Biol. 138, 1193–1206.
Engel, S.R., Dietrich, F.S., Fisk, D.G., Binkley, G., Balakrishnan, R., Costanzo, M.C., Dwight, S.S., Hitz, B.C., Karra, K., Nash, R.S., Weng, S., Wong, E.D., Lloyd, P., Skrzypek, M.S., Miyasato, S.R., Simison, M., Cherry, J.M., 2014. The reference genome sequence of Saccharomyces cerevisiae: then and now. G3 Bethesda Md 4, 389–398. https://doi.org/10.1534/g3.113.008995
Eriksson, M., Brown, W.T., Gordon, L.B., Glynn, M.W., Singer, J., Scott, L., Erdos, M.R., Robbins, C.M., Moses, T.Y., Berglund, P., Dutra, A., Pak, E., Durkin, S., Csoka, A.B., Boehnke, M., Glover, T.W., Collins, F.S., 2003. Recurrent de novo point mutations in lamin A cause Hutchinson-Gilford progeria syndrome. Nature 423, 293–298. https://doi.org/10.1038/nature01629
Erjavec, N., Larsson, L., Grantham, J., Nyström, T., 2007. Accelerated aging and failure to segregate damaged proteins in Sir2 mutants can be suppressed by overproducing the protein aggregation-remodeling factor Hsp104p. Genes Dev. 21, 2410–2421. https://doi.org/10.1101/gad.439307
Expósito-Serrano, M., Sánchez-Molina, A., Gallardo, P., Salas-Pino, S., Daga, R.R., 2020. Selective Nuclear Pore Complex Removal Drives Nuclear Envelope Division in Fission Yeast. Curr. Biol. 30, 3212-3222.e2. https://doi.org/10.1016/j.cub.2020.05.066
Falcón, A.A., Aris, J.P., 2003. Plasmid Accumulation Reduces Life Span in Saccharomyces cerevisiae *. J. Biol. Chem. 278, 41607–41617. https://doi.org/10.1074/jbc.M307025200
Fan, F., Liu, C.-P., Korobova, O., Heyting, C., Offenberg, H.H., Trump, G., Arnheim, N., 1997. cDNA Cloning and Characterization ofNpap60:A Novel Rat Nuclear Pore-Associated Protein with an Unusual Subcellular Localization during Male Germ Cell Differentiation. Genomics 40, 444–453. https://doi.org/10.1006/geno.1996.4557

Fares, H., Goetsch, L., Pringle, J.R., 1996. Identification of a developmentally regulated septin and involvement of the septins in spore formation in Saccharomyces cerevisiae. J. Cell Biol. 132, 399–411. https://doi.org/10.1083/jcb.132.3.399

Fawcett, D.W., Chemes, H.E., 1979. Changes in distribution of nuclear pores during differentiation of the male germ cells. Tissue Cell 11, 147–162. https://doi.org/10.1016/0040-8166(79)90015-6

Ferrandiz, N., Downie, L., Starling, G.P., Royle, S.J., 2022. Endomembranes promote chromosome missegregation by ensheathing misaligned chromosomes. J. Cell Biol. 221, e202203021. https://doi.org/10.1083/jcb.202203021

Feuerbach, F., Galy, V., Trelles-Sticken, E., Fromont-Racine, M., Jacquier, A., Gilson, E., Olivo-Marin, J.-C., Scherthan, H., Nehrbass, U., 2002. Nuclear architecture and spatial positioning help establish transcriptional states of telomeres in yeast. Nat. Cell Biol. 4, 214–221. https://doi.org/10.1038/ncb756

Flor-Parra, I., Iglesias-Romero, A.B., Salas-Pino, S., Lucena, R., Jimenez, J., Daga, R.R., 2018. Importin α and vNEBD Control Meiotic Spindle Disassembly in Fission Yeast. Cell Rep. 23, 933–941. https://doi.org/10.1016/j.celrep.2018.03.073

Foresti, O., Rodriguez-Vaello, V., Funaya, C., Carvalho, P., 2014. Quality control of inner nuclear membrane proteins by the Asi complex. Science 346, 751–755. https://doi.org/10.1126/science.1255638

Franz, C., Walczak, R., Yavuz, S., Santarella, R., Gentzel, M., Askjaer, P., Galy, V., Hetzer, M., Mattaj, I.W., Antonin, W., 2007. MEL-28/ELYS is required for the recruitment of nucleoporins to chromatin and postmitotic nuclear pore complex assembly. EMBO Rep. 8, 165–172. https://doi.org/10.1038/sj.embor.7400889

Frey, S., Görlich, D., 2007. A Saturated FG-Repeat Hydrogel Can Reproduce the Permeability Properties of Nuclear Pore Complexes. Cell 130, 512–523. https://doi.org/10.1016/j.cell.2007.06.024

Fuchs, J., Loidl, J., 2004. Behaviour of nucleolus organizing regions (NORs) and nucleoli during mitotic and meiotic divisions in budding yeast. Chromosome Res. Int. J. Mol. Supramol. Evol. Asp. Chromosome Biol. 12, 427–438. https://doi.org/10.1023/B:CHRO.0000034726.05374.db

Galy, V., Gadal, O., Fromont-Racine, M., Romano, A., Jacquier, A., Nehrbass, U., 2004. Nuclear retention of unspliced mRNAs in yeast is mediated by perinuclear Mlp1. Cell 116, 63–73. https://doi.org/10.1016/s0092-8674(03)01026-2

Gasset-Rosa, F., Chillon-Marinas, C., Goginashvili, A., Atwal, R.S., Artates, J.W., Tabet, R., Wheeler, V.C., Bang, A.G., Cleveland, D.W., Lagier-Tourenne, C., 2017. Polyglutamine-Expanded Huntingtin Exacerbates Age-Related Disruption of Nuclear Integrity and Nucleocytoplasmic Transport. Neuron 94, 48-57.e4. https://doi.org/10.1016/j.neuron.2017.03.027

Gerace, L., Blobel, G., 1980. The nuclear envelope lamina is reversibly depolymerized during mitosis. Cell 19, 277–287. https://doi.org/10.1016/0092-8674(80)90409-2
Gilbert, W., Siebel, C.W., Guthrie, C., 2001. Phosphorylation by Sky1p promotes Npl3p shuttling and mRNA dissociation. RNA N. Y. N 7, 302–313. https://doi.org/10.1017/s1355838201002369
Gillet, L.C., Navarro, P., Tate, S., Röst, H., Selevsek, N., Reiter, L., Bonner, R., Aebersold, R., 2012. Targeted data extraction of the MS/MS spectra generated by data-independent acquisition: a new concept for consistent and accurate proteome analysis. Mol. Cell. Proteomics MCP 11, O111.016717. https://doi.org/10.1074/mcp.O111.016717
Glover, J.R., Lindquist, S., 1998. Hsp104, Hsp70, and Hsp40: a novel chaperone system that rescues previously aggregated proteins. Cell 94, 73–82. https://doi.org/10.1016/s0092-8674(00)81223-4
Goodman, J.S., King, G.A., Ünal, E., 2020. Cellular quality control during gametogenesis. Exp. Cell Res. 396, 112247. https://doi.org/10.1016/j.yexcr.2020.112247
Gorsich, S.W., Shaw, J.M., 2004. Importance of mitochondrial dynamics during meiosis and sporulation. Mol. Biol. Cell 15, 4369–4381. https://doi.org/10.1091/mbc.e03-12-0875
Goudeau, J., Aguilaniu, H., 2010. Carbonylated proteins are eliminated during reproduction in C. elegans. Aging Cell 9, 991–1003. https://doi.org/10.1111/j.1474-9726.2010.00625.x
Grigaitis, R., Ranjha, L., Wild, P., Kasaciunaite, K., Ceppi, I., Kissling, V., Henggeler, A., Susperregui, A., Peter, M., Seidel, R., Cejka, P., Matos, J., 2020. Phosphorylation of the RecQ Helicase Sgs1/BLM Controls Its DNA Unwinding Activity during Meiosis and Mitosis. Dev. Cell 53, 706-723.e5. https://doi.org/10.1016/j.devcel.2020.05.016
Grigaitis, R., Susperregui, A., Wild, P., Matos, J., 2018. Chapter 16 - Characterization of DNA helicases and nucleases from meiotic extracts of S. cerevisiae, in: Maiato, H., Schuh, M. (Eds.), Methods in Cell Biology, Mitosis and Meiosis Part A. Academic Press, pp. 371–388. https://doi.org/10.1016/bs.mcb.2018.03.029
Grima, J.C., Daigle, J.G., Arbez, N., Cunningham, K.C., Zhang, K., Ochaba, J., Geater, C., Morozko, E., Stocksdale, J., Glatzer, J.C., Pham, J.T., Ahmed, I., Peng, Q., Wadhwa, H., Pletnikova, O., Troncoso, J.C., Duan, W., Snyder, S.H., Ranum, L.P.W., Thompson, L.M., Lloyd, T.E., Ross, C.A., Rothstein, J.D., 2017. Mutant Huntingtin Disrupts the Nuclear Pore Complex. Neuron 94, 93-107.e6. https://doi.org/10.1016/j.neuron.2017.03.023
Gruenbaum, Y., Foisner, R., 2015. Lamins: nuclear intermediate filament proteins with fundamental functions in nuclear mechanics and genome regulation. Annu. Rev. Biochem. 84, 131–164. https://doi.org/10.1146/annurev-biochem-060614-034115

Guan, T., Kehlenbach, R.H., Schirmer, E.C., Kehlenbach, A., Fan, F., Clurman, B.E., Arnheim, N., Gerace, L., 2000. Nup50, a Nucleoplasmically Oriented Nucleoporin with a Role in Nuclear Protein Export. Mol. Cell. Biol. 20, 5619–5630. https://doi.org/10.1128/MCB.20.15.5619-5630.2000

Gurskaya, N.G., Verkhusha, V.V., Shcheglov, A.S., Staroverov, D.B., Chepurnykh, T.V., Fradkov, A.F., Lukyanov, S., Lukyanov, K.A., 2006. Engineering of a monomeric green-to-red photoactivatable fluorescent protein induced by blue light. Nat. Biotechnol. 24, 461–465. https://doi.org/10.1038/nbt1191

Güttinger, S., Laurell, E., Kutay, U., 2009. Orchestrating nuclear envelope disassembly and reassembly during mitosis. Nat. Rev. Mol. Cell Biol. 10, 178–191. https://doi.org/10.1038/nrm2641

Haithcock, E., Dayani, Y., Neufeld, E., Zahand, A.J., Feinstein, N., Mattout, A., Gruenbaum, Y., Liu, J., 2005. Age-related changes of nuclear architecture in Caenorhabditis elegans. Proc. Natl. Acad. Sci. 102, 16690–16695. https://doi.org/10.1073/pnas.0506955102

Hakhverdyan, Z., Molloy, K.R., Keegan, S., Herricks, T., Lepore, D.M., Munson, M., Subbotin, R.I., Fenyö, D., Aitchison, J.D., Fernandez-Martinez, J., Chait, B.T., Rout, M.P., 2021. Dissecting the Structural Dynamics of the Nuclear Pore Complex. Mol. Cell 81, 153-165.e7. https://doi.org/10.1016/j.molcel.2020.11.032

Hampoelz, B., Andres-Pons, A., Kastritis, P., Beck, M., 2019. Structure and Assembly of the Nuclear Pore Complex. Annu. Rev. Biophys. 48, 515–536. https://doi.org/10.1146/annurev-biophys-052118-115308

Hartley, J.L., Temple, G.F., Brasch, M.A., 2000. DNA Cloning Using In Vitro Site-Specific Recombination. Genome Res. 10, 1788–1795. https://doi.org/10.1101/gr.143000

Haruki, H., Nishikawa, J., Laemmli, U.K., 2008. The Anchor-Away Technique: Rapid, Conditional Establishment of Yeast Mutant Phenotypes. Mol. Cell 31, 925–932. https://doi.org/10.1016/j.molcel.2008.07.020

Hatch, E.M., Fischer, A.H., Deerinck, T.J., Hetzer, M.W., 2013. Catastrophic nuclear envelope collapse in cancer cell micronuclei. Cell 154, 47–60. https://doi.org/10.1016/j.cell.2013.06.007

Hattersley, N., Cheerambathur, D., Moyle, M., Stefanutti, M., Richardson, A., Lee, K.-Y., Dumont, J., Oegema, K., Desai, A., 2016. A Nucleoporin Docks Protein Phosphatase 1 to Direct Meiotic Chromosome Segregation and Nuclear Assembly. Dev. Cell 38, 463–477. https://doi.org/10.1016/j.devcel.2016.08.006

Heald, R., McKeon, F., 1990. Mutations of phosphorylation sites in lamin A that prevent nuclear lamina disassembly in mitosis. Cell 61, 579–589. https://doi.org/10.1016/0092-8674(90)90470-Y

Henderson, K.A., Hughes, A.L., Gottschling, D.E., 2014. Mother-daughter asymmetry of pH underlies aging and rejuvenation in yeast. eLife 3, e03504. https://doi.org/10.7554/eLife.03504

Hetzer, M.W., 2010. The Nuclear Envelope. Cold Spring Harb. Perspect. Biol. 2, a000539. https://doi.org/10.1101/cshperspect.a000539

Ho, H.-C., 2010. Redistribution of nuclear pores during formation of the redundant nuclear envelope in mouse spermatids. J. Anat. 216, 525–532. https://doi.org/10.1111/j.1469-7580.2009.01204.x
Huang, J., Wang, H., Chen, Y., Wang, X., Zhang, H., 2012. Residual body removal during spermatogenesis in C. elegans requires genes that mediate cell corpse clearance. Dev. Camb. Engl. 139, 4613–4622. https://doi.org/10.1242/dev.086769
Hughes, A.L., Gottschling, D.E., 2012. An early age increase in vacuolar pH limits mitochondrial function and lifespan in yeast. Nature 492, 261–265. https://doi.org/10.1038/nature11654
Janke, C., Magiera, M.M., Rathfelder, N., Taxis, C., Reber, S., Maekawa, H., Moreno-Borchart, A., Doenges, G., Schwob, E., Schiebel, E., Knop, M., 2004. A versatile toolbox for PCR-based tagging of yeast genes: new fluorescent proteins, more markers and promoter substitution cassettes. Yeast Chichester Engl. 21, 947–962. https://doi.org/10.1002/yea.1142
Janssens, G.E., Meinema, A.C., González, J., Wolters, J.C., Schmidt, A., Guryev, V., Bischoff, R., Wit, E.C., Veenhoff, L.M., Heinemann, M., 2015. Protein biogenesis machinery is a driver of replicative aging in yeast. eLife 4, e08527. https://doi.org/10.7554/eLife.08527
Joseph, J., 2006. Ran at a glance. J. Cell Sci. 119, 3481–3484. https://doi.org/10.1242/jcs.03071
Kaeberlein, M., 2010. Lessons on longevity from budding yeast. Nature 464, 513–519. https://doi.org/10.1038/nature08981
Kalderon, D., Richardson, W.D., Markham, A.F., Smith, A.E., 1984. Sequence requirements for nuclear location of simian virus 40 large-T antigen. Nature 311, 33–38. https://doi.org/10.1038/311033a0
Kanki, T., Klionsky, D.J., 2008. Mitophagy in yeast occurs through a selective mechanism. J. Biol. Chem. 283, 32386–32393. https://doi.org/10.1074/jbc.M802403200
Katta, S.S., Smoyer, C.J., Jaspersen, S.L., 2014. Destination: inner nuclear membrane. Trends Cell Biol. 24, 221–229. https://doi.org/10.1016/j.tcb.2013.10.006
Keller, A., Nesvizhskii, A.I., Kolker, E., Aebersold, R., 2002. Empirical statistical model to estimate the accuracy of peptide identifications made by MS/MS and database search. Anal. Chem. 74, 5383–5392. https://doi.org/10.1021/ac025747h
Khmelinskii, A., Keller, P.J., Lorenz, H., Schiebel, E., Knop, M., 2010. Segregation of yeast nuclear pores. Nature 466, E1. https://doi.org/10.1038/nature09255
Khmelinskii, A., Meurer, M., Knop, M., Schiebel, E., 2011. Artificial tethering to nuclear pores promotes partitioning of extrachromosomal DNA during yeast asymmetric cell division. Curr. Biol. CB 21, R17-18. https://doi.org/10.1016/j.cub.2010.11.034
Kim, S.J., Fernandez-Martinez, J., Nudelman, I., Shi, Y., Zhang, W., Raveh, B., Herricks, T., Slaughter, B.D., Hogan, J.A., Upla, P., Chemmama, I.E.,

Pellarin, R., Echeverria, I., Shivaraju, M., Chaudhury, A.S., Wang, J., Williams, R., Unruh, J.R., Greenberg, C.H., Jacobs, E.Y., Yu, Z., de la Cruz, M.J., Mironska, R., Stokes, D.L., Aitchison, J.D., Jarrold, M.F., Gerton, J.L., Ludtke, S.J., Akey, C.W., Chait, B.T., Sali, A., Rout, M.P., 2018. Integrative structure and functional anatomy of a nuclear pore complex. Nature 555, 475–482. https://doi.org/10.1038/nature26003

King, G.A., Goodman, J.S., Schick, J.G., Chetlapalli, K., Jorgens, D.M., McDonald, K.L., Ünal, E., 2019. Meiotic cellular rejuvenation is coupled to nuclear remodeling in budding yeast. eLife 8, e47156. https://doi.org/10.7554/eLife.47156

King, G.A., Ünal, E., 2020. The dynamic nuclear periphery as a facilitator of gamete health and rejuvenation. Curr. Genet. 66, 487–493. https://doi.org/10.1007/s00294-019-01050-1

King, G.A., Wettstein, R., Varberg, J.M., Chetlapalli, K., Walsh, M.E., Gillet, L., Hernández-Armenta, C., Beltrao, P., Aebersold, R., Jaspersen, S.L., Matos, J., Ünal, E., 2022. Meiotic Nuclear Pore Complex Remodeling Provides Key Insights into Nuclear Basket Organization. https://doi.org/10.1101/2022.04.14.488376

King, M.C., Lusk, C.P., Blobel, G., 2006. Karyopherin-mediated import of integral inner nuclear membrane proteins. Nature 442, 1003–1007. https://doi.org/10.1038/nature05075

Klapholz, S., Waddell, C.S., Esposito, R.E., 1985. The role of the SPO11 gene in meiotic recombination in yeast. Genetics 110, 187–216. https://doi.org/10.1093/genetics/110.2.187

Knop, M., Strasser, K., 2000. Role of the spindle pole body of yeast in mediating assembly of the prospore membrane during meiosis. EMBO J. 19, 3657–3667. https://doi.org/10.1093/emboj/19.14.3657

Koch, B.A., Staley, E., Jin, H., Yu, H.-G., 2020. The ESCRT-III complex is required for nuclear pore complex sequestration and regulates gamete replicative lifespan in budding yeast meiosis. Nucl. Austin Tex 11, 219–236. https://doi.org/10.1080/19491034.2020.1812872

Komachi, K., Burgess, S.M., 2022. The Nup2 meiotic-autonomous region relieves inhibition of Nup60 to promote progression of meiosis and sporulation in Saccharomyces cerevisiae. Genetics iyac045. https://doi.org/10.1093/genetics/iyac045

Kremer, J.R., Mastronarde, D.N., McIntosh, J.R., 1996. Computer visualization of three-dimensional image data using IMOD. J. Struct. Biol. 116, 71–76. https://doi.org/10.1006/jsbi.1996.0013

Kumar, A., Sharma, P., Gomar-Alba, M., Shcheprova, Z., Daulny, A., Sanmartín, T., Matucci, I., Funaya, C., Beato, M., Mendoza, M., 2018. Daughter-cell-specific modulation of nuclear pore complexes controls cell cycle entry during asymmetric division. Nat. Cell Biol. 20, 432–442. https://doi.org/10.1038/s41556-018-0056-9

Kunszt, P., Blum, L., Hullár, B., Schmid, E., Srebniak, A., Wolski, W., Rinn, B., Elmer, F.-J., Ramakrishnan, C., Quandt, A., Malmström, L., 2015. iPortal: the swiss grid proteomics portal: Requirements and new features based on experience and usability considerations. Concurr. Comput. Pract. Exp. 27, 433–445. https://doi.org/10.1002/cpe.3294

Kutay, U., Jühlen, R., Antonin, W., 2021. Mitotic disassembly and reassembly of nuclear pore complexes. Trends Cell Biol. 31, 1019–1033. https://doi.org/10.1016/j.tcb.2021.06.011

Lam, C., Santore, E., Lavoie, E., Needleman, L., Fiacco, N., Kim, C., Neiman, A.M., 2014. A visual screen of protein localization during sporulation identifies new components of prospore membrane-associated complexes in budding yeast. Eukaryot. Cell 13, 383–391. https://doi.org/10.1128/EC.00333-13

Lam, H., Deutsch, E.W., Eddes, J.S., Eng, J.K., Stein, S.E., Aebersold, R., 2008. Building Consensus Spectral Libraries for Peptide Identification in Proteomics. Nat. Methods 5, 873–875. https://doi.org/10.1038/nmeth.1254

Laurell, E., Beck, K., Krupina, K., Theerthagiri, G., Bodenmiller, B., Horvath, P., Aebersold, R., Antonin, W., Kutay, U., 2011. Phosphorylation of Nup98 by Multiple Kinases Is Crucial for NPC Disassembly during Mitotic Entry. Cell 144, 539–550. https://doi.org/10.1016/j.cell.2011.01.012

Lee, B.H., Amon, A., 2003. Role of Polo-like kinase CDC5 in programming meiosis I chromosome segregation. Science 300, 482–486. https://doi.org/10.1126/science.1081846

Lee, C.-W., Wilfling, F., Ronchi, P., Allegretti, M., Mosalaganti, S., Jentsch, S., Beck, M., Pfander, B., 2020. Selective autophagy degrades nuclear pore complexes. Nat. Cell Biol. 22, 159–166. https://doi.org/10.1038/s41556-019-0459-2

Lee, K.K., Gruenbaum, Y., Spann, P., Liu, J., Wilson, K.L., 2000. C. elegans nuclear envelope proteins emerin, MAN1, lamin, and nucleoporins reveal unique timing of nuclear envelope breakdown during mitosis. Mol. Biol. Cell 11, 3089–3099. https://doi.org/10.1091/mbc.11.9.3089

Lee, W.C., Zabetakis, D., Mélèse, T., 1992. NSR1 is required for pre-rRNA processing and for the proper maintenance of steady-state levels of ribosomal subunits. Mol. Cell. Biol. 12, 3865–3871. https://doi.org/10.1128/mcb.12.9.3865-3871.1992

Lewinska, A., Miedziak, B., Kulak, K., Molon, M., Wnuk, M., 2014. Links between nucleolar activity, rDNA stability, aneuploidy and chronological aging in the yeast Saccharomyces cerevisiae. Biogerontology 15, 289–316. https://doi.org/10.1007/s10522-014-9499-y

Li, H.Y., Wirtz, D., Zheng, Y., 2003. A mechanism of coupling RCC1 mobility to RanGTP production on the chromatin in vivo. J. Cell Biol. 160, 635–644. https://doi.org/10.1083/jcb.200211004

Li, P., Jin, H., Hoang, M.L., Yu, H.-G., 2011. Tracking chromosome dynamics in live yeast cells: coordinated movement of rDNA homologs and anaphase disassembly of the nucleolus during meiosis. Chromosome Res. Int. J. Mol.

Supramol. Evol. Asp. Chromosome Biol. 19, 1013–1026. https://doi.org/10.1007/s10577-011-9253-0
Lieber, T., Jeedigunta, S.P., Palozzi, J.M., Lehmann, R., Hurd, T.R., 2019. Mitochondrial fragmentation drives selective removal of deleterious mtDNA in the germline. Nature 570, 380–384. https://doi.org/10.1038/s41586-019-1213-4
Lin, D.H., Hoelz, A., 2019. The Structure of the Nuclear Pore Complex (An Update). Annu. Rev. Biochem. 88, 725–783. https://doi.org/10.1146/annurev-biochem-062917-011901
Linder, M.I., Köhler, M., Boersema, P., Weberruss, M., Wandke, C., Marino, J., Ashiono, C., Picotti, P., Antonin, W., Kutay, U., 2017. Mitotic Disassembly of Nuclear Pore Complexes Involves CDK1- and PLK1-Mediated Phosphorylation of Key Interconnecting Nucleoporins. Dev. Cell 43, 141-156.e7. https://doi.org/10.1016/j.devcel.2017.08.020
Liu, S., Kwon, M., Mannino, M., Yang, N., Renda, F., Khodjakov, A., Pellman, D., 2018. Nuclear envelope assembly defects link mitotic errors to chromothripsis. Nature 561, 551–555. https://doi.org/10.1038/s41586-018-0534-z
Logie, C., Stewart, A.F., 1995. Ligand-regulated site-specific recombination. Proc. Natl. Acad. Sci. 92, 5940–5944. https://doi.org/10.1073/pnas.92.13.5940
Longo, V.D., Shadel, G.S., Kaeberlein, M., Kennedy, B., 2012. Replicative and chronological aging in Saccharomyces cerevisiae. Cell Metab. 16, 18–31. https://doi.org/10.1016/j.cmet.2012.06.002
Longtine, M.S., McKenzie, A., Demarini, D.J., Shah, N.G., Wach, A., Brachat, A., Philippsen, P., Pringle, J.R., 1998. Additional modules for versatile and economical PCR-based gene deletion and modification in Saccharomyces cerevisiae. Yeast Chichester Engl. 14, 953–961. https://doi.org/10.1002/(SICI)1097-0061(199807)14:10<953::AID-YEA293>3.0.CO;2-U
Lord, C.L., Timney, B.L., Rout, M.P., Wente, S.R., 2015. Altering nuclear pore complex function impacts longevity and mitochondrial function in S. cerevisiae. J. Cell Biol. 208, 729–744. https://doi.org/10.1083/jcb.201412024
Ludwig, C., Gillet, L., Rosenberger, G., Amon, S., Collins, B.C., Aebersold, R., 2018. Data-independent acquisition-based SWATH-MS for quantitative proteomics: a tutorial. Mol. Syst. Biol. 14, e8126. https://doi.org/10.15252/msb.20178126
Maier, P., Rathfelder, N., Maeder, C.I., Colombelli, J., Stelzer, E.H.K., Knop, M., 2008. The SpoMBe pathway drives membrane bending necessary for cytokinesis and spore formation in yeast meiosis. EMBO J. 27, 2363–2374. https://doi.org/10.1038/emboj.2008.168
Makarova, M., Gu, Y., Chen, J.-S., Beckley, J.R., Gould, K.L., Oliferenko, S., 2016. Temporal Regulation of Lipin Activity Diverged to Account for Differences in Mitotic Programs. Curr. Biol. 26, 237–243. https://doi.org/10.1016/j.cub.2015.11.061

Makio, T., Lapetina, D.L., Wozniak, R.W., 2013. Inheritance of yeast nuclear pore complexes requires the Nsp1p subcomplex. J. Cell Biol. 203, 187–196. https://doi.org/10.1083/jcb.201304047

Markossian, S., Suresh, S., Osmani, A.H., Osmani, S.A., 2015. Nup2 requires a highly divergent partner, NupA, to fulfill functions at nuclear pore complexes and the mitotic chromatin region. Mol. Biol. Cell 26, 605–621. https://doi.org/10.1091/mbc.E14-09-1359

Maro, B., Verlhac, M.-H., 2002. Polar body formation: new rules for asymmetric divisions. Nat. Cell Biol. 4, E281–E283. https://doi.org/10.1038/ncb1202-e281

Marston, A.L., Amon, A., 2004. Meiosis: cell-cycle controls shuffle and deal. Nat. Rev. Mol. Cell Biol. 5, 983–997. https://doi.org/10.1038/nrm1526

Martino, L., Morchoisne-Bolhy, S., Cheerambathur, D.K., Van Hove, L., Dumont, J., Joly, N., Desai, A., Doye, V., Pintard, L., 2017. Channel Nucleoporins recruit PLK-1 to Nuclear Pore Complexes to Direct Nuclear Envelope Breakdown in C. elegans. Dev. Cell 43, 157-171.e7. https://doi.org/10.1016/j.devcel.2017.09.019

Martins, F., Sousa, J., Pereira, C.D., da Cruz e Silva, O.A.B., Rebelo, S., 2020. Nuclear envelope dysfunction and its contribution to the aging process. Aging Cell 19, e13143. https://doi.org/10.1111/acel.13143

Matos, J., Blanco, M.G., Maslen, S., Skehel, J.M., West, S.C., 2011. Regulatory control of the resolution of DNA recombination intermediates during meiosis and mitosis. Cell 147, 158–172. https://doi.org/10.1016/j.cell.2011.08.032

Matos, J., Lipp, J.J., Bogdanova, A., Guillot, S., Okaz, E., Junqueira, M., Shevchenko, A., Zachariae, W., 2008. Dbf4-dependent CDC7 kinase links DNA replication to the segregation of homologous chromosomes in meiosis I. Cell 135, 662–678. https://doi.org/10.1016/j.cell.2008.10.026

McDonald, K., Müller-Reichert, T., 2002. Cryomethods for thin section electron microscopy. Methods Enzymol. 351, 96–123. https://doi.org/10.1016/s0076-6879(02)51843-7

McDonald, K.L., 2014. Out with the old and in with the new: rapid specimen preparation procedures for electron microscopy of sectioned biological material. Protoplasma 251, 429–448. https://doi.org/10.1007/s00709-013-0575-y

McDonald, K.L., Webb, R.I., 2011. Freeze substitution in 3 hours or less. J. Microsc. 243, 227–233. https://doi.org/10.1111/j.1365-2818.2011.03526.x

Meinema, A.C., Laba, J.K., Hapsari, R.A., Otten, R., Mulder, F.A.A., Kralt, A., van den Bogaart, G., Lusk, C.P., Poolman, B., Veenhoff, L.M., 2011. Long unfolded linkers facilitate membrane protein import through the nuclear pore complex. Science 333, 90–93. https://doi.org/10.1126/science.1205741

Mekhail, K., Moazed, D., 2010. The nuclear envelope in genome organization, expression and stability. Nat. Rev. Mol. Cell Biol. 11, 317–328. https://doi.org/10.1038/nrm2894

Mekhail, K., Seebacher, J., Gygi, S.P., Moazed, D., 2008. Role for perinuclear chromosome tethering in maintenance of genome stability. Nature 456, 667–670. https://doi.org/10.1038/nature07460
Melloy, P.G., Rose, M.D., 2017. Influence of the bud neck on nuclear envelope fission in Saccharomyces cerevisiae. Exp. Cell Res. 358, 390–396. https://doi.org/10.1016/j.yexcr.2017.07.013
Mészáros, N., Cibulka, J., Mendiburo, M.J., Romanauska, A., Schneider, M., Köhler, A., 2015. Nuclear pore basket proteins are tethered to the nuclear envelope and can regulate membrane curvature. Dev. Cell 33, 285–298. https://doi.org/10.1016/j.devcel.2015.02.017
Michaelis, C., Ciosk, R., Nasmyth, K., 1997. Cohesins: chromosomal proteins that prevent premature separation of sister chromatids. Cell 91, 35–45. https://doi.org/10.1016/s0092-8674(01)80007-6
Miller, M.P., Ünal, E., Brar, G.A., Amon, A., 2012. Meiosis I chromosome segregation is established through regulation of microtubule–kinetochore interactions. eLife 1, e00117. https://doi.org/10.7554/eLife.00117
Miyakawa, I., Aoi, H., Sando, N., Kuroiwa, T., 1984. Fluorescence microscopic studies of mitochondrial nucleoids during meiosis and sporulation in the yeast, Saccharomyces cerevisiae. J. Cell Sci. 66, 21–38. https://doi.org/10.1242/jcs.66.1.21
Mochida, K., Oikawa, Y., Kimura, Y., Kirisako, H., Hirano, H., Ohsumi, Y., Nakatogawa, H., 2015. Receptor-mediated selective autophagy degrades the endoplasmic reticulum and the nucleus. Nature 522, 359–362. https://doi.org/10.1038/nature14506
Moens, P.B., 1971. Fine structure of ascospore development in the yeast Saccharomyces cerevisiae. Can. J. Microbiol. 17, 507–510. https://doi.org/10.1139/m71-084
Moens, P.B., Rapport, E., 1971. Spindles, spindle plaques, and meiosis in the yeast Saccharomyces cerevisiae (Hansen). J. Cell Biol. 50, 344–361. https://doi.org/10.1083/jcb.50.2.344
Moore, D., Pilz, G., Araúzo-Bravo, M., Barral, Y., Jessberger, S., 2015. A mechanism for the segregation of age in mammalian neural stem cells. Science 349, 1334–1338. https://doi.org/10.1126/science.aac9868
Moreno-Borchart, A.C., Strasser, K., Finkbeiner, M.G., Shevchenko, A., Shevchenko, A., Knop, M., 2001. Prospore membrane formation linked to the leading edge protein (LEP) coat assembly. EMBO J. 20, 6946–6957. https://doi.org/10.1093/emboj/20.24.6946
Morlot, S., Song, J., Léger-Silvestre, I., Matifas, A., Gadal, O., Charvin, G., 2019. Excessive rDNA Transcription Drives the Disruption in Nuclear Homeostasis during Entry into Senescence in Budding Yeast. Cell Rep. 28, 408-422.e4. https://doi.org/10.1016/j.celrep.2019.06.032
Mortimer, R.K., Johnston, J.R., 1959. Life span of individual yeast cells. Nature 183, 1751–1752. https://doi.org/10.1038/1831751a0

Nakanishi, H., de los Santos, P., Neiman, A.M., 2004. Positive and negative regulation of a SNARE protein by control of intracellular localization. Mol. Biol. Cell 15, 1802–1815. https://doi.org/10.1091/mbc.e03-11-0798
Navarro, P., Kuharev, J., Gillet, L.C., Bernhardt, O.M., MacLean, B., Röst, H.L., Tate, S.A., Tsou, C.-C., Reiter, L., Distler, U., Rosenberger, G., Perez-Riverol, Y., Nesvizhskii, A.I., Aebersold, R., Tenzer, S., 2016. A multicenter study benchmarks software tools for label-free proteome quantification. Nat. Biotechnol. 34, 1130–1136. https://doi.org/10.1038/nbt.3685
Neiman, A.M., 2011. Sporulation in the budding yeast Saccharomyces cerevisiae. Genetics 189, 737–765. https://doi.org/10.1534/genetics.111.127126
Neiman, A.M., 1998. Prospore membrane formation defines a developmentally regulated branch of the secretory pathway in yeast. J. Cell Biol. 140, 29–37. https://doi.org/10.1083/jcb.140.1.29
Neumann, F.R., Nurse, P., 2007. Nuclear size control in fission yeast. J. Cell Biol. 179, 593–600. https://doi.org/10.1083/jcb.200708054
Neurohr, G.E., Terry, R.L., Sandikci, A., Zou, K., Li, H., Amon, A., 2018. Deregulation of the G1/S-phase transition is the proximal cause of mortality in old yeast mother cells. Genes Dev. https://doi.org/10.1101/gad.312140.118
Niepel, M., Molloy, K.R., Williams, R., Farr, J.C., Meinema, A.C., Vecchietti, N., Cristea, I.M., Chait, B.T., Rout, M.P., Strambio-De-Castillia, C., 2013. The nuclear basket proteins Mlp1p and Mlp2p are part of a dynamic interactome including Esc1p and the proteasome. Mol. Biol. Cell 24, 3920–3938. https://doi.org/10.1091/mbc.E13-07-0412
Niño, C.A., Guet, D., Gay, A., Brutus, S., Jourquin, F., Mendiratta, S., Salamero, J., Géli, V., Dargemont, C., 2016. Posttranslational marks control architectural and functional plasticity of the nuclear pore complex basket. J. Cell Biol. 212, 167–180. https://doi.org/10.1083/jcb.201506130
Nishimura, K., Fukagawa, T., Takisawa, H., Kakimoto, T., Kanemaki, M., 2009. An auxin-based degron system for the rapid depletion of proteins in nonplant cells. Nat. Methods 6, 917–922. https://doi.org/10.1038/nmeth.1401
Ocampo, A., Reddy, P., Martinez-Redondo, P., Platero-Luengo, A., Hatanaka, F., Hishida, T., Li, M., Lam, D., Kurita, M., Beyret, E., Araoka, T., Vazquez-Ferrer, E., Donoso, D., Roman, J.L., Xu, J., Rodriguez Esteban, C., Nuñez, G., Nuñez Delicado, E., Campistol, J.M., Guillen, I., Guillen, P., Izpisua Belmonte, J.C., 2016. In Vivo Amelioration of Age-Associated Hallmarks by Partial Reprogramming. Cell 167, 1719-1733.e12. https://doi.org/10.1016/j.cell.2016.11.052
Oelschlaegel, T., Schwickart, M., Matos, J., Bogdanova, A., Camasses, A., Havlis, J., Shevchenko, A., Zachariae, W., 2005. The yeast APC/C subunit Mnd2 prevents premature sister chromatid separation triggered by the meiosis-specific APC/C-Ama1. Cell 120, 773–788. https://doi.org/10.1016/j.cell.2005.01.032
O'Hara, L., Han, G.-S., Peak-Chew, S., Grimsey, N., Carman, G.M., Siniossoglou, S., 2006. Control of phospholipid synthesis by phosphorylation of the yeast lipin

Pah1p/Smp2p Mg2+-dependent phosphatidate phosphatase. J. Biol. Chem. 281, 34537–34548. https://doi.org/10.1074/jbc.M606654200
Olmos, Y., Hodgson, L., Mantell, J., Verkade, P., Carlton, J.G., 2015. ESCRT-III controls nuclear envelope reformation. Nature 522, 236–239. https://doi.org/10.1038/nature14503
Onischenko, E., Noor, E., Fischer, J.S., Gillet, L., Wojtynek, M., Vallotton, P., Weis, K., 2020. Maturation Kinetics of a Multiprotein Complex Revealed by Metabolic Labeling. Cell 183, 1785-1800.e26. https://doi.org/10.1016/j.cell.2020.11.001
Osmani, A.H., Davies, J., Liu, H.-L., Nile, A., Osmani, S.A., 2006. Systematic Deletion and Mitotic Localization of the Nuclear Pore Complex Proteins of Aspergillus nidulans. Mol. Biol. Cell 17, 4946–4961. https://doi.org/10.1091/mbc.e06-07-0657
Otsuka, S., Bui, K.H., Schorb, M., Hossain, M.J., Politi, A.Z., Koch, B., Eltsov, M., Beck, M., Ellenberg, J., 2016. Nuclear pore assembly proceeds by an inside-out extrusion of the nuclear envelope. eLife 5, e19071. https://doi.org/10.7554/eLife.19071
Otsuka, S., Steyer, A.M., Schorb, M., Hériché, J.-K., Hossain, M.J., Sethi, S., Kueblbeck, M., Schwab, Y., Beck, M., Ellenberg, J., 2018. Postmitotic nuclear pore assembly proceeds by radial dilation of small membrane openings. Nat. Struct. Mol. Biol. 25, 21–28. https://doi.org/10.1038/s41594-017-0001-9
Otto, G.M., Cheunkarndee, T., Leslie, J.M., Brar, G.A., 2021. Programmed cortical ER collapse drives selective ER degradation and inheritance in yeast meiosis. J. Cell Biol. 220, e202108105. https://doi.org/10.1083/jcb.202108105
Ozsarac, N., Bhattacharyya, M., Dawes, I.W., Clancy, M.J., 1995. The SPR3 gene encodes a sporulation-specific homologue of the yeast CDC3/10/11/12 family of bud neck microfilaments and is regulated by ABFI. Gene 164, 157–162. https://doi.org/10.1016/0378-1119(95)00438-c
Palancade, B., Zuccolo, M., Loeillet, S., Nicolas, A., Doye, V., 2005. Pml39, a Novel Protein of the Nuclear Periphery Required for Nuclear Retention of Improper Messenger Ribonucleoparticles. Mol. Biol. Cell 16, 5258–5268. https://doi.org/10.1091/mbc.E05-06-0527
Park, C.J., Park, J.-E., Karpova, T.S., Soung, N.-K., Yu, L.-R., Song, S., Lee, K.H., Xia, X., Kang, E., Dabanoglu, I., Oh, D.-Y., Zhang, J.Y., Kang, Y.H., Wincovitch, S., Huffaker, T.C., Veenstra, T.D., McNally, J.G., Lee, K.S., 2008. Requirement for the Budding Yeast Polo Kinase Cdc5 in Proper Microtubule Growth and Dynamics. Eukaryot. Cell 7, 444–453. https://doi.org/10.1128/EC.00283-07
Paxman, J., Zhou, Z., O'Laughlin, R., Li, Y., Tian, W., Su, H., Jiang, Y., Holness, S.E., Stasiowski, E., Tsimring, L.S., Pillus, L., Hasty, J., Hao, N., 2021. Age-dependent aggregation of ribosomal RNA-binding proteins links deterioration in chromatin stability with loss of proteostasis. https://doi.org/10.1101/2021.12.06.471495

Pemberton, L.F., Paschal, B.M., 2005. Mechanisms of Receptor-Mediated Nuclear Import and Nuclear Export. Traffic 6, 187–198. https://doi.org/10.1111/j.1600-0854.2005.00270.x

Petersen, J., Russell, P., 2016. Growth and the Environment of Schizosaccharomyces pombe. Cold Spring Harb. Protoc. 2016, pdb.top079764. https://doi.org/10.1101/pdb.top079764

Petronczki, M., Matos, J., Mori, S., Gregan, J., Bogdanova, A., Schwickart, M., Mechtler, K., Shirahige, K., Zachariae, W., Nasmyth, K., 2006. Monopolar Attachment of Sister Kinetochores at Meiosis I Requires Casein Kinase 1. Cell 126, 1049–1064. https://doi.org/10.1016/j.cell.2006.07.029

R Core Team, 2020. R: a language and environment for statistical computing. R Found. Stat. Comput. Vienna Austria.

Rabut, G., Doye, V., Ellenberg, J., 2004. Mapping the dynamic organization of the nuclear pore complex inside single living cells. Nat. Cell Biol. 6, 1114–1121. https://doi.org/10.1038/ncb1184

Rajoo, S., Vallotton, P., Onischenko, E., Weis, K., 2018. Stoichiometry and compositional plasticity of the yeast nuclear pore complex revealed by quantitative fluorescence microscopy. Proc. Natl. Acad. Sci. U. S. A. 115, E3969–E3977. https://doi.org/10.1073/pnas.1719398115

Rempel, I.L., Crane, M.M., Thaller, D.J., Mishra, A., Jansen, D.P., Janssens, G., Popken, P., Akşit, A., Kaeberlein, M., van der Giessen, E., Steen, A., Onck, P.R., Lusk, C.P., Veenhoff, L.M., 2019. Age-dependent deterioration of nuclear pore assembly in mitotic cells decreases transport dynamics. eLife 8, e48186. https://doi.org/10.7554/eLife.48186

Reynolds, E.S., 1963. The use of lead citrate at high pH as an electron-opaque stain in electron microscopy. J. Cell Biol. 17, 208–212. https://doi.org/10.1083/jcb.17.1.208

Ritchie, M.E., Phipson, B., Wu, D., Hu, Y., Law, C.W., Shi, W., Smyth, G.K., 2015. limma powers differential expression analyses for RNA-sequencing and microarray studies. Nucleic Acids Res. 43, e47. https://doi.org/10.1093/nar/gkv007

Roeder, A.D., Shaw, J.M., 1996. Vacuole partitioning during meiotic division in yeast. Genetics 144, 445–458. https://doi.org/10.1093/genetics/144.2.445

Romanauska, A., Köhler, A., 2021. Reprogrammed lipid metabolism protects inner nuclear membrane against unsaturated fat. Dev. Cell 56, 2562-2578.e3. https://doi.org/10.1016/j.devcel.2021.07.018

Romanauska, A., Köhler, A., 2018. The Inner Nuclear Membrane Is a Metabolically Active Territory that Generates Nuclear Lipid Droplets. Cell 174, 700-715.e18. https://doi.org/10.1016/j.cell.2018.05.047

Röst, H.L., Liu, Y., D'Agostino, G., Zanella, M., Navarro, P., Rosenberger, G., Collins, B.C., Gillet, L., Testa, G., Malmström, L., Aebersold, R., 2016. TRIC: an automated alignment strategy for reproducible protein quantification in targeted proteomics. Nat. Methods 13, 777–783. https://doi.org/10.1038/nmeth.3954

Röst, H.L., Rosenberger, G., Navarro, P., Gillet, L., Miladinović, S.M., Schubert, O.T., Wolski, W., Collins, B.C., Malmström, J., Malmström, L., Aebersold, R., 2014. OpenSWATH enables automated, targeted analysis of data-independent acquisition MS data. Nat. Biotechnol. 32, 219–223. https://doi.org/10.1038/nbt.2841

Roubinet, C., White, I.J., Baum, B., 2021. Asymmetric nuclear division in neural stem cells generates sibling nuclei that differ in size, envelope composition, and chromatin organization. Curr. Biol. CB 31, 3973-3983.e4. https://doi.org/10.1016/j.cub.2021.06.063

Saarikangas, J., Caudron, F., Prasad, R., Moreno, D.F., Bolognesi, A., Aldea, M., Barral, Y., 2017. Compartmentalization of ER-Bound Chaperone Confines Protein Deposit Formation to the Aging Yeast Cell. Curr. Biol. CB 27, 773–783. https://doi.org/10.1016/j.cub.2017.01.069

Sabath, N., Levy-Adam, F., Younis, A., Rozales, K., Meller, A., Hadar, S., Soueid-Baumgarten, S., Shalgi, R., 2020. Cellular proteostasis decline in human senescence. Proc. Natl. Acad. Sci. 117, 31902–31913. https://doi.org/10.1073/pnas.2018138117

Sari, F., Heinrich, M., Meyer, W., Braus, G.H., Irniger, S., 2008. The C-terminal Region of the Meiosis-specific Protein Kinase Ime2 Mediates Protein Instability and is Required for Normal Spore Formation in Budding Yeast. J. Mol. Biol. 378, 31–43. https://doi.org/10.1016/j.jmb.2008.02.001

Sarkar, T.J., Quarta, M., Mukherjee, S., Colville, A., Paine, P., Doan, L., Tran, C.M., Chu, C.R., Horvath, S., Qi, L.S., Bhutani, N., Rando, T.A., Sebastiano, V., 2020. Transient non-integrative expression of nuclear reprogramming factors promotes multifaceted amelioration of aging in human cells. Nat. Commun. 11, 1545. https://doi.org/10.1038/s41467-020-15174-3

Sawyer, E.M., Joshi, P.R., Jorgensen, V., Yunus, J., Berchowitz, L.E., Ünal, E., 2019. Developmental regulation of an organelle tether coordinates mitochondrial remodeling in meiosis. J. Cell Biol. 218, 559–579. https://doi.org/10.1083/jcb.201807097

Scaffidi, P., Misteli, T., 2006. Lamin A-Dependent Nuclear Defects in Human Aging. Science 312, 1059–1063. https://doi.org/10.1126/science.1127168

Scarcelli, J.J., Hodge, C.A., Cole, C.N., 2007. The yeast integral membrane protein Apq12 potentially links membrane dynamics to assembly of nuclear pore complexes. J. Cell Biol. 178, 799–812. https://doi.org/10.1083/jcb.200702120

Schindelin, J., Arganda-Carreras, I., Frise, E., Kaynig, V., Longair, M., Pietzsch, T., Preibisch, S., Rueden, C., Saalfeld, S., Schmid, B., Tinevez, J.-Y., White, D.J., Hartenstein, V., Eliceiri, K., Tomancak, P., Cardona, A., 2012. Fiji: an open-source platform for biological-image analysis. Nat. Methods 9, 676–682. https://doi.org/10.1038/nmeth.2019

Schubert, O.T., Gillet, L.C., Collins, B.C., Navarro, P., Rosenberger, G., Wolski, W.E., Lam, H., Amodei, D., Mallick, P., MacLean, B., Aebersold, R., 2015. Building high-quality assay libraries for targeted analysis of SWATH MS data. Nat. Protoc. 10, 426–441. https://doi.org/10.1038/nprot.2015.015

Schuller, A.P., Wojtynek, M., Mankus, D., Tatli, M., Kronenberg-Tenga, R., Regmi, S.G., Dip, P.V., Lytton-Jean, A.K.R., Brignole, E.J., Dasso, M., Weis, K., Medalia, O., Schwartz, T.U., 2021. The cellular environment shapes the nuclear pore complex architecture. Nature 598, 667–671. https://doi.org/10.1038/s41586-021-03985-3

Sehnal, D., Bittrich, S., Deshpande, M., Svobodová, R., Berka, K., Bazgier, V., Velankar, S., Burley, S.K., Koča, J., Rose, A.S., 2021. Mol* Viewer: modern web app for 3D visualization and analysis of large biomolecular structures. Nucleic Acids Res. 49, W431–W437. https://doi.org/10.1093/nar/gkab314

Sheff, M.A., Thorn, K.S., 2004. Optimized cassettes for fluorescent protein tagging in Saccharomyces cerevisiae. Yeast Chichester Engl. 21, 661–670. https://doi.org/10.1002/yea.1130

Shelton, S.N., Smith, S.E., Unruh, J.R., Jaspersen, S.L., 2021. A distinct inner nuclear membrane proteome in Saccharomyces cerevisiae gametes. G3 GenesGenomesGenetics 11, jkab345. https://doi.org/10.1093/g3journal/jkab345

Shou, W., Azzam, R., Chen, S.L., Huddleston, M.J., Baskerville, C., Charbonneau, H., Annan, R.S., Carr, S.A., Deshaies, R.J., 2002. Cdc5 influences phosphorylation of Net1 and disassembly of the RENT complex. BMC Mol. Biol. 3, 3. https://doi.org/10.1186/1471-2199-3-3

Shteynberg, D., Deutsch, E.W., Lam, H., Eng, J.K., Sun, Z., Tasman, N., Mendoza, L., Moritz, R.L., Aebersold, R., Nesvizhskii, A.I., 2011. iProphet: multi-level integrative analysis of shotgun proteomic data improves peptide and protein identification rates and error estimates. Mol. Cell. Proteomics MCP 10, M111.007690. https://doi.org/10.1074/mcp.M111.007690

Shu, T., Szórádi, T., Kidiyoor, G.R., Xie, Y., Herzog, N.L., Bazley, A., Bonucci, M., Keegan, S., Saxena, S., Ettefa, F., Brittingham, G., Lemiere, J., Fenyö, D., Chang, F., Delarue, M., Holt, L.J., 2022. nucGEMs probe the biophysical properties of the nucleoplasm. https://doi.org/10.1101/2021.11.18.469159

Sinclair, D.A., Guarente, L., 1997. Extrachromosomal rDNA circles--a cause of aging in yeast. Cell 91, 1033–1042. https://doi.org/10.1016/s0092-8674(00)80493-6

Sinclair, D.A., Mills, K., Guarente, L., 1997. Accelerated aging and nucleolar fragmentation in yeast sgs1 mutants. Science 277, 1313–1316. https://doi.org/10.1126/science.277.5330.1313

Sing, T.L., Brar, G.A., Ünal, E., 2022. Gametogenesis: Exploring an Endogenous Rejuvenation Program to Understand Cellular Aging and Quality Control. Annu. Rev. Genet. https://doi.org/10.1146/annurev-genet-080320-025104

Sipiczki, M., 2000. Where does fission yeast sit on the tree of life? Genome Biol. 1, reviews1011.1-reviews1011.4.

Smeal, T., Claus, J., Kennedy, B., Cole, F., Guarente, L., 1996. Loss of transcriptional silencing causes sterility in old mother cells of S. cerevisiae. Cell 84, 633–642. https://doi.org/10.1016/s0092-8674(00)81038-7

Smoyer, C.J., Jaspersen, S.L., 2014. Breaking down the wall: the nuclear envelope during mitosis. Curr. Opin. Cell Biol., Cell architecture 26, 1–9. https://doi.org/10.1016/j.ceb.2013.08.002

Smoyer, C.J., Katta, S.S., Gardner, J.M., Stoltz, L., McCroskey, S., Bradford, W.D., McClain, M., Smith, S.E., Slaughter, B.D., Unruh, J.R., Jaspersen, S.L., 2016. Analysis of membrane proteins localizing to the inner nuclear envelope in living cells. J. Cell Biol. 215, 575–590. https://doi.org/10.1083/jcb.201607043

Stafstrom, J.P., Staehelin, L.A., 1984. Dynamics of the nuclear envelope and of nuclear pore complexes during mitosis in the Drosophila embryo. Eur. J. Cell Biol. 34, 179–189.

Starr, D.A., Fridolfsson, H.N., 2010. Interactions between nuclei and the cytoskeleton are mediated by SUN-KASH nuclear-envelope bridges. Annu. Rev. Cell Dev. Biol. 26, 421–444. https://doi.org/10.1146/annurev-cellbio-100109-104037

Stevens, B., 1981. Mitochondrial structure., in: The Molecular Biology of the Yeast Saccharomyces: Life Cycle and Inheritance, J.N. Strathern, E.W. Jones, and J.R. Broach, Eds. Cold Spring Harbor Laboratory Press, Cold Spring Harbor, NY, pp. 471–505.

Storck, E.M., Özbalci, C., Eggert, U.S., 2018. Lipid Cell Biology: A Focus on Lipids in Cell Division. Annu. Rev. Biochem. 87, 839–869. https://doi.org/10.1146/annurev-biochem-062917-012448

Straight, A.F., Shou, W., Dowd, G.J., Turck, C.W., Deshaies, R.J., Johnson, A.D., Moazed, D., 1999. Net1, a Sir2-associated nucleolar protein required for rDNA silencing and nucleolar integrity. Cell 97, 245–256. https://doi.org/10.1016/s0092-8674(00)80734-5

Strambio-De-Castillia, C., Niepel, M., Rout, M.P., 2010. The nuclear pore complex: bridging nuclear transport and gene regulation. Nat. Rev. Mol. Cell Biol. 11, 490–501. https://doi.org/10.1038/nrm2928

Suda, Y., Nakanishi, H., Mathieson, E.M., Neiman, A.M., 2007. Alternative modes of organellar segregation during sporulation in Saccharomyces cerevisiae. Eukaryot. Cell 6, 2009–2017. https://doi.org/10.1128/EC.00238-07

Sun, N., Youle, R.J., Finkel, T., 2016. The Mitochondrial Basis of Aging. Mol. Cell 61, 654–666. https://doi.org/10.1016/j.molcel.2016.01.028

Suresh, S., Markossian, S., Osmani, A.H., Osmani, S.A., 2017. Mitotic nuclear pore complex segregation involves Nup2 in Aspergillus nidulans. J. Cell Biol. 216, 2813–2826. https://doi.org/10.1083/jcb.201610019

Sym, M., Engebrecht, J., Roeder, G.S., 1993. ZIP1 is a synaptonemal complex protein required for meiotic chromosome synapsis. Cell 72, 365–378. https://doi.org/10.1016/0092-8674(93)90114-6

Tachikawa, H., Bloecher, A., Tatchell, K., Neiman, A.M., 2001. A Gip1p–Glc7p phosphatase complex regulates septin organization and spore wall formation. J. Cell Biol. 155, 797–808. https://doi.org/10.1083/jcb.200107008

Teleman, J., Röst, H.L., Rosenberger, G., Schmitt, U., Malmström, L., Malmström, J., Levander, F., 2015. DIANA--algorithmic improvements for analysis of data-independent acquisition MS data. Bioinforma. Oxf. Engl. 31, 555–562. https://doi.org/10.1093/bioinformatics/btu686

Tiku, V., Jain, C., Raz, Y., Nakamura, S., Heestand, B., Liu, W., Späth, M., Suchiman, H.E.D., Müller, R.-U., Slagboom, P.E., Partridge, L., Antebi, A., 2017. Small nucleoli are a cellular hallmark of longevity. Nat. Commun. 8, 16083. https://doi.org/10.1038/ncomms16083

Toyama, B.H., Savas, J.N., Park, S.K., Harris, M.S., Ingolia, N.T., Yates, J.R., Hetzer, M.W., 2013. Identification of long-lived proteins reveals exceptional stability of essential cellular structures. Cell 154, 971–982. https://doi.org/10.1016/j.cell.2013.07.037

Troyer, D., Schwager, P., 1982. Evidence for nuclear membrane fluidity: Proacrosome migration and nuclear pore redistribution during grasshopper spermiogenesis. Cell Motil. 2, 355–367. https://doi.org/10.1002/cm.970020405

Ünal, E., Amon, A., 2011. Gamete Formation Resets the Aging Clock in Yeast. Cold Spring Harb. Symp. Quant. Biol. 76, 73–80. https://doi.org/10.1101/sqb.2011.76.011379

Unal, E., Kinde, B., Amon, A., 2011. Gametogenesis eliminates age-induced cellular damage and resets life span in yeast. Science 332, 1554–1557. https://doi.org/10.1126/science.1204349

Ungricht, R., Kutay, U., 2017. Mechanisms and functions of nuclear envelope remodelling. Nat. Rev. Mol. Cell Biol. 18, 229–245. https://doi.org/10.1038/nrm.2016.153

Varberg, J.M., Unruh, J.R., Bestul, A.J., Khan, A.A., Jaspersen, S.L., 2022. Quantitative analysis of nuclear pore complex organization in Schizosaccharomyces pombe. Life Sci. Alliance 5. https://doi.org/10.26508/lsa.202201423

Veatch, J.R., McMurray, M.A., Nelson, Z.W., Gottschling, D.E., 2009. Mitochondrial dysfunction leads to nuclear genome instability via an iron-sulfur cluster defect. Cell 137, 1247–1258. https://doi.org/10.1016/j.cell.2009.04.014

Verzijlbergen, K.F., Menendez-Benito, V., van Welsem, T., van Deventer, S.J., Lindstrom, D.L., Ovaa, H., Neefjes, J., Gottschling, D.E., van Leeuwen, F., 2010. Recombination-induced tag exchange to track old and new proteins. Proc. Natl. Acad. Sci. U. S. A. 107, 64–68. https://doi.org/10.1073/pnas.0911164107

Vollmer, B., Lorenz, M., Moreno-Andrés, D., Bodenhöfer, M., De Magistris, P., Astrinidis, S.A., Schooley, A., Flötenmeyer, M., Leptihn, S., Antonin, W., 2015. Nup153 Recruits the Nup107-160 Complex to the Inner Nuclear Membrane for Interphasic Nuclear Pore Complex Assembly. Dev. Cell 33, 717–728. https://doi.org/10.1016/j.devcel.2015.04.027

Walther, T.C., Alves, A., Pickersgill, H., Loïodice, I., Hetzer, M., Galy, V., Hülsmann, B.B., Köcher, T., Wilm, M., Allen, T., Mattaj, I.W., Doye, V., 2003a. The conserved Nup107-160 complex is critical for nuclear pore

complex assembly. Cell 113, 195–206. https://doi.org/10.1016/s0092-8674(03)00235-6
Walther, T.C., Askjaer, P., Gentzel, M., Habermann, A., Griffiths, G., Wilm, M., Mattaj, I.W., Hetzer, M., 2003b. RanGTP mediates nuclear pore complex assembly. Nature 424, 689–694. https://doi.org/10.1038/nature01898
Wente, S.R., Rout, M.P., 2010. The Nuclear Pore Complex and Nuclear Transport. Cold Spring Harb. Perspect. Biol. 2, a000562. https://doi.org/10.1101/cshperspect.a000562
Westrate, L.M., Lee, J.E., Prinz, W.A., Voeltz, G.K., 2015. Form follows function: the importance of endoplasmic reticulum shape. Annu. Rev. Biochem. 84, 791–811. https://doi.org/10.1146/annurev-biochem-072711-163501
Winey, M., Yarar, D., Giddings, T.H., Mastronarde, D.N., 1997. Nuclear Pore Complex Number and Distribution throughout the Saccharomyces cerevisiae Cell Cycle by Three-Dimensional Reconstruction from Electron Micrographs of Nuclear Envelopes. Mol. Biol. Cell 8, 2119–2132.
Witkin, K.L., Chong, Y., Shao, S., Webster, M.T., Lahiri, S., Walters, A.D., Lee, B., Koh, J.L.Y., Prinz, W.A., Andrews, B.J., Cohen-Fix, O., 2012. The Budding Yeast Nuclear Envelope Adjacent to the Nucleolus Serves as a Membrane Sink during Mitotic Delay. Curr. Biol. 22, 1128–1133. https://doi.org/10.1016/j.cub.2012.04.022
Xu, L., Ajimura, M., Padmore, R., Klein, C., Kleckner, N., 1995. NDT80, a meiosis-specific gene required for exit from pachytene in Saccharomyces cerevisiae. Mol. Cell. Biol. 15, 6572–6581. https://doi.org/10.1128/MCB.15.12.6572
Yam, C., He, Y., Zhang, D., Chiam, K.-H., Oliferenko, S., 2011. Divergent Strategies for Controlling the Nuclear Membrane Satisfy Geometric Constraints during Nuclear Division. Curr. Biol. 21, 1314–1319. https://doi.org/10.1016/j.cub.2011.06.052
Yang, L., Guan, T., Gerace, L., 1997. Integral membrane proteins of the nuclear envelope are dispersed throughout the endoplasmic reticulum during mitosis. J. Cell Biol. 137, 1199–1210. https://doi.org/10.1083/jcb.137.6.1199
Yesbolatova, A., Saito, Y., Kitamoto, N., Makino-Itou, H., Ajima, R., Nakano, R., Nakaoka, H., Fukui, K., Gamo, K., Tominari, Y., Takeuchi, H., Saga, Y., Hayashi, K., Kanemaki, M.T., 2020. The auxin-inducible degron 2 technology provides sharp degradation control in yeast, mammalian cells, and mice. Nat. Commun. 11, 5701. https://doi.org/10.1038/s41467-020-19532-z
Zetka, M., Paouneskou, D., Jantsch, V., 2020. The nuclear envelope, a meiotic jack-of-all-trades. Curr. Opin. Cell Biol., Cell Nucleus 64, 34–42. https://doi.org/10.1016/j.ceb.2019.12.010
Zhang, K., Donnelly, C.J., Haeusler, A.R., Grima, J.C., Machamer, J.B., Steinwald, P., Daley, E.L., Miller, S.J., Cunningham, K.M., Vidensky, S., Gupta, S., Thomas, M.A., Hong, I., Chiu, S.-L., Huganir, R.L., Ostrow, L.W., Matunis, M.J., Wang, J., Sattler, R., Lloyd, T.E., Rothstein, J.D., 2015. The C9orf72 repeat expansion disrupts nucleocytoplasmic transport. Nature 525, 56–61. https://doi.org/10.1038/nature14973

Zhang, W., Neuner, A., Rüthnick, D., Sachsenheimer, T., Lüchtenborg, C., Brügger, B., Schiebel, E., 2018. Brr6 and Brl1 locate to nuclear pore complex assembly sites to promote their biogenesis. J. Cell Biol. 217, 877–894. https://doi.org/10.1083/jcb.201706024

Zhao, X., Wu, C.-Y., Blobel, G., 2004. Mlp-dependent anchorage and stabilization of a desumoylating enzyme is required to prevent clonal lethality. J. Cell Biol. 167, 605–611. https://doi.org/10.1083/jcb.200405168

Zimmerli, C.E., Allegretti, M., Rantos, V., Goetz, S.K., Obarska-Kosinska, A., Zagoriy, I., Halavatyi, A., Hummer, G., Mahamid, J., Kosinski, J., Beck, M., 2021. Nuclear pores dilate and constrict in cellulo. Science 374, eabd9776. https://doi.org/10.1126/science.abd9776

Appendix A

Developing a genetic screen for factors involved in sequestration of nuclear material to the GUNC

A.1 Introduction

The endoplasmic reticulum (ER) is composed of a single continuous membrane but exhibits extensive sub-functionalization. The ER is divided into a cortical region (the cortical ER) and nuclear region (the nuclear envelope), which contain distinct proteomes and lipidomes. Within the cortical ER, tubules and sheets are specialized to perform lipid biogenesis and protein synthesis, respectively (reviewed in Westrate et al., 2015). Within the nuclear envelope, local membrane compartmentalization has also been observed, with membrane growth preferentially occurring near the nucleolus upon excess lipid synthesis (Witkin et al., 2012). However, the mechanisms that facilitate ER membrane compartmentalization remain poorly understood.

In many eukaryotes, ER compartmentalization can be established in a cell-cycle dependent manner to facilitate the asymmetric segregation of non-genetic material (Chao et al., 2014; Clay et al., 2014; Moore et al., 2015). In budding yeast mitosis, the bud neck has been suggested to organize a sphingolipid-based lateral diffusion barrier in the outer nuclear envelope, facilitating retention of age-induced damage in the mother cell (Clay et al., 2014). Our recent work provides evidence that a nuclear envelope diffusion barrier may also exist during budding yeast meiosis (King et al., 2019). Gamete plasma membranes establish two distinct membrane domains: the Gametogenesis Uninherited Nuclear Compartment (GUNC), which contains nuclear pore complexes and age-induced damage, and the inherited gamete nuclear envelope, which appears largely rejuvenated. Many genes involved in the establishment of the mitotic diffusion barrier are dispensable for this meiotic barrier (Chapter 2), suggesting the existence of meiosis-specific mechanisms. As such, it remains unknown how material is selectively sequestered into the GUNC.

In this section, we begin the process of designing and executing a genetic screen to identify factors involved in the establishment and/or maintenance of a meiotic nuclear envelope diffusion barrier. The screen uses gamete exclusion of extrachromosomal DNA (ecDNA), a plasmid carrying an excisable centromere and encoding a drug resistance cassette, as a genetic readout for proper GUNC formation. We hypothesized that a plasmid without a centromere would naturally be targeted to the GUNC in a manner similar to other types of ecDNA such as extrachromosomal rDNA circles, allowing for selection of mutants based of drug resistance. However, initial pilot experiments revealed that the acentromeric plasmid was not sequestered with high fidelity. To increase its sequestration and elimination, we developed a

strategy to tether the plasmid to the GUNC and performed initial work demonstrating its feasibility. Although further optimization is required prior to execution of a screen, our efforts lay the groundwork for identifying the enigmatic factors involved in this novel membrane compartmentalization event.

A.2 Results

A.2.1 Design of a genetic screen for factors involved in GUNC sequestration

In order to execute a genome-wide screen, we were interested in coupling the proper formation of the GUNC with the inheritance or disinheritance of a genetically selectable marker. Given that extrachromosomal rDNA circles were sequestered to the GUNC (Chapter 2), we hypothesized that other acentromeric genetic material might be similarly sequestered and eliminated. In support of this notion, artificial acentromeric plasmid DNA is asymmetrically inherited by mother cells during mitotic divisions, much like ecDNA (Denoth-Lippuner et al., 2014; Falcón and Aris, 2003). By placing a drug resistance cassette on this acentromeric plasmid, we could then select for mutants in GUNC formation by assaying for inheritance of drug resistance (Figure A.1A).

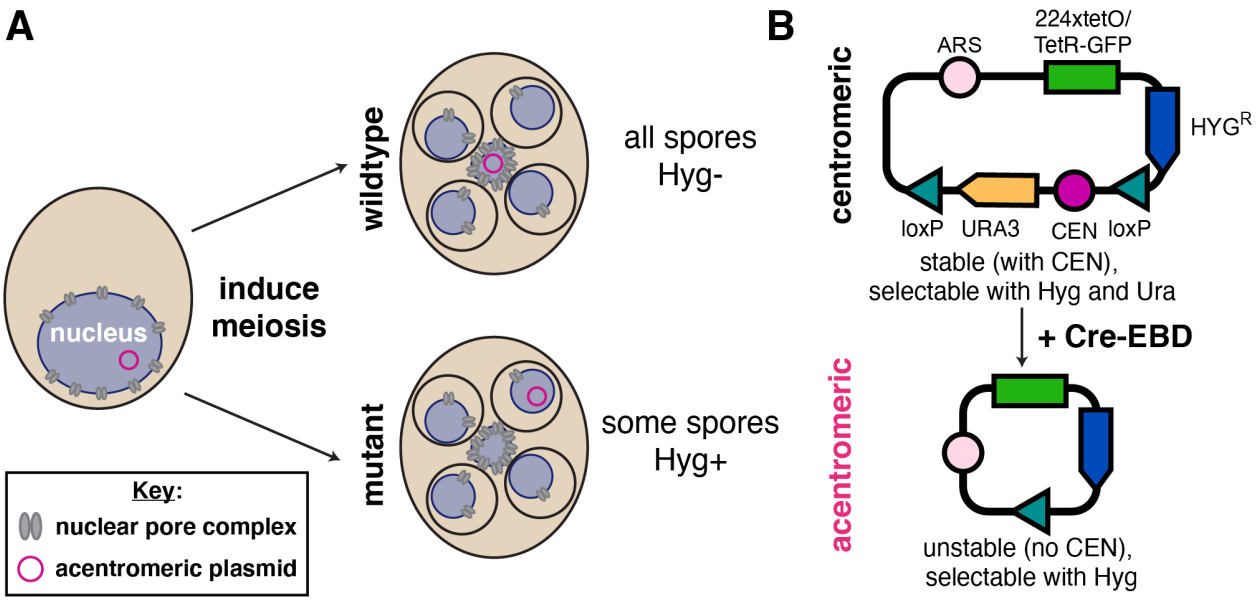

Figure A.1. Design of an acentromeric plasmid-based screen for factors involved in GUNC sequestration. A. Schematic depicting an acentromeric plasmid-based screen for GUNC sequestration factors. We hypothesized that an artificial acentromeric plasmid containing a drug resistance cassette would be targeted to the GUNC, similarly to extrachromosomal rDNA circles. In wild type cells, the plasmid would be eliminated and all gametes would be hygromycin sensitive ("Hyg-"). In cells mutant

for GUNC sequestration, the plasmid would be inherited by a gamete, resulting in hygromycin resistance ("Hyg+"). **B.** Schematic depicting the inducible acentromeric plasmid designed for the screen (pUB1898). A centromere (CEN) is flanked by two loxP sites, allowing it to be floxed out upon induction of Cre-EBD (a fusion of Cre and an estrogen binding domain, allowing activation by ß-estradiol). The backbone of the plasmid contains a hygromycin resistance cassette (HYG^R) and the floxable cassette contains an uracil synthesis gene (URA3), enabling selection for and differentiation between the centromeric and acentromeric plasmids. A tandem array of ~224x tet operator sequences (tetO) facilitates binding of TetR-GFP and visualization of the plasmid. ARS = autonomously replicating sequence.

We therefore constructed a plasmid carrying an excisable centromere for use in such a screen (Figure A.1B). The centromere is flanked by two loxP sites and can be removed upon activation of Cre recombinase. This feature enables the plasmid to be inherited faithfully and maintained at low copy number prior to the induction of Cre; if the excision is performed in stationary phase prior to gametogenesis, a large percentage of cells will begin the meiotic program with an acentromeric plasmid. The backbone of the plasmid also encodes an autonomously replicating sequence (ARS) to ensure its propagation. Importantly, the plasmid contains two selectable markers: a hygromycin resistance cassette (Hyg^R) on its backbone, allowing for selection of both centromeric and acentromeric plasmid-containing cells, and uracil synthesis gene (Ura3) in the floxable centromeric region, allowing for differentiation between centromeric and acentromeric plasmids. The inclusion of a *URA3* gene in the excisable centromeric region has the added benefit of enabling 5-Fluoroorotic acid (5-FOA) counter-selection against centromeric plasmids; double selection with hygromycin and 5-FOA allows for specific enrichment of cells with an acentromeric plasmid. Finally, the plasmid contains a tandem array of approximately 224 tetO repeats, allowing for the binding of TetR-GFP and direct visualization of plasmid inheritance using fluorescence microscopy.

A.2.2 Testing an inducible acentromeric plasmid for use in the screen

Upon cloning of this plasmid, we set out to determine whether it was sequestered to the GUNC with high fidelity. We performed a pilot experiment (Figure B.2A) that involved plating cells on YPD at various time points and replica plating to assess plasmid presence based on the ability to grow in the presence of hygromycin (centromeric and acentromeric plasmids) or absence of uracil (only centromeric plasmids). We first confirmed that the plasmid could be efficiently selected for prior to conversion, finding that over 80% of cells had the centromeric plasmid in a saturated YPD culture supplemented with hygromycin ("PRE" samples, Figure B.2A-B). We then induced Cre by adding of ß-estradiol and assessed the centromeric excision efficiency: over 90% of plasmid-containing cells had an acentromeric plasmid rather than centromeric plasmid after conversion ("POST" samples, Figure B.2A-B).

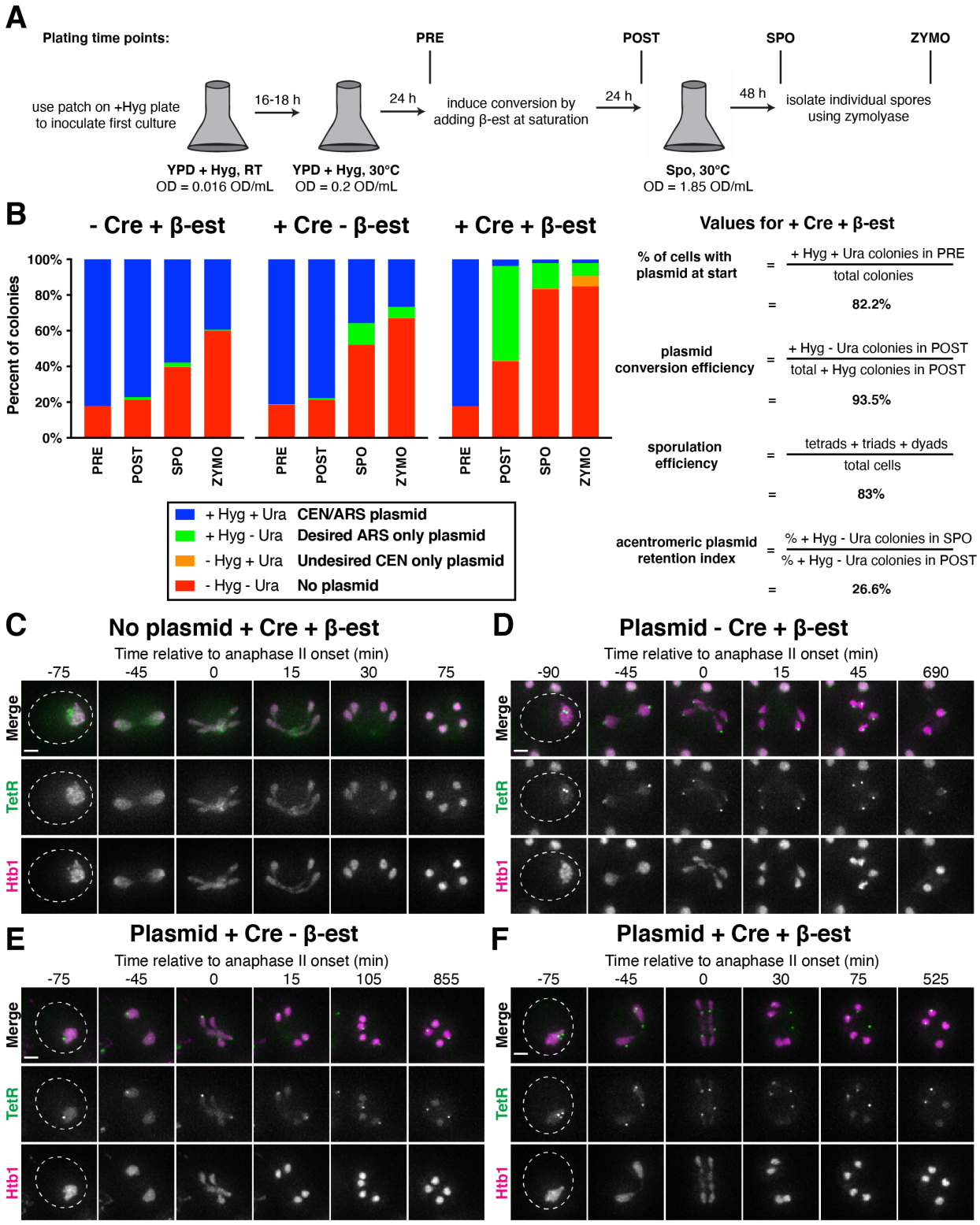
A
Plating time points:
PRE
POST
SPO
ZYMO
use patch on +Hyg plate to inoculate first culture
16-18 h
24 h
induce conversion by adding β-est at saturation
24 h
48 h
isolate individual spores using zymolyase
YPD + Hyg, RT
OD = 0.016 OD/mL
YPD + Hyg, 30°C
OD = 0.2 OD/mL
Spo, 30°C
OD = 1.85 OD/mL
B
- Cre + β-est
+ Cre - β-est
+ Cre + β-est
Percent of colonies
100%
80%
60%
40%
20%
0%
PRE
POST
SPO
ZYMO
+ Hyg + Ura CEN/ARS plasmid
+ Hyg - Ura Desired ARS only plasmid
- Hyg + Ura Undesired CEN only plasmid
- Hyg - Ura No plasmid
Values for + Cre + β-est
% of cells with plasmid at start = + Hyg + Ura colonies in PRE / total colonies = 82.2%
plasmid conversion efficiency = + Hyg - Ura colonies in POST / total + Hyg colonies in POST = 93.5%
sporulation efficiency = tetrads + triads + dyads / total cells = 83%
acentromeric plasmid retention index = % + Hyg - Ura colonies in SPO / % + Hyg - Ura colonies in POST = 26.6%
C
No plasmid + Cre + β-est
Time relative to anaphase II onset (min)
-75
-45
0
15
30
75
Merge
TetR
Htb1
D
Plasmid - Cre + β-est
Time relative to anaphase II onset (min)
-90
-45
0
15
45
690
Merge
TetR
Htb1
E
Plasmid + Cre - β-est
Time relative to anaphase II onset (min)
-75
-45
0
15
105
855
Merge
TetR
Htb1
F
Plasmid + Cre + β-est
Time relative to anaphase II onset (min)
-75
-45
0
30
75
525
Merge
TetR
Htb1

Figure A.2. Initial testing of an inducible acentromeric plasmid for use in the GUNC genetic screen. A. Schematic of the experimental design used in B-F to test the functionality of the acentromeric plasmid. Cells with the plasmid pUB1898 were induced to excise the centromere via activation of Cre fused to an estrogen binding domain (Cre-EBD) and allowed to progress through meiosis. At four time points, cells were plated on YPD and subsequently replica plated onto hygromycin (Hyg) or uracil-dropout (Ura) plates to assess plasmid retention: before induction of conversion (PRE), after induction of conversion (POST), after meiosis (SPO), and after single spore isolation (ZYMO). **B.** Plasmid retention for the experiment depicted in A. Three different conditions were tested: no Cre with 1 μM ß-estradiol ("-Cre +ß-est," UB26053); Cre with no ß-estradiol ("+Cre -ß-est," UB26049); and Cre with 1 μM ß-estradiol ("+Cre +ß-est," UB26049). At least 250 colonies were scored for each strain at each time point. Various metrics calculated using the plasmid frequencies are indicated to the right for the "+Cre +ß-est" sample. **C-F.** Montages of cells progressing through meiosis containing TetR-GFP under control of the *URA3* promoter to allow visualization of the tetO array-containing plasmid. Chromosomes were visualized with the histone marker Htb1-mCherry, and the first time point depicting anaphase II was defined as 0 minutes. **C.** a control strain without the plasmid but with Cre, treated with 1 μM ß-estradiol (UB26051). **D.** a strain with the plasmid but without Cre, treated with 1 μM ß-estradiol (UB26053). **E-F.** a strain with the plasmid and with Cre, either **E.** not treated or **F.** treated with 1 μM ß-estradiol (UB26049). Scale bars, 2 μm.

These cells were then induced to enter meiosis with high efficiency (~83% of cells formed packaged gametes), and plasmid retention of both centromeric and acentromeric plasmids was assessed (Figure A.2A). Centromeric plasmids behaved as expected, with a relatively high percentage of cells retaining a centromeric plasmid after meiosis (~75% of cells contain centromeric plasmids in "SPO" samples relative to "POST" samples for the "-Cre +ß-est" sample; Figure A.2A-B). Surprisingly, even though retained less efficiently, acentromeric plasmids were inherited at a rate much higher than expected (~27% of cells contain acentromeric plasmids in "SPO" samples relative to "POST" samples for the "+Cre +ß-est" sample; Figure A.2A-B). To confirm that these cells didn't represent unsporulated cells, we performed single spore isolation and observed a population of spores containing the acentromeric plasmid ("ZYMO," Figure A.2A-B). The high retention of acentromeric plasmids in the plating assays suggested that our artificial acentromeric plasmid was not behaving in the same way as other ecDNA, such as extrachromosomal rDNA circles (Figure 2.1).

To directly observe plasmid inheritance or disinheritance in individual cells, we performed microscopy of the same strains (Figure A.2C-F). We set out to visualize the behavior of individual plasmids using TetR-GFP bound to the tetO array on the plasmid, relative to dividing chromatin marked with Htb1-mCherry. We first confirmed that TetR-GFP is only punctate in the presence of the plasmid, observing

that the signal is diffuse in the absence of our screening plasmid (Figure A.2C). We then monitored the behavior of the plasmid with ("-Cre +ß-est" or "+Cre -ß-est;" Figure A.2D-E) or without ("+Cre +ß-est;" Figure A.2F) a centromere. When the centromere was present, the plasmid was segregated with high fidelity, localizing to the ends of the dividing meiotic spindle and likely to spindle pole bodies (Figure A.2D-E). When the centromere was absent, the plasmid behaved more randomly: it could either be sequestered to the GUNC or retained by gamete nuclei (Figure A.2F). Notably, the acentromeric plasmids that were retained did not behave like centromeric plasmids, localizing away from spindle pole bodies, indicating that centromere excision was largely successful (Figure A.2F). The microscopy therefore confirmed that acentromeric plasmids were able to be inherited by gamete nuclei, indicating that additional optimization was necessary prior to the plasmid being used in any screen.

A.2.3 Designing a GUNC-localized tether to drive acentromeric plasmid sequestration

We next aimed to increase sequestration of the acentromeric plasmid to the GUNC. To do this, we fused proteins thought to remain sequestered in the GUNC with TetR, such that they would bind to the tetO array within the plasmid and therefore target the plasmid to the GUNC (Figure A.3A). A similar approach was used in mitotic cells to alter acentromeric plasmid inheritance, with the tandem nature of the tetO array allowing for simultaneous visualization of the plasmid with TetR-GFP and tethering of the plasmid with a TetR fusion (Khmelinskii et al., 2011). We endogenously or ectopically tagged a number of putative GUNC-targeted proteins with TetR, including: Y-complex nucleoporins (Seh1 or Nup120), a protein aggregate-localized chaperone (Hsp104), and aggregate-prone nucleolar proteins (over-expressed Rlp7, Nop13, Nop15, and Sof1; Paxman et al., 2021). We then performed the same experiment as above, assessing the retention of the acentromeric plasmid through meiosis ("acentromeric plasmid retention index"; Figure A.3B). Excitingly, while the nucleoporin and chaperone constructs did not increase sequestration, two of the overexpressed nucleolar protein constructs – Nop15 and Sof1 – increased elimination of the acentromeric plasmid by up to ~60% (Figure A.3B). Surprisingly, both Nop15-GFP and Sof1-GFP exhibited only very weak sequestration to the GUNC, if any, when visualized directly (Figure A.3C-D). However, we confirmed that the increased plasmid elimination was reproducible and corresponded with increased sequestration to the GUNC by microscopy (personal communication with Benjamin Styler). We further validated that these constructs did not alter inheritance of the centromeric plasmid during meiosis (data not shown). Our data demonstrate that the GUNC tether approach is a promising direction for the genetic screen, although further optimization and characterization is required to ensure that the plasmid is sequestered with high fidelity by the endogenous mechanism.

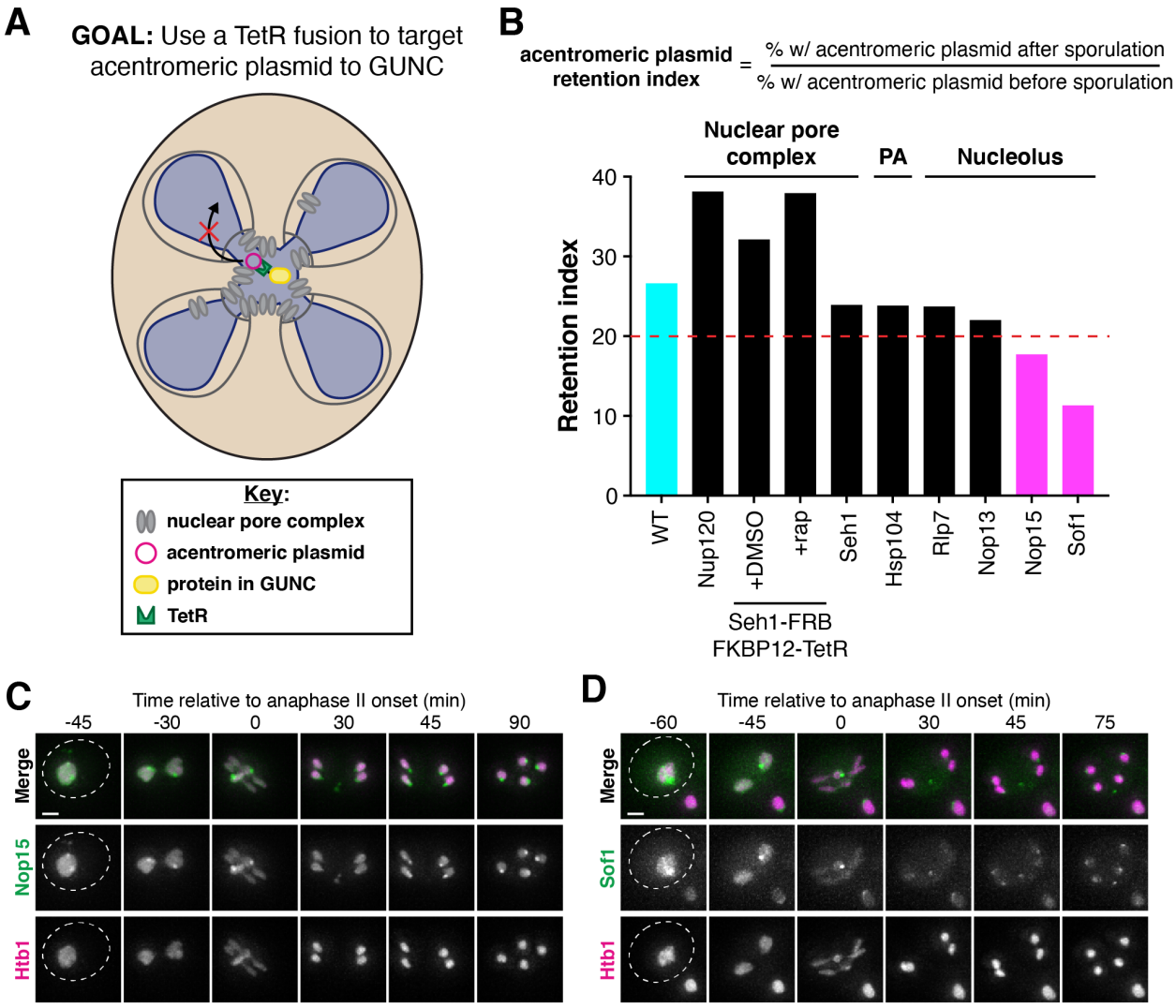

Figure A.3. Design of a GUNC tether to drive acentromeric plasmid sequestration and elimination. A. Schematic of the approach used to tether the acentromeric plasmid to the GUNC. Different proteins thought to localize to the GUNC were tagged with TetR at either an endogenous or ectopic locus; the TetR fusion should hopefully bind to the tetO array in the acentromeric plasmid, driving its sequestration and elimination. A similar approach was previously used in budding yeast mitosis to alter plasmid inheritance patterns (Khmelinskii et al., 2011). **B.** The acentromeric plasmid retention index for different TetR fusion constructs. The following constructs were tested: no tether (UB26049); Nup120-TetR (endogenous, UB30583); Seh1-FRB (endogenous) with *P_{URA3}-FKBP12-TetR* (UB28059); Seh1-TetR (endogenous, UB30589); Hsp104-TetR (endogenous, UB30577); Rlp7-TetR under the *ATG8* promoter (ectopic, UB33314); Nop13-TetR under the *ATG8* promoter (ectopic, UB33308); Nop15-TetR under the *ATG8* promoter (ectopic, UB33296); and Sof1-TetR

under the *ATG8* promoter (ectopic, UB33303). All experiments were performed as specified in A.2A. At least 250 colonies were scored for each strain at each time point. For the Seh1-FRB FKBP12-TetR tether, either DMSO or 10 μM rapamycin (rap) was added after 3 hours in Spo. The bar for wild type is cyan, and the bars for the two candidate tethers that increased sequestration are magenta. A red dotted line is placed at an acentromeric retention index of 20% to highlight to successful tethers. PA = protein aggregate. **C-D.** Montages of cells progressing through meiosis containing either **C.** Nop15-GFP (UB33284) or **D.** Sof1-GFP (UB33286) under control of the *ATG8* promoter. Chromosomes were visualized with the histone marker Htb1-mCherry, and the first time point depicting anaphase II was defined as 0 minutes. Scale bars, 2 μm.

A.3 Discussion

Our work in this section provides the conceptual basis for a genetic screen to identify mutants in GUNC formation and proof-of-concept experiments supporting this approach. We designed a screen that uses an acentromeric plasmid during meiosis to couple a genetic payload (a drug resistance cassette) and proper GUNC formation (Figure A.1). We constructed a well-behaved inducible acentromeric plasmid that exhibits seemingly random segregation during the meiotic divisions (Figure A.1-A.2). Finally, we tethered the plasmid to GUNC-localized proteins in order to increase its sequestration, such that its disinheritance serves as a proxy for proper GUNC formation (Figure A.3). Additional optimization must now be performed to increase the fidelity of plasmid sequestration and elimination even further.

It remains unclear why our artificial acentromeric plasmid was not sequestered to the GUNC as is observed for ecDNA (Figure A.2; Chapter 2). This difference between acentromeric plasmids and ecDNA in meiosis, when they behave similarly in mitosis, provides more evidence that a distinct meiotic diffusion barrier mechanism exists. The rDNA sequence itself may facilitate sequestration, perhaps by recruiting a protein that is itself sequestered. In support of this, tethering nucleolar proteins to our acentromeric plasmid resulted in increased sequestration and elimination (Figure A.3). Surprisingly, these nucleolar proteins were only weakly sequestrated themselves (Figure A.3). The combination of circular DNA and nucleolar proteins may be necessary for detection by the endogenous ecDNA-targeting pathway.

Testing tethers using GUNC-targeted proteins that exhibit greater sequestration, including other nucleolar proteins (e.g., Nhp2 or Nsr1) and various Y-complex nucleoporins (e.g., Nup84 and Nup133), may further increase sequestration of the plasmid. Alternatively, integrating a copy of the rDNA array into the plasmid could cause it to resemble and behave more like ecDNA. Of note, a screen that utilizes a specific GUNC component to drive plasmid sequestration has the potential to uncover both general and component-specific factors that contribute to sequestration.

Repeating the screen using tethers belonging to different classes of sequestered material (e.g., NPCs, nucleolar material, ecDNA) may enable differentiation between these general and component-specific pathways.

Key considerations remain in how the screen will be performed, with at least two alternate approaches to execution. (1) The screen could be performed via high-throughput microscopy, using a deletion collection. An arrayed library of deletions with the plasmid, tether, and TetR-GFP would be constructed and induced to undergo meiosis in a 96-well format. Automated image analysis before and after meiosis would allow identification of mutants that affect GUNC formation. (2) The screen could be performed via pooled selection, using random mutagenesis of a haploid strain able to sporulate (*spo11Δ spo13Δ*; Klapholz et al., 1985). Sequencing would be performed prior to meiosis and after outgrowth of spores in media containing hygromycin and 5-FOA. Since the centromere contains a selectable marker, the centromeric plasmid could be retransformed in and the meiotic retention experiment performed multiple times. While the former approach would allow for subtle phenotypes to be scored and for hits to be rapidly identified, the latter approach would allow for identification of alleles in essential genes and would be comparatively easy to perform. Initial piloting of both approaches is required to determine which is better suited for this screen.

Identification of factors involved in GUNC sequestration will provide important insight into how meiotic nuclear remodeling contributes to gamete health and rejuvenation. Moreover, the screen promises to shed light into the fundamental cell biological question of how compartmentalization of the nuclear envelope and, more generally, organellar membranes is achieved.

Appendix B

Additional tool development and results

B.1 Monitoring new and old NPCs during meiosis

B.1.1 Introduction

Meiosis in budding yeast is a cellular differentiation program that involves the dynamic regulation of almost all proteins in the genome (Brar et al., 2012; Cheng et al., 2018). In addition to regulation at the level of transcription and translation, protein levels are also regulated by programmed destruction (Eastwood et al., 2012; Eisenberg et al., 2018). Understanding this regulation and its potential implications for quality control requires the application of new techniques to differentiate between pre-existing and newly synthesized pools of proteins.

The nuclear pore complex (NPC) is one of the most stable structures in the eukaryotic cell (Toyama et al., 2013). In closed mitosis, NPCs remain largely intact during the cell cycle and only nucleophagy provides an opportunity for NPC turnover (Lee et al., 2020). As a consequence, NPCs undergo deterioration during replicative aging, resulting in compromised function (Lord et al., 2015; Rempel et al., 2019). Our previous work showed that meiosis is a unique developmental context allowing for large-scale turnover of core nucleoporins via their sequestration to the GUNC and eventual destruction by vacuolar proteases (King et al., 2019). However, the data in this paper did not allow for direct monitoring the of NPC inheritance and resynthesis.

In this work, we optimize two tools for general use in differentiating between new and old proteins in budding yeast meiosis: (1) photoconvertible tags (Dendra2; Gurskaya et al., 2006) and (2) recombination-induced tag exchange (RITE; Verzijlbergen et al., 2010). Both techniques are consistent with large-scale turnover of NPCs occurring during meiosis, with only a limited pool of nucleoporins being inherited by nascent gametes. Resynthesis of core subunits occurs during gamete development and may supply gametes with NPCs necessary for proper nucleocytoplasmic transport. We further anticipate that the tools developed here will be broadly useful for future studies of protein dynamics in our system.

B.1.2 Results

B.1.2.1 Photoconvertible tag approach

Photoconvertible fluorescent proteins are converted from emitting light in one wavelength (e.g., green light) to light in another wavelength (e.g., red light) via exposure to an activating light (e.g., blue light). As such, protein present at the time

of exposure to activating light (e.g., old protein) can be differentiated from protein synthesized afterwards (e.g., new protein). We used tandem copies of the photoconvertible protein Dendra2 to tag two different core nucleoporins (Gurskaya et al., 2006): Nup170, an inner ring nucleoporin, and Nup49, a channel nucleoporin. We then induced photoconversion during meiotic prophase and monitored the pool of pre-existing protein after the meiotic divisions (Figure B.1A).

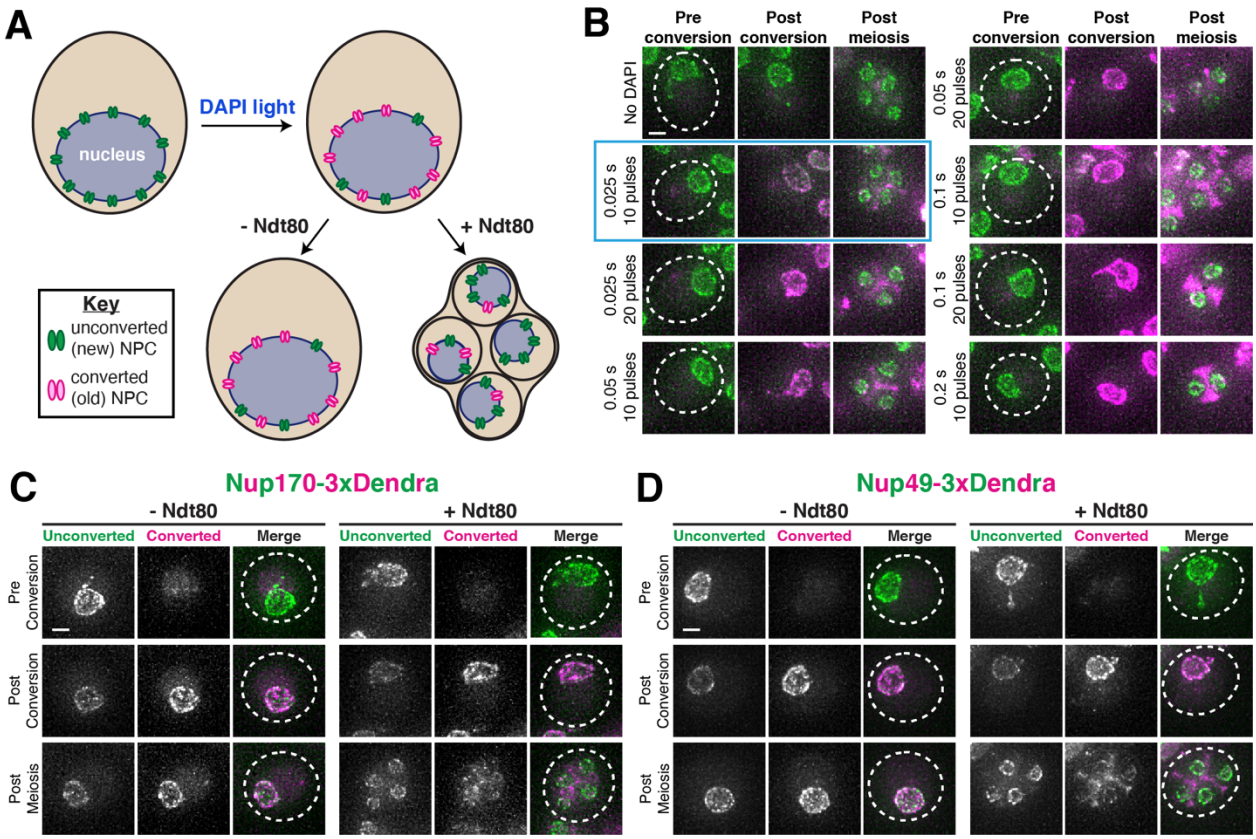

Figure B.1. Photoconvertible tags provide direct evidence for large-scale NPC turnover during meiosis. A. Schematic of the experiment performed, using a photoconvertible tag to monitor NPC turnover. Cells containing a nucleoporin tagged with the tandem photoconvertible tag, 3xDendra2, were exposed with an activating light, resulting in pre-existing protein being converted from emitting green light to emitting red light (Gurskaya et al., 2006). The converted NPCs (magenta) were therefore older than the newly synthesized and unconverted NPCs (green). Cells were then allowed to progress through meiosis, with the hypothesis that meiotic progression results in turnover of old NPCs. **B.** Optimization of photoconversion. Cells with Nup170-3xDendra2 were allowed to incubate in Spo for five hours and then induced to enter the meiotic divisions via activation of *P_{GAL}-NDT80* with 1 µM ß-estradiol (UB8837). Cells were loaded into the microfluidics chamber and then photoconverted with different DAPI light regimens. A representative cell for each regimen is shown before conversion, after conversion, and after meiosis (~24 hours).

The blue box indicates the conditions selected for the experiments in C-D. **C-D.** Representative cells with a photoconvertible nucleoporin before photoconversion, after photoconversion, and after meiosis (~24 hours). Cells were either arrested in prophase (P_{GAL}-*NDT80* + N/A, "-Ndt80") or allowed to progress through the meiotic divisions (P_{GAL}-*NDT80* + 1 µM ß-estradiol after 5 hours in Spo, "+Ndt80") **C.** Nup170-3xDendra2 (UB8837). **D.** Nup49-3xDendra2 (UB8839). Note that Nup49-3xDendra2 resulted in cells having a slight vegetative growth defect. Scale bars, 2 µm.

Initial optimization demonstrated that exposure to the activating light (UV light) resulted in reduction of sporulation efficiency, unless used at a very low initial level (Figure B.1B). We were therefore only able to achieve partial conversion of the existing protein pool, making this technique more useful for tracking old protein than new protein. Using the optimized photoconversion conditions, we monitored cells with Nup170-3xDendra2 or Nup49-3xDendra2 (Figure B.1C-D) that were either maintained in prophase arrest (P_{GAL}-*NDT80* without ß-estradiol; Carlile and Amon, 2008) or allowed to progress through the meiotic divisions (P_{GAL}-*NDT80* with ß-estradiol). For both nucleoporins, markedly more converted protein (e.g., old protein) was turned over in cells that progressed through meiosis than cells that remained in prophase (Figure B.1C-D). These results are consistent with NPC sequestration to the GUNC representing a large-scale protein turnover event (King et al., 2019). Resynthesis of new nucleoporins appeared stronger in cells that progressed through meiosis as well, although some resynthesis of Nup49 was apparent even in cells that remained in prophase (Figure B.1C-D). Altogether, these results provide direct evidence that NPCs undergo a massive remodeling event – involving both turnover and synthesis – during budding yeast meiosis.

B.1.2.2 Recombination inducible tag exchange approach

Recombination inducible tag exchange (RITE) is a technique that allows for genetic induction of tag switching on a protein of interest from one fluorescent protein to another (Verzijlbergen et al., 2010). In brief, an inducible Cre recombinase acts at loxP sites that flank one fluorescent protein (e.g., GFP) to bring another fluorescent protein (e.g., mCherry) in frame with the tagged protein (Figure B.2A). The protein synthesized before this conversion event (e.g., old protein) is therefore marked by a different color than the protein synthesized after this event (e.g., new protein). This technique has the added benefit of allowing for use of immunoblotting to monitor new and old protein pools, since distinct epitopes are present on the different fluorescent proteins.

We tagged the same nucleoporins – Nup170 and Nup49 – with a RITE cassette that could be induced to switch from encoding GFP to mCherry. Conversion was induced by addition of ß-estradiol to strains containing a fusion between Cre recombinase and an estrogen binding domain (Cre-EBD) under control of the *TDH3* promoter. This

conversion was specifically performed in non-dividing cultures to minimize dilution of old protein and synthesis of new protein prior to the induction of meiosis. Initial testing (Figure B.2B) demonstrated that RITE cassette switching occurred most efficiently in saturated reduced YPD cultures (~70-80% at 6 h), as opposed to saturated BYTA cultures (~30-50% at 6 h) or Spo cultures (~10-30% at 6 h; not shown). Allowing the conversion to proceed for 12 hours in reduced YPD consistently allowed for a conversion rate of ~95% in cells that were heterozygous or homozygous for the RITE cassette.

We then compared cells that were maintained in prophase arrest (*ndt80Δ*) or allowed to progress through the meiotic divisions (wild type) after RITE tag conversion. For Nup170-RITE, old protein (Nup170-GFP) decreased more strongly in meiotic cells than prophase-arrested cells (Figure B.2C), consistent with the results observed for Nup170-3xDendra2 (Figure B.1C). Nup170-GFP protein levels as monitored by Western also dramatically decreased during meiosis but not prophase arrest, concomitant with the appearance of a very weak free GFP band (Figure B.2E). New protein (Nup170-mCherry) increased weakly in prophase-arrested cells and more strongly in meiotic cells (Figure B2.C), although these changes were less apparent in protein levels as monitored by Western (Figure B2.E). For Nup49-RITE, old protein (Nup49-GFP) decreased and new protein (Nup149-mCherry) increased in both prophase-arrested and meiotic cells (Figure B2.D). This was in contrast to the clear difference observed between prophase-arrested and meiotic cells with Nup49-3xDendra2 (Figure B1.D). Confusingly, Nup49-GFP and Nup49-mCherry protein levels as monitored by Western did not match the results observed by microscopy (e.g., the relative stability of Nup49-GFP by Western; Figure B2.E). Overall, the results from the RITE-tagged constructs are consistent with high NPC turnover during meiosis. However, further troubleshooting is necessary to understand the discrepancy between protein levels as assayed by microscopy and immunoblot and to reconcile the differences between the photoconvertible and RITE results.

Despite these limitations, we were interested in using the RITE-tagged nucleoporins to confirm that gametes contain a mix of inherited and newly synthesized NPCs (Figure B.2F-G). Photoconvertible-tagged nucleoporins can experience inadvertent conversion during the process of imaging, since excitation in the FITC channel includes some wavelengths that can activate Dendra2 (Chudakov et al., 2007). RITE-tagged nucleoporins are not subject to the same limitations, allowing for more frequent imaging and increased confidence that even weak signal represents *bona fide* pre-existing protein. To assay inheritance, we monitored cells with converted RITE-tagged nucleoporins and BFP-tagged plasma membranes at three time points: before meiosis, shortly after meiosis II, and after gamete development. Excitingly, a limited pool of Nup170-GFP and Nup49-GFP were inherited by gametes, in addition to the large portion of each nucleoporin that remained sequestered to the GUNC (Figure B.2F-G). Subsequent synthesis of Nup170-mCherrry and Nup49-mCherry resulted in gamete nuclei that were chimeric for old and new NPCs (Figure B.2F-G).

These results confirm that, in spite of the large-scale nuclear remodeling that occurs, some NPCs are inherited from the pre-existing mother cell.

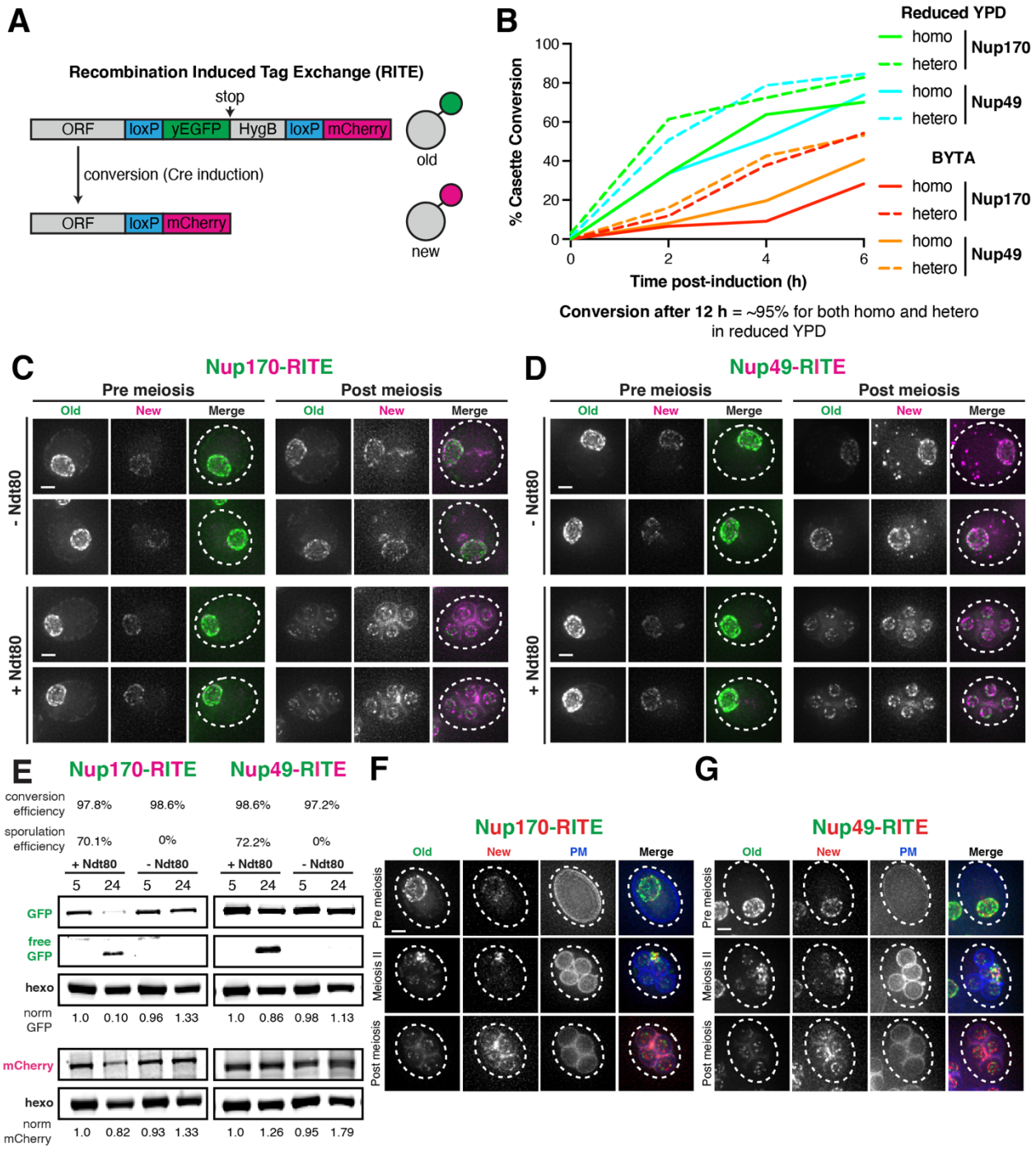

Figure B.2. Recombination inducible tag exchange (RITE) provides evidence that gamete nuclei contain both inherited and newly synthesized NPCs. A. Schematic of recombination inducible tag exchange (RITE) adapted from Verzijlbergen et al., 2010.

For a protein tagged with the RITE cassette, activation of Cre results in switching of fluorescent protein tags from GFP to mCherry. The old protein (pre-conversion) is marked with GFP**,** and the new protein (post-conversion) is marked with mCherry. **B.** Optimization of cassette conversion. Saturated YPD or BYTA cultures of cells containing a RITE-tagged nucleoporin and *P_{TDH3}-CRE-EBD78* were induced to undergo cassette conversion by addition of 1 μM ß-estradiol (homozygous Nup170-RITE = UB12926, heterozygous Nup170-RITE = UB13385, homozygous Nup49-RITE = UB12930, heterozygous Nup49-RITE = UB13387). Cassette conversion was monitored by plating cells and assessing loss of hygromycin resistance. The conversion conditions used for subsequent experiments in C-G and the approximate conversion efficiency achieved is specified below the plot. At least 100 colonies were counted for each strain at each time point. **C-D.** Representative cells with a RITE-tagged nucleoporin before (~5 h in Spo) and after (~24 h in Spo) meiosis. Cells were either maintained in prophase arrest (*ndt80Δ*, "-Ndt80") or allowed to progress through meiosis (wild type, "+Ndt80"). Two representative cells are shown for each strain in each condition. **C.** homozygous Nup170-RITE (wild type = UB12926, *ndt80Δ* = UB15666). **D.** homozygous Nup49-RITE (wild type = UB12930, *ndt80Δ* = UB15668). **E.** Immunoblots monitoring levels of GFP-tagged or mCherry-tagged nucleoporins before and after meiosis, corresponding to the experiments in C-D. The conversion and sporulation efficiency for each strain is indicated above the immunoblots (n ≥ 100 colonies per strain for conversion efficiency, n ≥ 300 cells per strain for sporulation efficiency). Hxk2 was used as a loading control. Background subtracted nucleoporin protein levels were divided by Hxk2 levels to control for loading and then normalized to the value of the respective wild type strain at 5 h in Spo. Note that the free GFP blots are adjusted to display pixels of much lower intensity than the normal GFP blots. **F-G.** Representative cells with a RITE-tagged nucleoporin and gamete plasma membranes marked with BFP-Spo20$^{51-91}$ before meiosis (~5 h in Spo), shortly after meiosis II (~8-10 h in Spo), and after meiosis (~24 h in Spo). **F.** homozygous Nup170-RITE (UB16640). **G.** homozygous Nup49-RITE (UB16642). Note that the intensity settings in C-D and F-G are consistent within each panel but not between panels. Scale bars, 2 μm.

B.1.3 Discussion

The work in this section establishes that core members of the nuclear pore complex undergo a large-scale turnover event during meiosis (Figure B.1 and B.2). This finding is consistent with our results demonstrating that a large fraction of core nucleoporins is sequestered to the GUNC during meiosis II and subsequently eliminated by vacuolar proteases (Chapter 2). Importantly, some mother NPCs are inherited by nascent gametes (Figure B.2), potentially explaining how gamete nuclei are transport-competent shortly after birth (Chapter 4).

Whether any selectivity exists in which NPCs are inherited remains an open question. In the experiments here, both older and newer NPCs appear to be sequestered to the GUNC in young cells (Figure B.2F-G). However, loss of NPC function during aging or upon other stresses may be a pre-requisite to observe selective inheritance. Notably, a similar RITE-based approach could be applied to monitor selective inheritance of new proteins in other damage-prone organelles such as mitochondria.

The presence of newly synthesized nucleoporins in gametes suggests that meiosis may also involve large-scale NPC insertion (Figure B.1 and B.2). Future work should determine whether this is the case and, if so, how this insertion is mediated. Attractive candidates to facilitate NPC synthesis include known insertion factors (e.g., Brl1, Brr6, and Apq12; Scarcelli et al., 2007; Zhang et al., 2018) and the lipid-binding domains of the returning nuclear basket (King et al., 2022, 2019; Mészáros et al., 2015; Vollmer et al., 2015). Meiosis represents an exciting new system to answer questions about the still enigmatic process of NPC assembly.

In all, the work here has improved our understanding of NPC death and birth during budding yeast meiosis. We anticipate that the same tools will help elucidate various quality control mechanisms in this strikingly dynamic process.

B.2 Monitoring nuclear lipid composition during meiosis

B.2.1 Introduction

During cell division, cells must properly partition organelles and other cellular material into daughter cells. This cellular remodeling often involves dramatic changes in lipid composition, in order to facilitate membrane growth and division (reviewed in Storck et al., 2018). In particular, the nuclear envelope must be remodeled to accommodate the division of genetic material. In open cell divisions, the nuclear envelope is disassembled and absorbed by the surrounding endoplasmic reticulum, allowing for proper spindle formation and chromosome segregation (reviewed in Ungricht and Kutay, 2017). In closed cell divisions, the nuclear envelope undergoes rapid expansion that is dependent on lipid synthesis (Neumann and Nurse, 2007; Witkin et al., 2012). Differences in lipid synthesis can underpin the dramatic differences in nuclear morphology observed between cell division programs of closely related organisms (Makarova et al., 2016). However, our understanding of lipid remodeling at the nuclear envelope during meiosis remains extremely limited.

Lipid biology has historically been limited by relatively few tools being available to visualize their behavior in vivo (Barrantes, 2021). A recent study developed genetically-coded sensors that allow for the monitoring of different lipid pools in both the nucleus and cytoplasm of vegetative budding yeast cells (Romanauska and Köhler, 2018). The sensors allow for detection of phosphatidic acid (PA), a precursor

of both the lipid growth and storage pathways, and diacylglycerol (DAG), a member of the lipid storage pathway (Figure B.3A). By monitoring these two species, the study was able to demonstrate that the inner nuclear membrane is an unexpectedly metabolically active compartment in budding yeast (Romanauska and Köhler, 2018). Here, we adapt these sensors for use in budding yeast meiosis to monitor changes in nuclear envelope shape and composition.

B.2.2 Results

We set out to monitor PA and DAG localization in both the nucleus and cytoplasm during budding yeast meiosis. To do this, we used a highly upregulated meiotic promoter (P_{ATG8}) to drive expression of either a PA sensor (the Opi1 Q2 domain) or a DAG sensor (the PKCß C1a+C1b domain) fused to GFP with or without the Nup60 NLS (Figure B.3B). We then brought this sensor into a strain with a fluorescently tagged histone, Htb1-mCherry, to track meiotic staging.

We first monitored the localization of PA, a precursor for both lipid growth and storage. During meiotic prophase, we confirmed the reported plasma membrane localization of the cytoplasmic PA sensor and the diffuse nucleoplasmic localization of the nuclear PA sensor (Figure B.3B-D). During meiosis, the cytoplasmic PA sensor transiently localized to the developing gamete plasma membranes (Figure B.3C). Intriguingly, this relocalization was far weaker than observed for another PA sensor, $Spo20^{51\text{-}91}$, which is a common tool used to monitor gamete plasma membranes (compare to Figure 2.14; Nakanishi et al., 2004). In contrast, the nuclear PA sensor lost its clear nucleoplasmic enrichment at the onset of meiosis II (Figure B.3D) for unknown reasons. One possibility is that the Nup60 nuclear localization signal no longer functions properly during this meiotic interval, although the loss of nuclear localization occurs earlier than virtual nuclear envelope breakdown (Chapter 4). The PA sensors therefore did not provide significant insight into nuclear envelope lipid composition during meiosis II.

We next monitored the localization of DAG, a member of the lipid storage pathway. During meiotic prophase, we confirmed the reported vacuolar localization of the cytoplasmic DAG sensor and the nuclear envelope localization of the nuclear DAG sensor (Figure B.3B, B.3E-F). During meiosis, the cytoplasmic DAG sensor strongly localized to the developing plasma membranes until closure (Figure B.3E). At this point, the sensor relocalized to what appear to be lipid droplets inside of the gamete (Figure B.3E). The nuclear DAG sensor robustly labelled the nuclear envelope during prophase and meiosis I (Figure B.3F), allowing for the observation of nuclear flares that likely coincide with prophase chromosome movements. However, upon entry into meiosis II, the sensor completely relocalized to the developing plasma membranes (Figure B.3F). This could be due to (1) gamete plasma membranes outcompeting the nuclear envelope for the sensor, (2) reduced nuclear envelope abundance of DAG due a shift towards growth instead of storage, or (3) an issue with the Nup60 NLS given

the similar loss of nuclear localization of the PA sensor. After meiosis II, the sensor again localized to the nuclear envelope, but exhibited more punctate distribution that may be consistent with nuclear lipid droplets (Figure B.3F). The DAG sensors therefore also did not provide significant insight into nuclear envelope lipid composition during meiosis II.

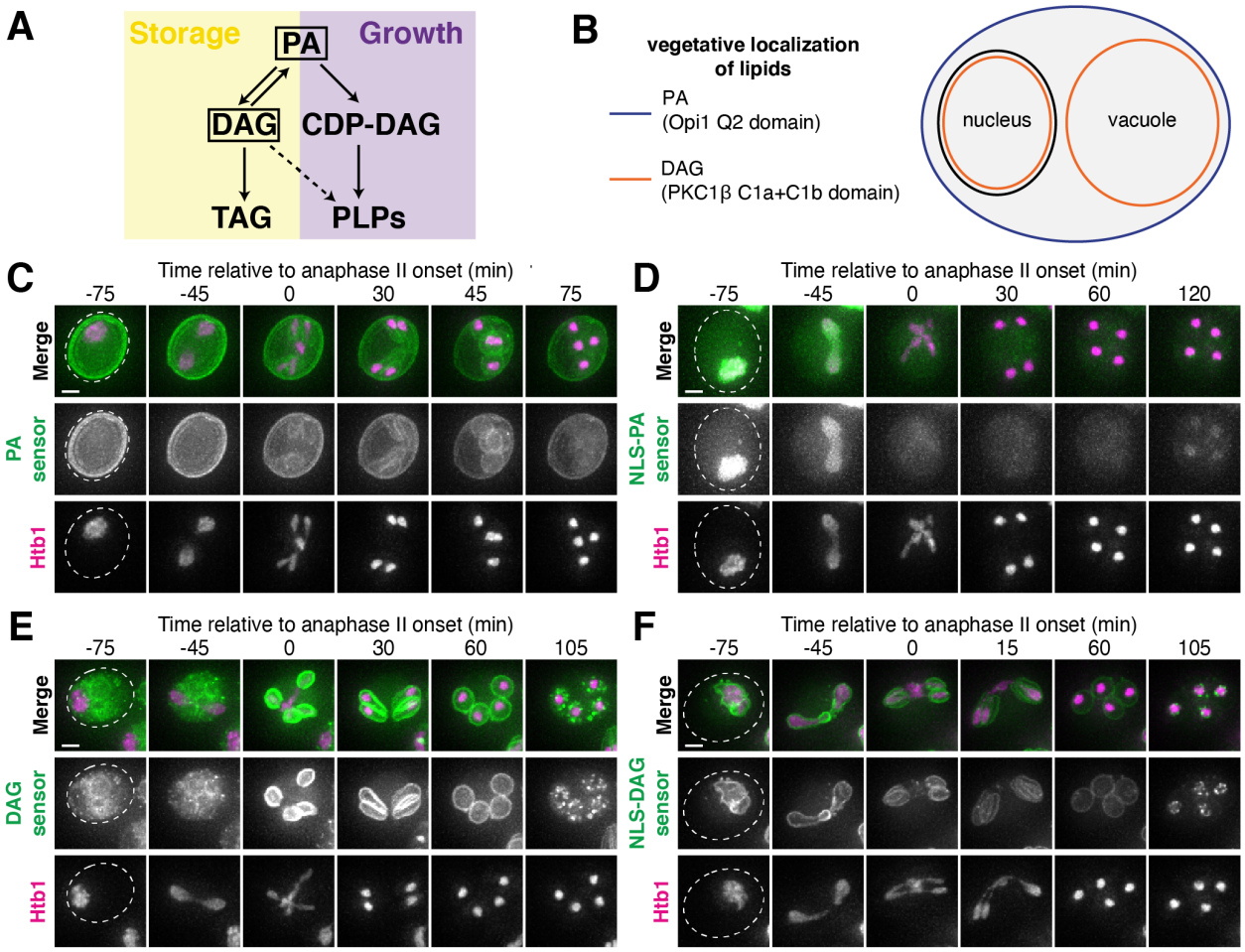

Figure B.3. Monitoring lipid dynamics during budding yeast meiosis using fluorescent lipid sensors. A. Schematic of lipid pathways in budding yeast adapted from Romanauska and Köhler, 2018. The boxed lipids are visualized by the lipid sensors in this figure. PA = phosphatidic acid, DAG = diacylglycerol, CDP-DAG = cytidine diphosphate diacylglycerol, TAG = triacylglycerol, PLPs = phospholipids. **B.** Schematic depicting the vegetative localization of the lipid sensors adapted from Romanauska and Köhler, 2018. The PA lipid sensors, which utilize the Opi1 Q2 domain, bind to the plasma membrane. The DAG lipid sensors, which utilize the PKCβ C1a+C1b domain, bind to the inner nuclear membrane and vacuolar membrane. **C-F.** Montages of cells progressing through meiosis containing the lipid sensors under control of the meiotically-upregulated *ATG8* promoter. Chromosomes were visualized with the histone marker Htb1-mCherry, and the first time point

depicting anaphase II was defined as 0 minutes. **C.** Q2-GFP, the cytoplasmic PA sensor (UB25974) **D.** NLS-Q2-GFP, the nuclear PA sensor (UB26043) **E.** C1a+C1b-GFP, the cytoplasmic DAG sensor (UB25976) **F.** 2xNLS-C1a+C1b-GFP, the nuclear DAG sensor (UB25978). Scale bars, 2 µm.

B.2.3 Discussion

Overall, the lipid sensors developed here proved to be of limited utility in monitoring nuclear envelope composition during meiosis. The nuclear DAG sensor works well to monitor prophase nuclear envelope dynamics and could therefore facilitate study of the nuclear envelope-chromosome contacts that facilitate proper homologous recombination (reviewed in Zetka et al., 2020). Additionally, the punctate nature of the nuclear DAG sensor's localization after meiosis may merit further investigation of nuclear lipid droplets during gamete development. However, further use of lipid sensors in monitoring nuclear envelope dynamics will require determining why both the nuclear PA and DAG sensors lost their nuclear localization during meiosis II. Optimization of the nuclear localization signal in the constructs may not help given the virtual nuclear envelope breakdown that occurs after anaphase II (Chapter 4).

The cytoplasmic lipid sensors did, however, provide unanticipated insights into gamete plasma membrane formation during meiosis. The cytoplasmic PA sensor only weakly bound to the plasma membrane, suggesting a difference in the Opi1 Q2 binding domain and $Spo20^{51\text{-}91}$ binding domain that merits further investigation. The cytoplasmic DAG sensor revealed that the inner gamete plasma membrane bilayer may be enriched for DAG, since DAG-containing lipid droplets formed only inside gametes after plasma membrane closure (Figure B.3E). Notably, both cytoplasmic lipid sensors localized away from the gamete plasma membrane shortly after closure, suggesting that dramatic lipid remodeling accompanies this event. The formation of *de novo* gamete plasma membranes may therefore require many as yet unknown lipid remodeling events.

Many questions remain with respect to lipid dynamics during meiosis. Continued development of tools to visualize different species will be important to understand how remodeling of the lipidome contributes to the formation of healthy gametes.

B.3 Identification of a marker for entry into the meiotic divisions

B.3.1 Introduction

The design of genetic screens requires appropriate controls to ensure that the genes identified specifically affect the phenotype of interest. In a developmental program like meiosis, mutations that prevent progression can often result in false positives.

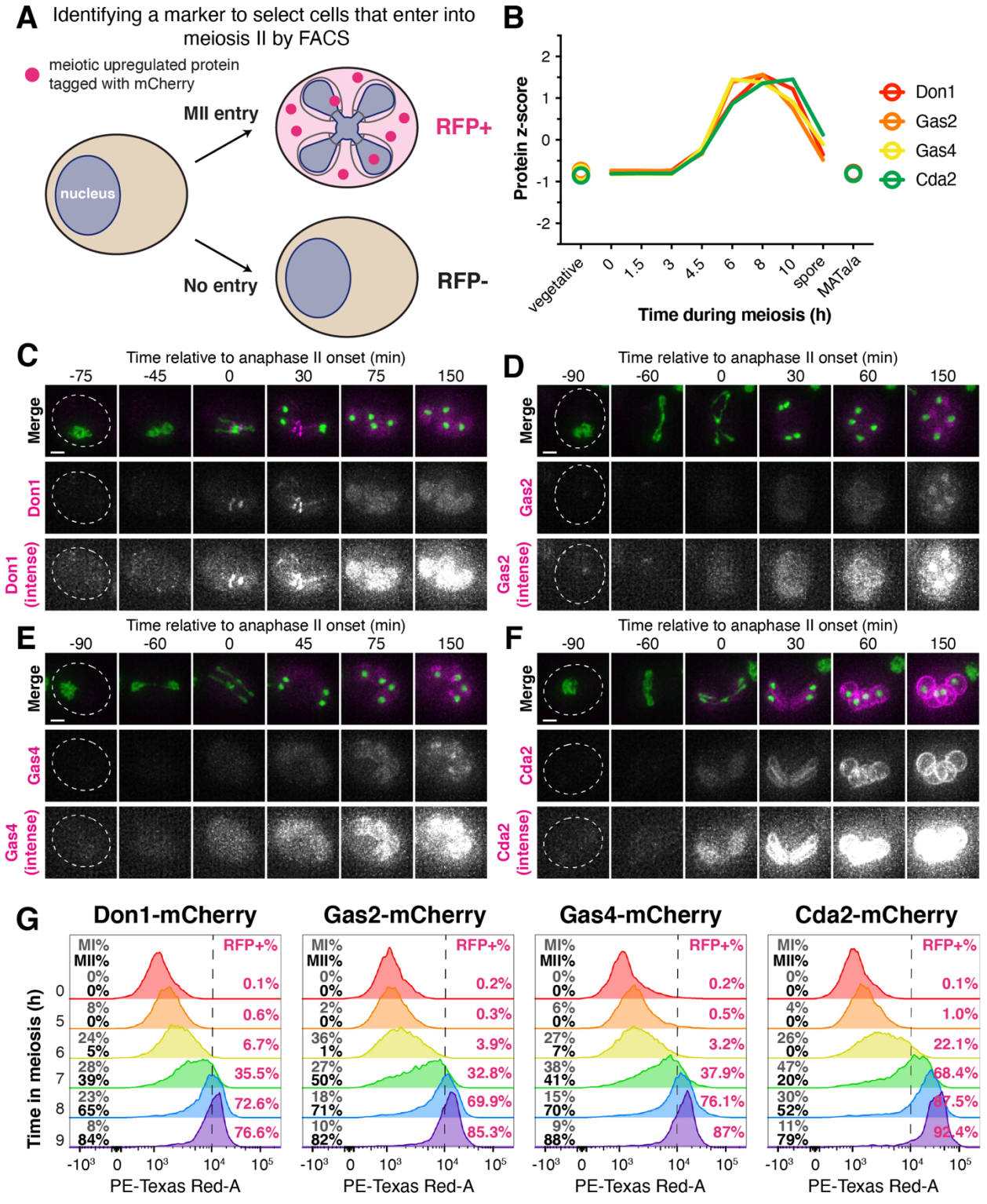

Figure B.4. Identification of Cda2 as a FACS-sortable marker of entry into the meiotic divisions. A. Schematic depicting the intended use of a highly upregulated meiotic

protein tagged with mCherry to differentiate between cells that enter into the meiotic divisions (RFP+) and cells that arrest prior to the meiotic divisions (RFP-). **B.** Protein abundance profiles from Cheng et al., 2018 for candidate proteins identified as having low expression prior to the meiotic divisions and high expression during the meiotic divisions. **C-F.** Montages of cells containing the candidate proteins tagged with mCherry progressing through meiosis. The candidate protein channel is shown in grayscale at two different intensities to highlight the extent of upregulation. Chromosomes were visualized with the histone marker Htb1-eGFP, and the first time point depicting anaphase II was defined as 0 minutes. **C.** Don1-mCherry (UB24483) **D.** Gas2-mCherry (UB23532) **E.** Gas4-mCherry (UB24364) **F.** Cda2-mCherry (UB23530). **G.** FACS profiles for RFP signal corresponding to the strains with different mCherry-tagged candidate proteins in C-F. Fixed samples were collected at different time points along a meiotic time course, before being analyzed by flow cytometry and scored for meiotic progression by Htb1-eGFP morphology. The percent of cells in meiosis I (two Htb1-eGFP lobes) and meiosis II (four Htb1-eGFP lobes) are indicated on the left of each plot; the percent of cells that are RFP+, as defined by having a signal greater than the dashed line, is indicated on the right of each plot. Scale bars, 2 μm.

Various markers have been identified that allow for assaying entry into different meiotic stages (e.g., Zip1-GFP for entry into pachytene; Sym et al., 1993); we were interested in identifying a protein that would allow for enrichment of cells that enter into the meiotic divisions (Figure B.4A). Here, we identify Cda2 as a highly abundant meiotic protein that allows cells in the meiotic divisions to be enriched for by FACS, establishing its utility in future screens.

B.3.2 Results

Using a dataset of protein abundance during the budding yeast meiotic program, we identified four candidate proteins that are highly upregulated specifically after upon entry into the meiotic divisions: Don1, Gas2, Gas4, and Cda2 (Cheng et al., 2018; Figure B.4B). We tagged the four proteins with mCherry and brought them into a strain with the meiotic staging marker Htb1-eGFP. We then monitored their abundance and localization by both microscopy and flow cytometry. By microscopy, all four proteins clearly exhibited upregulation during the meiotic divisions, particularly at and after anaphase II (Figure B.4C-F). Cda2-mCherry, which localized to gamete plasma membranes, was significantly more abundant than the three other proteins (Figure B.4F). We then used flow cytometry to determine whether these tags allow for differentiation between cells before and after entry into the meiotic divisions (Figure B.4G). For all four tags, almost no cells were RFP+ upon entry into meiosis (0 h) and at prophase (5 h). All tags exhibited an increase in RFP+ cells as progression through meiosis continued; however, Cda2-mCherry provided the clearest separation between RFP- and RFP+ cells, with over 90% of Cda2-mCherry cells scoring as RFP+

by 9 hours. Of note, Cda2-mCherry appears to allow enrichment for cells that have progressed through anaphase I or anaphase II, while the other three tags seem only to allow for enrichment for cells that have progressed through anaphase II. The different tags generated therefore allow for enrichment of cells in the meiotic divisions using a FACS-based approach.

B.3.3 Discussion

We anticipate that the tags generated here will be broadly useful for screens performed on phenotypes that occur after entry into the meiotic divisions. The different tags may be variably useful for screens that require entry into the meiotic divisions more generally (Cda2) or that require specific entry into meiosis II (Don1, Gas2, and Gas4). Further validation of the tags, including confirmation of their low expression in prophase-arrested cells (*ndt80Δ*), is necessary before use in in any full genetic screen. With the identification of a stage-specific marker for the meiotic divisions, we hope to facilitate study of the dynamic cellular remodeling required for the formation of gametes.

B.4 Additional tags generated

Monitoring dynamic protein localization during meiosis has resulted in unanticipated insights in this study and others. The following list are additional proteins which we tagged and monitored during the meiotic divisions, with their respective localization (Table B.1). Further studies may be able to utilize this information given the appropriate context.

Table B.1. Additional genes tagged with GFP and their meiotic localization. Movies of strains with the indicated allele and a meiotic staging marker (Htb1-mCherry) were generated. Tags that may be particularly useful are bolded and in red.

Allele	Strain	Localization
Chm7-GFP	UB8615 (w/ P_{GAL}-*NDT80* system)	Weak signal throughout meiosis
Nhp2-GFP	UB14607	Nucleolar protein that exhibits partial sequestration during meiosis II
Net1-GFP	UB17080	Nucleolar protein that becomes nucleoplasmic at the onset of anaphase I and anaphase II, resulting in its complete inheritance
Rpa135-GFP	UB17082	Nucleolar protein that exhibits behavior in between Net1 and Nhp2 – minor sequestration during meiosis II, in addition to partial dissolution at the onset of anaphase

Msc1-GFP	UB20072	ER protein enriched at the nuclear periphery that is extremely upregulated in spores
Hos3-GFP	UB25674	Weak signal, but will sometimes form foci especially in the GUNC
Nur1-GFP	UB25678	Weak signal throughout meiosis
Gip1-GFP	UB26799	Weak signal that increases during the meiotic divisions – localizes to septin bars during meiosis II, before relocalizing to the nucleus and eventually disappearing
GFP-Glc7	UB27323	Exhibits dynamic localization during meiosis: nuclear/punctate in prophase and meiosis I → septin bars during meiosis II → nuclear/ punctate after meiosis II → generally diffuse
Ulp1-GFP/ Ulp1-3xGFP	UB29048/ UB30626	Weakly localizes to the nuclear periphery during prophase and meiosis I; appears to detach with the nuclear basket during meiosis II and return to gamete nuclei

Appendix C

Methods

C.1 Yeast strains, plasmids, and culture methods

C.1.1 Strains and plasmids

All *S. cerevisiae* strains in this study are derivatives of SK1 and specified in Table C.1. Deletion and C-terminal tagging at endogenous loci were performed using previously described PCR-based methods unless otherwise specified (Janke et al., 2004; Longtine et al., 1998; Sheff and Thorn, 2004). Primer sequences used for strain construction are specified in Table C.2, and plasmids used for strain construction are specified in Table C.3.

Chapter 2
Strains UB17338, UB17509 and UB17532 are derivatives of strain HY2545 (a gift from Dr. Hong-Guo Yu). Deletion of *SSP1* and *SPS1* was performed by transforming cells with a PCR amplicon of the locus from the SK1 yeast deletion collection (a gift from Dr. Lars Steinmetz). The following alleles were constructed in a previous paper: *flo8Δ* (Boselli et al., 2009); Htb1-mCherry (Matos et al., 2008); Hsp104-eGFP (Unal et al., 2011); *ndt80Δ* (Xu et al., 1995); *spo21Δ* and *ama1Δ* (Sawyer et al., 2019); *cdc15-as1* (D'Aquino et al., 2005); and *atg39Δ* and *atg40Δ* (Otto et al., 2021).

To visualize the vacuole, we used either an eGFP-tagged version of Vph1 integrated at the *HIS3* locus or a mCherry-tagged version of Vph1 at its endogenous locus. To generate the eGFP-tagged version, we amplified the W303 genomic region from 1000 bp upstream to immediately before the stop codon of *VPH1* (2520 bp after the ORF start) and fused it to yeGFP in the *HIS3* integrating plasmid pNH603 (a gift from Leon Chan). We then performed integration of this plasmid (pUB691) at the *HIS3* locus by cutting the plasmid with PmeI. To generate the mCherry-tagged version, we constructed a new *HIS3*-selectable mCherry plasmid (pUB1197) by replacing eGFP in pYM28 (Janke et al., 2004) with mCherry. We then tagged the locus via traditional PCR-based methods.

To visualize the nuclear envelope, we generated an inner nuclear membrane-localizing reporter (eGFP-h2NLS-L-TM) by fusing eGFP and amino acids 93 to 378 of Heh2 (pUB1196; Meinema et al., 2011) under control of the *ARO10* promoter in the *LEU2* integrating plasmid pLC605 (a gift from Leon Chan). To visualize the prospore membrane, we used a reporter consisting of amino acids 51 to 91 from Spo20 fused to the C terminus of link-yeGFP under control of the *ATG8* promoter in a *LEU2* integrating plasmid (Sawyer et al., 2019). We also constructed a new variant with

mKate2 in place of yeGFP (pUB1104). All *LEU2* integration constructs were integrated into the genome by cutting the plasmids with PmeI.

To generate N-terminally tagged *NUP42* (yeGFP-Nup42) at the endogenous locus, CRISPR/Cas9-directed repair was used (Anand et al., 2017). Golden Gate Assembly was used to integrate a gRNA sequence (5'-ATTACAGTTGAGTCGTTGCT-3') binding upstream of the *NUP42* ORF into a *URA3*-marked centromeric plasmid containing Cas9 under control of the *PGK1* promoter (a gift from Gavin Schlissel and Jasper Rine). This plasmid (pUB1730) and a repair template – amplified from a plasmid (pUB257) and containing a mutation to abolish the PAM sequence (C→G at the -21nt position upstream of *NUP42*) – were co-transformed into yeast. The allele was confirmed by sequencing.

Chapter 3
The following alleles were constructed in a previous paper: P_{GPD}*-GAL4-ER* (Matos et al., 2008); P_{CUP1}*-CDC5* (Grigaitis et al., 2020); *ime2-as1* (Benjamin et al., 2003); *ndt80Δ::NatMX* (Matos et al., 2011); *SPC42-mCherry* (Miller et al., 2012); and *pCLB2-CDC5* (*cdc5-mn*) and *pCLB2-CDC20* (*cdc20-mn;* Lee and Amon, 2003).

To generate lipid-binding mutants (*nup60-ΔAH* [*nup60-Δ2-47*] and *nup60-I36R*) or phosphomutants (*NUP60-S89A*, *NUP60-Nterm3A*, *NUP60-Nterm5A*, *NUP60-Cterm4A*, and *NUP60-9A*; see Figure 3.8B for sites mutated in each allele) of *NUP60* at the endogenous locus, CRISPR/Cas9-directed repair was used unless otherwise noted (Anand et al., 2017). Golden Gate Assembly was used to integrate a gRNA sequence (5'-GTCGATTTTAGGATATCTCG-3') binding upstream of the *NUP60* ORF into a *URA3*-marked centromeric plasmid containing Cas9 under control of the *PGK1* promoter (a gift from Gavin Schlissel and Jasper Rine). This plasmid (pUB1729) and the appropriate repair template, amplified from a gBlock gene fragment (IDT), were co-transformed into yeast. All repair templates contained a mutation to abolish the PAM sequence (C→G at the -27nt position upstream of *NUP60*) and prevent re-cutting. The following nucleotide changes were introduced to achieve specific point mutations: I36R (5'-ATT-3' → 5'-CGT-3'), S89A (5'-TCC-3' → 5'-GCG-3'), T112A (5'-ACA-3' → 5'-GCA-3'), S118A (5'-TCC-3' → 5'-GCC-3'), S162A (5'-TCA-3' → 5'-GCA-3'), S171A (5'-TCG-3' → 5'-GCC-3'), S371A (5'-TCC-3' → 5'-GCC-3'), S374A (5'-TCA-3' → 5'-GCA-3'), S394A (5'-TCC-3' → 5'-GCC-3'), and S395A (5'-TCT-3' → 5'-GCT-3'). A similar approach was used to generate the N-terminally tagged FKBP12-Nup60, with a FKBP12-containing repair template amplified from a plasmid (pUB651). Following transformation into yeast, all alleles were confirmed by sequencing. To generate *NUP60-S89A-9myc*, a single point mutation in *NUP60-9myc* was introduced by site-directed mutagenesis using primers OML1096 and OML1018 (Table C.2). In brief, a mutagenic primer (S89A) was used to amplify the region coding for the C-terminus of *NUP60-9myc*, as well as the associated *TRP1* cassette. The PCR was then used to transform wild type cells, thus simultaneously introducing the S89A mutation and

the 9myc tag. The following nucleotide change was confirmed by sequencing: S89A (5'-TCC-3' → 5'-GCC-3').

To generate a lipid-binding mutant of *NUP1* (*nup1-ΔAH* [*nup1-Δ2-32*]) at the endogenous locus, a CRISPR/Cas9 approach was used. A Cas9 plasmid containing a gRNA (5'-CTGTCCCTATAACCCTTTCG-3') binding upstream of the *NUP1* ORF (pUB1727) was cloned, and the repair template – amplified from a gDNA gene block (IDT) – contained a mutation to abolish the PAM sequence (C→G at the -49nt position upstream of *NUP1*). To generate N-terminally tagged *MLP1* (*FKBP12-MLP1*) at the endogenous locus, a CRISPR/Cas9 approach was again used. A Cas9 plasmid containing a gRNA (5'-GCCACATTTTAGGATAATGT-3') overlapping with the 5'-end of the *MLP1* ORF was cloned (pUB2020), and the repair template – amplified from a plasmid (pUB651) – contained a mutation to abolish the PAM sequence (a synonymous G→C mutation at the +6 nt position of Mlp1). Both alleles were confirmed by sequencing.

To generate strains containing copper-inducible *CDC5* constructs (P_{CUP1}-*CDC5*^{KD}-*3xFLAG-10xHis* [pUB2047] and P_{CUP1}-*CDC5-3xFLAG-10xHis* [pUB2048]), we inserted the desired *CDC5* allele downstream of the *CUP1* promoter in a *TRP1* single integration vector backbone (pNH604, a gift from the Lim lab). The kinase-dead (KD) allele contained a K110M mutation (5'-AAA-3' → 5'-ATG-3') in the *CDC5* ORF (Charles et al., 1998). To generate strains carrying the ß-estradiol-inducible P_{GAL1}-*CDC5-eGFP* (pML118) or P_{GAL1}-*CDC5*^{KD}-*eGFP* (pML120) alleles, the respective *CDC5* sequences were inserted into the pAG304GAL-ccdB-EGFP::TRP1 destination vector by Gateway Cloning (Addgene 14183; Hartley et al., 2000). The constructs (pML118 and pML120) were integrated at the *TRP1* locus of a strain (YML 1110) carrying a P_{GPD}-*GAL4-ER* allele at the *URA3* locus. To generate strains containing a 5-Ph-IAA responsive F-box receptor osTIR1 (P_{CUP1}-*osTIR1*^{F74G}), KLD (kinase, ligase, and Dpn1) site-directed mutagenesis was performed for P_{CUP1}-*osTIR1* in a *HIS3* integrating vector. osTIR1^{F74G} exhibits lower background degradation, since it is non-responsive to the endogenous auxin present in yeast (Yesbolatova et al., 2020). All constructs were integrated into the genome following digestion with PmeI.

Chapter 4

The following alleles were constructed in a previous paper: *GAL4.ER* and P_{GAL}-*NDT80* (Benjamin et al., 2003; Carlile and Amon, 2008).

To visualize chromatin using a green fluorescent protein, we tagged Htb1 at its endogenous locus with GFP. Initial attempts to tag Htb1 resulted in an unanticipated rearrangement event involving potential duplication of the Htb1 locus, likely due to sickness associated with the allele (termed "old Htb1-GFP," used only in UB18822). We tested multiple linkers for fusing Htb1 and GFP, determining that a Knop linker (from pUB233) resulted in only minor sickness (this allele was used in all other strains). We note that this allele is still associated with a greater meiotic delay than

Htb1-mCherry, consistent with it representing a partial loss of function allele (data not shown).

To visualize the nucleoplasmic protein Npl3, we generated *a HIS3* single integration vector with a fusion between GFP and the ORF of *NPL3* (GFP-Npl3) downstream of the endogenous *NPL3* promoter (pUB931; derived from pKW551, a gift from the Weis lab, which is originally from Gilbert et al., 2001). To visualize the nucleoplasmic protein Trz1, we generated a *TRP1* single integration vector with a fusion between the ORF of *TRZ1* and GFP (Trz1-GFP) downstream of the endogenous *TRZ1* promoter (pUB1194). To generate the synthetic nucleoplasmic reporter 2xmCherry-SV40NLS, we generated a *LEU2* single integration vector with a fusion between two tandem copies of mCherry and the SV40 nuclear localization signal (SV40NLS; Kalderon et al., 1984) downstream of the *ARO10* promoter (pUB984). All constructs were integrated into the genome by cutting the plasmids with PmeI.

To facilitate inducible expression of a constitutively active allele of Ime2 (P_{GAL}-*IME2st*), we transformed a strain containing *IME2st* (an allele lacking its C-terminal 241 amino acids; Berchowitz et al., 2013; Sari et al., 2008) with a Pringle cassette placing the *GAL* promoter upstream of the ORF. The allele was verified by PCR.

Appendix A

The following alleles were constructed in a previous paper: P_{TDH3}-*CRE-EBD78* (Logie and Stewart, 1995, a gift from the van Leeuwen lab); P_{URA3}-*TetR-GFP* (Michaelis et al., 1997, a gift from the Koshland lab).

To generate the screening plasmid, we first generated a plasmid with a backbone containing a hygromycin resistance cassette HygMX and the autonomous replicating sequence ARSH4 and with an excisable cassette containing centromere CEN13 and the uracil synthesis gene *URA3* (pUB1765). We then used HindIII-SacI restriction cloning to integrate a 224xtetO array (from pAA951, a gift from the Amon lab) upstream of the HygMX cassette (pUB1898; Figure A.1B) and performed a restriction digest to confirm the ~10kb insertion. Due to the highly repetitive nature of the tetO array, the plasmid must be propagated in competent cells with reduced recombination (OneShot Stbl3 cells, Thermo Fisher).

For endogenous tagging of proteins with TetR, we generated a Pringle tagging plasmid with TetR and the NatMX selection cassette (pUB2127). To generate a rapamycin-inducible TetR tether (Haruki et al., 2008), we generated a *LEU2* single integration vector with the *FKBP12* ORF fused to TetR-GFP downstream of the *URA3* promoter (pUB1974). The *LEU2* integration construct was integrated into the genome by cutting the plasmid with AflII.

For ectopic meiotic overexpression of aggregate-protein nucleolar protein tethers, we generated *TRP1* single integration vectors with the SK1 sequences of nucleolar

proteins (*NOP15* [pUB2302], *SOF1* [pUB2303], *NOP13* [pUB2304], *RLP7* [pUB2305]; Paxman et al., 2021) fused to TetR downstream of an *ATG8* promoter. To visualize the overexpressed nucleolar proteins, we similarly generated *TRP1* single integration vectors with nucleolar proteins (*NOP15* [pUB2298] and *SOF1* [pUB2299]) fused to GFP downstream of an *ATG8* promoter. All *TRP1* integration constructs were integrated into the genome by cutting the plasmids with PmeI.

Appendix B

To generate nucleoporins with photoconvertible tags, we used a Pringle tagging vector with 3xDendra2 (Gurskaya et al., 2006; pUB1405, a gift from the Weis lab). To generate nucleoporins with a recombination inducible tag exchange (RITE) cassette (Verzijlbergen et al., 2010), we first replaced RFP in a RITE tagging cassette (V5-LoxP-HA-GFP-LoxP-T7-mRFP, a gift from the van Leeuwen lab) with mCherry (V5-LoxP-HA-GFP-LoxP-T7-mCherry, pUB1198). We then C-terminally tagged the nucleoporins at their endogenous locus with a standard PCR based approach using specific RITE adaptors.

To visualize lipids during meiosis, we integrated lipid sensors into either a *LEU2* or *TRP1* integrating plasmid downstream of an *ATG8* promoter. The lipid sensors consisted of either the Opi1 Q2 domain (for phosphatidic acid sensors) or the PKCβ C1a+C1b domain (for diacylglycerol sensors) with or without an NLS/2xNLS from *NUP60* (gifts from the Köhler lab). The following are the plasmid numbers: pUB1877 (Q2-GFP), pUB1879 (NLS-Q2-GFP), pUB1881 (C1a+C1b-GFP), pUB1883 (2xNLS-C1a+C1b-GFP). To visualize gamete plasma membranes membrane with BFP, we used a reporter consisting of amino acids 51 to 91 from Spo20 fused to the C terminus of mTagBFP under control of the *ATG8* promoter in a *LEU2* integrating plasmid (pUB1183). All *LEU2* or *TRP1* integration constructs were integrated into the genome by cutting the plasmids with PmeI.

To generate N-terminally tagged *GLC7* (yeGFP-Glc7) at the endogenous locus, CRISPR/Cas9-directed repair was used (Anand et al., 2017). Golden Gate Assembly was used to integrate a gRNA sequence (5'-TTTAATTTGAATGTATATTG-3') binding upstream of the *GLC7* ORF into a *URA3*-marked centromeric plasmid containing Cas9 under control of the *PGK1* promoter (a gift from Gavin Schlissel and Jasper Rine). This plasmid (pUB1938) and the repair template – amplified from a plasmid (pUB257) and containing a mutation to abolish the PAM sequence (C → G at the -25nt position upstream of *GLC7*) – were co-transformed into yeast. The allele was confirmed by sequencing.

Table C.1 Strains used in this study.

Strain	Genotype
SK1 wild-type	*ho::LYS2 lys2 ura3 leu2::hisG his3::hisG trp1::hisG*
UB3810	*MAT***a** */MATalpha Htb1-mCherry::HISMX6/Htb1-mCherry::HISMX6 Nup53-eGFP:KanMX6/Nup53-eGFP:KanMX6*
UB8615	*MAT***a** */MATalpha GAL-NDT80::TRP1/GAL-NDT80::TRP1 ura3::pGPD1-GAL4(848).ER::URA3/ura3::pGPD1-GAL4(848).ER::URA3 Chm7-GFP-HisMX/Chm7-GFP-HisMX HTB1-mCherry-HISMX6/HTB1-mCherry-HISMX6*
UB8746	*MAT***a** */MATalpha ura3::pGPD1-GAL4(848).ER::URA3/ ura3::pGPD1-GAL4(848).ER::URA3 GAL-NDT80::TRP1/GAL-NDT80::TRP1 Nup49-mCherry::KanMX/Nup49-mCherry::KanMX his3::GFP-Npl3::HIS3/his3::GFP-Npl3::HIS3*
UB8837	*MAT***a** */MATalpha GAL-NDT80::TRP1/GAL-NDT80::TRP1 ura3::pGPD1-GAL4(848).ER::URA3/ura3::pGPD1-GAL4(848).ER::URA3 Nup170-3xDendra-HisMX/Nup170-3xDendra-HisMX*
UB8839	*MAT***a** */MATalpha GAL-NDT80::TRP1/GAL-NDT80::TRP1 ura3::pGPD1-GAL4(848).ER::URA3/ura3::pGPD1-GAL4(848).ER::URA3 Nup49-3xDendra-HisMX/Nup49-3xDendra-HisMX*
UB9724	*MAT***a** */MATalpha Htb1-mCherry::HISMX6/Htb1-mCherry::HISMX6 Hsp104-eGFP::KanMX6/Hsp104-eGFP::KanMX6 flo8::KanMX6/ flo8::KanMX6*
UB11513	*MAT***a** */MATalpha Htb1-mCherry::HISMX6/Htb1-mCherry::HISMX6 Nup170-GFP::KanMX6/Nup170-GFP::KanMX6*
UB11821	*MAT***a** */MATalpha Hsp104-mCherry::NatMX6/Hsp104-mCherry::NatMX6 leu2::pATG8-link-yeGFP-SPO20(51-91)::LEU2/leu2::pATG8-link-yeGFP-SPO20(51-91)::LEU2 flo8::KanMX6/flo8::KanMX6*
UB12163	*MAT***a** */MATalpha flo8::KanMX6/flo8::KanMX6 Hsp104-mCherry::NatMX6/Hsp104-mCherry::NatMX6 his3::VPH1-eGFP::HIS3/ his3::VPH1-eGFP::HIS3*
UB12342	*MAT***a** */MATalpha leu2::pATG8-link-yeGFP-SPO20(51-91)::LEU2/ leu2::pATG8-link-yeGFP-SPO20(51-91)::LEU2 Nup49-mCherry::KanMX6/ Nup49-mCherry::KanMX6*
UB12414	*MAT***a** */MATalpha Ady3::HygB/Ady3::HygB Htb1-mCherry::HISMX6/ Htb1-mCherry::HISMX6 Nup170-*

	GFP::KanMX6/Nup170-GFP::KanMX6
UB12434	*MAT***a** */MATalpha leu2::pATG8-link-yeGFP-SPO20(51-91)::LEU2/ leu2::pATG8-link-yeGFP-SPO20(51-91)::LEU2 Htb1-mCherry::HISMX6/Htb1-mCherry::HISMX6*
UB12436	*MAT***a** */MATalpha Don1-GFP::KanMX6/Don1-GFP::KanMX6 Nup49-mCherry::KanMX6/Nup49-mCherry::KanMX6*
UB12438	*MAT***a** */MATalpha Don1-GFP::KanMX6/Don1-GFP::KanMX6 Htb1-mCherry::HISMX6/Htb1-mCherry::HISMX6*
UB12461	*MAT***a** */MATalpha Don1::HygB/Don1::HygB Nup170-GFP::KanMX6/Nup170-GFP::KanMX6 Htb1-mCherry::HISMX6/Htb1-mCherry::HISMX6*
UB12463	*MAT***a** */MATalpha Irc10::HygB/Irc10::HygB Nup170-GFP::KanMX6/Nup170-GFP::KanMX6 Htb1-mCherry::HISMX6/Htb1-mCherry::HISMX6*
UB12465	*MAT***a** */MATalpha ady3::HygB/ady3::HygB irc10::HygB/irc10::HygB Nup170-GFP::KanMX6/Nup170-GFP::KanMX6 Htb1-mCherry::HISMX6/ Htb1-mCherry::HISMX6*
UB12752	*MAT***a** */MATalpha Nsg1::HygMX/Nsg1::HygMX HTB1-mCherry-HISMX6/HTB1-mCherry-HISMX6 Nup170-GFP::KanMX/Nup170-GFP::KanMX*
UB12926	*MAT***a** */MATalpha Nup170-RITE (GFP->mCherry)::HygMX/Nup170-RITE (GFP->mCherry)::HygMX HIS3::pTDH3-Cre-EBD78-His3/HIS3::pTDH3-Cre-EBD78-His3*
UB12930	*MAT***a** */MATalpha Nup49-RITE (GFP->mCherry)::HygMX/Nup49-RITE (GFP->mCherry)::HygMX HIS3::pTDH3-Cre-EBD78-His3/HIS3::pTDH3-Cre-EBD78-His3*
UB12932	*MAT***a** */MATalpha leu2::pARO10-eGFP-h2NLS-L-TM::LEU2/leu2::pARO10-eGFP-h2NLS-L-TM::LEU2 Nup49-mCherry::KanMX6/ Nup49-mCherry::KanMX6*
UB12975	*MAT***a** */MATalpha Nup170-GFP::KanMX6/ Nup170-GFP::KanMX6 Hsp104-mCherry::NatMX6/Hsp104-mCherry::NatMX6 flo8::KanMX6/flo8::KanMX6*
UB13299	*MAT***a** */MATalpha Nsr1-GFP::KanMX6/ Nsr1-GFP::KanMX6 Hsp104-mCherry::NatMX6/Hsp104-mCherry::NatMX6 flo8::KanMX6/flo8::KanMX6*
UB13373	*MAT***a** */MATalpha ssp1::KanMX6/ ssp1::KanMX6 Nup170-GFP::KanMX6/Nup170-GFP::KanMX6 Htb1-mCherry::HISMX6/Htb1-mCherry::HISMX6*
UB13375	*MAT***a** */MATalpha Gip1::NatMX/Gip1::NatMX HTB1-mCherry-HISMX6/HTB1-mCherry-HISMX6 Nup170-GFP::KanMX/Nup170-GFP::KanMX*

UB13377	*MAT***a** */MATalpha spo21::HygB/spo21::HygB Nup170-GFP::KanMX6/Nup170-GFP::KanMX6 Htb1-mCherry::HISMX6/Htb1-mCherry::HISMX6*
UB13379	*MAT***a** */MATalpha Sps1::KanMX/Sps1::KanMX HTB1-mCherry-HISMX6/HTB1-mCherry-HISMX6 Nup170-GFP::KanMX/Nup170-GFP::KanMX*
UB13381	*MAT***a** */MATalpha Smk1::HygB/Smk1::HygB HTB1-mCherry-HISMX6/HTB1-mCherry-HISMX6 Nup170-GFP::KanMX/Nup170-GFP::KanMX*
UB13383	*MAT***a** */MATalpha ama1::KanMX6/ama1::KanMX6 HTB1-mCherry-HISMX6/HTB1-mCherry-HISMX6 Nup170-GFP::KanMX/Nup170-GFP::KanMX*
UB13385	*MAT***a** */MATalpha Nup170-RITE (GFP->mCherry)::HygMX/+ HIS3::pTDH3-Cre-EBD78-His3 HIS3::pTDH3-Cre-EBD78-His3*
UB13387	*MAT***a** */MATalpha Nup49-RITE (GFP->mCherry)::HygMX/+ HIS3::pTDH3-Cre-EBD78-His3/HIS3::pTDH3-Cre-EBD78-His3*
UB13473	*MAT***a** */MATalpha ssp1::KanMX6/ ssp1::KanMX6 leu2::pATG8-link-yeGFP-SPO20(51-91)::LEU2/ leu2::pATG8-link-yeGFP-SPO20(51-91)::LEU2 Nup49-mCherry::KanMX6/ Nup49-mCherry::KanMX6*
UB13475	*MAT***a** */MATalpha ssp1::KanMX6/ ssp1::KanMX6 leu2::pATG8-link-yeGFP-SPO20(51-91)::LEU2/ leu2::pATG8-link-yeGFP-SPO20(51-91)::LEU2 Htb1-mCherry::HISMX6/Htb1-mCherry::HISMX6*
UB13497	*MAT***a** */MATalpha Nup84-GFP::KanMX6/ Nup84-GFP::KanMX6 Htb1-mCherry::HISMX6/Htb1-mCherry::HISMX6*
UB13499	*MAT***a** */MATalpha Nup120-GFP::KanMX6/Nup120-GFP::KanMX6 Htb1-mCherry::HISMX6/Htb1-mCherry::HISMX6*
UB13503	*MAT***a** */MATalpha Pom34-GFP::KanMX6/Pom34-GFP::KanMX6 Htb1-mCherry::HISMX6/Htb1-mCherry::HISMX6*
UB13505	*MAT***a** */MATalpha Nup188-GFP::KanMX6/Nup188-GFP::KanMX6 Htb1-mCherry::HISMX6/Htb1-mCherry::HISMX6*
UB13509	*MAT***a** */MATalpha Nup49-GFP::KanMX6/Nup49::KanMX6 Htb1-mCherry::HISMX6/Htb1-mCherry::HISMX6*
UB13513	*MAT***a** */MATalpha cdc15-as1:URA3/cdc15-as1:URA3 HTB1-mCherry-HISMX6/HTB1-mCherry-HISMX6 Nup170-GFP::KanMX/Nup170-GFP::KanMX*
UB13568	*MAT***a** */MATalpha spo21::HygB/spo21::HygB Hsp104-mCherry::NatMX6/ Hsp104-mCherry::NatMX6 Nup170-GFP::KanMX6/Nup170-GFP::KanMX6 flo8::KanMX6/flo8::KanMX6*
UB13583	*MAT***a** */MATalpha ady3::HygB/ady3::HygB Irc10::HygB/Irc10::HygB leu2::pATG8-link-yeGFP-SPO20(51-91)::LEU2/ leu2::pATG8-link-yeGFP-SPO20(51-91)::LEU2 Nup49-mCherry::KanMX6/ Nup49-mCherry::KanMX6*

UB13585	*MAT***a** */MATalpha ady3::HygB/ady3::HygB Irc10::HygB/Irc10::HygB leu2::pATG8-link-yeGFP-SPO20(51-91)::LEU2/ leu2::pATG8-link-yeGFP-SPO20(51-91)::LEU2 Htb1-mCherry::HISMX6/Htb1-mCherry::HISMX6*
UB14372	*MAT***a** */MATalpha atg39::NatMX/atg39::NatMX HTB1-mCherry-HISMX6/HTB1-mCherry-HISMX6 Nup170-GFP::KanMX/Nup170-GFP::KanMX*
UB14374	*MAT***a** */MATalpha atg40::KanMX/atg40::KanMX HTB1-mCherry-HISMX6/HTB1-mCherry-HISMX6 Nup170-GFP::KanMX/Nup170-GFP::KanMX*
UB14376	*MAT***a** */MATalpha Chm7::HisMX/Chm7::HisMX HTB1-mCherry-HISMX6/HTB1-mCherry-HISMX6 Nup170-GFP::KanMX/Nup170-GFP::KanMX*
UB14378	*MAT***a** */MATalpha Heh1::NatMX/Heh1::NatMX HTB1-mCherry-HISMX6/HTB1-mCherry-HISMX6 Nup170-GFP::KanMX/Nup170-GFP::KanMX*
UB14380	*MAT***a** */MATalpha Heh2::NatMX/Heh2::NatMX HTB1-mCherry-HISMX6/HTB1-mCherry-HISMX6 Nup170-GFP::KanMX/Nup170-GFP::KanMX*
UB14382	*MAT***a** */MATalpha Heh1::NatMX/Heh1::NatMX Heh2::NatMX/ Heh2::NatMX HTB1-mCherry-HISMX6/HTB1-mCherry-HISMX6 Nup170-GFP::KanMX/Nup170-GFP::KanMX*
UB14386	*MAT***a** */MATalpha Nvj1::NatMX/Nvj1::NatMX HTB1-mCherry-HISMX6/HTB1-mCherry-HISMX6 Nup170-GFP::KanMX/Nup170-GFP::KanMX*
UB14391	*MAT***a** */MATalpha Heh1-3xeGFP::KanMX6/Heh1-3xeGFP::KanMX6 Nup49-mCherry::KanMX6/ Nup49-mCherry::KanMX6*
UB14393	*MAT***a** */MATalpha Heh1-3xeGFP::KanMX6/Heh1-3xeGFP::KanMX6 Htb1-mCherry::HISMX6/ Htb1-mCherry::HISMX6*
UB14418	*MAT***a** */MATalpha Htb1-mCherry::HISMX6/Htb1-mCherry::HISMX6 Hsp104-eGFP::KanMX6/Hsp104-eGFP::KanMX6 flo8::KanMX6/ flo8::KanMX6 spo21::HygB/spo21::HygB*
UB14419	*MAT***a** */MATalpha Htb1-mCherry::HISMX6/Htb1-mCherry::HISMX6 Nsr1-GFP::KanMX6/ Nsr1-GFP::KanMX6 spo21::HygB/spo21::HygB*
UB14425	*MAT***a** */MATalpha Nsr1-GFP::KanMX6/ Nsr1-GFP::KanMX6 Nup49-mCherry::KanMX6/ Nup49-mCherry::KanMX6 spo21::HygB/spo21::HygB*
UB14607	*MAT***a** */MATalpha Nhp2-GFP-TRP1/Nhp2-GFP-TRP1 HTB1-mCherry-HISMX6/HTB1-mCherry-HISMX6*
UB14646	*MAT***a** */MATalpha Nup60-GFP::KanMX6/ Nup60-GFP::KanMX6 Htb1-mCherry::HISMX6/Htb1-mCherry::HISMX6*

UB14648	*MAT***a** */MATalpha Mlp1-GFP-KanMX/Mlp1-GFP-KanMX HTB1-mCherry-HISMX6/HTB1-mCherry-HISMX6*
UB14650	*MAT***a** */MATalpha Nup159-GFP::KanMX6/ Nup159-GFP::KanMX6 Htb1-mCherry::HISMX6/Htb1-mCherry::HISMX6*
UB14652	*MAT***a** */MATalpha Nup82-GFP::KanMX6/ Nup82-GFP::KanMX6 Htb1-mCherry::HISMX6/Htb1-mCherry::HISMX6*
UB14654	*MAT***a** */MATalpha Nup57-GFP::KanMX6/Nup57-GFP::KanMX6 Htb1-mCherry::HISMX6/Htb1-mCherry::HISMX6*
UB15118	*MAT***a** */MATalpha Nsr1-GFP::KanMX6/ Nsr1-GFP::KanMX6 Htb1-mCherry::HISMX6/Htb1-mCherry::HISMX6*
UB15301	*MAT***a** */MATalpha Ndc1-GFP::KanMX6/ Ndc1-GFP::KanMX6 Htb1-mCherry::HISMX6/Htb1-mCherry::HISMX6*
UB15303	*MAT***a** */MATalpha Nup1-GFP::KanMX6/ Nup1-GFP::KanMX6 Htb1-mCherry::HISMX6/Htb1-mCherry::HISMX6*
UB15305	*MAT***a** */MATalpha Nup2-GFP::KanMX6/ Nup2-GFP::KanMX6 Htb1-mCherry::HISMX6/Htb1-mCherry::HISMX6*
UB15307	*MAT***a** */MATalpha spr3::HygB/ spr3::HygB Nup170-GFP::KanMX6/ Nup170-GFP::KanMX6 Htb1-mCherry::HISMX6/ Htb1-mCherry::HISMX6*
UB15426	*MAT***a** */MATalpha spr28::HygB/ spr28::HygB Nup170-GFP::KanMX6/ Nup170-GFP::KanMX6 Htb1-mCherry::HISMX6/ Htb1-mCherry::HISMX6*
UB15428	*MAT***a** */MATalpha spr3::HygB/ spr3::HygB spr28::HygB/ spr28::HygB Nup170-GFP::KanMX6/ Nup170-GFP::KanMX6 Htb1-mCherry::HISMX6/ Htb1-mCherry::HISMX6*
UB15666	*MAT***a** */MATalpha ndt80::LEU2/ndt80::LEU2 Nup170-RITE (GFP->mCherry)::HygMX/Nup170-RITE (GFP->mCherry)::HygMX HIS3::pTDH3-Cre-EBD78-His3/HIS3::pTDH3-Cre-EBD78-His3*
UB15668	*MAT***a** */MATalpha ndt80::LEU2/ndt80::LEU2 Nup49-RITE (GFP->mCherry)::HygMX/Nup49-RITE (GFP->mCherry)::HygMX HIS3::pTDH3-Cre-EBD78-His3/HIS3::pTDH3-Cre-EBD78-His3*
UB15672	*MAT***a** */MATalpha Nup2-GFP::KanMX6/ Nup2-GFP::KanMX6 Nup49-mCherry::KanMX6/ Nup49-mCherry::KanMX6*
UB15890	*MAT***a** */MATalpha Nup170-GFP::KanMX6/Nup170-GFP::KanMX6 Vph1-mCherry::HisMX6/Vph1-mCherry::HisMX6*
UB16640	*MAT***a** */MATalpha Nup170-RITE (GFP->mCherry)::HygMX/Nup170-RITE (GFP->mCherry)::HygMX HIS3::pTDH3-Cre-EBD78-His3/HIS3::pTDH3-Cre-EBD78-His3 leu2:pATG8-link-mTagBFP-Spo20(51-91)::LEU2/leu2:pATG8-link-mTagBFP-Spo20(51-91)::LEU2*
UB16642	*MAT***a** */MATalpha Nup49-RITE (GFP->mCherry)::HygMX/Nup49-RITE (GFP->mCherry)::HygMX HIS3::pTDH3-Cre-EBD78-*

	His3/HIS3::pTDH3-Cre-EBD78-His3 leu2:pATG8-link-mTagBFP-Spo20(51-91)::LEU2/leu2:pATG8-link-mTagBFP-Spo20(51-91)::LEU2
UB16708	*MAT***a** */MATalpha Nsr1-GFP::KanMX6/ Nsr1-GFP::KanMX6 Nup49-mCherry::KanMX6/ Nup49-mCherry::KanMX6 flo8/flo8*
UB16710	*MAT***a** */MATalpha Nsr1-GFP::KanMX6/ Nsr1-GFP::KanMX6 leu2::pATG8-link-mKate-SPO20(51-91)::LEU2/leu2::pATG8-link-mKate-SPO20(51-91)::LEU2 flo8/flo8*
UB16712	*MAT***a** */MATalpha Nsr1-GFP::KanMX6/ Nsr1-GFP::KanMX6 Htb1-mCherry::HISMX6/ Htb1-mCherry::HISMX6 flo8/flo8*
UB17080	*MAT***a** */MATalpha Net1-GFP::KanMX/Net1-GFP::KanMX HTB1-mCherry-HISMX6/HTB1-mCherry-HISMX6*
UB17082	*MAT***a** */MATalpha Rpa135-GFP::KanMX/Rpa135-GFP::KanMX HTB1-mCherry-HISMX6/HTB1-mCherry-HISMX6*
UB17338	*MAT***a** */MATalpha Hta1-mApple::HIS5/ Hta1-mApple::HIS5 rDNA-5xtetO/rDNA pREC8-TetR-GFP::LEU2/ pREC8-TetR-GFP::LEU2 flo8/flo8 * Derived from HY2545*
UB17509	*MAT***a** */MATalpha Hta1-mApple::HIS5/ Hta1-mApple::HIS5 pREC8-TetR-GFP::LEU2/ pREC8-TetR-GFP::LEU2 flo8/flo8 * Derived from HY2545*
UB17532	*MAT***a** */MATalpha Nup49-mCherry::KanMX6/ Nup49-mCherry::KanMX6 rDNA-5xtetO/+ pREC8-TetR-GFP::LEU2/ pREC8-TetR-GFP::LEU2 flo8/flo8 * Derived from HY2545*
UB18509	*MAT***a** */MATalpha his3::GFP-Npl3::HIS3/his3::GFP-Npl3::HIS3 HTB1-mCherry-HISMX6/HTB1-mCherry-HISMX6*
UB18511	*MAT***a** */MATalpha his3::GFP-Npl3::HIS3/his3::GFP-Npl3::HIS3 leu2::pATG8-link-mKate-SPO20(51-91)::LEU2/leu2::pATG8-link-mKate-SPO20(51-91)::LEU2*
UB18822	*MAT***a** */MATalpha spo21::HygB/spo21::HygB Leu2::2xmCherry-SV40NLS::LEU2/ Leu2::2xmCherry-SV40NLS::LEU2 HTB1-eGFP::KanMX [NOTE: OLD Htb1-GFP]/HTB1-eGFP::KanMX [NOTE: OLD Htb1-GFP]*
UB18824	*MAT***a** */MATalpha Gip1::NatMX/Gip1::NatMX his3::GFP-Npl3::HIS3/his3::GFP-Npl3::HIS3 HTB1-mCherry-HISMX6/HTB1-mCherry-HISMX6*
UB18859	*MAT***a** */MATalpha spo21::HygB/spo21::HygB his3::GFP-Npl3::HIS3/his3::GFP-Npl3::HIS3 HTB1-mCherry-HISMX6/HTB1-mCherry-HISMX6*
UB19927	*MAT***a** */MATalpha Htb1-mCherry::HISMX6/Htb1-mCherry::HISMX6 Nup170-GFP::KanMX6/Nup170-GFP::KanMX6 ndt80::LEU2/ndt80::LEU2*
UB19229	*MAT***a** */MATalpha Nup84-GFP::KanMX6/ Nup84-GFP::KanMX6 Htb1-mCherry::HISMX6/Htb1-mCherry::HISMX6*

	ndt80::LEU2/ndt80::LEU2
UB19752	*MAT***a** */MATalpha Hsp104-mCherry::NatMX6/Hsp104-mCherry::NatMX6 leu2::pATG8-link-yeGFP-SPO20(51-91)::LEU2/leu2::pATG8-link-yeGFP-SPO20(51-91)::LEU2 flo8::KanMX6/flo8::KanMX6 spr3::HygB/ spr3::HygB*
UB19754	*MAT***a** */MATalpha Hsp104-mCherry::NatMX6/Hsp104-mCherry::NatMX6 leu2::pATG8-link-yeGFP-SPO20(51-91)::LEU2/leu2::pATG8-link-yeGFP-SPO20(51-91)::LEU2 flo8::KanMX6/flo8::KanMX6 spr28::HygB/ spr28::HygB*
UB19756	*MAT***a** */MATalpha Hsp104-mCherry::NatMX6/Hsp104-mCherry::NatMX6 leu2::pATG8-link-yeGFP-SPO20(51-91)::LEU2/leu2::pATG8-link-yeGFP-SPO20(51-91)::LEU2 flo8::KanMX6/flo8::KanMX6 don1::HygB/ don1::HygB*
UB19758	*MAT***a** */MATalpha Hsp104-mCherry::NatMX6/Hsp104-mCherry::NatMX6 leu2::pATG8-link-yeGFP-SPO20(51-91)::LEU2/leu2::pATG8-link-yeGFP-SPO20(51-91)::LEU2 flo8::KanMX6/flo8::KanMX6 ady3::HygB/ ady3::HygB*
UB19760	*MAT***a** */MATalpha Hsp104-mCherry::NatMX6/Hsp104-mCherry::NatMX6 leu2::pATG8-link-yeGFP-SPO20(51-91)::LEU2/leu2::pATG8-link-yeGFP-SPO20(51-91)::LEU2 flo8::KanMX6/flo8::KanMX6 spr3::HygB/ spr3::HygB spr28::HygB/ spr28::HygB*
UB19762	*MAT***a** */MATalpha Hsp104-mCherry::NatMX6/Hsp104-mCherry::NatMX6 leu2::pATG8-link-yeGFP-SPO20(51-91)::LEU2/leu2::pATG8-link-yeGFP-SPO20(51-91)::LEU2 flo8::KanMX6/flo8::KanMX6 irc10::HygB/ irc10::HygB*
UB20072	*MAT***a** */MATalpha Msc1-GFP-KanMX/Msc1-GFP-KanMX HTB1-mCherry-HISMX6/HTB1-mCherry-HISMX6*
UB20074	*MAT***a** */MATalpha Sma2::HygMX/Sma2::HygMX HTB1-mCherry-HISMX6/HTB1-mCherry-HISMX6 Nup170-GFP::KanMX/Nup170-GFP::KanMX*
UB20076	*MAT***a** */MATalpha Spo19::HygMX/Spo19::HygMX HTB1-mCherry-HISMX6/HTB1-mCherry-HISMX6 Nup170-GFP::KanMX/Nup170-GFP::KanMX*
UB20080	*MAT***a** */MATalpha Nup2-GFP-KanMX/Nup2-GFP-KanMX Pom34-mCherry-HISMX/Pom34-mCherry-HISMX*
UB20153	*MAT***a** */MATalpha Rna1-3xEGFP::KanMX/Rna1-3xEGFP::KanMX HTB1-mCherry-HISMX6/HTB1-mCherry-HISMX6*
UB20155	*MAT***a** */MATalpha Rna1-3xEGFP::KanMX/Rna1-3xEGFP::KanMX Leu2::2xmCherry-SV40NLS::LEU2/Leu2::2xmCherry-SV40NLS::LEU2*

UB20157	*MAT***a** */MATalpha Heh1::NatMX/ Heh1::NatMX his3::GFP-Npl3::HIS3/his3::GFP-Npl3::HIS3 HTB1-mCherry-HISMX6/HTB1-mCherry-HISMX6*
UB20159	*MAT***a** */MATalpha Ssp1::KanMX/Ssp1::KanMX his3::GFP-Npl3::HIS3/his3::GFP-Npl3::HIS3 HTB1-mCherry-HISMX6/HTB1-mCherry-HISMX6*
UB20161	*MAT***a** */MATalpha Prp20-GFP-HisMX/Prp20-GFP-HisMX HTB1-mCherry-HISMX6/HTB1-mCherry-HISMX6*
UB20163	*MAT***a** */MATalpha his3::GFP-Npl3::HIS3/his3::GFP-Npl3::HIS3 HTB1-mCherry-HISMX6/HTB1-mCherry-HISMX6 Heh2::NatMX/Heh2::NatMX*
UB20218	*MAT***a** */MATalpha Msc1::HygMX/Msc1::HygMX HTB1-mCherry-HISMX6/HTB1-mCherry-HISMX6 Nup170-GFP::KanMX/Nup170-GFP::KanMX*
UB20274	*MAT***a** */MATalpha Heh1::NatMX/Heh1::NatMX Heh2::NatMX/ Heh2::NatMX his3::GFP-Npl3::HIS3/his3::GFP-Npl3::HIS3 HTB1-mCherry-HISMX6/HTB1-mCherry-HISMX6*
UB20605	*MAT***a** */MATalpha Sma2::HygMX/Sma2::HygMX his3::GFP-Npl3::HIS3/his3::GFP-Npl3::HIS3 HTB1-mCherry-HISMX6/HTB1-mCherry-HISMX6*
UB20607	*MAT***a** */MATalpha ama1::KanMX6/ama1::KanMX6 his3::GFP-Npl3::HIS3/his3::GFP-Npl3::HIS3 HTB1-mCherry-HISMX6/HTB1-mCherry-HISMX6*
UB20609	*MAT***a** */MATalpha trp1::TRZ1-WT-yEGFP::TRP1/trp1::TRZ1-WT-yEGFP::TRP1 HTB1-mCherry-HISMX6/HTB1-mCherry-HISMX6*
UB20613	*MAT***a** */MATalpha Nup170-GFP::KanMX/Nup170-GFP::KanMX Don1-mCherry-HisMX/Don1-mCherry-HisMX*
UB20615	*MAT***a** */MATalpha Nup170-GFP::KanMX/Nup170-GFP::KanMX leu2::pATG8-link-mKate-SPO20(51-91)::LEU2/leu2::pATG8-link-mKate-SPO20(51-91)::LEU2*
UB20617	*MAT***a** */MATalpha his3::GFP-Npl3::HIS3/his3::GFP-Npl3::HIS3 Leu2::2xmCherry-SV40NLS::LEU2/Leu2::2xmCherry-SV40NLS::LEU2*
UB20761	*MAT***a** */MATalpha Sma2::HygMX/Sma2::HygMX Ssp1::KanMX/Ssp1::KanMX his3::GFP-Npl3::HIS3/his3::GFP-Npl3::HIS3 HTB1-mCherry-HISMX6/HTB1-mCherry-HISMX6*
UB20765	*MAT***a** */MATalpha Sma2::HygMX/Sma2::HygMX Nup170-GFP::KanMX/Nup170-GFP::KanMX Don1-mCherry-HisMX/Don1-mCherry-HisMX*
UB20767	*MAT***a** */MATalpha Sma2::HygMX/Sma2::HygMX Nup170-GFP::KanMX/Nup170-GFP::KanMX leu2::pATG8-link-mKate-SPO20(51-91)::LEU2/leu2::pATG8-link-mKate-SPO20(51-91)::LEU2*

UB20863	*MAT***a** */MATalpha Chm7::HygMX/Chm7::HygMX his3::GFP-Npl3::HIS3/his3::GFP-Npl3::HIS3 HTB1-mCherry-HISMX6/HTB1-mCherry-HISMX6*
UB20983	*MAT***a** */MATalpha Chm7::HygMX/Chm7::HygMX Heh1::NatMX/Heh1::NatMX his3::GFP-Npl3::HIS3/his3::GFP-Npl3::HIS3 HTB1-mCherry-HISMX6/HTB1-mCherry-HISMX6*
UB21079	*MAT***a** */MATalpha Nup84-GFP::KanMX/Nup84-GFP::KanMX Pom34-mCherry-HISMX/Pom34-mCherry-HISMX*
UB21380	*MAT***a** */MATalpha Htb1-EGFP-KanMX/Htb1-EGFP-KanMX Leu2::2xmCherry-SV40NLS::LEU2/Leu2::2xmCherry-SV40NLS::LEU2*
UB21612	*MAT***a** */MATalpha spo21::HygB/spo21::HygB Htb1-EGFP-KanMX/Htb1-EGFP-KanMX Leu2::2xmCherry-SV40NLS::LEU2/Leu2::2xmCherry-SV40NLS::LEU2*
UB21614	*MAT***a** */MATalpha Gip1::NatMX/Gip1::NatMX Htb1-EGFP-KanMX/Htb1-EGFP-KanMX Leu2::2xmCherry-SV40NLS::LEU2/Leu2::2xmCherry-SV40NLS::LEU2*
UB21660	*MAT***a** */MATalpha Nup100-GFP-KanMX/Nup100-GFP-KanMX Htb1-mCherry-HISMX6/Htb1-mCherry-HISMX6*
UB21817	*MAT***a** */MATalpha Ssp1::KanMX/Ssp1::KanMX Htb1-EGFP-KanMX/Htb1-EGFP-KanMX Leu2::2xmCherry-SV40NLS::LEU2/ Leu2::2xmCherry-SV40NLS::LEU2*
UB22741	*MAT***a** */MATalpha Gle1-GFP-KanMX/Gle1-GFP-KanMX Htb1-mCherry-HISMX6/Htb1-mCherry-HISMX6*
UB22987	*MAT***a** */MATalpha Spr3::HygMX/Spr3::HygMX his3::GFP-Npl3::HIS3/his3::GFP-Npl3::HIS3 HTB1-mCherry-HISMX6/HTB1-mCherry-HISMX6*
UB23087	*MAT***a** */MATalpha spo21::HygB/spo21::HygB Nup2-GFP-KanMX/Nup2-GFP-KanMX Pom34-mCherry-HISMX/Pom34-mCherry-HISMX*
UB23203	*MAT***a** */MATalpha Spr28::HygMX/Spr28::HygMX his3::GFP-Npl3::HIS3/his3::GFP-Npl3::HIS3 HTB1-mCherry-HISMX6/HTB1-mCherry-HISMX6*
UB23530	*MAT***a** */MATalpha Cda2-mCherry-HISMX6/Cda2-mCherry-HISMX6 Htb1-EGFP-KanMX/Htb1-EGFP-KanMX*
UB23532	*MAT***a** */MATalpha Gas2-mCherry-HISMX6/Gas2-mCherry-HISMX6 Htb1-EGFP-KanMX/Htb1-EGFP-KanMX*
UB23658	*MAT***a** */MATalpha Nup60::HygMX/Nup60::HygMX his3::GFP-Npl3::HIS3/his3::GFP-Npl3::HIS3 Htb1-mCherry-HISMX6/Htb1-mCherry-HISMX6*
UB23866	*MAT***a** */MATalpha Spr3::HygMX/Spr3::HygMX Spr28::HygMX/Spr28::HygMX his3::GFP-Npl3::HIS3/his3::GFP-Npl3::HIS3 HTB1-mCherry-HISMX6/HTB1-mCherry-HISMX6*

UB24011	*MAT***a** */MATalpha yeGFP-Nup42 (unmarked)/yeGFP-Nup42 (unmarked) HTB1-mCherry-HISMX6/HTB1-mCherry-HISMX6*
UB24018	*MAT***a** */MATalpha Sps1::KanMX/Sps1::KanMX Nup2-GFP-KanMX/Nup2-GFP-KanMX Pom34-mCherry-HISMX/Pom34-mCherry-HISMX*
UB24020	*MAT***a** */MATalpha Smk1::HygB/Smk1::HygB Nup2-GFP-KanMX/Nup2-GFP-KanMX Pom34-mCherry-HISMX/Pom34-mCherry-HISMX*
UB24022	*MAT***a** */MATalpha ime2-as1/ime2-as1 Nup2-GFP-KanMX/Nup2-GFP-KanMX Pom34-mCherry-HISMX/Pom34-mCherry-HISMX*
UB24130	*MAT***a** */MATalpha cdc15-as1:URA3/cdc15-as1:URA3 Nup2-GFP-KanMX/Nup2-GFP-KanMX Pom34-mCherry-HISMX/Pom34-mCherry-HISMX*
UB24364	*MAT***a** */MATalpha Gas4-mCherry-HISMX6/Gas4-mCherry-HISMX6 Htb1-EGFP-KanMX/Htb1-EGFP-KanMX*
UB24483	*MAT***a** */MATalpha Don1-mCherry-HisMX/Don1-mCherry-HisMX Htb1-EGFP-KanMX/Htb1-EGFP-KanMX*
UB24613	*MAT***a** */MATalpha Seh1-GFP-KanMX/Seh1-GFP-KanMX HTB1-mCherry-HISMX6/HTB1-mCherry-HISMX6*
UB25072	*MAT***a** */MATalpha Nup60::HygMX/Nup60::HygMX Htb1-EGFP-KanMX/+ Leu2::2xmCherry-SV40NLS::LEU2/Leu2::2xmCherry-SV40NLS::LEU2*
UB25445	*MAT***a** */MATalpha Gip1::NatMX/Gip1::NatMX Nup2-GFP-KanMX/Nup2-GFP-KanMX Pom34-mCherry-HISMX/Pom34-mCherry-HISMX*
UB25650	*MAT***a** */MATalpha ama1::KanMX6/ama1::KanMX6 Htb1-EGFP-KanMX/Htb1-EGFP-KanMX Leu2::2xmCherry-SV40NLS::LEU2/Leu2::2xmCherry-SV40NLS::LEU2*
UB25672	*MAT***a** */MATalpha Hos3::HygMX/Hos3::HygMX Nup170-GFP::KanMX/Nup170-GFP::KanMX HTB1-mCherry-HISMX6/ HTB1-mCherry-HISMX6*
UB25674	*MAT***a** */MATalpha Hos3-GFP-KanMX/Hos3-GFP-KanMX HTB1-mCherry-HISMX6/HTB1-mCherry-HISMX6*
UB25676	*MAT***a** */MATalpha Nur1::HygMX/Nur1::HygMX Nup170-GFP::KanMX/Nup170-GFP::KanMX HTB1-mCherry-HISMX6/ HTB1-mCherry-HISMX6*
UB25678	*MAT***a** */MATalpha Nur1-GFP-KanMX/Nur1-GFP-KanMX HTB1-mCherry-HISMX6/HTB1-mCherry-HISMX6*
UB25727	*MAT***a** */MATalpha Nup1-delta2-32-GFP-KanMX/Nup1-delta2-32-GFP-KanMX HTB1-mCherry-HISMX6/HTB1-mCherry-HISMX6*
UB25731	*MAT***a** */MATalpha Nup60-delta2-47-GFP-KanMX/Nup60-delta2-47-GFP-KanMX HTB1-mCherry-HISMX6/HTB1-mCherry-HISMX6*

UB25843	*MAT***a** */MATalpha Fpr1::HygMX/Fpr1::HygMX FKBP12-Nup60 (unmarked)/FKBP12-Nup60 (unmarked) Seh1-FRB-KanMX/Seh1-FRB-KanMX Nup2-GFP-KanMX/Nup2-GFP-KanMX Pom34-mCherry-HISMX/Pom34-mCherry-HISMX*
UB25974	*MAT***a** */MATalpha leu2::pATG8-Q2-GFP::LEU2/leu2::pATG8-Q2-GFP::LEU2 HTB1-mCherry-HISMX6/HTB1-mCherry-HISMX6*
UB25976	*MAT***a** */MATalpha trp1::pATG8-C1a+C1b-GFP::TRP1/trp1::pATG8-C1a+C1b-GFP::TRP1 HTB1-mCherry-HISMX6/HTB1-mCherry-HISMX6*
UB25978	*MAT***a** */MATalpha trp1::pATG8-2xNLS-C1a+C1b-GFP::TRP1/trp1::pATG8-2xNLS-C1a+C1b-GFP::TRP1 HTB1-mCherry-HISMX6/HTB1-mCherry-HISMX6*
UB26043	*MAT***a** */MATalpha leu2::pATG8-NLS-Q2-GFP::LEU2/leu2::pATG8-NLS-Q2-GFP::LEU2 HTB1-mCherry-HISMX6/HTB1-mCherry-HISMX6*
UB26049	*MAT***a** */MATalpha HIS3::pTDH3-Cre-EBD78-His3/+ pUB1898 (pFA6a-224xtetO-HygMX-loxP-CEN13-Ura3-loxP-ARSH4) leu2::pURA3-TetR-GFP::LEU2/leu2::pURA3-TetR-GFP::LEU2 HTB1-mCherry-HISMX6/HTB1-mCherry-HISMX6*
UB26051	*MAT***a** */MATalpha HIS3::pTDH3-Cre-EBD78-His3/+ leu2::pURA3-TetR-GFP::LEU2/leu2::pURA3-TetR-GFP::LEU2 HTB1-mCherry-HISMX6/HTB1-mCherry-HISMX6*
UB26053	*MAT***a** */MATalpha pUB1898 (pFA6a-224xtetO-HygMX-loxP-CEN13-Ura3-loxP-ARSH4) leu2::pURA3-TetR-GFP::LEU2/leu2::pURA3-TetR-GFP::LEU2 HTB1-mCherry-HISMX6/HTB1-mCherry-HISMX6*
UB26148	*MAT***a** */MATalpha Sps1::KanMX/Sps1::KanMX his3::GFP-Npl3::HIS3/his3::GFP-Npl3::HIS3 HTB1-mCherry-HISMX6/HTB1-mCherry-HISMX6*
UB26150	*MAT***a** */MATalpha Sps1::KanMX/Sps1::KanMX Htb1-EGFP-KanMX/Htb1-EGFP-KanMX Leu2::2xmCherry-SV40NLS::LEU2/Leu2::2xmCherry-SV40NLS::LEU2*
UB26152	*MAT***a** */MATalpha spo21::HygB/spo21::HygB ama1::KanMX6/ama1::KanMX6 his3::GFP-Npl3::HIS3/his3::GFP-Npl3::HIS3 HTB1-mCherry-HISMX6/HTB1-mCherry-HISMX6*
UB26154	*MAT***a** */MATalpha spo21::HygB/spo21::HygB Gip1::NatMX/ Gip1::NatMX his3::GFP-Npl3::HIS3/his3::GFP-Npl3::HIS3 HTB1-mCherry-HISMX6/HTB1-mCherry-HISMX6*
UB26156	*MAT***a** */MATalpha spo21::HygB/spo21::HygB Gip1::NatMX/ Gip1::NatMX Htb1-EGFP-KanMX/Htb1-EGFP-KanMX Leu2::2xmCherry-SV40NLS::LEU2/ Leu2::2xmCherry-SV40NLS::LEU2*
UB26364	*MAT***a** */MATalpha ama1::KanMX6/ama1::KanMX6 Sps1::KanMX/Sps1::KanMX his3::GFP-Npl3::HIS3/his3::GFP-*

	Npl3::HIS3 HTB1-mCherry-HISMX6/HTB1-mCherry-HISMX6
UB26283	*MAT***a** */MATalpha ama1::KanMX6/ama1::KanMX6 Sps1::KanMX/ Sps1::KanMX Htb1-EGFP-KanMX/Htb1-EGFP-KanMX Leu2::2xmCherry-SV40NLS::LEU2/Leu2::2xmCherry-SV40NLS::LEU2*
UB26767	*MAT***a** */MATalpha GAL-NDT80::TRP1/GAL-NDT80::TRP1 ura3::pGPD1-GAL4(848).ER::URA3/ura3::pGPD1-GAL4(848).ER::URA3 ime2-as1/ime2-as1 his3::GFP-Npl3::HIS3/ his3::GFP-Npl3::HIS3 HTB1-mCherry-HISMX6/HTB1-mCherry-HISMX6*
UB26769	*MAT***a** */MATalpha GAL-NDT80::TRP1/GAL-NDT80::TRP1 ura3::pGPD1-GAL4(848).ER::URA3/ura3::pGPD1-GAL4(848).ER::URA3 ime2-as1/ime2-as1 Htb1-EGFP-KanMX/Htb1-EGFP-KanMX Leu2::2xmCherry-SV40NLS::LEU2/ Leu2::2xmCherry-SV40NLS::LEU2*
UB26799	*MAT***a** */MATalpha Gip1-GFP-KanMX/Gip1-GFP-KanMX HTB1-mCherry-HISMX6/HTB1-mCherry-HISMX6*
UB27143	*MAT***a** */MATalpha Fpr1::HygMX/Fpr1::HygMX FKBP12-Nup60 (unmarked)/FKBP12-Nup60 (unmarked) Seh1-FRB-KanMX/Seh1-FRB-KanMX Nup1-GFP-KanMX/Nup1-GFP-KanMX Pom34-mCherry-HISMX/Pom34-mCherry-HISMX*
UB27189	*MAT***a** */MATalpha Nup60-I36R-GFP-KanMX/Nup60-I36R-GFP-KanMX HTB1-mCherry-HISMX6/HTB1-mCherry-HISMX6*
UB27197	*MAT***a** */MATalpha ndt80::LEU2/ndt80::LEU2 ura3::pGPD1-GAL4(848).ER::URA3/ ura3::pGPD1-GAL4(848).ER::URA3 KanMX-pGAL-IME2st/+ his3::GFP-Npl3::HIS3/his3::GFP-Npl3::HIS3 HTB1-mCherry-HISMX6/HTB1-mCherry-HISMX6*
UB27298	*MAT***a** */MATalpha FKBP12-Nup60-GFP-KanMX/FKBP12-Nup60-GFP-KanMX Pom34-mCherry-HISMX/Pom34-mCherry-HISMX Fpr1::HygMX/Fpr1::HygMX Seh1-FRB-KanMX/Seh1-FRB-KanMX*
UB27323	*MAT***a** */MATalpha GFP-Glc7 (unmarked)/GFP-Glc7 (unmarked) HTB1-mCherry-HISMX6/HTB1-mCherry-HISMX6*
UB27725	*MAT***a** */MATalpha Fpr1::HygMX/Fpr1::HygMX FKBP12-Nup60 (unmarked)/FKBP12-Nup60 (unmarked) Seh1-FRB-KanMX/Seh1-FRB-KanMX Mlp1-GFP-KanMX/Mlp1-GFP-KanMX Pom34-mCherry-HISMX/Pom34-mCherry-HISMX*
UB28059	*HIS3::pTDH3-Cre-EBD78-His3/+ pUB1898 (pFA6a-224xtetO-HygMX-loxP-CEN13-Ura3-loxP-ARSH4) Fpr1::KanMX/ Fpr1::KanMX Seh1-FRB-KanMX/Seh1-FRB-KanMX leu2::pURA3-NLS-FKBP12-TetR-GFP::LEU2/leu2::pURA3-NLS-FKBP12-TetR-GFP::LEU2 HTB1-mCherry-HISMX6/HTB1-mCherry-HISMX6*

UB28201	*MAT***a** */MATalpha SPC42-mCherry::NAT/SPC42-mCherry::NAT Nup60-GFP-KanMX/Nup60-GFP-KanMX*
UB28211	*MAT***a** */MATalpha cdc20::pCLB2-CDC20::TRP1/cdc20::pCLB2-CDC20::TRP1 Nup60-GFP-KanMX/Nup60-GFP-KanMX HTB1-mCherry-HISMX6/HTB1-mCherry-HISMX6*
UB28213	*MAT***a** */MATalpha cdc20::pCLB2-CDC20::TRP1/cdc20::pCLB2-CDC20::TRP1 Nup60-delta2-47-GFP-KanMX/Nup60-delta2-47-GFP-KanMX HTB1-mCherry-HISMX6/HTB1-mCherry-HISMX6*
UB28492	*MAT***a** */MATalpha cdc5::pCLB2-CDC5::KanMX6/cdc5::pCLB2-CDC5::KanMX6 Nup60-GFP-KanMX/Nup60-GFP-KanMX HTB1-mCherry-HISMX6/HTB1-mCherry-HISMX6*
UB28494	*MAT***a** */MATalpha cdc5::pCLB2-CDC5::KanMX6/cdc5::pCLB2-CDC5::KanMX6 Nup60-delta2-47-GFP-KanMX/Nup60-delta2-47-GFP-KanMX HTB1-mCherry-HISMX6/HTB1-mCherry-HISMX6*
UB28614	*MAT***a** */MATalpha cdc20::pCLB2-CDC20::TRP1/cdc20::pCLB2-CDC20::TRP1 cdc5::pCLB2-CDC5::KanMX6/cdc5::pCLB2-CDC5::KanMX6 Nup60-GFP-KanMX/Nup60-GFP-KanMX HTB1-mCherry-HISMX6/HTB1-mCherry-HISMX6*
UB28616	*MAT***a** */MATalpha cdc20::pCLB2-CDC20::TRP1/cdc20::pCLB2-CDC20::TRP1 cdc5::pCLB2-CDC5::KanMX6/cdc5::pCLB2-CDC5::KanMX6 Nup60-delta2-47-GFP-KanMX/Nup60-delta2-47-GFP-KanMX HTB1-mCherry-HISMX6/HTB1-mCherry-HISMX6*
UB29048	*MAT***a** */MATalpha Ulp1-GFP-KanMX/Ulp1-GFP-KanMX HTB1-mCherry-HISMX6/HTB1-mCherry-HISMX6*
UB29069	*MAT***a** */MATalpha ndt80::LEU2/ndt80::LEU2 trp1::pCUP1-Cdc5[KD]-3xFLAG-10xHIS::TRP1/trp1::pCUP1-Cdc5[KD]-3xFLAG-10xHIS::TRP1 Nup60-GFP-KanMX/Nup60-GFP-KanMX HTB1-mCherry-HISMX6/HTB1-mCherry-HISMX6*
UB29071	*MAT***a** */MATalpha ndt80::LEU2/ndt80::LEU2 trp1::pCUP1-Cdc5-3xFLAG-10xHIS::TRP1/trp1::pCUP1-Cdc5-3xFLAG-10xHIS::TRP1 Nup60-delta2-47-GFP-KanMX/Nup60-delta2-47-GFP-KanMX HTB1-mCherry-HISMX6/HTB1-mCherry-HISMX6*
UB29073	*MAT***a** */MATalpha ndt80::LEU2/ndt80::LEU2 trp1::pCUP1-Cdc5[KD]-3xFLAG-10xHIS::TRP1/trp1::pCUP1-Cdc5[KD]-3xFLAG-10xHIS::TRP1 Nup60-delta2-47-GFP-KanMX/Nup60-delta2-47-GFP-KanMX HTB1-mCherry-HISMX6/HTB1-mCherry-HISMX6*
UB29129	*MAT***a** */MATalpha ndt80::LEU2/ndt80::LEU2 trp1::pCUP1-Cdc5-3xFLAG-10xHIS::TRP1/trp1::pCUP1-Cdc5-3xFLAG-10xHIS::TRP1 Nup60-GFP-KanMX/Nup60-GFP-KanMX HTB1-mCherry-HISMX6/HTB1-mCherry-HISMX6*
UB29249	*MAT***a** */MATalpha cdc20::pCLB2-CDC20::TRP1/cdc20::pCLB2-CDC20::TRP1 cdc5::pCLB2-CDC5::KanMX6/cdc5::pCLB2-CDC5::KanMX6 SPC42-mCherry::NAT/SPC42-mCherry::NAT Nup60-GFP-KanMX/Nup60-GFP-KanMX*

UB29251	*MAT***a** */MATalpha cdc5::pCLB2-CDC5::KanMX6/cdc5::pCLB2-CDC5::KanMX6 SPC42-mCherry::NAT/SPC42-mCherry::NAT Nup60-GFP-KanMX/Nup60-GFP-KanMX*
UB29255	*MAT***a** */MATalpha cdc20::pCLB2-CDC20::TRP1/cdc20::pCLB2-CDC20::TRP1 cdc5::pCLB2-CDC5::KanMX6/cdc5::pCLB2-CDC5::KanMX6 SPC42-mCherry::NAT/SPC42-mCherry::NAT Nup60-delta2-47-GFP-KanMX/Nup60-delta2-47-GFP-KanMX*
UB29257	*MAT***a** */MATalpha cdc5::pCLB2-CDC5::KanMX6/cdc5::pCLB2-CDC5::KanMX6 SPC42-mCherry::NAT/SPC42-mCherry::NAT Nup60-delta2-47-GFP-KanMX/Nup60-delta2-47-GFP-KanMX*
UB29259	*MAT***a** */MATalpha cdc20::pCLB2-CDC20::TRP1/cdc20::pCLB2-CDC20::TRP1 SPC42-mCherry::NAT/SPC42-mCherry::NAT Nup60-delta2-47-GFP-KanMX/Nup60-delta2-47-GFP-KanMX*
UB29253	*MAT***a** */MATalpha cdc20::pCLB2-CDC20::TRP1/cdc20::pCLB2-CDC20::TRP1 SPC42-mCherry::NAT/SPC42-mCherry::NAT Nup60-GFP-KanMX/Nup60-GFP-KanMX*
UB29265	*MAT***a** */MATalpha Nup60-S89A-GFP-KanMX/Nup60-S89A-GFP-KanMX HTB1-mCherry-HISMX6/HTB1-mCherry-HISMX6*
UB29267	*MAT***a** */MATalpha Nup60-Cterm4A-GFP-KanMX/Nup60-Cterm4A-GFP-KanMX HTB1-mCherry-HISMX6/HTB1-mCherry-HISMX6*
UB29337	*MAT***a** */MATalpha Fpr1::HygMX/Fpr1::HygMX Seh1-FRB-KanMX/Seh1-FRB-KanMX FKBP12-Mlp1-GFP-KanMX/FKBP12-Mlp1-GFP-KanMX Pom34-mCherry-HISMX/Pom34-mCherry-HISMX*
UB29358	*MAT***a** */MATalpha Nup60-9A-GFP-KanMX/Nup60-9A-GFP-KanMX HTB1-mCherry-HISMX6/HTB1-mCherry-HISMX6*
UB29441	*MAT***a** */MATalpha Nup60-Nterm3A-GFP-KanMX/Nup60-Nterm3A-GFP-KanMX HTB1-mCherry-HISMX6/HTB1-mCherry-HISMX6*
UB29443	*MAT***a** */MATalpha Nup60-Nterm5A-GFP-KanMX/Nup60-Nterm5A-GFP-KanMX HTB1-mCherry-HISMX6/HTB1-mCherry-HISMX6*
UB29560	*MAT***a** */MATalpha ndt80::LEU2/ndt80::LEU2 trp1::pCUP1-Cdc5-3xFLAG-10xHIS::TRP1/trp1::pCUP1-Cdc5-3xFLAG-10xHIS::TRP1 Nup60-S89A-GFP-KanMX/Nup60-S89A-GFP-KanMX HTB1-mCherry-HISMX6/HTB1-mCherry-HISMX6*
UB29562	*MAT***a** */MATalpha ndt80::LEU2/ndt80::LEU2 trp1::pCUP1-Cdc5-3xFLAG-10xHIS::TRP1/trp1::pCUP1-Cdc5-3xFLAG-10xHIS::TRP1 Nup60-Cterm4A-GFP-KanMX/Nup60-Cterm4A-GFP-KanMX HTB1-mCherry-HISMX6/HTB1-mCherry-HISMX6*
UB29564	*MAT***a** */MATalpha ndt80::LEU2/ndt80::LEU2 trp1::pCUP1-Cdc5-3xFLAG-10xHIS::TRP1/trp1::pCUP1-Cdc5-3xFLAG-10xHIS::TRP1 Nup60-9A-GFP-KanMX/Nup60-9A-GFP-KanMX HTB1-mCherry-HISMX6/HTB1-mCherry-HISMX6*

UB29636	*MAT***a** */MATalpha ndt80::LEU2/ndt80::LEU2 trp1::pCUP1-Cdc5-3xFLAG-10xHIS::TRP1/trp1::pCUP1-Cdc5-3xFLAG-10xHIS::TRP1 Nup60-Nterm3A-GFP-KanMX/Nup60-Nterm3A-GFP-KanMX HTB1-mCherry-HISMX6/HTB1-mCherry-HISMX6*
UB29638	*MAT***a** */MATalpha ndt80::LEU2/ndt80::LEU2 trp1::pCUP1-Cdc5-3xFLAG-10xHIS::TRP1/trp1::pCUP1-Cdc5-3xFLAG-10xHIS::TRP1 Nup60-Nterm5A-GFP-KanMX/Nup60-Nterm5A-GFP-KanMX HTB1-mCherry-HISMX6/HTB1-mCherry-HISMX6*
UB30166	*MAT***a** */MATalpha Fpr1::HygMX/Fpr1::HygMX Seh1-FRB-KanMX/Seh1-FRB-KanMX FKBP12-Mlp1 (unmarked)/FKBP12-Mlp 1(unmarked) Nup1-GFP-KanMX/Nup1-GFP-KanMX Pom34-mCherry-HISMX/Pom34-mCherry-HISMX*
UB30168	*MAT***a** */MATalpha Fpr1::HygMX/Fpr1::HygMX Seh1-FRB-KanMX/Seh1-FRB-KanMX FKBP12-Mlp1 (unmarked)/FKBP12-Mlp1 (unmarked) Nup2-GFP-KanMX/Nup2-GFP-KanMX Pom34-mCherry-HISMX/Pom34-mCherry-HISMX*
UB30174	*MAT***a** */MATalpha Fpr1::HygMX/Fpr1::HygMX Seh1-FRB-KanMX/Seh1-FRB-KanMX FKBP12-Mlp1 (unmarked)/FKBP12-Mlp1 (unmarked) Nup60-GFP-KanMX/Nup60-GFP-KanMX Pom34-mCherry-HISMX/Pom34-mCherry-HISMX*
UB30327	*MAT***a** */MATalpha cdc20::pCLB2-CDC20::TRP1/cdc20::pCLB2-CDC20::TRP1 Nup60-S89A-GFP-KanMX/Nup60-S89A-GFP-KanMX SPC42-mCherry::NAT/SPC42-mCherry::NAT*
UB30329	*MAT***a** */MATalpha cdc20::pCLB2-CDC20::TRP1/cdc20::pCLB2-CDC20::TRP1 Nup60-Nterm3A-GFP-KanMX/Nup60-Nterm3A-GFP-KanMX SPC42-mCherry::NAT/SPC42-mCherry::NAT*
UB30331	*MAT***a** */MATalpha cdc20::pCLB2-CDC20::TRP1/cdc20::pCLB2-CDC20::TRP1 Nup60-Nterm5A-GFP-KanMX/Nup60-Nterm5A-GFP-KanMX SPC42-mCherry::NAT/SPC42-mCherry::NAT*
UB30333	*MAT***a** */MATalpha cdc20::pCLB2-CDC20::TRP1/cdc20::pCLB2-CDC20::TRP1 Nup60-Cterm4A-GFP-KanMX/Nup60-Cterm4A-GFP-KanMX SPC42-mCherry::NAT/SPC42-mCherry::NAT*
UB30438	*MAT***a** */MATalpha cdc20::pCLB2-CDC20::TRP1/cdc20::pCLB2-CDC20::TRP1 Nup60-9A-GFP-KanMX/Nup60-9A-GFP-KanMX Spc42-mCherry/Spc42-mCherry*
UB30577	*MAT***a** */MATalpha HIS3::pTDH3-Cre-EBD78-His3/+ pUB1898 (pFA6a-224xtetO-HygMX-loxP-CEN13-Ura3-loxP-ARSH4) Hsp104-TetR-NatMX/ Hsp104-TetR-NatMX leu2::pURA3-TetR-GFP::LEU2/leu2::pURA3-TetR-GFP::LEU2 HTB1-mCherry-HISMX6/HTB1-mCherry-HISMX6*
UB30583	*MAT***a** */MATalpha HIS3::pTDH3-Cre-EBD78-His3/+ pUB1898 (pFA6a-224xtetO-HygMX-loxP-CEN13-Ura3-loxP-ARSH4) Nup120-TetR-NatMX/Nup120-TetR-NatMX leu2::pURA3-TetR-GFP::LEU2/ leu2::pURA3-TetR-GFP::LEU2 HTB1-mCherry-HISMX6/HTB1-*

	mCherry-HISMX6
UB30589	*MAT***a** */MATalpha HIS3::pTDH3-Cre-EBD78-His3/+ pUB1898 (pFA6a-224xtetO-HygMX-loxP-CEN13-Ura3-loxP-ARSH4) Seh1-TetR-NatMX/Seh1-TetR-NatMX leu2::pURA3-TetR-GFP::LEU2/ leu2::pURA3-TetR-GFP::LEU2 HTB1-mCherry-HISMX6/HTB1-mCherry-HISMX6*
UB30626	*MAT***a** */MATalpha Ulp1-3xeGFP-KanMX/Ulp1-3xeGFP-KanMX HTB1-mCherry-HISMX6/HTB1-mCherry-HISMX6*
UB30628	*MAT***a** */MATalpha Nup60-delta2-47 (unmarked)/Nup60-delta2-47 (unmarked) Nup1-GFP-KanMX/Nup1-GFP-KanMX HTB1-mCherry-HISMX6/HTB1-mCherry-HISMX6*
UB30630	*MAT***a** */MATalpha Nup60-delta2-47 (unmarked)/Nup60-delta2-47 (unmarked) Nup2-GFP-KanMX/Nup2-GFP-KanMX HTB1-mCherry-HISMX6/HTB1-mCherry-HISMX6*
UB30632	*MAT***a** */MATalpha Nup60-delta2-47 (unmarked)/Nup60-delta2-47 (unmarked) Mlp1-GFP-KanMX/Mlp1-GFP-KanMX HTB1-mCherry-HISMX6/HTB1-mCherry-HISMX6*
UB30640	*MAT***a** */MATalpha Nup60-I36R (unmarked)/Nup60-I36R (unmarked) Mlp1-GFP-KanMX/Mlp1-GFP-KanMX HTB1-mCherry-HISMX6/HTB1-mCherry-HISMX6*
UB31262	*MAT***a** */MATalpha Nup60::HygMX/Nup60::HygMX Mlp1-GFP-KanMX/Mlp1-GFP-KanMX HTB1-mCherry-HISMX6/HTB1-mCherry-HISMX6*
UB31600	*MAT***a** */MATalpha Nup60::HygMX/Nup60::HygMX Nup2-GFP-KanMX/Nup2-GFP-KanMX HTB1-mCherry-HISMX6/HTB1-mCherry-HISMX6*
UB32238	*MAT***a** */MATalpha his3::pCup1-OsTIR1-F74G (codon optimized)::HIS3/his3::pCup1-OsTIR1-F74G (codon optimized)::HIS3 Nup60-3V5-IAA17-KanMX (Vinny linker)/Nup60-3V5-IAA17-KanMX (Vinny linker) ndt80::LEU2/ndt80::LEU2 Nup2-GFP-KanMX/Nup2-GFP-KanMX HTB1-mCherry-HISMX6/HTB1-mCherry-HISMX6*
UB32240	*MAT***a** */MATalpha Nup60-3V5-IAA17-KanMX (Vinny linker)/Nup60-3V5-IAA17-KanMX (Vinny linker) ndt80::LEU2/ndt80::LEU2 Nup2-GFP-KanMX/Nup2-GFP-KanMX HTB1-mCherry-HISMX6/HTB1-mCherry-HISMX6*
UB32246	*MAT***a** */MATalpha his3::pCup1-OsTIR1-F74G (codon optimized)::HIS3 his3::pCup1-OsTIR1-F74G (codon optimized)::HIS3 Nup60-3V5-IAA17-KanMX (Vinny linker)/Nup60-3V5-IAA17-KanMX (Vinny linker) ndt80::LEU2/ndt80::LEU2 Mlp1-GFP-KanMX/Mlp1-GFP-KanMX HTB1-mCherry-HISMX6/HTB1-mCherry-HISMX6*

UB32248	*MAT***a** */MATalpha Nup60-3V5-IAA17-KanMX (Vinny linker)/Nup60-3V5-IAA17-KanMX (Vinny linker) ndt80::LEU2/ndt80::LEU2 Mlp1-GFP-KanMX/Mlp1-GFP-KanMX HTB1-mCherry-HISMX6/HTB1-mCherry-HISMX6*
UB33284	*MAT***a** */MATalpha trp1::pATG8-Nop15-GFP::TRP1/trp1::pATG8-Nop15-GFP::TRP1 HTB1-mCherry-HISMX6/HTB1-mCherry-HISMX6*
UB33286	*MAT***a** */MATalpha trp1::pATG8-Sof1-GFP::TRP1/trp1::pATG8-Sof1-GFP::TRP1 HTB1-mCherry-HISMX6/HTB1-mCherry-HISMX6*
UB33296	*MAT***a** */MATalpha HIS3::pTDH3-Cre-EBD78-His3/+ pUB1898 (pFA6a-224xtetO-HygMX-loxP-CEN13-Ura3-loxP-ARSH4) trp1::pATG8-Nop15-TetR::TRP1/trp1::pATG8-Nop15-TetR::TRP1 leu2::pURA3-TetR-GFP::LEU2/leu2::pURA3-TetR-GFP::LEU2 HTB1-mCherry-HISMX6/HTB1-mCherry-HISMX6*
UB33303	*MAT***a** */MATalpha HIS3::pTDH3-Cre-EBD78-His3/+ pUB1898 (pFA6a-224xtetO-HygMX-loxP-CEN13-Ura3-loxP-ARSH4) trp1::pATG8-Sof1-TetR::TRP1/trp1::pATG8-Sof1-TetR::TRP1 leu2::pURA3-TetR-GFP::LEU2/leu2::pURA3-TetR-GFP::LEU2 HTB1-mCherry-HISMX6/HTB1-mCherry-HISMX6*
UB33308	*MAT***a** */MATalpha HIS3::pTDH3-Cre-EBD78-His3/+ pUB1898 (pFA6a-224xtetO-HygMX-loxP-CEN13-Ura3-loxP-ARSH4) trp1::pATG8-Nop13-TetR::TRP1/trp1::pATG8-Nop13-TetR::TRP1 leu2::pURA3-TetR-GFP::LEU2/leu2::pURA3-TetR-GFP::LEU2 HTB1-mCherry-HISMX6/HTB1-mCherry-HISMX6*
UB33314	*MAT***a** */MATalpha HIS3::pTDH3-Cre-EBD78-His3/+ pUB1898 (pFA6a-224xtetO-HygMX-loxP-CEN13-Ura3-loxP-ARSH4) trp1::pATG8-Rlp7-TetR::TRP1/trp1::pATG8-Rlp7-TetR::TRP1 Leu2::pURA3-TetR-GFP::LEU2/Leu2::pURA3-TetR-GFP::LEU2 HTB1-mCherry-HISMX6/HTB1-mCherry-HISMX6*
YML 1110	*MAT***a** *ndt80Δ::NatMX4 ura3::pGPD-GAL4-ER-URA3*
YML 3993	*MAT***a** */MATalpha ndt80Δ::NatMX4/ndt80Δ::NatMX4 ura3::pGPD-GAL4-ER-URA3/ura3::pGPD-GAL4-ER-URA3 trp1::pGAL1-CDC5-WT-eGFP-TRP1/trp1::pGAL1-CDC5-WT-eGFP-TRP1*
YML 3994	*MAT***a** */MATalpha ndt80Δ::NatMX4/ndt80Δ::NatMX4 ura3::pGPD-GAL4-ER-URA3/ura3::pGPD-GAL4-ER-URA3 trp1::pGAL1-CDC5-KD-eGFP-TRP1/trp1::pGAL1-CDC5-KD-eGFP-TRP1*
YML 6662	*MAT***a** */MATalpha NUP60-myc9::KITRP1/NUP60-myc9::KITRP1*
YML 6665	*MAT***a** */MATalpha NUP60-myc9::KITRP1/NUP60-myc9::KITRP1 cdc20::P_{CLB2}-CDC20::KanMX6/cdc20::P_{CLB2}-CDC20::KanMX6*
YML 6664	*MAT***a** */MATalpha NUP60-myc9::KITRP1/NUP60-myc9::KITRP1 cdc20::P_{CLB2}-CDC20::KanMX6/cdc20::P_{CLB2}-CDC20::KanMX6*

	cdc5::P_{CLB2}-CDC5::HphMX4/cdc5::P_{CLB2}-CDC5::HphMX4
YML 7956	*MAT**a** /MATalpha NUP60^{S89A}-myc9::KITRP1/NUP60^{S89A}-myc9::KITRP1 cdc20::P_{CLB2}-CDC20::KanMX6/cdc20::P_{CLB2}-CDC20::KanMX6*
YML 7800	*MAT**a** /MATalpha SLK19-myc9::KITRP1/SLK19-myc9::KITRP1 cdc20::P_{CLB2}-CDC20::KanMX6/cdc20::P_{CLB2}-CDC20::KanMX6*
YML 7801	*MAT**a** /MATalpha SLK19-myc9::KITRP1/SLK19-myc9::KITRP1 cdc20::P_{CLB2}-CDC20::KanMX6/cdc20::P_{CLB2}-CDC20::KanMX6 cdc5::P_{CLB2}-CDC5::HphMX4/cdc5::P_{CLB2}-CDC5::HphMX4*
YML 8836	*MAT**a** /MATalpha SWI6-myc9::KITRP1/SWI6-myc9::KITRP1 cdc20::P_{CLB2}-CDC20::KanMX6/cdc20::P_{CLB2}-CDC20::KanMX6*
YML 8837	*MAT**a** /MATalpha SWI6-myc9::KITRP1/SWI6-myc9::KITRP1 cdc20::P_{CLB2}-CDC20::KanMX6/cdc20::P_{CLB2}-CDC20::KanMX6 cdc5::P_{CLB2}-CDC5::HphMX4/cdc5::P_{CLB2}-CDC5::HphMX4*
YML 12334	*MAT**a**/MATalpha NUP60-myc9::KITRP1/NUP60-myc9::KITRP1 ndt80Δ::HIS3/ndt80Δ::HIS3 natNT2::pCUP1-1-CDC5/natNT2::pCUP1-1-CDC5*
fySLJ456	*h-, Ppc89-mCherry-HygMX6, his3-D1, leu1-32, ura4-D18, ade6-M210*
fySLJ479	*h+, Ppc89-mCherry-HygMX6, his3-D1, leu1-32, ura4-D18, ade6-M210*
fySLJ730	*h-, Nup60-GFP-KanMX, his3-D1, leu1-32, ura4-D18, ade6-M210*
fySLJ840	*h-, Nup61-GFP-KanMX, his3-D1, leu1-32, ura4-D18, ade6-M210*
fySLJ842	*h-, Alm1-GFP-KanMX, his3-D1, leu1-32, ura4-D18, ade6-M210*
fySLJ989	*h+, Nup124-GFP-KanMX, his3-DA, leu1-34, ura4-D18, ade6-M210*
fySLJ990	*h+, Nup211-GFP-KanMX, his3-DA, leu1-34, ura4-D18, ade6-M210*
fySLJ1242	*h-, Pom34-GFP-KanMX, Ppc89-mCherry-HygMX6, his3-DA, leu1-34, ura4-D18, ade6-M210*
fySLJ1243	*h+, Pom34-GFP-KanMX, Ppc89-mCherry-HygMX6, his3-DA, leu1-34, ura4-D18, ade6-M210*

Table C.2 Primers used in this study.

Construct name	Forward primer	Reverse primer
HEH1-3xeGFP	GGAACTCAATGAACCTAA GGATTCCGCTGAAAACAA AATA**cggatccccgggttaattaa**	TTTGAGAAGAGAAAACTAC GTTTGAGTTTCATTTTGTG GG**GAATTCGAGCTCGTTTA AAC**
NUP53-eGFP	AAATAGATTGAATAATTGG TTATTTGGATGGAATGATT TG**ggtgacggtgctggttta**	AATCGCACCAAAGCACTAC ATTTGGGGGTAAGGTTTTT CA**tcgatgaattcgagc**
NUP84-GFP	GTATCTGGATCTCGTTGCT CGCACAGCAACCCTTTCGA AT**CGGATCCCCGGGTTAAT TAA**	TTACTTAAAATATAAACTT ATTCTGCAATACATTAATT GA**GAATTCGAGCTCGTTTA AAC**
NUP120-GFP *NUP120-TetR*	GGTTACTTTAACTGATTTA AGAGATGAGTTACGAGGT CTA**CGGATCCCCGGGTTA ATTAA**	ATTTTTTAAATGAAGTATT AATTTACAGTTTATATATT CA**GAATTCGAGCTCGTTTA AAC**
NUP170-GFP *Nup170-3xDendra2*	GAACAGCGGCAATAATTT GGGGATTTGTTTCTACAAA GAA**CGGATCCCCGGGTTA ATTAA**	ACGTACATTACCCTGCTAT CTATATGTCGAACATGAAT TT**GAATTCGAGCTCGTTTA AAC**
POM34-GFP *POM34-mCherry*	TGCATATATGATGAACTCA CAGTCCCCAAGGGGTAAA ATA**CGGATCCCCGGGTTA ATTAA**	TATATAGCTATGGAAAGTA TTAAATGTTTTTTTGCTGT TT**GAATTCGAGCTCGTTTA AAC**
NUP188-GFP	AGACATTAAAGCATTACAA GATTCACTATTCAAGGACG TT**CGGATCCCCGGGTTAAT TAA**	ATTATTATATTATGTAGCT TTACATAACTTACAAAATA AG**GAATTCGAGCTCGTTTA AAC**
NDC1-GFP	GTTTCTAGAAGTGTACGCC TCAGGCAACCCTAATGCTA CG**CGGATCCCCGGGTTAA TTAA**	ACATGAAATGGGAGGAGG GGTGCTCCTCGGTTGAATT GTA**GAATTCGAGCTCGTTT AAAC**
HSP104-mCherry *HSP104-TetR*	CGATAATGAGGACAGTAT GGAAATTGATGATGACCTA GAT**CGGATCCCCGGGTTA ATTAA**	ATTCTTGTTCGAAAGTTTT TAAAAATCACACTATATTA AA**GAATTCGAGCTCGTTTA AAC**
ssp1Δ	GGCGACACAAAATCATGA AG	TGATGTTTATGTATAGATC TCTCGA

NSR1-GFP	AAATACCGCTTCTTTCGCT GGTTCAAAGAAAACATTTG AT**CGGATCCCCGGGTTAAT** **TAA**	AAGAGAAAAAATTGAAATT GAAATTCATTTCATTTTCT CA**GAATTCGAGCTCGTTTA** **AAC**
don1Δ	TTTGGCTGGTATTTAAACA CAAGTAAGAGAAGCATCA AAC**CGGATCCCCGGGTTA** **ATTAA**	GCACTTTGCCGAAAGAGTT AATAAACATTACCGCTATA CA**GAATTCGAGCTCGTTTA** **AAC**
DON1-GFP *DON1-mCherry*	AAAGCAGGTTCATCCATCT AGACAAGAATTAAGTTTTA CG**CGGATCCCCGGGTTAA** **TTAA**	GCACTTTGCCGAAAGAGTT AATAAACATTACCGCTATA CA**GAATTCGAGCTCGTTTA** **AAC**
ady3Δ	TTTTGAATGGGATAGTTGA ATACAACAAACTTCTCCGA AT**CGGATCCCCGGGTTAAT** **TAA**	ACACCATTGAATATATTAG TTCTAAATAAAAAAAAAAA AG**GAATTCGAGCTCGTTTA** **AAC**
irc10Δ	AGTCTGCGGTATAATCACC TGGCCTAGTGCTTTTTCAA TC**CGGATCCCCGGGTTAAT** **TAA**	CTATATGTCAAGGGTGTCC CAAAATAAAAACTAACAGT AC**GAATTCGAGCTCGTTTA** **AAC**
NUP60-GFP *FKBP12-NUP60-GFP* *NUP60$^{\Delta AH}$-GFP* *NUP60^{I36R}-GFP* *NUP60^{S89A}-GFP* *NUP60^{Nterm3A}-GFP* *NUP60^{Nterm5A}-GFP* *NUP60^{Cterm4A}-GFP* *NUP60^{9A}-GFP*	TGAAAATAAAGTTGAGGCT TTCAAGTCCCTATATACCT TT**CGGATCCCCGGGTTAAT** **TAA**	GGGCTATACGGTAATTATG TCACGGCTAAAATTTTCAT TA**GAATTCGAGCTCGTTTA** **AAC**
NUP159-GFP	GCAAATTGGTGATTTCTTC AAAAATTTGAACATGGCAA AA**CGGATCCCCGGGTTAA** **TTAA**	TTATTAACGGCACTAACAA CGTACATATAGCTAAATAT CA**GAATTCGAGCTCGTTTA** **AAC**
NUP82-GFP	ATTGTTACAAGTTTCTCAG GAATTTACTACTAAAACTC AA**CGGATCCCCGGGTTAA** **TTAA**	TAGCGTACATATATGATAG CAGACTATGCAAGTCGCTT AC**GAATTCGAGCTCGTTTA** **AAC**
NUP57-GFP	GAAAGATGCTGCAATTGTA AAAAAATATAAAAATAAAA CG**CGGATCCCCGGGTTAA** **TTAA**	CGATCTTTATACAATTCAG TCATTGATTTAAGTAACCT GA**GAATTCGAGCTCGTTTA** **AAC**
NUP1-GFP *NUP1$^{\Delta AH}$-GFP*	GGCGAACAGAAAGATTGC AAGAATGAGGCACTCTAA	TTCAGAAAAGCAACACAAT ACCTAATTACATAACCGAT

	AAGG**CGGATCCCCGGGTTAATTAA**	AT**GAATTCGAGCTCGTTTAAAC**
NUP2-GFP	ATTTACGAAAGCTATTGAAGATGCTAAAAAAGAAATGAAA**CGGATCCCCGGGTTAATTAA**	AGGGTTCTATTCTATTTAAAATTGTTAACTGTATTTACTC**GAATTCGAGCTCGTTTAAAC**
spr3Δ	TAAAAACCTAAAATTCCTTTTGCGTCATTGAATTTTTATT**CGGATCCCCGGGTTAATTAA**	TTGCGCGAAATTATTGGCTTTTTTTTTTTTTTAATTAATA**GAATTCGAGCTCGTTTAAAC**
spr28Δ	AAAGAGCTACTATACGTACATAAAGTCAGTAAATAATCAA**CGGATCCCCGGGTTAATTAA**	ATTTCATATGTATCTAACGCTAACAAGGCCGTATATTTAT**GAATTCGAGCTCGTTTAAAC**
VPH1-mCherry	GGAAGTCGCTGTTGCTAGTGCAAGCTCTTCCGCTTCAAGC**CGTACGCTGCAGGTCGAC**	AGTACTTAAATGTTTCGCTTTTTTTAAAAGTCCTCAAAAT**ATCGATGAATTCGAGCTCG**
NUP49-GFP *NUP49-mCherry* *NUP49-3xDendra2*	GAATCGCCGTGTTACATCAAAAAACGAAAACACTGGCATCATTGAGCATA**cggatccccgggttaattaa**	AGACATTTGTACTTGTTATACGCACTATATAAACTTTCAGGGCGATTTAC**gaattcgagctcgtttaaac**
NUP100-GFP	AGGCACCTATAGTTACACCATAGATCACCCAGTTTTAACT**CGGATCCCCGGGTTAATTAA**	CTTAGACGATACAAGGATTCTCTACAAAAATTATTCCGGT**GAATTCGAGCTCGTTTAAAC**
GLE1-GFP	GCAAAATAATAATATGGAGTCCTTTCCGGAAATGTCTCCT**CGGATCCCCGGGTTAATTAA**	AGTGTATTAGCATAATGTGCATATATAAGTTCAGAATTTT**GAATTCGAGCTCGTTTAAAC**
sma2Δ	AATATATATATTCTTTCTGTCATAATATAAAAGGGCGAGC**CGGATCCCCGGGTTAATTAA**	ACATATTTACTGTCATTTGAAAAAAAAGTTCTGTGGTGAA**GAATTCGAGCTCGTTTAAAC**
chm7Δ	CACCACCAAAGCCAGCCAAATAGTATCTCACTGTATCTGAC**GGATCCCCGGGTTAATTAA**	TATTTATACATATATATTTATTTATTAGTCACTCAGTTCG**GAATTCGAGCTCGTTTAAAC**
heh1Δ	ACAAACAGTAGAACGGTAGCAGTACTCAGTTAGTGCCGCGC**GGATCCCCGGGTTAATTAA**	TTTGAGAAGAGAAAACTACGTTTGAGTTTCATTTTGTGGG**GAATTCGAGCTCGTTTAAAC**
heh2Δ	AATAGTAGAAAAGGAAGTTTCCTATCTTCACTAATCG	AAGAAAAGTAACAAAAAGTGGTTTGAAGACGGAAAT

	ACAC**GGATCCCCGGGTTA ATTAA**	ACGA**GAATTCGAGCTCGTT TAAAC**
sps1Δ	GAAAGCAAACCAGCATTT GC	GCAGGTAAATAATCAAAAA CACATG
smk1Δ	TCATATCGATAGAAATGTA GACGTGCTCAACGCTCCA AGA**CGGATCCCCGGGTTA ATTAA**	AGAATATAACTTCATGATA TACCTATTTGTGTAGTGGT TA**GAATTCGAGCTCGTTTA AAC**
gip1Δ	CAAATTTTTTGGTGAAGAG CTATTCAATTATTAGCTAA TT**CGGATCCCCGGGTTAAT TAA**	AATTTTACAGAGTATTGGC AGTTAAGTGTTGTTTTTTC GC**GAATTCGAGCTCGTTTA AAC**
nvj1Δ	ATCAAAAAAGCTACAAATA TAATTGTAAAATATAATAA GC**CGGATCCCCGGGTTAA TTAA**	TAAGTGACGATGATAACC GAGATGACGGAAATATAG TACA**GAATTCGAGCTCGTT TAAAC**
nsg1Δ	GCAAGTGAGAAAAAAAAA ATTTAAACAGAGGAGGTTA CTA**CGGATCCCCGGGTTA ATTAA**	ACACATCGATACTAATCAT TGAACGCCCCTATGGGAA CAC**GAATTCGAGCTCGTTT AAAC**
spo19Δ	AAATCATCACTAACAAATA TAAGATCACGCTATACTAT CA**CGGATCCCCGGGTTAA TTAA**	TAGCCAACAATATTTCTTA TTTAAATAAAATAATGATC TA**GAATTCGAGCTCGTTTA AAC**
msc1Δ	AGGAGACAACTACAAAAG AACTGTTAATTAAGAGAAG AAG**CGGATCCCCGGGTTA ATTAA**	AAATTGGGGAGAAAAGTA CATTACGTTGACACCCCAA TCA**GAATTCGAGCTCGTTT AAAC**
hos3Δ	AAGGGCTCTGGAAGTAAA CAGAGAAATTCGACGATAT AAT**cggatccccgggttaattaa**	TCTTTAGTGGGTTCAAGAC AACATTATATATGCATTGG TA**GAATTCGAGCTCGTTTA AAC**
nur1Δ	TTGTGCAGTAGAGAGCTTT ACATTTACCTTCGGCAGTA AA**cggatccccgggttaattaa**	TTTTACGTAACTGTATATA CTTAGACATAATTAAGAAA CG**GAATTCGAGCTCGTTTA AAC**
fpr1Δ	AACTCGAGTATAAGCAAAA AATCAATCAAAACAAGTAA TA**cggatccccgggttaattaa**	TAAAAAGCAGAAAGGCGG CTCAATTGATAGTACTTTG CTT**GAATTCGAGCTCGTTT AAAC**
SEH1-FRB *SEH1-GFP* *SEH1-TetR*	AAATGAATTTAAGTGTATG TCAGTAATTACTGCCCAAC AA**CGGATCCCCGGGTTAA TTAA**	AAGTACCAATATATAATGT TATGTATACATATATTCTT AT**GAATTCGAGCTCGTTTA AAC**

NUP60-3V5-IAA17	TGAAAATAAAGTTGAGGCT TTCAAGTCCCTATATACCT TT**gcggccgctctagaactagtgg**	GGGCTATACGGTAATTATG TCACGGCTAAAATTTTCAT TA**ccccctcgaggtcgacggtatcg**
nup60Δ	ATCAAATAAGCACCGCAA GATATCCTAAAATCGACAT CCA**CGGATCCCCGGGTTA ATTAA**	GGGCTATACGGTAATTATG TCACGGCTAAAATTTTCAT TA**GAATTCGAGCTCGTTTA AAC**
MLP1-GFP FKBP12-MLP1-GFP	AGAAAAAGAAACCGATAA GGTGAATGACGAGAACAG TATA**cggatccccgggttaattaa**	AAGGTTTAGTTTGTATTGA TCCCTTGTTTTTACTATCT CCT**GAATTCGAGCTCGTTT AAAC**
NUP60-myc9	GCTTGGTTGATGAAAATAA AGTTGAGGCTTTCAAGTCC CTATATACCTTT**TCCGGTT CTGCTGCTAG**	GTATTGAGTTGGGCTATAC GGTAATTATGTCACGGCTA AAATTTTCATTA**CCTCGAG GCCAGAAGAC**
*NUP60^{S89A}-myc9**	GGAGGTTATTTCCATTCTG AGATATCCCCAGATTCTAC TGTAAACCGT**G**CCGTAGTT GTT**G**CTGCAGTGGGTG	TTATAAGAGCCGCTAAAG GT
SpNUP60-GFP	ATGGAAAGCACCCAGGAA TTACCTAAATTCTCATTTT CAGTTTTGAAGGAAGAAA AGAACCGGATCCCCGGG TTAATTAA	AATTTATCTAGTCTAAATA GATATATGCCATTGAATAA AAGTATATTAATGCCAAAA AGTGAATTCGAGCTCGTTT AAAC
SpNUP61-GFP	AGTACTGCGGAAAAGTTAT TAGCCGAATTGAATGAGA AAAAGGTCTCAAAGTCAG AGAACCGGATCCCCGGGT TAATTAA	ATGTACATTTAATAGACCA AAAATAAAGGAATAAATAG TGACTGAATCAATCACTGC TTTGAATTCGAGCTCGTTT AAAC
SpNUP211-GFP	AAAAGACAACGTGACGAT GCGAACAAAGGAGGATCC AGTTCGAACCAAAAGAAA GCAAAACGGATCCCCGGG TTAATTAA	AAATCATGTTAACTAAATA TGAATAGTCCTAAGAGTGA TTTATGAACCATATGAAAA CATGAATTCGAGCTCGTTT AAAC
SpALM1-GFP	CCTAAACGGTCCAGTTCAG ACGCTGGTATGGATGTTTC CAATGATGTTAAGAAAGCC AAACGGATCCCCGGGTTA ATTAA	CTGTTTACAAACTCTTAAG AAACATTAAAAAGGGCATT ATACCAAAAAATTCATATT TTAGAATTCGAGCTCGTTT AAAC
SpNUP124-GFP	TCACAAACAAATGCGCCCC CGGGCCGTAAAATTGCTG TGCCCCGAAGTCGAAGAA	ATCATATACCCAACCGCAA TGTTTTGTCATATTGTCTT GTCAACATGTCATAATATT

	AACGTCGGATCCCCGGGT TAATTAA	AATGAATTCGAGCTCGTTT AAAC
PRP20-GFP	TGATGAGGACGCAGAAAA GAGAGCGGATGAAATGGA TGAT**CGGATCCCCGGGTT AATTAA**	ATTATGTCGATTTTCTTTT ATTTATCTTTGTACTACTA CC**GAATTCGAGCTCGTTTA AAC**
RNA1-3xEGFP	AGATGATCTTGCTGAACGT TTAGCTGAAACTGAAATCA AA**CGGATCCCCGGGTTAA TTAA**	GTCCACAGTTGATTGTGTT TATTTTTACTTTTATTCATA G**GAATTCGAGCTCGTTTAA AC**
HTB1-EGFP (old)	TACTAGAGCTGTTACCAAG TACTCTTCCTCTACTCAAG CA**GGTGACGGTGCTGGTT TA**	TAAATAATAATATTAATTA TAACCAAAGGAAGTGATTT CA**TCGATGAATTCGAGC**
HTB1-EGFP (new)	TACTAGAGCTGTTACCAAG TACTCTTCCTCTACTCAAG CA**CGTACGCTGCAGGTCG AC**	TAAATAATAATATTAATTA TAACCAAAGGAAGTGATTT CA**ATCGATGAATTCGAGCT CG**
P_{GAL}-IME2st	AATAAAAGAAGAGTACTAA GCTTAACTTAATAGGTCAT TT**gaattcgagctcgtttaaac**	AGCCACTACTGGAACTCTG TCTACTACGTTTTTCAAC**ca ttttgagatccgggtttt**
NUP170-RITE	GAACAGCGGCAATAATTT GGGGATTTGTTTCTACAAA GAA**GGTGGATCTGGTGGA TCT**	ACGTACATTACCCTGCTAT CTATATGTCGAACATGAAT TT**TGATTACGCCAAGCTCG**
NUP49-RITE	GTTACATCAAAAAACGAAA ACACTGGCATCATTGAGCA TA**GGTGGATCTGGTGGAT CT**	ACTTGTTATACGCACTATA TAAACTTTCAGGGCGATTT AC**TGATTACGCCAAGCTCG**
CHM7-GFP	TAATGAGATAAGAAAAATC ATGATGGAAGAACAACCA CGT**CGGATCCCCGGGTTA ATTAA**	TATTTATACATATATATTT ATTTATTAGTCACTCAGTT CG**GAATTCGAGCTCGTTTA AAC**
NHP2-GFP	GGAATCTTTCAACGAAGTT GTCAAAGAAGTTCAAGCTT TA**cggatccccgggttaattaa**	TTCTTCTAGATTTCTAATA TGGTTAAGAAGCGAACTTT TT**GAATTCGAGCTCGTTTA AAC**
NET1-GFP	TGGTGGATTTGCATCATTA ATAAAAGATTTCAAGAAAA AA**CGGATCCCCGGGTTAA TTAA**	TAGCTTTCTGTGACGTGTA TTCTACTGAGACTTTCTGG TA**GAATTCGAGCTCGTTTA AAC**
RPA135-GFP	CGCAATGGGTATAAGATT GCGTTATAATGTAGAGCCC	ATTTACCATTCTATATCAA TTTGGAAAGAAGGGTATTT

	AAA**CGGATCCCCGGGTTA ATTAA**	CT**GAATTCGAGCTCGTTTA AAC**
MSC1-GFP	TAACGTTAAAAACTGGTCG AAAAGCATATTAGGGTTCA AC**CGGATCCCCGGGTTAA TTAA**	AAATTGGGGAGAAAAGTA CATTACGTTGACACCCCAA TCA**GAATTCGAGCTCGTTT AAAC**
CDA2-mCherry	TTGTGTCGGCGGAATTGAT TACATAAAAGAATTCTTGT CC**CGTACGCTGCAGGTCG AC**	GTAATTTAATTCTTCCTTA TTTTCTTCAATTCCCTGAA AA**ATCGATGAATTCGAGCT CG**
GAS2-mCherry	TATACTTCTAATTTCTATG ATAGCTGCTGGAATTCTTC TA**CGTACGCTGCAGGTCG AC**	ACTATCAATTTATAACTTC ATTGAATATTAAATGAATT TT**ATCGATGAATTCGAGCT CG**
GAS4-mCherry	TGGGTTGTGTTTGCTTTTT TTTACTTTTAGTTTATTTTT T**CGTACGCTGCAGGTCGA C**	TATGTATTTACTCTTTAAA AAGGGAGAACGACATTAA AGT**ATCGATGAATTCGAGC TCG**
HTB1-EGFP	TACTAGAGCTGTTACCAAG TACTCTTCCTCTACTCAAG CA**CGTACGCTGCAGGTCG AC**	TAAATAATAATATTAATTA TAACCAAAGGAAGTGATTT CA**ATCGATGAATTCGAGCT CG**
HOS3-GFP	TGTTTCAAGAAAACATACA ACAAGAAGTGGTGGAAGA TGG**cggatccccgggttaattaa**	TCTTTAGTGGGTTCAAGAC AACATTATATATGCATTGG TA**GAATTCGAGCTCGTTTA AAC**
NUR1-GFP	TCTTCGCTCTCCAAAGAAA AAGAAGAACTATCACAAAA GA**cggatccccgggttaattaa**	TTTTACGTAACTGTATATA CTTAGACATAATTAAGAAA CG**GAATTCGAGCTCGTTTA AAC**
GIP1-GFP	TCAAGGGGCACAAATTATA TCGCTTGATGAGGATGTCT TT**CGTACGCTGCAGGTCG AC**	AATTTTACAGAGTATTGGC AGTTAAGTGTTGTTTTTTC GC**ATCGATGAATTCGAGCT CG**
ULP1-GFP *ULP1-3xeGFP*	AAGATTTATTGCCCATTTG ATTTTAACCGACGCTTTAA AA**cggatccccgggttaattaa**	TTCTACTTATGTATAATAA TTGTATATTATAAAAGAAT AA**GAATTCGAGCTCGTTTA AAC**

***** NOTE: Mutagenic primer can be used to introduce two mutations simultaneously: S89A and S93A. Single mutants were distinguished from double mutants and selected based on sequencing of potential transformants. I highlighted the nucleotides deviating from WT sequence in bold font.

Table C.3. Plasmids used for strain construction.

Plasmid Name	Description
pUB3	pFA6a-His3MX6
pUB4/pSJ2445	pFA6a-GFP(S65T)-KanMX6
pUB5	pFA6a-GFP(S65T)-TRP1
pUB6	pFA6a-GFP(S65T)-His3MX6
pUB16	pFA6a-kanMX6-PGAL1
pUB72	pFA6a-mCherry-KanMX6
pUB73	pFA6a-mCherry-NatMX6
pUB76	pFA6a-link-yeGFP-Kan
pUB153	pFA6a-NatMX4
pUB217	pFA6a-HphNT1
pUB233	pYM27 (C-terminal EGFP-KanMX Knop tagging plasmid)
pUB257	pYM-N4 (N-terminal yeGFP Knop tagging plasmid)
pUB595	pFA6a-FRB-KanMX6
pUB651	pNH604-pGPD1-FKBP12-CTEV
pUB691	pNH603-HIS3-VPH1-eGFP
pUB916	pFA6a-mCherry-His3MX6
pUB931	GFP-Npl3 His3 single integration vector
pUB984	pLC605-pARO10-2xmCherry-SV40NLS
pUB985	pFA6a-3xeGFP-KanMX6
pUB1104	pLC605-pATG8-link-mKate-SPO20(51-91)
pUB1183	pATG8-BFP-Spo20(51-91) Leu2 single integration vector
pUB1194	Trz1-eGFP Trp1 single integration vector
pUB1196	pLC605-pARO10-eGFP-h2NLS-L-TM
pUB1197	pYM28-mCherry-His3MX6
pUB1198	RITE V5-LoxP-HA-GFP->LoxP-T7-mCherry
pUB1305	pL245-3V5-IAA17
pUB1405	pFA6a-3xDendra2-HisMX6 (pKW2208)
pUB1727	Cas9-Nup1 gRNA4 Ura CEN plasmid
pUB1729	Cas9-Nup60 gRNA4 Ura CEN plasmid
pUB1730	Cas9-Nup42 gRNA1 Ura CEN plasmid
pUB1765	Screen plasmid 2.0 (pFA6a-HygMX-loxP-CEN13-Ura3-loxP-ARSH4)
pUB1877	pATG8-Q2-GFP Leu2 single integration vector
pUB1879	pATG8-NLS-Q2-GFP Leu2 single integration vector
pUB1881	pATG8-C1+C1b-GFP Trp1 single integration vector
pUB1883	pATG8-2xNLS-C1a+C1b-GFP Trp1 single integration vector
pUB1898	Screen plasmid 2.0 with tetO array (pFA6a-224xtetO-HygMX-loxP-CEN13-Ura3-loxP-ARSH4)

pUB1938	Cas9-Glc7 gRNA1 Ura CEN plasmid
pUB1974	pURA3-NLS-FKBP12-TetR-GFP Leu2 single integration vector
pUB2020	Cas9-Mlp1 gRNA1 Ura CEN plasmid
pUB2047	pCUP1-Cdc5-3xFLAG-10xHis Trp single integration vector
pUB2048	pCUP1-Cdc5[KD]-3xFLAG-10xHis Trp single integration vector
pUB2120	pCup-OsTIR-F74G His3 Integrating Vector
pUB2127	pFA6a-TetR-NatMX
pUB2298	pATG8-Nop15-GFP Trp1 single integration vector
pUB2299	pATG8-Sof1-GFP Trp1 single integration vector
pUB2302	pATG8-Nop15-TetR Trp1 single integration vector
pUB2303	pATG8-Sof1-TetR Trp1 single integration vector
pUB2304	pATG8-Nop13-TetR Trp1 single integration vector
pUB2305	pATG8-Rlp7-TetR Trp1 single integration vector
pML67	pWZV87 (pUC19-Myc9-KITRP1)
pML118	pAG304GAL-Cdc5WT-EGFP-TRP1
pML120	pAG304GAL-Cdc5KD-EGFP-TRP1
pSJ2392	pFA6a-mCherry-hphMX6; Addgene #105156

C.1.2 Sporulation conditions

Sporulation was induced using the traditional starvation method unless otherwise indicated. Diploid cells were first grown in YPD (1% yeast extract, 2% peptone, 2% glucose, 22.4 mg/L uracil, and 80 mg/L tryptophan) at room temperature for around 24 hours until the cultures reached a cell density of $OD_{600} \geq 10$. The cultures were then diluted in BYTA (1% yeast extract, 2% bacto tryptone, 1% potassium acetate, and 50 mM potassium phthalate) to $OD_{600} = 0.25$ and grown for 12-16 hours at 30°C. After reaching an $OD_{600} \geq 5$, the cells were pelleted, washed in sterile MilliQ water, and resuspended in the sporulation media (referred to as SPO in chapter 2, SPM in chapter 3) to $OD_{600} = 1.85$. SPO was 0.5% potassium acetate alone, 1% potassium acetate alone, or 2% potassium acetate supplemented with amino acids (0.04 g/L adenine, 0.04 g/L uracil, 0.01 g/L histidine, 0.01 g/L leucine and 0.01 g/L tryptophan); the media's pH was adjusted to 7 with acetic acid and 0.02% raffinose was sometimes added to improve sporulation. Meiotic cultures were shaken at 30°C for the duration of the experiment. At all stages, the flask size was 10 times the culture volume to ensure proper aeration.

To selectively enrich for the formation of dyads and triads (Figure 2.17), diploid cells were induced to sporulate in reduced carbon media (Eastwood et al., 2012). Cells were grown in YPD and BYTA as described above and then resuspended in SPO with reduced potassium acetate (0.1% potassium acetate, 0.02% raffinose, pH7) to an $OD_{600} = 1.85$. After 5 hours at 30°C, the cells were then pelleted, washed in sterile MilliQ, and resuspended in 0.15% KCl.

For Figures 3.6, 3.7C-E, and 3.7H-I: Meiotic time courses were performed with diploid SK1 strains obtained from mating *MAT***a** and *MATα* haploids, as previously described (Oelschlaegel et al., 2005; Petronczki et al., 2006). In brief, cells were grown for 48 h at 30°C on YPG (2% glycerol) plates as single colonies and subsequently propagated as a thin lawn on YPD plates. Cells were used to inoculate pre-sporulation medium YPA (2% potassium acetate) at OD_{600} = 0.3 and cultured for 11 h (30°C) on a shaker. Meiotic induction was initiated by switching cells to sporulation medium (SPM*, 2% potassium acetate) at OD_{600} = 3.5 – 4. The time of inoculation in SPM* was defined as t = 0. Cultures were upscaled to a 10 L fermenter system for MS sample collection, as previously described (Grigaitis et al., 2018). P_{GAL1}-*CDC5-eGFP* or P_{GAL1}-$CDC5^{KD}$-*eGFP* were induced by addition of β-estradiol to a final concentration of 2 µM. Cell cycle stage distribution was tracked by analyzing the cellular DNA content using propidium iodide staining on a FACS Canto cell sorter.

For *S. pombe,* strains were mated on sporulation agar medium with supplements (SPA5S; Petersen and Russell, 2016). After 15-18 h, a small toothpick of the mating patch was resuspended in 100 µL ddH20 and 10 µL was spotted onto a new SPA5S plate. This region was then removed and transferred to a 35-mm glass bottom dish (MaTek, no. 1.5 coverslip) for imaging.

C.1.3 Aged cell isolation and sporulation

Aged cells were enriched using a biotin-labeling and magnetic-sorting assay (Smeal et al., 1996). Cells were grown in YPD at room temperature or 30°C overnight until saturation ($OD_{600} \geq 10$) and then diluted to a cell density of OD_{600} = 0.2 in a new YPD culture. Cells were harvested before the cultures reached OD_{600} = 1 and were labeled with 8 mg/ml EZ-Link Sulfo-NHS-LC-biotin (ThermoFisher Scientific) for 30 minutes at 4°C. Biotinylated cells were grown for 6-8 generations in YPD with 100 µg/ml ampicillin at 30°C. Cells were subsequently harvested and mixed with 100 µl of anti-biotin magnetic beads (Miltenyi Biotechnology) for 15 minutes at 4°C. Cell were washed with PBS pH 7.4, 0.5% BSA buffer and sorted magnetically using LS depletion columns with a QuadroMacs sorter following the manufacturer's protocol. A fraction of the flow-through (biotin-negative) was kept as young cells and was bud scar labeled with eluted aged cells (biotin-positive) for 20 minutes at room temperature using 1 µg/ml Wheat Germ Agglutinin, Alexa Fluor™ 350 Conjugate (ThermoFisher Scientific). A mixture of aged and young cells was subsequently washed twice in H_2O and once with SPO (0.5% or 1% potassium acetate, 0.02% raffinose, pH 7.0). The cell mixture was resuspended with SPO at a cell density of OD_{600} = 1.85 with 100 µg/ml ampicillin and incubated at 30°C. The number of doublings in subsequent experiments was measured by counting the number of bud scars.

C.1.4 Cre-induced recombination experiments

For experiments involving Cre-induced recombination (e.g., the inducible acentromeric plasmid in Appendix A or the RITE tags in appendix B), diploid cells were taken out of the freezer on a YPG plate before being transferred to a hygromycin plate to maintain selection for either the plasmid or the intact RITE cassette. Cultures of YPD with hygromycin (200 µg/mL) were inoculated at a very low OD_{600} (<0.05 OD/mL) using yeast from the hygromycin plate resuspended in YPD. The cultures were allowed to grow at room temperature for ~16-18 h until reaching log phase (0.2 OD/mL < OD_{600} < 2.0 OD/mL). For the inducible acentromeric plasmid experiments, the cultures were back-diluted into YPD with hygromycin (200 µg/mL) at an OD_{600} = 0.2 OD/mL and allowed to grow for ~24 h until reaching saturation. Plasmid conversion was induced by addition of 1 µM ß-estradiol and allowed to continue for ~24 h. For the RITE experiments, the cultures were back-diluted into reduced YPD (same as YPD except 1% glucose and no tryptophan; no hygromycin) at an OD_{600} = 0.2 OD/mL and allowed to grow for ~12 h until reaching saturation. Cassette conversion was induced by addition of 1 µM ß-estradiol and allowed to continue for ~12 h. Cells were then induced to sporulate in Spo, as above.

At various time points, cells were plated onto YPD, with a dilution series performed to get ~200-400 cells per plate. After ~48 hours of growth at 30°C, the colonies were replica plated onto hygromycin and sometimes uracil-dropout plates. Colony growth was scored after either 24 h (for the RITE experiments and centromeric plasmids) or after 48 h (for the weak growing acentromeric plasmids). For the plasmid conversion experiments, an extra single spore isolation step was sometimes performed (the "ZYMO" samples, Figure A.2). Here, 5 mL of Spo culture was spun down and then resuspended in 1 mL MilliQ. The sample was then transferred to a low adhesion tube (Posi-Click, Denville; note that these tubes are far superior for pelleting yeast than any other low adhesion tubes tested). Digestion of mother cell asci and unsporulated cells was achieved by addition of 100 µL 1 mg/mL zymolyase (final concentration: 0.1 mg/mL) and 2 µL ß-mercaptoethanol, followed by incubation at 30°C overnight (~14-20 h). After this incubation, the samples were pelleted and washed in 1 mL MilliQ. The samples were resuspended in 1 mL MilliQ and transferred to a Bioruptor tube (Diagenode) with ~300 µL Bioruptor beads (Diagenode). Spores were then sonicated in the Bioruptor using a 30 s ON/ 30 s OFF program repeated 20 times. Single spore purity (usually >95%) was assessed under the microscope using a hemocytometer, prior to dilution and plating. For reasons that remain unclear, acentromeric plasmid-containing yeast grow more slowly on hygromycin plates after zymolyase treatment (data not shown), resulting in our preferential use of the "SPO" samples in assessing plasmid retention.

C.2 Light Microscopy

C.2.1 Fluorescence microscopy

All *S. cerevisiae* mages were acquired using a DeltaVision Elite wide-field fluorescence microscope (GE Healthcare). Live cell images were generated using a 60x/1.42 NA oil-immersion objective; fixed cell images were generated using a 100x/1.40 NA oil-immersion objective. Images were deconvolved using softWoRx imaging software (GE Healthcare). Unless otherwise noted, images were maximum intensity z-projected over the range of acquisition in FIJI (RRID: SCR_002285, Schindelin et al., 2012).

All *S. pombe* fluorescence microscopy was performed on a Nikon Ti-E microscope with a CSI W1 spinning disk (Yokogawa) using a 100x 1.4 NA Olympus Plan Apo oil objective and an iXon DU897 Ultra EMCCD camera (Andor).

C.2.2 Live-cell imaging

For *S. cerevisiae*, live cells were imaged in an environmental chamber heated to 30°C, using either the CellASIC ONIX Microfluidic Platform (EMD Millipore) or concanavalin A-coated, glass-bottom 96-well plates (Corning). All live imaging experiments used conditioned sporulation media (SPO filter-sterilized after five hours of sporulation at 30°C), as this was found to enhance meiotic progression. With the CellASIC system, cultures in SPO (OD_{600} = 1.85) were transferred to a microfluidic Y04D or Y04E plate and were loaded with a pressure of 8 psi for 5 seconds. Conditioned SPO was subsequently applied with a constant flow rate pressure of 2 psi for 15-20 hours. With the 96-well plates, cells were adhered to the bottom of the wells and 250 µl of conditioned SPO was added to each well. Images were acquired every 5 minutes for 8 hours or every 15 minutes for 15-18 hours.

For *S. pombe*, time lapse imaging of meiosis was performed in 35-mm glass bottom dishes (MaTek, no. 1.5 coverslip) maintained at 25°C using an Oko Lab stage top incubator. Fluorophores were excited at 488 nm (GFP) and 561 nm (mCherry) and collected through an ET525/36m (GFP) or ET605/70m (mCherry) bandpass filters. Images were collected over a z-volume of 8 µm with 0.5 µm spacing for 4-5 h, at 5-minute intervals.

C.2.3 Fixed-cell imaging

Fixed cells were prepared by treating 500-1000 µl of meiotic culture with 3.7% formaldehyde for 15 minutes at room temperature. Cells were permeabilized with either 1% Triton X-100 or 70% ethanol. (1) For Figure 2.8, cells were washed with 0.1 M potassium phosphate pH 6.4 and subsequently treated with 0.05 µg DAPI and 1% Triton in KPi sorbitol (0.1 M potassium phosphate, 1.2 M sorbitol, pH 7.5). Cells were

then immediately washed with KPi sorbitol before imaging. (2) For Figure 2.12A-B, cells were treated for five minutes with 1% Triton in KPi sorbitol and then resuspended in KPi sorbitol. Cells were then adhered on a poly-lysine treated multi-well slide and mounted with Vectashield Mounting Medium with DAPI (Vector Labs). (3) For Figures 2.9A-B, 2.17C-D, 2.17F, 2.19, cells were washed with 0.1 M potassium phosphate pH 6.4 and then resuspended in KPi sorbitol buffer. Cells were then adhered to a poly-lysine treated multi-well slide, quickly permeabilized with 70% ethanol, and mounted with Vectashield Mounting Medium with DAPI (Vector Labs).

For time course staging or flow cytometry, 500 µL of meiotic culture was fixed in 3.7% formaldehyde for 15 minutes at room temperature. Cells were washed in 0.1 M potassium phosphate pH 6.4, resuspended in KPi sorbitol buffer (0.1 M potassium phosphate, 1.2 M sorbitol, pH 7.5), and stored at 4°C prior to imaging. For flow cytometry, samples were resuspended in phosphate-buffered saline (PBS), before being passed through a Cell Strainer Snap Cap (Corning) and collected in a falcon tube (Corning). The data were collected on a BD Bioscience LSR Fortessa flow cytometer and were analyzed using FlowJo Flow Cytometry Analysis Software.

C.2.4 Super-resolution microscopy

Samples for structured illumination microscopy (SIM) were prepared by fixing 500 µL of meiotic cultures in 4% paraformaldehyde supplemented with 200 mM glucose for 15-20 minutes at room temperature. Cells were then washed and resuspended in phosphate buffered-saline (PBS), prior to being stored at 4°C until imaging. Fixed cells were imaged in PBS on an Applied Precision OMX Blaze V4 (GE Healthcare) microscope using a 60x 1.42 NA Olympus Plan Apo oil objective and two PCO Edge sCMOS cameras. GFP and mCherry were imaged with 488 nm (GFP) or 561 nm (mCherry) lasers with alternating excitation, using a 405/488/561/640 dichroic with 504-552 nm and 590-628 nm emission filters. Image stacks were acquired over a volume covering the full nucleus (typically 3-4 um) with a z-spacing of 125 nm. Images were reconstructed in SoftWoRx (Applied Precision Ltd) using a Wiener filter of 0.001.

C.2.5 Image quantification and statistics

Chapter 2
To quantify the percentage of Nsr1 sequestration, measurements of Nsr1-GFP signal intensity were taken with Fiji (RRID:SCR_002285, from maximum intensity z-projection movies of young and aged cells that eventually formed tetrads. Nsr1 signal was measured after nucleolus segregation to the four dividing nuclei, determined by the appearance of four Nsr1 foci in the four nuclei. Percent sequestration was measured by calculating the raw integrated intensity in the fifth compartment and dividing it by the sum of the signal present in the four nuclei and the fifth compartment. The mean intensity measured from non-cellular background was subtracted in each field of view before quantifying Nsr1 levels.

For the vacuolar lysis experiments, the timing of vacuolar membrane disruption and either excluded nucleoporin or protein aggregate disappearance were scored in cells that eventually became tetrads. Vacuolar membrane disruption was defined as the time point at which Vph1 signal becomes diffuse, instead of localizing to the membrane. Protein aggregate and NPC disappearance was defined as the time point at which the excluded fluorescence signal was no longer visible. Only cells in which both vacuolar membrane disruption and nucleoporin or protein aggregate disappearance could be confidently called were included in our analysis. In less than 25% of cells, the vacuole appeared to crumple and collapse over more than an hour prior to vacuolar membrane disappearance. Since we were unable to interpret these changes in vacuolar morphology, these cells were not included in our quantification.

For protein aggregate and nucleolar sequestration experiments, sequestration was scored in wild type cells that formed tetrads and *spo21Δ* cells that progressed through anaphase II, as tetrad formation cannot be assessed in *spo21Δ* cells. Protein aggregate sequestration was scored in aged cells and was defined as the aggregate no longer associating with chromatin after the four anaphase II nuclei became distinct. Nucleolar sequestration was scored in young cells and was defined as the presence of a fifth focus that did not associate with a gamete nucleus after the four anaphase II nuclei became distinct.

Chapter 3

All image analysis was performed in FIJI (RRID:SCR_002285; Schindelin et al., 2012). Maximum z-projection and single z-slices are shown for each image and were modified for presentation using linear brightness and contrast adjustments in FIJI. For any experiments in which successful sporulation was possible, only cells that became normally-packaged tetrads were analyzed.

To quantify nucleoporin detachment, individual cells were cropped from deconvolved images with background subtracted using a rolling ball method with a radius of 15 pixels. For the time points of interest, the individual z-slices containing the middle of the nucleus were selected and a nuclear mask was generated using the Htb1-mCherry signal. This nuclear mask was eroded and then dilated to generate masks for the nucleoplasmic and nuclear envelope regions, respectively. These masks were used to measure the intensities for each region in the Nup-GFP channel. Signal corresponding to the nuclear envelope was derived by subtracting the nucleoplasmic intensity from the total nuclear intensity. The detachment index (DI) was calculated for each nucleus image by dividing the mean nucleoplasmic intensity by the mean nuclear envelope intensity. Individual DI values were normalized to the mean intensity of a reference group, as indicated in the figure legends. We note that changes in nuclear geometry during the meiotic divisions likely affect DI measurements, as a smaller effective nuclear volume (e.g., a single nuclear lobe during anaphase I vs. the entire nucleus during prophase I) can result in more "nucleoplasmic" signal from out of focus z-slices. As such, we used Pom34-GFP, a

transmembrane nucleoporin, as our reference for different meiotic stages when initially assessing detachment (compare "pre" and "anaphase I" values for Pom34-GFP, Figure 3.1C). Downstream analysis, plotting, and statistics were conducted using R 4.1.1 (R Core Team, 2020). Information on the specific statistical test used for each experiment is provided in the corresponding figure legends. All source code used for analysis is provided at https://github.com/jmvarberg/King_et_al_2022. For all experiments, asterisks represent the following p-values: *, $p < 0.05$; **, $p < 0.01$; ***, $p < 0.001$; ****, $p < 0.0001$.

To visualize nucleoporin detachment in *S. pombe*, line profiles were measured In FIJI using a line width of 5 pixels on a single middle image of nuclei at the indicated time points relative to SPB separation (visualized using SpPpc89-mCherry). Individual line profiles were normalized (min-max) and plotted in GraphPad Prism (v. 9.0).

To quantify timing of Nup60 detachment relative to other meiotic events (Figures 3.2A and 3.5B), the following definitions were used: "detachment" was defined as the first time point with near maximum relocalization of Nup60-GFP to the nucleoplasm, and "reattachment" was defined as the first time point with near maximum relocalization of Nup60-GFP to the nuclear periphery. To quantify Mlp1-GFP mislocalization (Figures 3.13F and 3.14E), the following definitions were used: "normal localization" was defined as Mlp1-GFP signal/puncta distributed relatively evenly around the nuclear periphery; "mild mislocalization" was defined as one or two major Mlp1-GFP puncta with additional weaker peripheral Mlp1-GFP localization, or clustered and uneven peripheral Mlp1-GFP signal; "severe mislocalization" was defined as almost all Mlp1-GFP signal existing in one or two major puncta; and "diffuse signal" was defined as no clear enrichment of Mlp1-GFP at the nuclear periphery.

C.3 Electron Microscopy

Yeast cells were concentrated by vacuum filtration onto a nitrocellulose membrane and then scrape-loaded into 50- or 100- µm-deep high pressure freezing planchettes (McDonald and Müller-Reichert, 2002). Freezing was done in a Bal-Tec HPM-010 high-pressure freezer (Bal-Tec AG).

High pressure frozen cells stored in liquid nitrogen were transferred to cryovials containing 1.5 ml of fixative consisting of 1% osmium tetroxide, 0.1% uranyl acetate, and 5% water in acetone at liquid nitrogen temperature (-195˚C) and processed for freeze substitution according to the method of McDonald and Webb (McDonald, 2014; McDonald and Webb, 2011). Briefly, the cryovials containing fixative and cells were transferred to a cooled metal block at -195˚C; the cold block was put into an insulated container such that the vials were horizontally oriented and shaken on an orbital shaker operating at 125 rpm. After 3 hours the block and cryovials had warmed to 20˚C and were transitioned to resin infiltration.

Resin infiltration was accomplished by a modification of the method of McDonald (McDonald, 2014). Briefly, cells were rinsed 4-5 times in pure acetone and infiltrated with Epon-Araldite resin in increasing increments of 25% over 3 hours plus 3 changes of pure resin at 30 minutes each. Cells were removed from the planchettes at the beginning of the infiltration series and spun down at 6,000 x g for 1 minute between solution changes. The cells in pure resin were placed in between 2 PTFE-coated microscope slides and polymerized over 2 hours in an oven set to 100˚C.

Cells were cut out from the thin layer of polymerized resin and remounted on blank resin blocks for sectioning. Serial sections of 70 nm were cut on a Reichert-Jung Ultracut E microtome and picked up on 1 x 2 mm slot grids covered with a 0.6% Formvar film. Sections were post-stained with 1% aqueous uranyl acetate for 10 minutes and lead citrate for 10 minutes (Reynolds, 1963). Images of cells on serial sections were taken on an FEI Tecnai 12 electron microscope operating at 120 kV equipped with a Gatan Ultrascan 1000 CCD camera.

Models were constructed from serial sections with the IMOD package (Kremer et al., 1996), using 3DMOD version 4.9.8. Initial alignment was performed using the Midas tool in the ETomo interface of the IMOD package; afterwards, sections were rotated and minorly warped in Midas to improve alignment. The plasma membrane, nuclear envelope, and nucleoli were segmented in IMOD by manual tracing using the Drawing Tools plugin created by Andrew Noske.

C.4 Protein methods

C.4.1 Immunoblotting

For each meiotic time point, 3.33 or 3.7 OD_{600} equivalents of cells were pelleted and resuspended in 5% trichloroacetic acid and incubated at 4°C for ≥ 10 minutes. The cells were subsequently washed with 1 mL 10 mM Tris pH 8.0 and then 1 mL of acetone, before being left to dry overnight. Glass beads (~100 µL) and 100 µL protein breakage buffer (50 mM Tris-HCl pH 8.0, 1 mM EDTA, 20 mM Tris pH 9.5, 3 mM DTT, 1X cOmplete EDTA-free inhibitor cocktail [Roche]) were added to the samples, which were then pulverized for 5 minutes using the Mini-Beadbeater-96 (BioSpec). In Chapter 2 and Appendix B, the samples were then treated with 50 µl of 3X SDS sample buffer (187.5 mM Tris pH 6.8, 6% ß-mercaptoethanol, 30% glycerol, 9% SDS, 0.05% bromophenol blue) and heated at 37°C for 5 minutes. In Chapter 3, the samples were then treated with 50 µL of 3x SDS buffer (250 mM Tris pH 6.8, 8% ß-mercaptoethanol, 40% glycerol, 12% SDS, 0.00067% bromophenol blue) was added to the samples prior to incubation at 95°C for five minutes.

Proteins were separated by polyacrylamide gel electrophoresis using 4–12% Bis-Tris Bolt gels (Thermo Fisher) and transferred onto nitrocellulose membranes (0.45 µm,

Bio-Rad). The Nup84-GFP blot in Figure 2.16E was generated using a semi-dry transfer apparatus (Trans-Blot Turbo Transfer System, Bio-Rad). All other blots were generated using a Mini-PROTEAN Tetra tank (Bio-Rad) filled with 25 mM Tris, 195 mM glycine, and 15% methanol, run at 180 mA (max 80 V) for 3 hours at 4°C. The membranes were blocked for at least 30 minutes with PBS Blocking Buffer (LI-COR Biosciences) at room temperature. Ponceau S (Sigma) staining was often performed to assess protein transfer, followed by blocking in PBS Blocking Buffer (LI-COR Biosciences). Blots were incubated overnight in primary antibody diluted in PBS Blocking Buffer at 4°C. The following primary antibodies were used: 1:2000 mouse anti-GFP (RRID:AB_2313808, 632381, Clontech); 1:2000 mouse anti-3V5 (RRID:AB_2556564, Invitrogen); 1:10000 rabbit anti-hexokinase (RRID:AB_219918, 100-4159, Rockland); and 1:1000 rabbit anti-FLAG (RRID:AB_2217020, 2368, Cell Signaling Technology). Blots were then washed in PBST (PBS with 0.1% Tween-20) and incubated in secondary antibody diluted in PBS Blocking Buffer + 0.1% Tween-20 for 3-6 h at RT. The following secondary antibodies were used: 1:15000 donkey anti-mouse conjugated to IRDye 800CW (RRID:AB_621847, 926–32212, LI-COR Biosciences) and 1:15000 goat anti-rabbit conjugated to IRDye 680RD (RRID:AB_10956166, 926–68071, LI-COR Biosciences). Blots were then washed in PBST and PBS, before imaging using the Odyssey CLx system (LI-COR Biosciences). Image analysis and quantification was performed in FIJI (RRID:SCR_002285, Schindelin et al., 2012).

For Figures 3.6, 3.7C-E, and 3.7H-I: TCA extracts were performed as described previously (Matos et al., 2008). Briefly, pellets from meiotic cultures (OD_{600} ~3.5, 10 ml) were disrupted in 10% TCA using glass beads. Precipitates were collected by centrifugation, resuspended in 2x NuPAGE sample buffer (50% 4X NuPAGE, 30% H_2O, 20% DTT 1M), and neutralized with 1 M Tris-Base. Samples were incubated for 10 min at 95°C, cleared by centrifugation, and separated in NuPAGE 3-8% Tris-Acetate gels (Invitrogen). Proteins were then transferred onto PVDF membranes (Amersham Hybond 0.45 µm, GE Healthcare). For immunoblotting, the following antibodies were used: 1:15000 rabbit anti-Myc HRP-conjugated (RRID: AB_299800), 1:5000 rabbit anti-Crm1 (a gift from K. Weis, ETH Zurich), 1:5000 rabbit anti-Puf6 (a gift from V. Panse, University of Zurich), 1:2500 mouse anti-Cdc5 clone 4F10 (MM-0192-1-100, Médimabs). The following secondary antibodies were used: 1:5000 goat anti-mouse immunoglobulin conjugated to HRP (RRID:AB_2617137, P0447, Agilent) and 1:5000 swine anti-rabbit immunoglobulin HRP conjugated (RRID:AB_2617141, P0399, Agilent).

C.4.2 **MS data acquisition and analysis**

Sample preparation: 100 mL of meiotic yeast culture OD_{600} = 3.5 in SPM* (2% KAc) was collected per time point and supplemented with 100% Trichloroacetic acid (TCA) to a final concentration of 6.25%. Samples were washed twice with cold acetone, pelleted and snap frozen in liquid nitrogen. Proteins were extracted in batches of 12

samples by 5 minutes bead beating using 400 µl of 425-600 µm glass beads in a cell Disruptor Genie and 400 µl of lysis buffer (8 M urea, 100 mM ammonium bicarbonate, 5 mM EDTA, pH = 8). The samples were then centrifuged at 16,000 x g for 10 min and the supernatant collected. The extraction procedure was repeated a total of 5 times using 400 µL fresh lysis buffer each time. Total amount of protein was measured with bicinchoninic acid (BCA) assay (Pierce) and 3 mg of total protein was further used per sample. Samples were sequentially incubated with (1) 5 mM Tris (2-carboxyethyl) phosphine (TCEP) for 1h at 25°C, (2) 12 mM Iodoacetamide for 1h at 25°C in dark, (3) diluted 8 times with 100 mM ammonium bicarbonate (reducing urea to 1M), and (4) trypsin digested overnight at 37°C (protein to trypsin ratio 1:100). Sample pH was reduced to ~2.5 with formic acid (FA) and peptides were enriched on C18 silica reversed-phase chromatography column (Sep-Pak C18 3cc, Waters). Peptides were eluted in 50% acetonitrile (ACN) and 0.1% FA, speedvac-dried, and reconstituted in 50 µL 0.1% FA. For the total proteome assessment ("non-enriched"), 1 µL was taken up and diluted to 1 µg/µL. The remaining sample was used for phosphopeptide enrichment by TiO_2 affinity purification. To this end, samples were incubated 1h RT on a rotator with 6.25 mg of TiO_2 resin (GL Science) pre-equilibrated twice with methanol and twice with lactic acid binding buffer (5 ml ACN, 2.92 ml lactic acid, 20 µl 50% TFA, filled with H_2O to 10 ml). Beads were washed sequentially twice with lactic acid binding buffer, then 80% ACN, 0.1% TFA and 0.1% TFA. Phosphopeptides were eluted in 50 mM ammonium phosphate pH 10.8 and acidified immediately to pH 2 with 50% FA. Samples were cleaned on C18 Micro Spin Columns (The Nest group), eluted in 50% ACN 0.1% FA, speedvac-dried, and resuspended in 0.1% FA. All samples were spiked with iRT reference peptides (Biognosys). Samples for library preparation consisted of the following triplicate pools of selected time points after Cdc5 or $Cdc5^{KD}$ induction: t = 0.5h, t = 2h, t = 5h.

Mass spectrometry data acquisition: 1 µg of peptides was injected on a 6600 Sciex TripleTOF mass spectrometer interfaced with an Eksigent NanoLC Ultra 1D Plus system. The peptides were separated on a 75-µm-diameter, 20cm-long new Objective emitter packed with Magic C18 AQ 3 µm resin (Michrom BioResources) and eluted at 300 nL/min with a linear gradient of 2-to-30% Buffer B for 60 min (Buffer B: 98% ACN, 0.1% FA). MS data acquisition for the individual meiotic time course samples was performed in data-independent acquisition (DIA) SWATH-MS mode using 64 variable precursor isolation windows with 1 Da overlaps acquired each for 50 ms plus one MS1 scan acquired for 250ms, as described in Gillet et al., 2012. Library generation was performed in data-dependent acquisition mode (DDA, top20, with 20 s dynamic exclusion after 1 MS/MS). For either mode, the mass ranges recorded were 360-1460 m/z for MS1 and 50-2000 m/z for MS2, and the collision energy was set to 0.0625 × m/z - 6.5 with a 15-eV collision energy spread regardless of the precursor charge state.

Data-dependent acquisition (DDA) mode data analysis: The DDA search and spectral library were performed essentially as described in Schubert et al., 2015. In short, the

raw DDA files were converted to mzXML using gtofpeakpicker (Proteowizzard v 3.0.9992) and further to mgf using MzXML2Search (TPP 4.7). The converted files were searched with Comet (2014.02 rev. 0) and Mascot (version 2.5.1) using the yeast SGD database (release 13.01.2015) appended with the SK1 (for a total of containing 12,043 proteins including one protein entry for the concatenated sequence of the iRT peptides and as many decoy protein entries generated by pseudo-reversing the tryptic peptide sequences) or the W303 entries (for a total of containing 12,071 proteins including one protein entry for the concatenated sequence of the iRT peptides and as many decoy protein entries generated by pseudo-reversing the tryptic peptide sequences) for data acquired for the SK1 or W303 strain, respectively. The search parameters were as follows: +/- 25ppm tolerance for MS1 and MS2, fixed cysteine carbamidomethylation, either variable methionine oxidation (for the non-enriched datasets) or variable methionine oxidation and variable serine/threonine/tyrosine phosphorylation (for the phospho-enriched datasets), semi-tryptic and 2 missed cleavages allowed. The comet and mascot search results were further processed using peptideProphet (Keller et al., 2002) and aggregated using iProphet (Shteynberg et al., 2011; TPP v4.7 rev 0). The search results were filtered for an iProphet cutoff of 1% false discovery rate. The pep.xml file was further processed with LuciPhor for determining the confidence in the phosphorylation site localization. Two consensus spectral libraries were generated using spectrast (Lam et al., 2008) depending on the confidence in phosphorylation-site localization and the two assay libraries thereof were exported using the spectrast2tsv.py script (Schubert et al., 2015) with the following parameters: 5 highest intensity fragments (of charge 1+ or 2+) per peptide, within the mass range 350-2000 m/z, allowing fragments with -79.97 or -97.98 neutral losses, and excluding the fragments within the precursor isolation window of the corresponding swath. The final library retained in priority assays from the high confidence localization and then the assays from the low confidence localization. The assay library was finally exported to TraML with shuffled decoys appended as described in Schubert et al., 2015.

SWATH-MS targeted data extraction and data filtering: The SWATH-MS data were extracted with the above mentioned assay library through the iPortal interface (Kunszt et al., 2015) with openSWATH (Röst et al., 2014; openMS 2.1.0), pyProphet (Teleman et al., 2015), and TRIC alignement (Röst et al., 2016) using the same parameters as described in Navarro et al., 2016 and further processed in R. The precursor intensities were first $\log_2$-transformed and normalized (mean-centering). Assays identified in two out of three triplicates for at least one condition were kept. The missing values were imputed at the precursor level using either a random value amongst a distribution centered at the mean of the other replicate values of that triplicate series (when at least 1 value was found for that triplicate) or centered on a value 3-fold lower than the lowest value of that precursor, and with a standard deviation equal to the mean standard deviation of all the replicate precursor values. All the precursor intensities were then summed to a protein intensity value for the non-enriched datasets.

The raw dataset consisted of 14,710 phosphopeptides with single and multi-phosphorylated sites that were annotated to the yeast proteomes W303 and SK1 (17,387 proteins; Engel et al., 2014). W303 is identical to the proteome release S288C_reference_genome_R64-2-1_20150113.tgz available at http://sgd-archive.yeastgenome.org/sequence/S288C_reference/genome_releases/. The median intensities of phosphosites mapping to the same amino acid and position per protein were merged to generate 7,552 unique phosphopeptides. Additionally, multi-phosphorylated peptides were split into single phosphosites and they were retained for further analysis if they were not part of the set of mono-phosphorylated peptides.

The $\log_2$ ratios in Figure 3.6B-C comparing $Cdc5^{WT}$ vs $Cdc5^{KD}$ were calculated using the mean values across biological replicates and time points (2, 3, 4 and 5 h after Cdc5 induction). The reported p-values were corrected for false discovery rate (FDR) and tested against an alpha value of 0.05. All statistical methods were implemented using R v3.5.1 (R Core Team, 2020) and the limma package v3.38.3 (Ritchie et al., 2015).

A few considerations are important to correctly interpret this dataset. (1) Cdc5-mediated phosphorylation of a peptide may not necessarily lead to an increase in its abundance. Protein phosphorylation can be linked to the co-occurrence of other PTMs or to protein degradation, which could lead to a decrease in the ability of our approach to detect the phosphorylated peptide. In addition, the low expression level of some proteins could intrinsically limit their detection by SWATH-MS. As such, some, possibly many, Cdc5 targets may be absent in the current dataset. (2) Phosphorylation of a peptide that is pre-phosphorylated at a different site can result in a decrease in the abundance of the pre-phosphorylated peptide, without the detection of the double phosphorylated peptide species. A possible example of this is shown in Figures 3.6D and 3.7H, in which Swi6 phosphorylation at S176 decreases sharply upon Cdc5 expression. This could be explained by modification of additional sites in the vicinity, which would render the double/multiple phosphorylated peptide difficult to monitor by MS. Therefore, a decrease in abundance in cells expressing Cdc5 ($Cdc5/Cdc5^{KD}$) could indicate that another site in the vicinity is phosphorylated in response to Cdc5. (3) Given the complexity of the samples analyzed, it is likely that the putative Cdc5 target sites identified constitute only a subset of all residues phosphorylated in cells. Due to these considerations, complementary approaches should be used to further validate individual Cdc5 targets, as well as to expand on the identity of the phosphorylation sites when studying them in-depth.